# Dry and Wet Surface Enhanced Raman Scattering Substrates

by

Ahmed Mahmoud

A thesis submitted in partial fulfillment of the requirements for the degree of

Doctor of Philosophy

Department of Chemistry
University of Alberta

# Abstract

In the past few decades, surface enhanced Raman scattering (SERS) has been evolving as a powerful analytical technique for the detection of a wide of chemical and biological molecules. The technique can reach a sensitivity of single molecule detection, which triggered plenty of ongoing research. In addition, technological advancements in photonics and nanoscience have resulted in the advent of portable and handheld Raman systems. These devices help SERS analysis move from expensive heavy-equipped research labs to low cost field deployable-research. The development of efficient SERS substrates that can provide signal enhancement by many orders of magnitude is a core component for SERS. The SERS substrates market and research are generally dominated by rigid solid substrates that are fabricated mostly by micro/nanofabrication techniques. Although these methods can provide reproducible substrates, they suffer from usability constraints because of their high cost of fabrication.

The work presented in this thesis explored cost-effective approaches to develop and optimize SERS substrates. The substrates investigated are divided into two main categories, membrane-based SERS substrates and in-solution SERS substrates. The membrane-based SERS substrates were fabricated by equipment-free methods. In these deviceless methods, gold and silver nanostructures were incorporated in-situ within the micropores of polyvinylidene fluoride (PVDF) membranes by seed mediated and seedless protocols, respectively. The SERS performance of these substrates was investigated and optimized by controlling the loading of plasmonic nanostructures. These flexible inexpensive substrates have the advantages of being easy to fabricate and

to use. In addition, the variation in the SERS performance of these substrate was less than 20% within the same substrate and from substrate-to-substrate, which reflects acceptable reproducibility. Analytical applications of these substrates were demonstrated using a Raman microscope as well as a handheld Raman spectrometer.

The second category of the SERS substrates studied was based on the optimization of gold nanostars and graphene–silver nanocomposites for water dispersible SERS measurements. In-solution SERS platforms are not used as commonly as solid-based substrates; however, these wet platforms can provide some advantages over the dried-based ones in terms of cost, reproducibility, and analysis time. The SERS performance of gold nanostars with different branch lengths was optimized based on the type of Good's buffer, the ratio of buffer to gold concentration, and their aggregation. Our results were counterintuitive in that the gold nanostars with the shorter branches provided the largest in-solution SERS intensity. These findings can be attributed to higher surface coverage of the Raman probe rather than enhanced electromagnetic effects. Graphene–silver nanocomposites were investigated also as in-solution SERS substrates with a large 2D surface area. The SERS behavior of these nanocomposites were studied using graphene, a thiolated Raman probe, and a dye labelled ssDNA to simulate different possible interactions. The SERS and plasmonic performance of these nanocomposites can be tuned by the size of silver nanoparticles on these substrates. The nanocomposites were more stable and showed superior SERS performance when compared to commercial silver nanoparticles. The contributions of this work can pave the way for flexible membrane-based and in-solution SERS substrates to be accompanied with a handheld Raman device for field-deployable SERS measurements.

# Preface

This thesis is an original work by Ahmed Mahmoud under the supervision of Professor Mark T. McDermott. The work in this thesis was based on the collaborative research contributions of many people. Below are details of each experimental chapter.

Chapter 2 was conducted in collaboration with Dr. Nikola Pekas, a research officer at the National Research Council Nanotechnology Research Centre (Edmonton). Dr. Pekas developed the seed mediated protocol to incorporate gold nanostructures into PVDF membranes. Dr. McDermott and Dr. Pekas have contributed with critical inputs and suggestions. I have optimized and merged the seed mediated protocol with the SILAR-like seeding protocol and have performed most of the experimental work, all data analysis, and writing of this chapter. Helium ion microscopy was performed through the nanoFAB facility at the University of Alberta by Peng Li. FTIR and UV-vis diffuse reflectance measurements were collected through the Analytical and Instrumentation Laboratory at the department of chemistry. Wayne Moffat and I have collected UV-vis diffuse reflectance measurements.

Chapter 3 also was conducted in collaboration with Dr. Pekas. Both Dr. McDermott and Dr. Pekas have contributed with critical inputs and suggestions. I have performed most of the experimental work, data analysis, and writing of this chapter. Helium ion microscopy was performed through the nanoFAB facility by Dr. Shihong Xu. FTIR and UV-vis diffuse reflectance measurements were collected through the Analytical and Instrumentation Laboratory at the department of chemistry. W. Moffat and I collected UV-vis diffuse reflectance. A patent filing is intended for this chapter in near future.

A part of Chapter 4 was published recently as Mahmoud, A. Y. F.; Rusin, C. J.; McDermott, M. T., Gold nanostars as a colloidal substrate for in-solution SERS measurements using a handheld Raman spectrometer. *Analyst* **2020,** *145* (4), 1396-1407. Dr. McDermott, C. Rusin, and I have composed the manuscript with equal contribution between C. Rusin and I. This chapter was a collaborative work with Casey Rusin, including data collection, analysis, and discussion. Critical inputs, suggestions, and recommendations were given by Dr. McDermott. Synthesis of gold nanostars and related extinction spectroscopy measurements were performed by C. Rusin and me. C. Rusin took a lead in the electron microscopy and differential light scanning experiments in this work., while I performed almost all Raman and SERS measurements. The impact of centrifugation on the SERS performance of the nanostars was conducted by C. Rusin. Part of the data related to the comparison between the three Raman spectrometers was also collected and analyzed by C. Rusin.

I conducted the experiments in Chapter 5 under the supervision of Dr. McDermott. I performed most of the experimental work of this chapter with, critical inputs from Dr. McDermott. FTIR spectra were collected through the Analytical and Instrumentation Laboratory at the department of chemistry. A transmission electron microscopy micrograph of graphene oxide was collected by Dr. Lida Hadidi, I performed scanning electron microscopy through the nanoFAB facility with Peng Li and Dr. Anqiang He. I carried out the data analysis and chapter writing.

During my PhD, I was involved in other collaborative projects not described in this thesis, which resulted in the following publications:

1. Li, X.; Chen, Y.; Kumar, A.; Mahmoud, A.; Nychka, J. A.; Chung, H.-J., Sponge-Templated Macroporous Graphene Network for Piezoelectric ZnO Nanogenerator. *ACS Applied Materials & Interfaces* **2015,** *7* (37), 20753-20760. I Performed the Raman spectroscopy charcterization and related data analysis.

2. Hadidi, L.; Mahmoud, A. Y. F.; Purkait, T. K.; McDermott, M. T.; Veinot, J. G. C., Cellulose nanocrystal-derived hollow mesoporous carbon spheres and their application as a metal-free catalyst. *Nanotechnology* **2017,** *28* (50), 505606. This project was a collaboration between Dr. Jonathan Veinot and Dr. McDermott. I worked with Dr. Lida Hadidi in this project, who took a lead in the synthesis and characterization part, while I performed the Raman spectroscopy characterization and the catalytic application of mesoporous carbon derived from cellulose nanocrystals. Dr. Hadidi and I contributed equally in data analysis, discussion, and manuscript writing, with critical inputs, suggestions, and help from Dr. McDermott and Dr. Veinot.

# Dedication

To the memory of my father, Yousef, and my aunt, Bothaina, both of you will be in my heart and in my thoughts always. I missed your continuous support and encouragement through my PhD program.

# Acknowledgments

The work of this thesis would not have been possible without the help and support of a lot of people that I was lucky to have at the department of chemistry and at the University of Alberta. First and foremost, I would like to thank Dr. Mark McDermott, my PhD supervisor, for his continuous help, guidance, support, and patience. Dr. McDermott provided me with a unique learning and research experience over the years, working in his labs with awesome co-workers. I cannot find enough words that can express my gratitude, appreciation, and respect to Dr. McDermott. I would like to extend my gratitude to my committee members, Dr. Richard McCreery and Dr. Robert Campbell, for their valuable comments and suggestions through the annual progress report reading and meetings. I thank Dr. Jonathan Veinot for stepping in as a committee member to replace Dr. Campbell for my defense.

In addition, I would like to thank all the current and previous members of McDermott's group, including Casey Rusin, Sunil Rajput, Shereen Elbayomy, Kenny Xu, Thuy Nguyen, Greg Kaufman, Nicole Jankovic, Khandaker Shahriar, Abdelhaq Benkaddour, Taylor Lynk, Huijun Mao, Ibrahim Bushnak, Rongbing Du, Lars Laurentius, John Toman and Cici Cao. Each one of you has helped me during my PhD, and you have been a family for me.

I would like to thank all the staff members of the chemistry department, especially Anita Weiler, Laura Pham, Esther Moibi, Gareth Lambkin, Wayne Moffat, and many other awesome people in the department. I am indebted to all the people who have been

working in storerooms, glass shop, and machine shop at the department of chemistry for their help, understanding, and support.

My teaching skills were improved through working with a great teaching team, including Dr. Yoram Apelblat, Dr. Norman Gee, Dr. Greg Kiema, Dr. Eric Flaim, Dr. James Harynuk, and Dr. Vladimir Michaelis. I would like to thank each one of you for being helpful and understanding. I am very grateful to Dr. Charles Lucy, who provided me with a great learning and teaching opportunity through the chemical education program. Thank you, Chuck, for this wonderful experience.

I am indebted to Dr. Anna Jordan who has been helping me in thesis editing. Anna, with her positive attitude and cheerful smile, made thesis editing a fun thing to do with less stress. Thank you, Anna, for being kind, understanding, and encouraging. Special thanks to Dr. Jonathan Veinot and Dr. Lida Hadidi for their collaboration. In addition, I am very thankful and grateful to Dr. Maria Stepanova who hired me before my PhD defense. Thank you, Maria, for encouraging and motivating me to finish.

Moreover, I would like to thank and acknowledge some old and new friends who have been supporting and helping me in one way or another through my PhD program, including Osama Elshenawy, Wael Elhenawy, Ahmed Belal, Ahmed Saed, Mahmoud Bahnasy, Amgad Roushdy, Eiman Osman, Abdullah Elshemimry, Karim Atta, Ahmed Ali, Ahmed Ibrahim, Nayyera Fouad, Seham Helmi, Karim Elgammal, Ahmed Foda, Loay Elalfy, Omnia Fayed, Islam Ali, and Amro Gharib.

Last but not least, special thanks to all my family members who have been supporting me in many ways during my PhD here at the university of Alberta. Thank you, Mom, for all your continuous help, support, encouragement, and prayers. I am also

thankful and grateful to all my siblings, including Fatima ElZahraa, Mohamed, Fouad, Bothaina, and Mahmoud. I would like to acknowledge all my nephews and nieces who were also supportive and kept encouraging me to finish my work including Sohaila, Basmella, Yousef AbdelHakim, Yousef Fouad, Farida, Ziad, Hamza, Yousef Mahmoud, Mustafa, Farah, and Ahmed.

# Table of contents

# List of Tables

# List of Figures

# List of Abbreviations

| | |
|---|---|
| 4-MBA | 4-mercaptobenzoic acid |
| ACN | Acetonitrile |
| Ag | Silver |
| $AgNO_3$ | Silver nitrate |
| AgNPs | Silver nanoparticles |
| AFM | Atomic force microscopy |
| a.u | Arbitrary unit |
| Au | Gold |
| Au NS | Gold nanostars |
| cDNA | Complementary deoxyribonucleic acid |
| CE | Chemical mechanism |
| Cipro | Ciprofloxacin |
| CMC | Carboxymethylcellulose |
| CT | Charge transfer |
| CTAB | Cetyltrimethylammonium bromide |
| CV | Crystal violet |
| CVD | Chemical vapor deposition |
| Cy5 | Cyanine 5 |
| DI | Deionized water |
| DLS | Dynamic light scattering |
| DNA | Deoxyribonucleic acid |

| | |
|---|---|
| E-beam | Electron beam |
| EF | Enhancement factor |
| EM | Electromagnetic mechanism |
| EPPS | 4-(2-hydroxyethyl)-1-piperazinepropanesulfonic acid |
| FFT | Fast Fourier Transform |
| FIB | Focused ion beam |
| FRET | Fluorescence resonance energy transfer |
| FTIR | Fourier transform infrared |
| FWHM | Full width at half maximum |
| GERS | Graphene enhanced Raman scattering |
| GO | Graphene oxide |
| $HAuCl_4$ | Chloroauric acid |
| HCl | Hydrochloric acid |
| HH | Hydroxylamine hydrochloride |
| HEPES | 4-(2-hydroxyethyl)-1-piperazineethanesulfonic acid |
| HIM | Helium ion microscopy |
| HIV | Human Immunodeficiency Virus |
| $H_2O_2$ | Hydrogen peroxide |
| $H_3PO_4$ | Phosphoric acid |
| $H_2SO_4$ | Sulfuric acid |
| inc | Incoming |
| $K_2HPO_4$ | Potassium phosphate dibasic |
| $KH_2PO_4$ | Potassium phosphate monobasic |

| | |
|---|---|
| LC | Liquid chromatography |
| LOD | Limit of detection |
| LSPR | Localized surface plasmon resonance |
| LUMO | Lowest unoccupied molecular orbital |
| MBN | 4-Mercabtobenzonitrile |
| Mel | Melamine |
| MG | Malachite green |
| $MgCl_2$ | Magnesium chloride |
| min | Minute |
| MOPS | 3-(N-morpholino)propanesulfonic acid |
| MRL | Maximum residue limit |
| MRSA | Methicillin-resistant Staphylococcus aureus |
| MS | Mass spectrometry |
| MTZ | Methimazole |
| MWCO | Molecular weight cut-off |
| N.A | Numerical aperture |
| $NaBH_4$ | Sodium borohydride |
| NaCl | Sodium chloride |
| NaOH | Sodium hydroxide |
| NBT | 4-nitrobenzenthiol |
| NCs | Nanocomposites |
| PC | Phthalocyanine |
| PLLA | Poly (l-lactic acid) |

| | |
|---|---|
| PPB | Potassium phosphate buffer |
| ppb | Parts per billion |
| ppm | Parts per million |
| PPP | Protoporphyrin IX |
| PVDF | Polyvinylidene fluoride |
| PVP | Polyvinyl pyrrolidone |
| R6G | Rhodamine 6G |
| RGO | Reduced graphene oxide |
| RhB | Rhodamine B |
| RNA | Ribonucleic acid |
| RPM | Revolutions per minute |
| RSD | Relative standard deviation |
| S.D | Standard deviation |
| SEM | Scanning electron microscope |
| SERS | Surface enhanced Raman scattering |
| Si | Silicon |
| SILAR | Successive ionic layer absorption and reaction |
| ssDNA | Single stranded deoxyribonucleic acid |
| TBZ | Thiabendazole |
| TEM | Transmission electron microscopy |
| US EPA | The United States Environmental Protection Agency |
| Vib | Vibrational |

# List of Symbols

| | |
|---|---|
| a | Average radius of curvature of the nanoparticle |
| α | Polarizability |
| °C | Degree Celsius |
| cm | Centimeter |
| $cm^{-1}$ | Wavenumber |
| Da | Dalton |
| E | Electric field |
| $\varepsilon_m$ | Dielectric function of the surrounding medium |
| $\varepsilon_{metal}$ | Dielectric function of a metal |
| h | Hour |
| $\lambda_{max}$ | Absorption band maximum / position |
| µL | Microliter |
| µM | Micromolar |
| mg | Milligram |
| mL | Milliliter |
| mM | Millimolar |
| mm | Millimeter |
| µW | Micro Watts |
| mW | Milli Watts |
| MΩ-cm | Mega ohm centimeter |
| M | Molar |

| | |
|---|---|
| $\nu_0$ | Frequency of the incident laser |
| $\nu_j$ | Characteristic harmonic frequency of the jth normal mode |
| nm | Nanometer |
| nM | Nano molar |
| nmole | Nanomole |
| $\omega$ | Angular frequency |
| P | Polarization |
| pM | Picomolar |
| Qj | Normal molecular vibration modes |
| r | Distance between the adsorbed molecule and the metal surface |
| $R^2$ | Correlation coefficient |
| s | Second |
| W | Watts |
| w/w | Weight per weight |

# Chapter 1

## General Introduction

## 1.1 Research Scope and Objectives

Technological advancements in Raman systems with portable options and single molecule detection capability of surface enhanced Raman scattering (SERS) have made SERS a powerful analytical technique.[1-6] These have led to the expansion of fields where SERS can be applied, such as surgery, security, quality control of pharmaceuticals, investigation of artwork, environmental monitoring, and many more.[7-11] Besides the advantage of single molecule detection, SERS has the advantages of normal Raman. It is (1) a non-destructive technique, (2) it can provide chemical information of molecules from their vibrational fingerprints, (3) it is water compatible, (4) it requires minimal sample preparation, (5) it has remote analysis and on-site analysis capabilities, and (6) it has a multiplexing capability.[5-6] In addition, SERS as a technique has been combined with other techniques, such as chromatographic and electrochemical techniques.[12-15]

A nanostructured substrate is a vital component for SERS and is responsible for the Raman signal being enhanced by several orders of magnitude. The development of efficient SERS substrates is challenged always by reproducibility and the cost of fabrication. Nanosphere lithography, oblique angle metal film evaporation, electron beam (e-beam) lithography, and focused ion beam (FIB) milling are some examples of micro/nanofabrication techniques that are used widely in SERS substrates fabrication.[16-20] These methods can yield SERS substrates with highly ordered nanopatterns and high enhancement factors; however, they require very specialized equipment, highly trained personnel, and a high cost to operate.[21]

The motivation behind this thesis is the exploration of cost-effective approaches that can be used to develop and optimize SERS substrates for applications in analytical

chemistry. The research work within this thesis is divided into two major parts. The first part is focused on the development of flexible SERS substrates using in-situ synthesis approaches. These approaches are used to incorporate plasmonic nanostructures into the 3D porous network of polyvinylidene fluoride (PVDF) filters. The plasmonic behaviour and the SERS performance of these substrates are studied using different techniques. The second part is focused on the exploration and optimization of the in-solution SERS behaviour of gold nanostars and graphene–silver nanocomposites.

The main experimental research objectives of this thesis include: (1) the development of equipment-free methods to incorporate metal nanostructures into PVDF membranes to be used as SERS substrates; (2) the optimization of gold nanostars with different branch lengths as in-solution SERS substrates; (3) the exploration of graphene–silver nanocomposites as in-solution SERS substrates; and (4) the demonstration of potential applications using these substrates.

This chapter aims to introduce some relevant topics that are fundamental to understanding the development of inexpensive SERS substrates. Raman scattering and SERS theories will be discussed briefly. A particular focus on the development of cost-effective SERS substrates will be presented in this chapter. SERS substrates based on membranous materials and in-suspension SERS substrates are emphasized, as these substrates are relevant to this thesis. The current market of SERS substrates and commercially available SERS substrates are highlighted at the end of this chapter.

## 1.2 Raman Scattering

Raman scattering is an inelastic light scattering phenomenon that was described first by Chandrasekhara Venkata Raman in a Nature paper entitled "A New Type of Secondary Radiation" in 1928.[22] This new type of secondary radiation, Raman scattering, granted C. V. Raman the Nobel prize in physics in 1930. His discovery used a simple setup consisting of a telescope, coloured filters, sunlight as a light source, and eye as a detector.[23] The effect had been predicted theoretically five years before C.V Raman's experiment by A. Smekal in 1923.[23] Seventy years after the discovery of the Raman effect, the American Chemical Society considered Raman scattering a national historic landmark for its analytical capability in molecular level characterization of gases, liquids, and solids.[24]

When light interacts with matter, the large majority of the scattered photons are of the same frequency as the incident light (Rayleigh scattering). Raman scattered light, on the other hand, has frequencies other than the incident light.[6] The frequency shift between the incident and scattered light in Raman scattering is equal to vibrational transitions.[6] Figure 1-1 is a graphical representation that shows the difference between Rayleigh and Raman scattering. The virtual state in Figure 1-1 is a very short-lived distortion of the electron cloud produced by the oscillating electric field of the light, and it is not a true quantum state.[6]

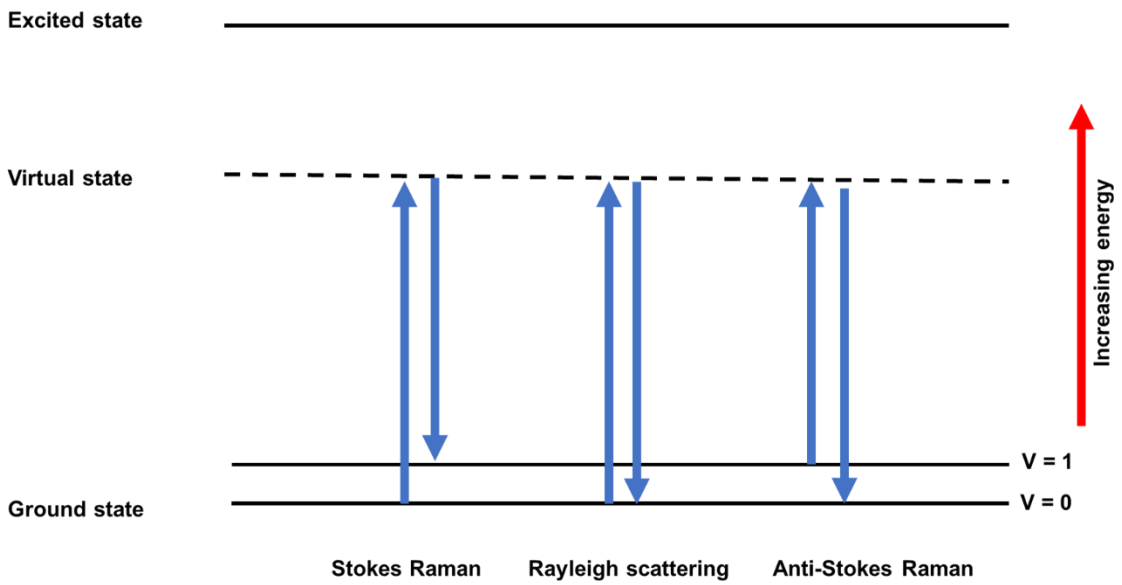


**Figure 1-1. Rayleigh, Stokes and Anti-Stokes Raman scattering.**

The following section contains a summary of a few equations that describe Raman scattering.[6] The classical and quantum mechanics explanation of Raman scattering depend on Equation 1-1:

$$P = \alpha E \qquad \text{(Eq1-1)}$$

where $P$ is a polarization induced in the molecule by the oscillating electric field ($E$) of the incoming light, and $\alpha$ is the polarizability.[6] The induced polarization is proportional to the polarizability and the strength of electric field $E$, which can be expressed in Equation 1-2 as

$$E = E_0 \cos 2\pi\nu_0 t \qquad \text{(Eq1-2)}$$

where $\nu_0$ is the frequency of the incident laser light, and $t$ is the irradiation time.[6] A molecule with number of atoms ($N$) will have its normal molecular vibration modes, $Qj$.[6]

$$Qj = Q^0 j \cos 2\pi\nu_j t \qquad \text{(Eq1-3)}$$

where $\nu_j$ is referred to the characteristic harmonic frequency of the jth normal mode.[6] Since the molecular vibrations can control the polarizability of electrons in the molecule, polarizability, $\alpha$, can be expressed as:

$$\alpha = \alpha_0 + \left(\frac{\delta\alpha}{\delta Q_j}\right) Q_j + .. \qquad \text{(Eq1-4)}$$

By substituting Equations 1-2 and 1-4 into Equation 1-1 and disregarding higher order in Equation 1-4, polarization, *P*, can be expressed as:

$$P = \alpha_0 E_0 \cos 2\pi\nu_0 t + E_0 Q^0{}_j \left(\frac{\delta\alpha}{\delta Q_j}\right) \frac{\cos 2\pi(\nu_0+\nu_j) + \cos 2\pi(\nu_0-\nu_j)}{2} \qquad \text{(Eq1-5)}$$

Equation 1-5 shows that light will be scattered with three possible frequencies, with the assumption that that the polarized electrons will radiate light at the frequency of their oscillations.[6] The first part of the equation, $\alpha_0 E_0 \cos 2\pi\nu_0 t$, refers to Rayleigh scattering, where the scattered light has the same frequency as the incident light. The second part refers to the anti-Stokes Raman scattering, where the scattered light will have a higher frequency than the incident light, $(\nu_0 + \nu_j)$.[6] The third part refers to the Stokes Raman scattering, where the scattered light will have a lower frequency than the incident light, $(\nu_0 - \nu_j)$.[6] This means that Raman frequencies may have lower or higher frequencies when compared to the incident light frequency.[6] While the last equation was based on a classical derivation and is incomplete, it can offer some significant understandings about Raman scattering.[6] From Equation 1-5, we can deduce that polarization and scattering intensities are in a linear relationship with the incident intensity for Rayleigh and Raman scattering.[6] In addition, Raman scattering will be produced only by vibrations that can result in a change in the polarizability, where $\frac{\delta\alpha}{\delta Q_j} \neq 0$ is considered as the primary selection rule for Raman scattering.[6]

Although Raman scattering as a technique offers some advantages that we discussed earlier in this chapter, Raman scattering is considered as an insensitive technique due to two main limitations, low intensity and fluorescence interference.[6] The low intensity is a result of only one photon in approximately 10 million photons being Raman scattered.[25] Although fluorescence interference can be reduced by using lasers with longer wavelengths (785 and 1064 nm), this will result in low intensity, as scattering scales with the fourth power of the frequency of the incident laser.[6] Besides, the Raman cross section is many orders of magnitudes lower than that of fluorescence.[6]

## 1.3 Surface Enhanced Raman Scattering (SERS)

The journey of the discovery of SERS was started in 1974 by Fleischmann et al.[26] An intense Raman signal of pyridine was observed when it was adsorbed onto a roughened silver electrode.[26] The researchers initially assumed that the electrochemical surface roughening of the electrode resulted in increasing its surface area and, consequently, increased the number of adsorbed pyridine molecules.[26] However, SERS was explained independently three years later by two different research groups in 1977.[27-28] The two research groups established that there is an enhancement mechanism that led to such an intense Raman signal and that the large surface area postulation is not adequate to account for it solely. An electric field enhancement mechanism was suggested by Jeanmarie and Van Duyne.[27] Albrecht and Creighton, on the other hand, proposed that the electronic energy levels of pyridine got broadened upon adsorption onto the roughened electrode, which may have induced resonant Raman scattering through the interaction between the adsorbed molecules and surface plasmons.[28] Afterward,

Moskovits suggested that the enhancement was due to the optical excitation of the collective oscillation of the surface electrons of the metal nanostructures.[29-30] The SERS effect is attributed to two main mechanisms: an electromagnetic enhancement mechanism (EM) and a chemical enhancement mechanism (CE).[27-32]

The two enhancement mechanisms can be explained by the direct relationship between the intensity of Raman scattering and the square of the induced dipole moment.[32] This induced dipole moment is the product of the Raman polarizability and the strength of the incident electromagnetic field; as a result of exciting the localized surface plasmon resonance (LSPR) of nanofeatures on a metal surface, the local electromagnetic field is enhanced.[32] The dominant enhancement mechanism in SERS is the EM mechanism, which can contribute a $10^4$-$10^8$ enhancement factor, while the CE mechanism may contribute to an enhancement factor of $10^2$.[32] An enhancement factor up to $10^9$–$10^{10}$ can result from combining SERS and resonance Raman scattering.[32] Although there is always a debate about the exact contribution of these enhancement mechanisms in SERS,[33] the capability of SERS to reach a single molecule detection limit has made SERS a powerful analytical technique.[1-2]

### 1.3.1 Electromagnetic Enhancement Mechanism

As stated in the last section, the main enhancement mechanism in SERS is the electromagnetic (EM) mechanism, as illustrated in Figure 1-2 for a gold nanoparticle. This enhancement mechanism results from the excitation of LSPR of metal nanoparticles by the incident laser with a frequency of ($\omega_{inc}$) and strength of ($E_0$), leading to charge separation and the amplification of the electromagnetic field.[34]

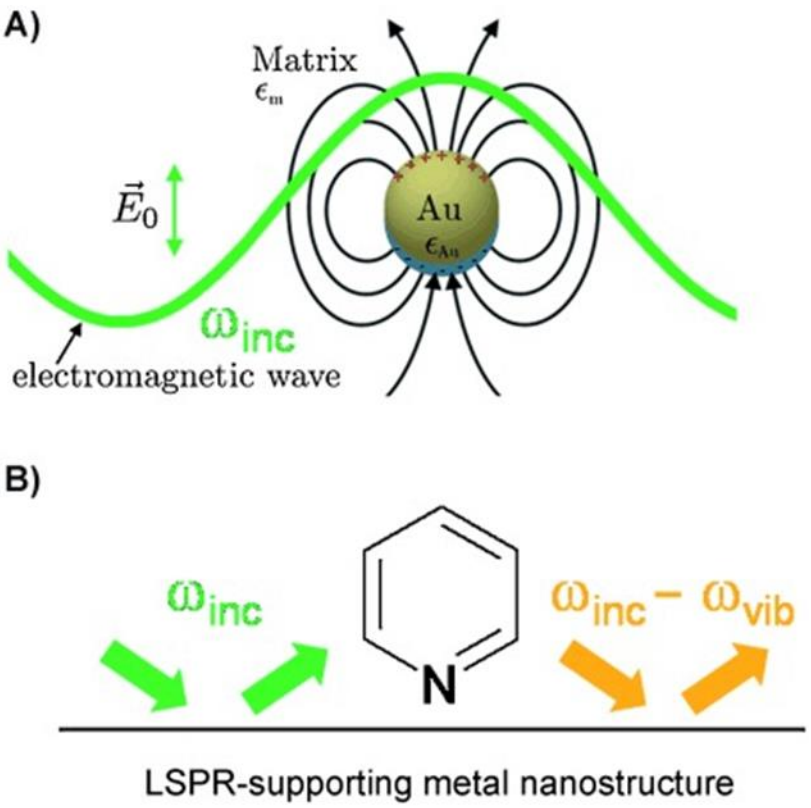


**Figure 1-2. Electromagnetic enhancement in SERS.** (A) A gold nanoparticle acts as a nanoantenna by excitation of a dipolar localized surface plasmon resonance (LSPR). (B) Both the "incoming" field ($\omega_{inc}$, green) and the "outgoing" field ($\omega_{inc}-\omega_{vib}$, orange) are enhanced by elastic light scattering off the LSPR-supporting metal nanostructure. Reproduced with permission from *Angewandte Chemie, International Edition* 2014, *53* (19), 4756-4795.[34]

The LSPR of metal nanoparticles varies mainly with the dielectric functions of the metal ($\varepsilon_{metal}$) and the surrounding medium ($\varepsilon_m$).[34] The polarizability of the metal and incident electric field strength can determine the induced dipole of the metal.[34] As a result of exciting the LSPR of the metal nanoparticle with the incident laser, a nanoantenna is generated that can emit light at the same frequency, $\omega_{inc}$, as shown in Figure 1-2.[34] Figure 1-2A shows an elastic light scattering off a gold nanoparticle, which resulted in enhancing the local electric field of the incident light close to the surface of the metal nanoparticle.[34]

Figure 1-2B illustrates the interaction between the local electric field ($\omega_{inc}$) and pyridine as an example of a Raman reporter near the gold nanoparticle surface with the exciting LSPR.[34] It also illustrates the interaction between the outgoing stokes scattered light ($\omega_{inc}-\omega_{vib}$) and the LSPR of the gold nanoparticle.[34] This interaction means that the SERS intensity is dependent on both the incident ($\omega_{inc}$) and scattered ($\omega_{inc} - \omega_{vib}$) electric fields:

$$I_{SERS}=I_{inc}(\omega_{inc})I(\omega_{inc} - \omega_{vib})=|E_{inc}(\omega_{inc})|^2 \, |E(\omega_{inc} - \omega_{vib})|^2 \qquad \text{(Eq 1-6)}$$

Equation 1-6 shows that the intensity of SERS scales to $E^4$ approximately when the frequency of the incident laser light and stokes Raman scattering for a certain vibration are close to each other.[34]

Optimum SERS enhancements can be achieved when both incident and scattered light are in resonance with the plasmon band of the metal nanoparticle.[34] Van Duyne and co-workers showed that the strongest SERS enhancements could be achieved when the excitation wavelength is shorter, i.e., blue-shifted, than that of the $\lambda_{max}$ of the LSPR of the metal nanoparticles.[35] Another important aspect of the EM mechanism and SERS, generally, is its distance dependence. The field enhancement close to a spherical metal nanoparticles scales as $r^{-3}$, where $r$ is the distance between the adsorbed molecule and the metal surface.[32, 34, 36] Therefore, the total distance dependence scales with $r^{-12}$ with the $E^4$ approximation.[32, 34, 36] However, one should take into account the increased surface area scaling factor of about $r^2$, considering that shells of adsorbed molecules at an increased distance from the metal surface result in $r^{-10}$ distance dependence:

$$I_{SERS}= (a+r/a)^{-10} \qquad \text{(Eq 1-6)}$$

where *a* is the average radius of curvature of the nanoparticle.[32, 36] Overall, the EM enhancement mechanism can be summarized briefly as a result of an increase in the local electric field upon excitation of LSPR of metal nanoparticles, leading to a significant enhancement in the SERS signal compared to normal Raman scattering.

### 1.3.2 Chemical Enhancement Mechanism

The overall SERS enhancement cannot be explained exclusively using the EM enhancement mechanism. For example, different molecular species with similar polarizability display vastly different enhancement when they are adsorbed on the same metallic substrate.[37-38] The chemical (molecular/electronic) enhancement (CE) is the second mechanism responsible for SERS enhancement. This mechanism involves an increase in the molecular polarizability tensor $\alpha_{molecule}$, which will result in a larger Raman cross-section.[39-40] The formation of a metal–adsorbate chemical bond and the existence of specific active sites are some of the requirements of this short-range mechanism, described by Otto as the first-layer effect.[41] Although the CE mechanism is not understood fully, it is assumed to have resulted from different processes, including molecular excitation resonances, charge-transfer (CT) resonances, and non-resonant changes in the polarizability of the molecule upon adsorption onto the metal surface.[42-45] The CE mechanism can be explained by a general model, including a CT between the adsorbed molecules and the metal surface.[40, 46] Figure 1-3 shows a schematic representation of the CT model of SERS CE.[46] In this model, an electron from the Fermi level ($E_f$) of the metal is transferred to the lowest unoccupied molecular orbital (LUMO) of the adsorbed molecule.[46] The newly formed metal–adsorbate complex is in a CT transition, which is in resonance with the incident photon frequency $\omega_{inc}$, followed by

electron relaxation back to the metal.[46] The scattered photon ($\omega_s = \omega_{inc} - \omega_{vib}$) will have vibrational information of the molecule ($\omega_{vib}$). Controlling the energy of $E_f$ can be managed by the excitation wavelength or by an externally applied potential in the case of a metallic electrode.[46]

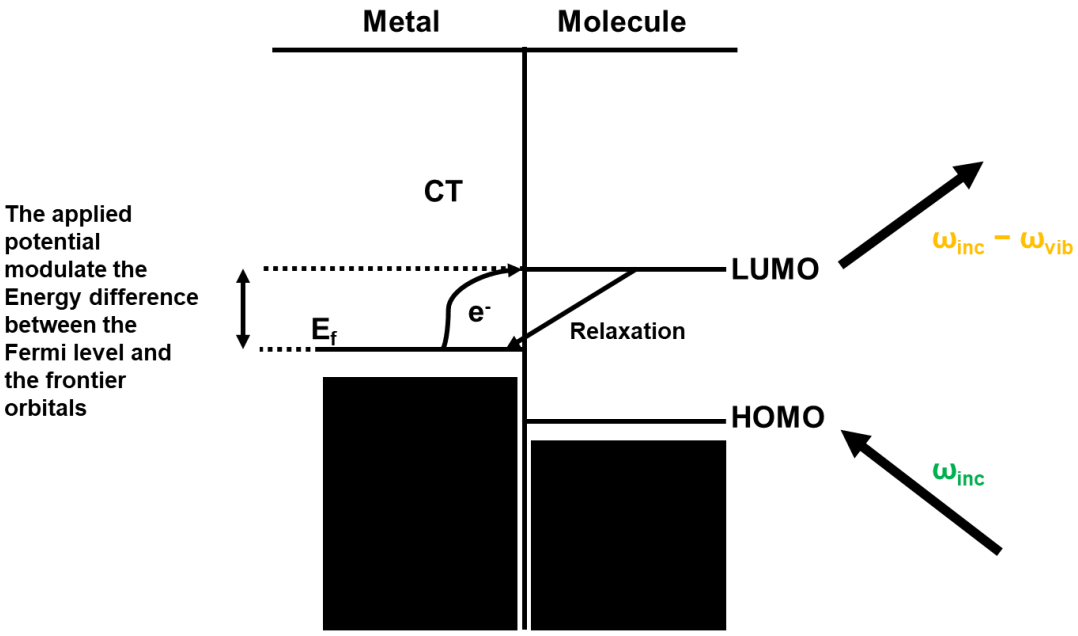


**Figure 1- 3. Charge transfer model of SERS chemical enhancement.** For adsorbed molecules containing empty low energy π* orbitals, an electron is transferred from the metal's Fermi level to the LUMO. This process is in resonance with the energy of the incident photon ($\omega_{inc}$). The applied potential can modulate the energy of the Fermi level; the energy of the Fermi level either increases or decreases as a negative or positive potential, respectively, is applied. Adapted with permission from *Journal of Molecular Structure* 1997, *405* (1), 29-44.[46]

The CE contribution to the SERS enhancement of a factor of $10^0$–$10^3$ is less than that of the EM mechanism.[45, 47-49] However, CE does not require nanoscale features when compared to EM. For example, Campion and co-workers have shown a SERS enhancement of a factor of 100 on a smooth copper surface, attributed to CE.[42] It is very complicated to distinguish between CE and EM in SERS clearly. One way to distinguish

between them is by studying the dependence of SERS spectra on the laser excitation wavelength, which can prove the CT mechanism of CE.[50] Sun and co-workers presented a visualized method based on charge density difference calculations to provide a clear evidence of a CT mechanism and to differentiate between CT and EM mechanisms.[51] The importance of the EM in SERS has driven researchers to develop substrates with nanoscale features that provide a high level of plasmonic enhancement.

## 1.4 Development of Cost-Effective SERS Substrates

A significant component in any SERS platform is the SERS substrate, where enhancement of the Raman signal will take place. Natan and Lin et al. have outlined some properties for an ideal SERS substrate, which include: (1) the SERS substrate should demonstrate reproducible signals over a large area, with a variation of less than 20% from spot-to-spot and substrate-to-substrate; (2) the substrate should have a high enhancement to provide high sensitivity; (3) the substrate should have a clean surface and should be applicable to strong and weak adsorbates; (4) a good stability over a long period of time should be provided by an ideal SERS substrate.[52-53] Other significant desired features are the ease of fabrication and use as well as the overall cost.[5] However, it is difficult to find a universal SERS substrate with all of the above-noted features, therefore, there always will be trade-offs dictated by the desired applications.[53] For example, SERS substrates with huge enhancements will be required for trace analysis, and substrates with reproducible results will be required for quantitative analysis.[53]

Generally, SERS substrates can be categorized into three major platforms: i) nanostructures fabricated directly on solid substrates by micro/nanofabrication

techniques, ii) nanoparticles immobilized and incorporated on solid substrates, and iii) nanoparticles in suspension.[5, 54] Since the work in this thesis is focused on cost-effective approaches for developing SERS substrates, we will present some examples of inexpensive methods to fabricate SERS substrates, emphasizing the incorporation of nanoparticles into 3D structures of membranous materials and nanoparticles in suspensions. The reader is directed to these comprehensive reviews for micro/nanofabrication techniques reported to develop SERS substrates.[5, 54-56]

### 1.4.1 SERS Substrates Based on Porous Materials

The development of efficient SERS substrates by alternative, cost-effective methods to the micro/nanofabrication methods is an active field of research. Integration of plasmonic nanostructures into flexible scaffolds, such as paper, membranes, and fabrics, is one approach.[57-58] These scaffolds can be exploited easily to fabricate SERS substrates where metal nanoparticles are incorporated and stabilized.[59] Paper-based SERS substrates were introduced by Vo-Dinh et al. in 1984.[60] The authors developed a two-step process to a create a paper SERS substrate.[60] The first step was to coat paper with polystyrene spheres. The second step was to vacuum deposit silver nanostructures on the coated paper by thermal evaporation.[60] Later, Vo-Dinh and co-workers published another article using a one-step process to develop a paper SERS substrate.[61] The authors thermally evaporated silver nanostructures directly onto the paper surface, without a polystyrene coating, as before.[61] In the following section, we present some examples of experimental approaches about how plasmonic nanoparticles have been incorporated into these types of scaffolds with a 3D fibrous network of paper and other related

materials. Table 1-1 shows a few examples of the approaches that will be discussed later. The enhancement factor range of these approaches ranges from $10^4$ to $10^7$, with a limit of detection range from nM to pM.

**Table 1- 1. Examples of Some Approaches to Develop SERS Substrates Based on Porous Scaffolds**

| Approach | Nanoparticles | Porous platform | Analyte/s and (limit of detection) | Enhancement factor |
|---|---|---|---|---|
| In-situ synthesis[62] | Gold nanoparticles | Whatman cellulose chromatography paper (Grade 1) | 2-naphthalenethiol (1 pM) | $7.8 \times 10^8$ |
| Immersion[63] | Gold nanoparticles | Filter paper (Whatman No. 4) | Trans-1,2-bis(4-pyridyl)ethylene[a] | $\sim 3 \times 10^4$ |
| Spotting[64] | Gold nanorods | Hydrophobic nanofibrous PLLA paper | R6G (0.1 nM) and malachite green (0.1 nM) | $1.08 \times 10^7$ |
| Brushing[65] | Silver nanoparticles | Filter paper (Whatman No. 1) | R6G (1 nM) and malachite green (10 nM) | $2.2 \times 10^7$ |
| Inkjet printing[66] | Silver nanoparticles | Fisherbrand chromatography paper | R6G[a] | $2 \times 10^5$ |
| Screen printing[67] | Silver nanoparticles | fibre glass plates | R6G ($1.6 \times 10^{-13}$ M) | $4.4 \times 10^6$ |
| Spraying[68] | Silver nanoparticles | Filter paper (Whatman chromatography No.1 paper) | R6G (1 nM) | $\sim 2 \times 10^7$ |
| Filtration[69] | Silver nanoparticles | Nylon and PVDF membranes | R6G (10 nM), melamine (6.3 ppb), and malathion (61.5 ppb) | $\sim 1.5 \times 10^6$ |

[a]Limit of detection was not reported. R6G: Rhodamine 6G

#### 1.4.1.1 In-situ Synthesis Approach

Many research groups have explored the in-situ synthesis approach to incorporate plasmonic nanoparticles within porous membranes to develop paper-based SERS substrates. For example, Winefordner's group immersed filter papers in a silver nitrate solution and then sprayed sodium borohydride from a distance with a nebulizer to deposit silver nanostructures in-situ.[70-72] Marque et al. synthesized a cellulosic fibre-

silver nanocomposite sponge by immersing cellulose fibres into a silver nitrate solution.[73] They used sodium citrate with boiling to reduce the silver nanoparticles within the fibres.[73] A silver mirror reaction also was used for in-situ deposition of silver nanoparticles into filter paper with or without previous chemical modifications of the paper.[74-75] For example, Zhu and co-workers used a silver mirror reaction at room temperature to synthesize silver nanostructures within the 3D fibrous network of a filter paper.[74] They used formaldehyde to reduce Tollen's reagent without any pretreatment of the filter paper.[74] However, Li and co-workers have modified this protocol by imparting aldehyde groups on the paper, which can reduce Tollen's reagent without using an external reducing agent, such as formaldehyde.[75] However, their protocol involved heating.[75]

All the previous examples depended on a single cycle of reduction to synthesize plasmonic nanoparticles. Choi's group has introduced a protocol that involved multiple cycles of reduction in fabricating paper-based SERS substrates.[62, 76-78] In their protocol, plasmonic nanoparticles have been incorporated into filter paper through a successive ionic layer absorption and reaction (SILAR) technique.[62, 76-78] The group has merged the knowledge of early reports to fabricate SERS substrates based on filter papers and the principles of the SILAR technique from solar cells fabrication.[62, 76-78] In their approach, filter papers were immersed in succession into a metal ion (silver or gold) solution, water, reducing agent solution ($NaBH_4$), and water through repeated reaction cycles.[62, 76-78] This resulted in the direct synthesis of plasmonic nanoparticles at the reaction sites.[62, 76-78] The researchers studied how they can optimize the SERS enhancement based on the concentration of the reagents and the number of SILAR cycles used.[62, 76-78] Figure

1-4 shows a graphical representation of the SILAR protocol. The protocol discussed above depends on a wax pre-treatment step of the filter papers before starting the multiple SILAR cycles. The waxing step was implemented to create hydrophobic barrier regions that can result in concentrating the plasmonic nanoparticles in the hydrophilic regions for SERS measurements.[62, 76-77] In addition, the wax treatment step was essential to improve the mechanical stability of the filter paper; otherwise, the material would deform after multiple cycles of dipping in various chemical reagents in the SILAR protocol.[62, 76-77]

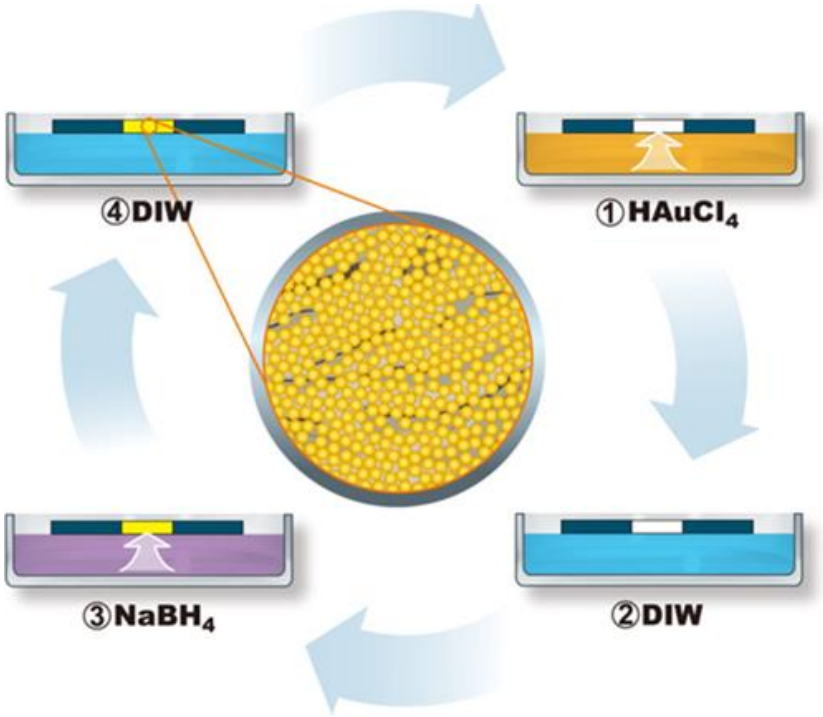


**Figure 1-4. Graphical representation of the SILAR protocol to incorporate gold nanoparticles into filter paper.** One SILAR cycle consists of four successive steps, which are: (1) immersion in gold solution, (2) washing with deionized water to remove excess reagent from the previous step, (3) immersion in $NaBH_4$ solution, where reduction of gold takes place, and (4) washing again with deionized water to remove excess reagent and unattached particles. Synthesis of gold nanoparticles took place only at the hydrophilic regions (white or yellow) of the paper, not at the wax-printed hydrophobic regions (black). Reproduced with permission from *Analytical Chemistry* 2016, *88* (10), 5531-5537.[62]

#### 1.4.1.4 Immersion Approach

The immersion or dip-coating approach is another protocol to incorporate plasmonic nanoparticles into porous supports to be used as SERS substrates. In this approach, the porous scaffolds are immersed in previously synthesized colloidal solutions of plasmonic nanoparticles for a prolonged time (typically 1-2 days). Singamaneni's group presented this protocol to deposit gold nanorods and gold nanobipyramids into filter papers.[79-81] Mehn and co-workers deposited star-shaped gold nanoparticles into filter paper, which reflected the capability of this approach to incorporate anisotropic nanostructures easily within the 3D porous architecture.[82] Ngo et al. used the immersion protocol to incorporate spherical gold nanoparticles into filter paper.[83] The authors observed that the SERS performance of these substrates was higher than that on a hydrophobic paper and a silicon wafer.[83] They rationalized that the z-distribution of the nanoparticles into the 3D structures of filter paper, where interlayer plasmon coupling took place, leads to a higher SERS enhancement.[83] Mirkin and co-workers incorporated previously aggregated nanoparticles into paper using the immersion approach.[63] In addition, the same group applied the immersion approach to attach previously synthesized nanoparticles into a paper to act as seeds before growing them into anisotropic nanostructures.[84]

In this approach, pre-treatment of filter papers was investigated to improve the loading of plasmonic nanostructures and their SERS performance. For example, dipping filter papers in a NaCl solution before immersing them into the colloidal solution of silver nanoparticles was employed to increase the adsorption of silver nanoparticles and thus improve SERS performance.[85-86] Surface modification can reduce the time needed in the

immersion approach. For example, Kong and co-workers modified the surface of regenerated fibres from wood sawdust and de-inked pulp by glycidyltrimethylammonium chloride.[87] This modification imparted ammonium groups on the surface of the fibres, facilitating the self-assembly of citrate capped silver nanoparticles by electrostatic interaction in only five minutes dipping time.[87]

#### 1.4.1.5 Spotting Approach

Spotting of plasmonic nanoparticles on porous membranes is one of the methods used to fabricate paper-based SERS substrates. For example, Fang's group developed SERS substrates by just dropping previously synthesized colloidal silver and gold nanoparticles onto slow-speed filter papers and microporous films.[88-90] They applied their substrates to study 4-hyrdroxybenzoic acid, C60, C70, and single-walled carbon nanotubes.[88-90] The impact of the paper grade in terms of grams per square meter on the SERS performance was shown in one study using the spotting approach.[91] In this study, silver nanoparticles were pipetted on different papers with different grades, and their SERS performance was compared.[91]

Other examples employed other spotting techniques rather than dropping and pipetting, such as a semi-automatic thin layer chromatography sample applicator[92] and a capillary tube.[64] For example, Chen et al. spot-aggregated silver nanoparticles by NaCl onto filter paper that was pretreated with polyvinyl pyrrolidone (PVP) using a semi-automatic thin layer chromatography sample applicator.[92] They used PVP to enhance the adhesion of the aggregated silver nanoparticles onto the paper.[92] Another example was presented by Shao and co-workers, where they used a glass capillary tube (inner

diameter 0.3 mm) to spot cetyltrimethylammonium bromide (CTAB) capped gold nanorods onto a hydrophobic poly(l-lactic acid) (PLLA) nanofibrous paper.[64] Their platform depended on the electrostatic attraction between CTAB capped gold nanorods and PLLA.[64]

#### 1.4.1.6 Writing and Brushing Approaches

In this approach, previously synthesized and concentrated plasmonic nanostructures were applied to paper materials using pens[93-94] and brushes[65, 95] to develop paper-based SERS substrates. In one report, a fountain pen was used to write plasmonic inks containing nanostructures with different shapes onto paper.[93] In this example, concentrated spherical gold nanoparticles, spherical silver nanoparticles, and gold nanorods were used as plasmonic inks.[93] In another report, a ballpoint pen was used to write gold nanorods as a plasmonic ink on paper.[94] Painting plasmonic inks of silver and gold nanostructures have been shown also by brushing on paper to develop SERS substrates.[65, 95]

#### 1.4.1.7 Inkjet Printing Approach

Another method to integrate plasmonic nanoparticles into the 3D porous architecture of paper materials is inkjet printing. A commercial inexpensive inkjet printer can be used to propel plasmonic ink onto paper substrates using refillable printing cartridges.[66] This approach was introduced by the White group as a cost-effective approach to fabricating SERS sensors in comparison to micro and nanofabrication approaches.[66, 96-104] In their first report, colloidal silver nanoparticles were used to prepare a silver ink that printed

onto paper using a low-cost inkjet printer.[66] The fabrication of silver nanoparticles paper-based SERS substrates consisted of three major steps.[66] The first step was to inkjet print hexadecenyl succinic anhydride on the paper substrate to make it hydrophobic.[66] The second step was the synthesis, purification, and concentration of the silver nanoparticles to make the silver ink.[66] The third step was to inkjet print the silver ink onto the hydrophobic papers for five cycles to increase the concentration of the nanoparticles.[66] Figure 1-5 shows silver nanoparticles inkjet printed on a filter paper, along with its scanning electron micrograph and the SERS spectrum of R6G collected from such a substrate.

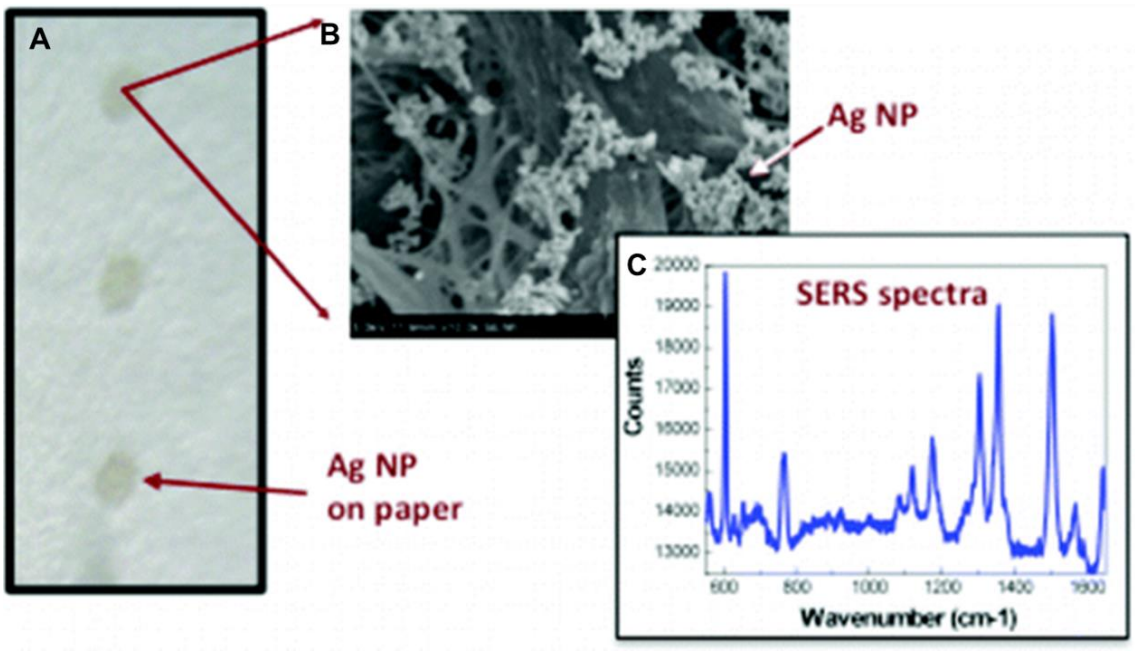


**Figure 1-5. An example of inkjet printed SERS substrate.** (A) A photo of an array of silver nanoparticles inkjet printed on a filter paper. (B) Scanning electron micrograph of a printed spot showing clusters of silver nanoparticles. (C) SERS spectrum of R6G collected from this substrate. Adapted with permission from *Analytical Chemistry* 2010, *82* (23), 9626-9630.[66]

Other groups have merged the inkjet printing and in-situ synthesis approaches to pattern plasmonic nanoparticles on paper.[105-106] For example, Liao et al. developed disposable paper-based SERS substrates without any chemical treatment on the paper by inkjet printing lecithin and potassium iodide first on an A4 paper.[105] Then, gold nanoparticles were formed by immersing the paper in the $HAuCl_4$ solution.[105] Another report used "a print–expose–develop process" where silver and halide solutions were inkjet printed onto paper first.[106] Networks of silver nanowires were formed afterward by light exposure and immersing the paper into a standard photographic developer solution.[106]

#### 1.4.1.8 Screen Printing Approach

In this approach, the plasmonic ink is squeezed through a woven mesh with various image areas by applying force using a screen-printing machine.[67] This results in having screen printed features on the substates under the woven mesh.[67] The screen printing approach can increase the number of nanoparticles attached to the porous membranes compared to the inkjet printing approach.[58] Long's group has developed disposable SERS substrates based on screen printing of arrays of plasmonic nanoparticles. In one report, silver nanoparticles were used to prepare silver ink after concentration and mixing with carboxymethylcellulose (CMC) as a viscosity-enhancing agent.[67] Fibre glass plates were used as a scaffold over filter papers and glass in this report, as they showed a higher SERS performance. The authors reproducibly demonstrated a large batch production of SERS substrates by screen printing arrays of silver nanoparticles on fibre glass plates.[67]

In another report, the same group has merged the screen-printing approach and microfluidics to develop SERS substrates.[107] The authors deposited bimetallic (gold and silver) plasmonic nanoparticles by screen printing silver and gold ink in successive steps on a cellulose paper.[107] The sensor had two areas in the shape of a dumbbell connected with a microfluidic channel made of insulating ink.[107] The first zone was for sample introduction, where it can be filtered by the capillary action of the paper to the second zone, while the second zone was the SERS sensing zone.[107] No external pumps were required for that sensor because of the capillary action of the paper.[107] Kim et al. used the screen printing approach to deposit gold nanoparticles on filter paper.[108] They used citrate capped gold nanoparticles mixed with CMC as the plasmonic ink.[108] The group optimized the SERS performance, based on the size of gold nanoparticles, the CMC concentration, the volume ratio of CMC solution and gold nanoparticles, and the number of the printing cycles.[108]

#### 1.4.1.9 Spraying Approach

In this approach, plasmonic nanoparticles, in the form of an ink similar to the one used in the inkjet printing approach, can be sprayed over membranous platforms to develop SERS substrates using spraying bottles or airbrush devices.[68, 109] For example, Li et al. have sprayed silver nanoparticles from a spraying bottle on a microfluidic paper-based device in order to fabricate paper-SERS substrates.[68] The authors have optimized the SERS substrate, based on the number of sprayed cycles needed and the type of paper to be used.[68] The authors reported a cost of US$ 20 for 1000 substrates. [68] In another report, Bolz and co-workers have employed an airbrush spray setup to deposit silver

nanoparticles on porous platforms to develop a paper-based SERS substrate.[109] The authors have optimized their SERS substrates based on the type of paper and the deposition technique of silver nanoparticles.[109] The spraying approach was similar to the inkjet printing approach, where the nanoparticles have to be synthesized first, purified, and concentrated before their deposition onto the paper substrates.

#### 1.4.1.10 Filtration Approach

Filtration is another simple approach to incorporate plasmonic nanostructures into porous membranes to develop SERS substrates.[69, 110] For example, Yu and White have demonstrated a simple approach to develop flexible SERS substrates, based on syringe filtration.[69] In their approach, previously synthesized and salt-aggregated silver nanoparticles were entrapped into nylon and PVDF filters.[69] The SERS performance of the substrates was optimized, based on the volume of aggregated nanoparticles to be incorporated into the filter and the volume of the sample to be used.[69] In another similar report, Gao et al. have developed SERS substrates, based on filtering previously salt-aggregated silver nanoparticles through PVDF membranes.[110] The authors optimized the SERS performance, based on the volume of aggregated nanoparticles to be filtered through the membrane and applied it to detect antibiotics.[110]

### 1.4.2 In-Solution SERS Substrates

The advancement in synthesis and characterization of plasmonic nanoparticles, especially silver and gold, has provided a simple and inexpensive route in SERS as SERS substrates. These nanoparticles can be prepared in large volumes without the need for

sophisticated lab equipment. The in-solution SERS substrates field is dominated by the use of silver and gold spherical nanoparticles, with many examples.[111-116] These nanoparticles are synthesized usually by reducing a metal precursor, such as $AgNO_3$ or $HAuCl_4$, using sodium citrate in the water, where sodium citrate works as a reducing and a capping agent at the same time.[117-118] These nanoparticles have LSPR bands ranging between 400 and 600 nm, which can be red-shifted by increasing the particle size.[119-120]

Many factors can influence the SERS performance of metallic nanoparticles, such as the type of metal, its nanoparticle size, and its shape. For example, silver nanoparticles, in general, can provide higher SERS enhancement by one to two orders of magnitude than that of gold nanoparticles with a similar size.[121] However, gold nanoparticles have a better biocompatibility than silver nanoparticles, especially when it comes to biological applications.[122] This means that the type of application may dictate which metal is to be used. Another significant factor that can have a crucial effect on the SERS behaviour of gold and silver nanoparticles is the size of these nanoparticles.[123-125] An optimal size range between about 10 to 100 nm has been suggested to be used in SERS.[126]

The shape of the nanoparticles is another significant factor that can play a crucial role in SERS platforms. A variety of different shapes of nanostructures has been synthesized, such as nanocubes,[127] nanoprisms,[128] nanobipyramids,[129] nanostars,[130-132] nanocages,[133] nanorods,[134-135] etc. These shapes offer the control and tunability of the LSPR over a broad range of wavelengths in comparison to spherical counterparts with an intense electric field at their sharp edges.[136-139] Plasmonic excitation of anisotropic nanostructures with sharp edges can have significant SERS enhancement due to the "lightning rod" effect.[136-140] For example, Tian et al. have investigated the effect of

different shapes on the SERS enhancement.[141] They studied the SERS enhancement of R6G as a Raman reporter when mixed with gold nanospheres, aggregated gold nanospheres, gold nanotriangles, and gold nanostars.[141] They have shown that the SERS performance of the nanostars was the highest, followed by the nanotriangles, then the aggregated nanospheres.[141] The authors observed a negligible SERS enhancement from the non-aggregated nanosphere.[141] They rationalized this behaviour due to the significant increase in the strength and number of local field hotspots at nanostructures with sharp edges when compared to spherical nanoparticles.[141] Chapter 4 provides a more detailed introduction about gold nanostars synthesis and their applications in SERS.

The SERS behavior of anisotropic nanoparticles is investigated mostly on dry surfaces rather than within the suspension of the nanoparticles. Extrapolation of the SERS performance of these nanostructures on planar substrates may not be the same as within their suspensions. For example, Murphy and co-workers have demonstrated that the colloidal SERS performance of gold nanorods was higher by using a laser with a wavelength red-shifted with respect to the LSPR of the gold nanorods.[142] This was the opposite of what they expected by aligning the excitation wavelength of the laser near the LSPR of gold nanorods.[142] They explained that on the basis of a competition between extinction and enhancement.[142]

Aggregation of nanoparticles is one of the ways to improve their SERS performance, which can increase the number of interstitial hot spots where molecules would be adsorbed under optimized conditions.[5, 113, 143-147] There are a lot of aggregating agents that can be used, such as $MgSO_4$, halide ions, spermine, poly-L-lysine, etc.[143]

Although aggregating of plasmonic nanoparticles is a straightforward approach to enhance SERS signals, it is challenging to control the aggregation and hence the reproducibility.[143] Many approaches were presented to control the aggregation of the nanoparticles to improve the SERS reproducibility. For example, Etchegoin and co-workers have optimized the aggregation of citrate capped silver nanoparticles using KCl.[111] They optimized the experimental conditions to reach a long-living metastable state of nanoaggregates, preventing the sedimentation of large clusters.[111] These metastable nanoaggregates showed stable and reproducible SERS signals using 3-methoxy-4-(5'-azobenzotriazolyl)phenylamine and R6G as Raman probes.[111]

Another example was presented by Tantra et al. to improve the reproducibility of colloidal SERS of aggregated silver nanoparticles using R6G as a Raman reporter.[112] The authors studied the effect of some experimental conditions, such as filtration, vortex time, and storage conditions, on the reproducibility of SERS data produced from silver nanoparticles after aggregation. They showed that increasing the vortexing time after inducing the aggregation was the most critical parameter to optimize the SERS reproducibility due to the formation of reproducible silver nanoaggregates under forced convection.[112] However, filtration, and sonication, as pretreatment conditions, and different storage conditions of silver nanoparticles had minimal effects on the SERS reproducibility in this study.[112] Recently, Van Duyne and co-workers have proposed a reproducible approach to control the aggregation of gold nanoparticles by encapsulating the aggregates by polyvinylpyrrolidone (PVP) for an in-SERS solution, as shown in Figure 1-6.[113] PVP was used to prevent further aggregation and sedimentation of the nanoparticles.[113] They applied their approach for label-free detection of five

neurotransmitters, including epinephrine, dopamine, serotonin, histamine, and norepinephrine in the nM range.[113]

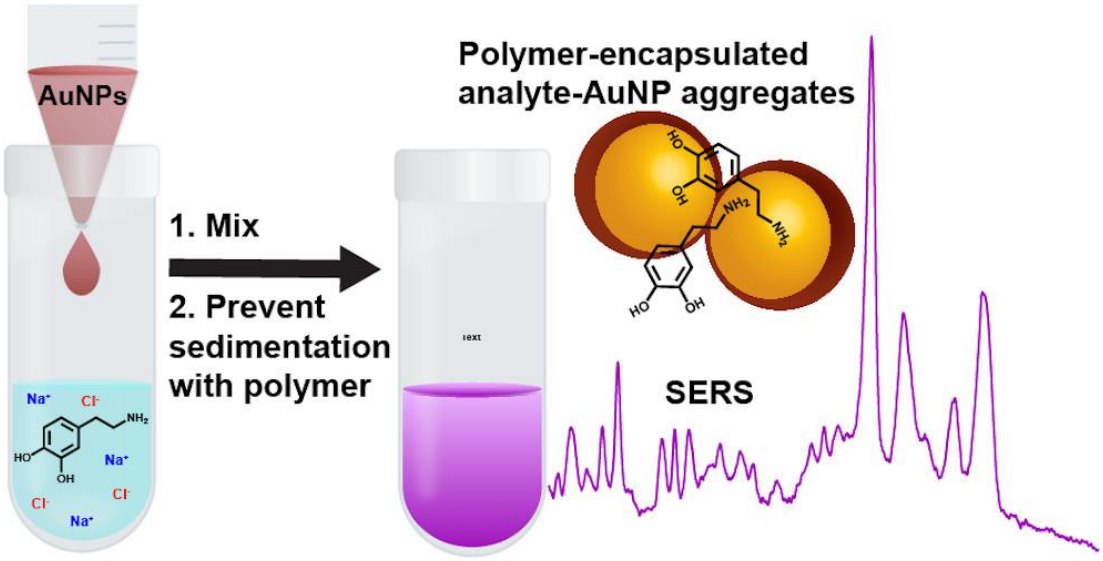


**Figure 1-6. A strategy to control plasmonic nanoparticles aggregation for in-solution SERS by PVP.** Reproduced with permission from *Analytical Chemistry* 2019, *91* (15), 9554-9562.[113]

Incorporation of metal nanoparticles into 2D scaffolds like graphene is another approach where nanoparticles can be packed closely together. Graphene–plasmonic nanocomposites can provide another approach to have metal nanoparticles in near proximity to each other, and hence many hot-spots can be generated and exploited for in-solution SERS. Chapter 5 provides a more detailed introduction about graphene–plasmonic nanocomposites to be used as a SERS substrate.

## 1.5 Current Market and Commercialization of SERS Substrates

The technological advancements in nanoscience, generally, and in Raman systems, especially, have created a market need for active SERS substrates to be commercialized for various applications. Most of these SERS substrates are sold by companies that are specialized in photonics and Raman systems manufacturing, for example, Horiba Scientific, Ocean Optics, Real-Time Analyzers, OndaVia, Enhanced Spectrometry, StellarNet, and Hamamatsu. A few companies, such as Mesophotonics (acquired by Renishaw), SERSitive, Nanova Inc., Diagnostic anSERS (acquired by Metrohm), SILMECO, and Ato ID, etc, are specialized only in fabricating SERS substrates rather than Raman spectrometers. However, the business of SERS substrates is very dynamic, where big companies may acquire small ones, which adds more complexity to find details about these substrates. In addition, information about how these substrates were fabricated is not provided by most of these companies.[54] Moreover, comparisons between these substrates are scarce in the literature.[54, 148-149] The SERS substrates market is dominated by companies that fabricate rigid SERS substrates rather than by companies that produce flexible SERS substrates. We will discuss some examples of these substrates in the following section.

The dynamic oblique vacuum evaporation technique has been used by Horiba Scientific to fabricate SERS substrates that are coated with gold nanorods.[54] The manufacturer offers two sizes, including squares of 12 and 35 $mm^2$.[54, 150] Ocean Optics offers three types of SERS substrates, based on nanostructures that are composed of gold,

silver, and gold/silver on borosilicate glass slides.[151] The substrates are circles of an active area of 15.9 $mm^2$ for Au and Ag substrates, and squares of an active area of 16 $mm^2$ for Au/Ag substrates.[151] The company's recommendation is to drop cast 10–15 μL of the sample and to use different lasers, depending on the substrate used.[151] For example, 532, 633, and 785 nm lasers are recommended for Ag, Au/Ag, and Au substrates, respectively.[151] Real-Time Analyzers has a unique set of SERS products, based on their patented sol-gel SERS substrates.[152] Their products include SERS vials, SERS microplates, SERS capillaries, and a SERS assay kit for Listeria.[152] OndaVia has merged SERS with chemical separation using microfluidics.[153] The manufacturer offers specific SERS microfluidic cartridges kits for some analytes, with detection limits ranging from ppm to ppb.[154] For example, kits are available for the detection of perchlorate, nitrate, chromium, selenium, morpholine, etc.[154] Cartridges to detect other analytes, such as boron, acrolein, glutaraldehyde, and other analytes, are under development by the company.[154]

Enhanced spectrometry offers rectangular-shaped substrates with two active circular SERS zones, with a diameter of 4 mm.[155] The plasmonic nanostructures are deposited on glass or silicon substrates.[155] Although the company has no information about the fabrication of their SERS substrates, some information can be found in an article published by Zavyalova and co-workers.[156] A thin film of silver was deposited on the silicon substrates to have silver nanoparticles with an average size of 20 nm.[156] The substrates were optimized to be used with a 532 nm laser.[156] The substrates were used in a sandwich aptasensor assay to detect the influenza virus.[156] StellarNet offers SERS strips based on gold nanoparticles on cellulose membranes, with a rectangular SERS active area of 45 $mm^2$.[157] The company recommends the use of 785 nm as the optimal

excitation laser, but 633 and 1064 nm also can be used.[157] The substrates enhancement factor is approximately up to $10^6$, depending on the analyte.[157] Pipetting, immersion, and swabbing are possible sampling techniques using these strips.[157] Hamamatsu offers disposable SERS substrates, based on gold nanostructures on polypropylene slides, with a square-shaped SERS active area of 7.29 $mm^2$.[158] The recommended wavelength of the excitation laser is 785 nm, and the recommended sample volume is 6 μL to be deposited on the SERS active area.[158] No details can be found about how these substrates are fabricated. Similarly, S.T.Japan developed SERS substrates, based on gold nanorod arrays on glass slides.[159] The recommended excitation wavelength is 785 nm, however 633 and 830 nm can be used too.[159] The company offers two chips with two different rectangular sizes of SERS active zones of 12 and 35 $mm^3$, with an approximate enhancement factor of $10^4$–$10^6$.[159]

Klarite SERS substrates originally have been developed by Mesophotonics, which later was acquired by Renishaw Diagnostics Limited.[54, 160] These substrates are considered one of the most characterized SERS substrates.[54] Klarite is fabricated by photolithographic etching of a silicon wafer to induce arrays of square pyramidal pits on the silicon surface, followed by coating with a rough gold layer.[161-162] The SERS performance of Klarite can be controlled by the dimensions of these pits.[162] There are many examples of work where Klarite is used as an active SERS substrate, such as label-free detection of bacteria,[163] determination of explosives,[148] as a standard to evaluate the performance of other SERS substrates,[148, 164-165] etc. Klarite also was used as a plasmonic substrate in methods other than SERS, such as fluorescence lifetime and

cathodoluminescence measurements, to evaluate the radiative emission rates of fluorophores.[166]

SERSitive is another company that is specialized in fabricating SERS substrates, based on electrodeposition of silver and gold nanoparticles on indium tin oxide and fluorine-doped glass.[149, 167-169] The SERS active area is a rectangular shape, with an area of 20 $mm^2$.[169] The company recommends using a 785 nm laser, but other wavelengths can also be used, such as 532 and 633 nm.[169] Immersion and drop deposition sampling techniques are recommended by the manufacturer.[169] These substrates have been used to detect and identify pathogens and to evaluate the SERS performance of other SERS substrates.[149, 167-168]

Nanova Inc. has developed SERS substrates, Q-SERS, based on gold nanoparticles with an average diameter of 40–60 nm on silicon substrates.[170-171] The SERS active area is a square of 25 $mm^2$ attached to a regular glass slide.[170] The company developed two types of substrates to be used in various applications, one with a hydrophilic surface and the other one with a hydrophobic surface.[170] Lai et al. compared the SERS performance of Klarite and Q-SERS substrates using chloramphenicol and crystal violet.[171] Although Q-SERS substrates were superior to Klarite using crystal violet, Klarite showed superior performance when chloramphenicol was used.[171] Q-SERS substrates were used to determine three pesticides, including azinphosmethyl, carbaryl, and phosmet, in apples and tomatoes with ppm levels of detection.[172] Q-SERS also was used for the detection of malachite green, leucomalachite green, and furazolidone in fish products.[173-174] P-SERS substrates originally were developed by Diagnostic anSERS Inc., which was acquired by Metrohm Raman afterwards.[175] These substrates are fabricated by the inkjet printing

approach that developed by the White group to provide flexible inexpensive SERS substrates, as previously discussed in this chapter.

SILMECO developed, SERStrate, a SERS substrate, based on metal over silicon nanopillars.[17] Reactive ion etching of silicon is used to fabricate these substrates, which is followed by gold or silver deposition using sputtering or electron beam evaporation in a maskless process.[17] These substrates have a shape of a square, with a SERS active area of 16 $mm^2$.[176-177] Like other solid substrates, sampling techniques involve immersion, vapour deposition, and drop-casting.[176-177] The recommended excitation wavelength for the silver substrates spans from 514 to 785nm, while 780–785 nm excitation is recommended only for the gold substrates.[176-177] Some examples of work where these substrates have been used are the detection of nerve gases,[178] hydrogen cyanide,[179-181] volatile organic compounds,[182] and bacterial metabolites.[183-184]

Ato ID developed SERS substrates, based on gold and silver nanostructures on soda-lime glass substrates.[185-186] An ultra-short pulse laser is used to induce nanofeatures on these substrates to be coated with silver or gold.[185-186] Immersion and liquid and vapour deposition can be used as sampling techniques.[185-186] The company recommends using these substrates within two months from their manufacturing date and store them under vacuum.[185-186] The company offers substrates with a square active SERS area of 16 $mm^2$ and other substrates with a rectangular active SERS area of 15 $mm^2$.[185-186] The recommended excitation wavelength for the silver substrates ranges from 440 nm to near-infrared, while it is from 600 nm to near-infrared for the gold substrates.[186] The company showed that the SERS performance of their gold substrate was approximately eight times higher than that of Klarite substrates using benzenethiol

as a Raman probe.[186] However, He et al. showed that the enhancement factor of Ato ID silver substrates was comparable to substrates fabricated on filter paper, and their enhancement factor was in the range of $10^4$ using crystal violet as a Raman probe.[187] From all the above mentioned companies, only two offer flexible SERS substrates based on paper substrates. A summary of the above-mentioned companies and their substrates can be found in Table 1-2.

**Table 1- 2. Examples of SERS Substrates Companies**

| Company | Nanoparticles | Platform Type | Price per Substrate(CAD$) |
|---|---|---|---|
| Horiba Scientific[54, 150] | Gold nanorods | Rigid (glass) | Not listed |
| Ocean Optics[151] | Gold, silver, and gold-silver nanoparticles | Rigid (glass) | ≈ 17–19 |
| Real-Time Analyzers[152] | Sol-gel plasmonic nanoparticles | Rigid (capillaries, vials, and microplates) | Not listed |
| OndaVia[153] | Not listed | Rigid (microfluidic cartridges kits) | ≈ 53 |
| Enhanced spectrometry[155, 156] | Silver nanoparticles | Rigid (glass and silicon substrates) | Not listed |
| StellarNet[157] | Gold nanoparticles | Paper-based | ≈ 8 |
| Hamamatsu[158] | Gold nanostructures | Rigid (polypropylene slides) | Not listed |
| S.T.Japan[159] | Arrays of gold nanorods | Rigid (glass) | Not listed |
| Renishaw Diagnostics Limited[160] | Gold nanostructures | Rigid (silicon wafer) | Not listed |
| SERSitive[169] | Gold and silver nanostructures | Rigid (indium tin oxide and glass) | ≈ 25–44 |
| Nanova Inc.[170] | Gold nanoparticles | Rigid (silicon substrates) | ≈ 33 |
| Metrohm Raman[175] | Gold and silver nanoparticles | Paper-based | Not listed |
| SILMECO[176-177] | Gold and silver nanostructures | Rigid (silicon substrate) | ≈ 66–106 |
| Ato ID[185-186] | Gold and silver nanostructures | Rigid (glass) | ≈ 22–44 |

## 1.6 Thesis Outline

This thesis contributes to the SERS field in two major aspects. The first aspect is the development of inexpensive, flexible SERS substrates using in-situ equipment-free methods. The development of such substrates is achieved by incorporating plasmonic nanostructures of gold and silver into the 3D microporous network of PVDF membranes (Chapters 2 and 3). The second aspect is the exploration and optimization of gold nanostars and graphene–silver nanocomposite as in-suspension SERS substrates (Chapters 4 and 5).

Chapter 2 presents a seed-mediated in-situ synthetic protocol to develop SERS substrates, based on the incorporation of gold nanostructures into the 3D porous network of PVDF membranes. The synthetic approach is an equipment-free one that depends on merging a SILAR-like seeding and growth protocol together. This chapter investigates the plasmonic behaviour, SERS optimization, and potential applications of these substrates. The reproducibility of the SERS data is studied within the same substrate and from substrate-to-substrate.

Chapter 3 presents PVDF–silver nanocorals SERS substrates. The substrates are developed through a seedless in-situ equipment-free protocol based on the incorporation of silver nanostructures into the 3D porous network of PVDF membranes. A handheld Raman spectrometer is used in this chapter to study the SERS performance, reproducibility, and applications of these substrates.

Chapter 4 explores the use of gold nanostars as in-solution SERS substrates. The primary drive behind this chapter is to perform a systematic study to optimize the SERS performance of Good's buffers nanostars within their suspensions using a handheld

Raman spectrometer. The impact of using different Good's buffers and different gold-to-buffer molar ratios on the SERS performance of these nanostars are studied. Post functionalization stability and the effect of using salt to aggregate these nanostars also are investigated, with some potential applications.

Chapter 5 explores the use of graphene–silver nanocomposites as in-solution SERS substrates. The effect of increasing the silver content of these nanocomposites on the SERS performance is examined. In addition, this chapter investigates the SERS performance of these nanocomposites in dry form and within their suspensions. The interaction between dye-labelled single-strand DNA molecules with these nanocomposites are studied before and after the introduction of their complementary strands.

## 1.7 References


1. Kneipp, K.; Wang, Y.; Kneipp, H.; Perelman, L. T.; Itzkan, I.; Dasari, R. R.; Feld, M. S., Single Molecule Detection Using Surface-Enhanced Raman Scattering (SERS). *Physical Review Letters* **1997,** *78* (9), 1667-1670.

2. Nie, S.; Emory, S. R., Probing Single Molecules and Single Nanoparticles by Surface-Enhanced Raman Scattering. *Science* **1997,** *275* (5303), 1102-1106.

3. Sharaabi, Y.; Shegai, T.; Haran, G., Two-state analysis of single-molecule Raman spectra of crystal violet. *Chemical Physics* **2005,** *318* (1), 44-49.

4. Le Ru, E. C.; Meyer, M.; Etchegoin, P. G., Proof of Single-Molecule Sensitivity in Surface Enhanced Raman Scattering (SERS) by Means of a Two-Analyte Technique. *The Journal of Physical Chemistry B* **2006,** *110* (4), 1944-1948.

5. Pilot, R.; Signorini, R.; Durante, C.; Orian, L.; Bhamidipati, M.; Fabris, L., A Review on Surface-Enhanced Raman Scattering. *Biosensors (Basel)* **2019,** *9* (2), 57.

6. McCreery, R. L., Raman spectroscopy for chemical analysis. John Wiley & Sons: New York :, 2000.

7. Chen, N.; Ding, P.; Shi, Y.; Jin, T.; Su, Y.; Wang, H.; He, Y., Portable and Reliable Surface-Enhanced Raman Scattering Silicon Chip for Signal-On Detection of Trace Trinitrotoluene Explosive in Real Systems. *Analytical Chemistry* **2017,** *89* (9), 5072-5078.

8. Mojica, E.-R. E.; Zapata, J.; Vedad, J.; Desamero, R. Z. B.; Dai, Z., Analysis of Over-the-Counter Drugs Using Raman Spectroscopy. In *Raman Spectroscopy in the Undergraduate Curriculum*, American Chemical Society: 2018; Vol. 1305, pp 69-91.

9. Sarfo, D. K.; Izake, E. L.; O'Mullane, A. P.; Ayoko, G. A., Molecular recognition and detection of Pb(II) ions in water by aminobenzo-18-crown-6 immobilised onto a nanostructured SERS substrate. *Sensors and Actuators B: Chemical* **2018,** *255*, 1945-1952.

10. Saviello, D.; Di Gioia, A.; Turenne, P.-I.; Trabace, M.; Giorgi, R.; Mirabile, A.; Baglioni, P.; Iacopino, D., Handheld surface-enhanced Raman scattering identification of dye chemical composition in felt-tip pen drawings. *Journal of Raman Spectroscopy* **2019,** *50* (2), 222-231.

11. Karabeber, H.; Huang, R.; Iacono, P.; Samii, J. M.; Pitter, K.; Holland, E. C.; Kircher, M. F., Guiding Brain Tumor Resection Using Surface-Enhanced Raman Scattering Nanoparticles and a Hand-Held Raman Scanner. *ACS Nano* **2014,** *8* (10), 9755-9766.

12. Sequaris, J. M. L.; Koglin, E., Direct analysis of high-performance thin-layer chromatography spots of nucleic purine derivatives by surface-enhanced Raman scattering spectrometry. *Analytical Chemistry* **1987,** *59* (3), 525-527.

13. Carron, K. T.; Kennedy, B. J., Molecular-specific chromatographic detector using modified SERS substrates. *Analytical Chemistry* **1995,** *67* (18), 3353-3356.

14. Kennedy, B. J.; Milofsky, R.; Carron, K. T., Development of a Cascade Flow Cell for Dynamic Aqueous Phase Detection Using Modified SERS Substrates. *Analytical Chemistry* **1997,** *69* (22), 4708-4715.

15. Bailey, M. R.; Pentecost, A. M.; Selimovic, A.; Martin, R. S.; Schultz, Z. D., Sheath-Flow Microfluidic Approach for Combined Surface Enhanced Raman Scattering and Electrochemical Detection. *Analytical Chemistry* **2015,** *87* (8), 4347-4355.

16. Haynes, C. L.; Van Duyne, R. P., Nanosphere Lithography: A Versatile Nanofabrication Tool for Studies of Size-Dependent Nanoparticle Optics. *The Journal of Physical Chemistry B* **2001,** *105* (24), 5599-5611.

17. Schmidt, M. S.; Hübner, J.; Boisen, A., Large Area Fabrication of Leaning Silicon Nanopillars for Surface Enhanced Raman Spectroscopy. *Advanced Materials* **2012,** *24* (10), OP11-OP18.

18. Kahl, M.; Voges, E.; Kostrewa, S.; Viets, C.; Hill, W., Periodically structured metallic substrates for SERS. *Sensors and Actuators B: Chemical* **1998,** *51* (1), 285-291.

19. Saracut, V.; Giloan, M.; Gabor, M.; Astilean, S.; Farcau, C., Polarization-Sensitive Linear Plasmonic Nanostructures via Colloidal Lithography with Uniaxial Colloidal Arrays. *ACS Applied Materials & Interfaces* **2013,** *5* (4), 1362-1369.

20. Brolo, A. G.; Arctander, E.; Gordon, R.; Leathem, B.; Kavanagh, K. L., Nanohole-Enhanced Raman Scattering. *Nano Letters* **2004,** *4* (10), 2015-2018.

21. Shi, R.; Liu, X.; Ying, Y., Facing Challenges in Real-Life Application of Surface-Enhanced Raman Scattering: Design and Nanofabrication of Surface-Enhanced Raman Scattering Substrates for Rapid Field Test of Food Contaminants. *Journal of Agricultural and Food Chemistry* **2018,** *66* (26), 6525-6543.

22. Raman, C. V.; Krishnan, K. S., A New Type of Secondary Radiation. *Nature* **1928,** *121* (3048), 501-502.

23. Krishnan, R. S.; Shankar, R. K., Raman effect: History of the discovery. *Journal of Raman Spectroscopy* **1981,** *10* (1), 1-8.

24. American Chemical Society International Historic Chemical Landmarks. The Raman Effect. http://www.acs.org/content/acs/en/education/whatischemistry/landmarks/ramaneffect.html (accessed November 2, 2019).

25. Liang, D.; Bowers, J. E., Recent progress in lasers on silicon. *Nature Photonics* **2010,** *4* (8), 511-517.

26. Fleischmann, M.; Hendra, P. J.; McQuillan, A. J., Raman spectra of pyridine adsorbed at a silver electrode. *Chemical Physics Letters* **1974,** *26* (2), 163-166.

27. Jeanmaire, D. L.; Van Duyne, R. P., Surface raman spectroelectrochemistry: Part I. Heterocyclic, aromatic, and aliphatic amines adsorbed on the anodized silver electrode. *Journal of Electroanalytical Chemistry and Interfacial Electrochemistry* **1977,** *84* (1), 1-20.

28. Albrecht, M. G.; Creighton, J. A., Anomalously intense Raman spectra of pyridine at a silver electrode. *Journal of the American Chemical Society* **1977,** *99* (15), 5215-5217.

29. Moskovits, M., Surface roughness and the enhanced intensity of Raman scattering by molecules adsorbed on metals. *The Journal of Chemical Physics* **1978,** *69* (9), 4159-4161.

30. Moskovits, M., Surface-enhanced spectroscopy. *Reviews of Modern Physics* **1985,** *57* (3), 783-826.

31. Ding, S.-Y.; You, E.-M.; Tian, Z.-Q.; Moskovits, M., Electromagnetic theories of surface-enhanced Raman spectroscopy. *Chemical Society Reviews* **2017,** *46* (13), 4042-4076.

32. Stiles, P. L.; Dieringer, J. A.; Shah, N. C.; Duyne, R. P. V., Surface-Enhanced Raman Spectroscopy. *Annual Review of Analytical Chemistry* **2008,** *1* (1), 601-626.

33. Goodacre, R.; Graham, D.; Faulds, K., Recent developments in quantitative SERS: Moving towards absolute quantification. *TrAC Trends in Analytical Chemistry* **2018,** *102*, 359-368.

34. Schlücker, S., Surface-Enhanced Raman Spectroscopy: Concepts and Chemical Applications. *Angewandte Chemie International Edition* **2014,** *53* (19), 4756-4795.

35. McFarland, A. D.; Young, M. A.; Dieringer, J. A.; Van Duyne, R. P., Wavelength-Scanned Surface-Enhanced Raman Excitation Spectroscopy. *The Journal of Physical Chemistry B* **2005,** *109* (22), 11279-11285.

36. Kennedy, B. J.; Spaeth, S.; Dickey, M.; Carron, K. T., Determination of the Distance Dependence and Experimental Effects for Modified SERS Substrates Based on Self-Assembled Monolayers Formed Using Alkanethiols. *The Journal of Physical Chemistry B* **1999,** *103* (18), 3640-3646.

37. Otto, A., Surface-enhanced Raman scattering of adsorbates. *Journal of Raman Spectroscopy* **1991,** *22* (12), 743-752.

38. Otto, A.; Mrozek, I.; Grabhorn, H.; Akemann, W., Surface-enhanced Raman scattering. *Journal of Physics: Condensed Matter* **1992,** *4* (5), 1143-1212.

39. McCreery, R. L., Raman Spectroscopy of Surfaces. In *Raman Spectroscopy for Chemical Analysis*, WINEFORDNER, J. D., Ed. Wiely: 2000; pp 373-413.

40. LeRu, E. C.; Etchegoin, P. G., *Principles of Surface-Enhanced Raman Spectroscopy: And Related Plasmonic Effects*. 2009; p 1-663.

41. Otto, A., The 'chemical' (electronic) contribution to surface-enhanced Raman scattering. *Journal of Raman Spectroscopy* **2005,** *36* (6-7), 497-509.

42. Kambhampati, P.; Child, C. M.; Foster, M. C.; Campion, A., On the chemical mechanism of surface enhanced Raman scattering: Experiment and theory. *The Journal of Chemical Physics* **1998,** *108* (12), 5013-5026.

43. Lombardi, J. R.; Birke, R. L., A Unified Approach to Surface-Enhanced Raman Spectroscopy. *The Journal of Physical Chemistry C* **2008,** *112* (14), 5605-5617.

44. Morton, S. M.; Ewusi-Annan, E.; Jensen, L., Controlling the non-resonant chemical mechanism of SERS using a molecular photoswitch. *Physical Chemistry Chemical Physics* **2009,** *11* (34), 7424-7429.

45. Valley, N.; Greeneltch, N.; Van Duyne, R. P.; Schatz, G. C., A Look at the Origin and Magnitude of the Chemical Contribution to the Enhancement Mechanism of Surface-Enhanced Raman Spectroscopy (SERS): Theory and Experiment. *The Journal of Physical Chemistry Letters* **2013,** *4* (16), 2599-2604.

46. Brolo, A. G.; Irish, D. E.; Smith, B. D., Applications of surface enhanced Raman scattering to the study of metal-adsorbate interactions. *Journal of Molecular Structure* **1997,** *405* (1), 29-44.

47. Zhao; Jensen, L.; Schatz, G. C., Pyridine–Ag20 Cluster: A Model System for Studying Surface-Enhanced Raman Scattering. *Journal of the American Chemical Society* **2006,** *128* (9), 2911-2919.

48. Jensen, L.; Zhao, L. L.; Schatz, G. C., Size-Dependence of the Enhanced Raman Scattering of Pyridine Adsorbed on Agn (n = 2–8, 20) Clusters. *The Journal of Physical Chemistry C* **2007,** *111* (12), 4756-4764.

49. Morton, S. M.; Silverstein, D. W.; Jensen, L., Theoretical Studies of Plasmonics using Electronic Structure Methods. *Chemical Reviews* **2011,** *111* (6), 3962-3994.

50. Srnová-Šloufová, I.; Vlčková, B.; Snoeck, T. L.; Stufkens, D. J.; Matějka, P., Surface-Enhanced Raman Scattering and Surface-Enhanced Resonance Raman Scattering Excitation Profiles of Ag-2,2‘-Bipyridine Surface Complexes and of [Ru(bpy)3]2+ on Ag Colloidal Surfaces: Manifestations of the Charge-Transfer Resonance Contributions to the Overall Surface Enhancement of Raman Scattering. *Inorganic Chemistry* **2000,** *39* (16), 3551-3559.

51. Xia, L.; Chen, M.; Zhao, X.; Zhang, Z.; Xia, J.; Xu, H.; Sun, M., Visualized method of chemical enhancement mechanism on SERS and TERS. *Journal of Raman Spectroscopy* **2014,** *45* (7), 533-540.

52. Natan, M. J., Concluding Remarks Surface enhanced Raman scattering. *Faraday Discussions* **2006,** *132* (0), 321-328.

53. Lin, X.-M.; Cui, Y.; Xu, Y.-H.; Ren, B.; Tian, Z.-Q., Surface-enhanced Raman spectroscopy: substrate-related issues. *Analytical and Bioanalytical Chemistry* **2009,** *394* (7), 1729-1745.

54. Mosier-Boss, P. A., Review of SERS Substrates for Chemical Sensing. *Nanomaterials* **2017,** *7* (6), 142.

55. Fan, M.; Andrade, G. F. S.; Brolo, A. G., A review on the fabrication of substrates for surface enhanced Raman spectroscopy and their applications in analytical chemistry. *Analytica Chimica Acta* **2011,** *693* (1), 7-25.

56. Langer, J.; Jimenez de Aberasturi, D.; Aizpurua, J.; Alvarez-Puebla, R. A.; Auguié, B.; Baumberg, J. J.; Bazan, G. C.; Bell, S. E. J.; Boisen, A.; Brolo, A. G.; Choo, J.; Cialla-May, D.; Deckert, V.; Fabris, L.; Faulds, K.; García de Abajo, F. J.; Goodacre, R.; Graham, D.; Haes, A. J.; Haynes, C. L.; Huck, C.; Itoh, T.; Käll, M.; Kneipp, J.; Kotov, N. A.; Kuang, H.; Le Ru, E. C.; Lee, H. K.; Li, J.-F.; Ling, X. Y.; Maier, S. A.; Mayerhöfer, T.; Moskovits, M.; Murakoshi, K.; Nam, J.-M.; Nie, S.; Ozaki, Y.; Pastoriza-Santos, I.; Perez-Juste, J.; Popp, J.; Pucci, A.; Reich, S.; Ren, B.; Schatz, G. C.; Shegai, T.; Schlücker, S.; Tay, L.-L.; Thomas, K. G.; Tian, Z.-Q.; Van Duyne, R. P.; Vo-

Dinh, T.; Wang, Y.; Willets, K. A.; Xu, C.; Xu, H.; Xu, Y.; Yamamoto, Y. S.; Zhao, B.; Liz-Marzán, L. M., Present and Future of Surface-Enhanced Raman Scattering. *ACS Nano* **2020,** *14* (1), 28-117.

57. Prikhozhdenko, E. S.; Bratashov, D. N.; Gorin, D. A.; Yashchenok, A. M., Flexible surface-enhanced Raman scattering-active substrates based on nanofibrous membranes. *Nano Research* **2018,** *11* (9), 4468-4488.

58. Restaino, S. M.; White, I. M., A critical review of flexible and porous SERS sensors for analytical chemistry at the point-of-sample. *Analytica Chimica Acta* **2019,** *1060*, 17-29.

59. Schmucker, A. L.; Tadepalli, S.; Liu, K.-K.; Sullivan, C. J.; Singamaneni, S.; Naik, R. R., Plasmonic paper: a porous and flexible substrate enabling nanoparticle-based combinatorial chemistry. *RSC Advances* **2016,** *6* (5), 4136-4144.

60. Vo-Dinh, T.; Hiromoto, M. Y. K.; Begun, G. M.; Moody, R. L., Surface-enhanced Raman spectrometry for trace organic analysis. *Analytical Chemistry* **1984,** *56* (9), 1667-1670.

61. Vo-Dinh, T.; Uziel, M.; Morrison, A. L., Surface-Enhanced Raman Analysis of Benzo[A]Pyrene-DNA Adducts on Silver-Coated Cellulose Substrates. *Applied Spectroscopy* **1987,** *41* (4), 605-610.

62. Kim, W.; Lee, J.-C.; Shin, J.-H.; Jin, K.-H.; Park, H.-K.; Choi, S., Instrument-Free Synthesizable Fabrication of Label-Free Optical Biosensing Paper Strips for the Early Detection of Infectious Keratoconjunctivitides. *Analytical Chemistry* **2016,** *88* (10), 5531-5537.

63. Ross, M. B.; Ashley, M. J.; Schmucker, A. L.; Singamaneni, S.; Naik, R. R.; Schatz, G. C.; Mirkin, C. A., Structure–Function Relationships for Surface-Enhanced Raman Spectroscopy-Active Plasmonic Paper. *The Journal of Physical Chemistry C* **2016,** *120* (37), 20789-20797.

64. Shao, J.; Tong, L.; Tang, S.; Guo, Z.; Zhang, H.; Li, P.; Wang, H.; Du, C.; Yu, X.-F., PLLA Nanofibrous Paper-Based Plasmonic Substrate with Tailored Hydrophilicity for Focusing SERS Detection. *ACS Applied Materials & Interfaces* **2015,** *7* (9), 5391-5399.

65. Zhang, W.; Li, B.; Chen, L.; Wang, Y.; Gao, D.; Ma, X.; Wu, A., Brushing, a simple way to fabricate SERS active paper substrates. *Analytical Methods* **2014,** *6* (7), 2066-2071.

66. Yu, W. W.; White, I. M., Inkjet Printed Surface Enhanced Raman Spectroscopy Array on Cellulose Paper. *Analytical Chemistry* **2010,** *82* (23), 9626-9630.

67. Qu, L.-L.; Li, D.-W.; Xue, J.-Q.; Zhai, W.-L.; Fossey, J. S.; Long, Y.-T., Batch fabrication of disposable screen printed SERS arrays. *Lab on a Chip* **2012,** *12* (5), 876-881.

68. Li, B.; Zhang, W.; Chen, L.; Lin, B., A fast and low-cost spray method for prototyping and depositing surface-enhanced Raman scattering arrays on microfluidic paper based device. *ELECTROPHORESIS* **2013,** *34* (15), 2162-2168.

69. Yu, W. W.; White, I. M., A simple filter-based approach to surface enhanced Raman spectroscopy for trace chemical detection. *Analyst* **2012,** *137* (5), 1168-1173.

70. Berthod, A.; Laserna, J. J.; Winefordner, J. D., Analysis by surface enhanced Raman spectroscopy on silver hydrosols and silver coated filter papers. *Journal of Pharmaceutical and Biomedical Analysis* **1988,** *6* (6), 599-608.

71. Laserna, J. J.; Campiglia, A. D.; Winefordner, J. D., Surface-enhanced Raman spectrometry on a silver-coated filter paper substrate. *Analytica Chimica Acta* **1988,** *208*, 21-30.

72. Laserna, J. J.; Campiglia, A. D.; Winefordner, J. D., Mixture analysis and quantitative determination of nitrogen-containing organic molecules by surface-enhanced Raman spectrometry. *Analytical Chemistry* **1989,** *61* (15), 1697-1701.

73. Marques, P. A. A. P.; Nogueira, H. I. S.; Pinto, R. J. B.; Neto, C. P.; Trindade, T., Silver-bacterial cellulosic sponges as active SERS substrates. *Journal of Raman Spectroscopy* **2008,** *39* (4), 439-443.

74. Zhu, Y.; Li, M.; Yu, D.; Yang, L., A novel paper rag as 'D-SERS' substrate for detection of pesticide residues at various peels. *Talanta* **2014,** *128*, 117-124.

75. Li, Y.; Zhang, K.; Zhao, J.; Ji, J.; Ji, C.; Liu, B., A three-dimensional silver nanoparticles decorated plasmonic paper strip for SERS detection of low-abundance molecules. *Talanta* **2016,** *147*, 493-500.

76. Kim, W.; Kim, Y.-H.; Park, H.-K.; Choi, S., Facile Fabrication of a Silver Nanoparticle Immersed, Surface-Enhanced Raman Scattering Imposed Paper Platform through Successive Ionic Layer Absorption and Reaction for On-Site Bioassays. *ACS Applied Materials & Interfaces* **2015,** *7* (50), 27910-27917.

77. Kim, W.; Lee, J.-C.; Lee, G.-J.; Park, H.-K.; Lee, A.; Choi, S., Low-Cost Label-Free Biosensing Bimetallic Cellulose Strip with SILAR-Synthesized Silver Core–Gold Shell Nanoparticle Structures. *Analytical Chemistry* **2017,** *89* (12), 6448-6454.

78. Lee, J.-C.; Kim, W.; Park, H.-K.; Choi, S., Controlling successive ionic layer absorption and reaction cycles to optimize silver nanoparticle-induced localized surface plasmon resonance effects on the paper strip. *Spectrochimica Acta Part A: Molecular and Biomolecular Spectroscopy* **2017,** *174*, 37-43.

79. Lee, C. H.; Tian, L.; Singamaneni, S., Paper-Based SERS Swab for Rapid Trace Detection on Real-World Surfaces. *ACS Applied Materials & Interfaces* **2010,** *2* (12), 3429-3435.

80. Lee, C. H.; Hankus, M. E.; Tian, L.; Pellegrino, P. M.; Singamaneni, S., Highly Sensitive Surface Enhanced Raman Scattering Substrates Based on Filter Paper Loaded with Plasmonic Nanostructures. *Analytical Chemistry* **2011,** *83* (23), 8953-8958.

81. Abbas, A.; Brimer, A.; Slocik, J. M.; Tian, L.; Naik, R. R.; Singamaneni, S., Multifunctional Analytical Platform on a Paper Strip: Separation, Preconcentration, and Subattomolar Detection. *Analytical Chemistry* **2013,** *85* (8), 3977-3983.

82. Mehn, D.; Morasso, C.; Vanna, R.; Bedoni, M.; Prosperi, D.; Gramatica, F., Immobilised gold nanostars in a paper-based test system for surface-enhanced Raman spectroscopy. *Vibrational Spectroscopy* **2013,** *68*, 45-50.

83. Ngo, Y. H.; Li, D.; Simon, G. P.; Garnier, G., Gold Nanoparticle–Paper as a Three-Dimensional Surface Enhanced Raman Scattering Substrate. *Langmuir* **2012,** *28* (23), 8782-8790.

84. Ashley, M. J.; Bourgeois, M. R.; Murthy, R. R.; Laramy, C. R.; Ross, M. B.; Naik, R. R.; Schatz, G. C.; Mirkin, C. A., Shape and Size Control of Substrate-Grown Gold Nanoparticles for Surface-Enhanced Raman Spectroscopy Detection of Chemical Analytes. *The Journal of Physical Chemistry C* **2018,** *122* (4), 2307-2314.

85. Hasi, W.-L.-J.; Lin, X.; Lou, X.-T.; Lin, S.; Yang, F.; Lin, D.-Y.; Lu, Z.-W., Chloride ion-assisted self-assembly of silver nanoparticles on filter paper as SERS substrate. *Applied Physics A* **2015,** *118* (3), 799-807.

86. Huang, Z.; Cao, G.; Sun, Y.; Du, S.; Li, Y.; Feng, S.; Lin, J.; Lei, J., Evaluation and Optimization of Paper-Based SERS Substrate for Potential Label-Free Raman Analysis of Seminal Plasma. *Journal of Nanomaterials* **2017,** *2017*, 8.

87. Kong, X.-M.; Reza, M.; Ma, Y.-B.; Hinestroza, J.-P.; Ahvenniemi, E.; Vuorinen, T., Assembly of metal nanoparticles on regenerated fibers from wood sawdust and de-inked pulp: flexible substrates for surface enhanced Raman scattering (SERS) applications. *Cellulose* **2015,** *22* (6), 3645-3655.

88. Wu, D.; Fang, Y., The adsorption behavior of p-hydroxybenzoic acid on a silver-coated filter paper by surface enhanced Raman scattering. *Journal of Colloid and Interface Science* **2003,** *265* (2), 234-238.

89. Luo, Z.; Fang, Y., SERS of C60/C70 on gold-coated filter paper or filter film influenced by the gold thickness. *Journal of Colloid and Interface Science* **2005,** *283* (2), 459-463.

90. Niu, Z.; Fang, Y., Surface-enhanced Raman scattering of single-walled carbon nanotubes on silver-coated and gold-coated filter paper. *Journal of Colloid and Interface Science* **2006,** *303* (1), 224-228.

91. Chamuah, N.; Hazarika, A.; Hatiboruah, D.; Nath, P., SERS on paper: an extremely low cost technique to measure Raman signal. *Journal of Physics D: Applied Physics* **2017,** *50* (48), 485601.

92. Chen, Y.; Cheng, H.; Tram, K.; Zhang, S.; Zhao, Y.; Han, L.; Chen, Z.; Huan, S., A paper-based surface-enhanced resonance Raman spectroscopic (SERRS) immunoassay using magnetic separation and enzyme-catalyzed reaction. *Analyst* **2013,** *138* (9), 2624-2631.

93. Polavarapu, L.; Porta, A. L.; Novikov, S. M.; Coronado-Puchau, M.; Liz-Marzán, L. M., Pen-on-Paper Approach Toward the Design of Universal Surface Enhanced Raman Scattering Substrates. *Small* **2014,** *10* (15), 3065-3071.

94. Tian, L.; Tadepalli, S.; Farrell, M. E.; Liu, K.-K.; Gandra, N.; Pellegrino, P. M.; Singamaneni, S., Multiplexed charge-selective surface enhanced Raman scattering based on plasmonic calligraphy. *Journal of Materials Chemistry C* **2014,** *2* (27), 5438-5446.

95. Hassanain, W. A.; Izake, E. L.; Schmidt, M. S.; Ayoko, G. A., Gold nanomaterials for the selective capturing and SERS diagnosis of toxins in aqueous and biological fluids. *Biosensors and Bioelectronics* **2017,** *91*, 664-672.

96. Yu, W. W.; White, I. M., Paper-based optofluidic SERS using ink-jet-printed substrates. *Proc. SPIE* **2011,** *7911* (Plasmonics in Biology and Medicine VIII), 791105/1-791105/6.

97. White, I. M., Optofluidic SERS on inkjet-fabricated paper-based substrates. *Proc. SPIE* **2012,** *8264* (Integrated Optics: Devices, Materials, and Technologies XVI), 826414/1-826414/6.

98. Hoppmann, E. P.; White, I. M., A paper-based inkjet-fabricated substrate for SERS detection and differentiation of PCR products. *Proc. SPIE* **2013,** *8718* (Advanced Environmental, Chemical, and Biological Sensing Technologies X), 871804/1-871804/6.

99. Hoppmann, E. P.; Yu, W. W.; White, I. M., Highly sensitive and flexible inkjet printed SERS sensors on paper. *Methods* **2013,** *63* (3), 219-224.

100. Yu, W. W.; White, I. M., Chromatographic separation and detection of target analytes from complex samples using inkjet printed SERS substrates. *Analyst (Cambridge, U. K.)* **2013,** *138* (13), 3679-3686.

101. Betz, J. F.; Yu, W. W.; Cheng, Y.; White, I. M.; Rubloff, G. W., Simple SERS substrates: powerful, portable, and full of potential. *Phys. Chem. Chem. Phys.* **2014,** *16* (6), 2224-2239.

102. Hoppmann, E. P.; Yu, W. W.; White, I. M., Inkjet-printed fluidic paper devices for chemical and biological analytics using surface enhanced Raman spectroscopy. *IEEE J. Sel. Top. Quantum Electron.* **2014,** *20* (3), 7300510/1-7300510/10.

103. Hoppmann, E. P.; Yu, W. W.; White, I. M., Detection of deoxyribonucleic acid (DNA) targets using polymerase chain reaction (PCR) and paper surface-enhanced Raman spectroscopy (SERS) chromatography. *Appl. Spectrosc.* **2014,** *68* (8), 909-915.

104. Berger, A. G.; Restaino, S. M.; White, I. M., Vertical-flow paper SERS system for therapeutic drug monitoring of flucytosine in serum. *Anal. Chim. Acta* **2017,** *949*, 59-66.

105. Liao, W.-J.; Roy, P. K.; Chattopadhyay, S., An ink-jet printed, surface enhanced Raman scattering paper for food screening. *RSC Advances* **2014,** *4* (76), 40487-40493.

106. Joshi, P.; Santhanam, V., Paper-based SERS active substrates on demand. *RSC Advances* **2016,** *6* (72), 68545-68552.

107. Qu, L.-L.; Song, Q.-X.; Li, Y.-T.; Peng, M.-P.; Li, D.-W.; Chen, L.-X.; Fossey, J. S.; Long, Y.-T., Fabrication of bimetallic microfluidic surface-enhanced Raman scattering sensors on paper by screen printing. *Analytica Chimica Acta* **2013,** *792*, 86-92.

108. Kim, W.-S.; Shin, J.-H.; Park, H.-K.; Choi, S., A low-cost, monometallic, surface-enhanced Raman scattering-functionalized paper platform for spot-on bioassays. *Sensors and Actuators B: Chemical* **2016,** *222*, 1112-1118.

109. Bolz, A.; Panne, U.; Rurack, K.; Buurman, M., Glass fibre paper-based test strips for sensitive SERS sensing. *Analytical Methods* **2016,** *8* (6), 1313-1318.

110. Au - Gao, S.; Au - Glasser, J.; Au - He, L., A Filter-based Surface Enhanced Raman Spectroscopic Assay for Rapid Detection of Chemical Contaminants. *JoVE* **2016,** (108), e53791.

111. Meyer, M.; Le Ru, E. C.; Etchegoin, P. G., Self-Limiting Aggregation Leads to Long-Lived Metastable Clusters in Colloidal Solutions. *The Journal of Physical Chemistry B* **2006,** *110* (12), 6040-6047.

112. Tantra, R.; Brown, R. J. C.; Milton, M. J. T., Strategy to improve the reproducibility of colloidal SERS. *Journal of Raman Spectroscopy* **2007,** *38* (11), 1469-1479.

113. Vander Ende, E.; Bourgeois, M. R.; Henry, A.-I.; Chávez, J. L.; Krabacher, R.; Schatz, G. C.; Van Duyne, R. P., Physicochemical Trapping of Neurotransmitters in Polymer-Mediated Gold Nanoparticle Aggregates for Surface-Enhanced Raman Spectroscopy. *Analytical Chemistry* **2019,** *91* (15), 9554-9562.

114. Izquierdo-Lorenzo, I.; Sanchez-Cortes, S.; Garcia-Ramos, J. V., Trace detection ofaminoglutethimide drug by surface-enhanced Raman spectroscopy: a vibrational and adsorption study on gold nanoparticles. *Analytical Methods* **2011,** *3* (7), 1540-1545.

115. Izquierdo-Lorenzo, I.; Sanchez-Cortes, S.; Garcia-Ramos, J. V., Adsorption of Beta-Adrenergic Agonists Used in Sport Doping on Metal Nanoparticles: A Detection Study Based on Surface-Enhanced Raman Scattering. *Langmuir* **2010,** *26* (18), 14663-14670.

116. Izquierdo-Lorenzo, I.; García-Ramos, J. V.; Sanchez-Cortes, S., Vibrational characterization and surface-enhanced Raman scattering detection of probenecid doping drug. *Journal of Raman Spectroscopy* **2013,** *44* (10), 1422-1427.

117. Lee, P. C.; Meisel, D., Adsorption and surface-enhanced Raman of dyes on silver and gold sols. *The Journal of Physical Chemistry* **1982,** *86* (17), 3391-3395.

118. Turkevich, J.; Stevenson, P. C.; Hillier, J., The Formation of Colloidal Gold. *The Journal of Physical Chemistry* **1953,** *57* (7), 670-673.

119. Link, S.; Wang, Z. L.; El-Sayed, M. A., Alloy Formation of Gold–Silver Nanoparticles and the Dependence of the Plasmon Absorption on Their Composition. *The Journal of Physical Chemistry B* **1999,** *103* (18), 3529-3533.

120. Evanoff, D. D.; Chumanov, G., Size-Controlled Synthesis of Nanoparticles. 2. Measurement of Extinction, Scattering, and Absorption Cross Sections. *The Journal of Physical Chemistry B* **2004,** *108* (37), 13957-13962.

121. Abalde-Cela, S.; Aldeanueva-Potel, P.; Mateo-Mateo, C.; Rodríguez-Lorenzo, L.; Alvarez-Puebla, R. A.; Liz-Marzán, L. M., Surface-enhanced Raman scattering biomedical applications of plasmonic colloidal particles. *Journal of The Royal Society Interface* **2010,** *7* (suppl_4), S435-S450.

122. Murphy, C. J.; Gole, A. M.; Stone, J. W.; Sisco, P. N.; Alkilany, A. M.; Goldsmith, E. C.; Baxter, S. C., Gold Nanoparticles in Biology: Beyond Toxicity to Cellular Imaging. *Accounts of Chemical Research* **2008,** *41* (12), 1721-1730.

123. Njoki, P. N.; Lim, I. I. S.; Mott, D.; Park, H.-Y.; Khan, B.; Mishra, S.; Sujakumar, R.; Luo, J.; Zhong, C.-J., Size Correlation of Optical and Spectroscopic Properties for Gold Nanoparticles. *The Journal of Physical Chemistry C* **2007,** *111* (40), 14664-14669.

124. Seney, C. S.; Gutzman, B. M.; Goddard, R. H., Correlation of Size and Surface-Enhanced Raman Scattering Activity of Optical and Spectroscopic Properties for Silver Nanoparticles. *The Journal of Physical Chemistry C* **2009,** *113* (1), 74-80.

125. Emory, S. R.; Haskins, W. E.; Nie, S., Direct Observation of Size-Dependent Optical Enhancement in Single Metal Nanoparticles. *Journal of the American Chemical Society* **1998,** *120* (31), 8009-8010.

126. Moskovits, M., Surface-enhanced Raman spectroscopy: a brief retrospective. *Journal of Raman Spectroscopy* **2005,** *36* (6-7), 485-496.

127. Sau, T. K.; Murphy, C. J., Room Temperature, High-Yield Synthesis of Multiple Shapes of Gold Nanoparticles in Aqueous Solution. *Journal of the American Chemical Society* **2004,** *126* (28), 8648-8649.

128. Pelaz, B.; Grazu, V.; Ibarra, A.; Magen, C.; del Pino, P.; de la Fuente, J. M., Tailoring the Synthesis and Heating Ability of Gold Nanoprisms for Bioapplications. *Langmuir* **2012,** *28* (24), 8965-8970.

129. Kou, X.; Ni, W.; Tsung, C.-K.; Chan, K.; Lin, H.-Q.; Stucky, G. D.; Wang, J., Growth of Gold Bipyramids with Improved Yield and Their Curvature-Directed Oxidation. *Small* **2007,** *3* (12), 2103-2113.

130. Ahsan, H.; Masaaki, T.; Guang, W. Y., Formation of Gold Nanoparticles by Good's Buffers. *Bulletin of the Chemical Society of Japan* **2005,** *78* (2), 262-269.

131. Xie, J.; Lee, J. Y.; Wang, D. I. C., Seedless, Surfactantless, High-Yield Synthesis of Branched Gold Nanocrystals in HEPES Buffer Solution. *Chemistry of Materials* **2007,** *19* (11), 2823-2830.

132. Nehl, C. L.; Liao, H.; Hafner, J. H., Optical Properties of Star-Shaped Gold Nanoparticles. *Nano Letters* **2006,** *6* (4), 683-688.

133. Skrabalak, S. E.; Au, L.; Li, X.; Xia, Y., Facile synthesis of Ag nanocubes and Au nanocages. *Nature Protocols* **2007,** *2*, 2182.

134. Nikoobakht, B.; El-Sayed, M. A., Preparation and Growth Mechanism of Gold Nanorods (NRs) Using Seed-Mediated Growth Method. *Chemistry of Materials* **2003,** *15* (10), 1957-1962.

135. Gole, A.; Murphy, C. J., Seed-Mediated Synthesis of Gold Nanorods: Role of the Size and Nature of the Seed. *Chemistry of Materials* **2004,** *16* (19), 3633-3640.

136. Murphy, C. J.; Gole, A. M.; Hunyadi, S. E.; Stone, J. W.; Sisco, P. N.; Alkilany, A.; Kinard, B. E.; Hankins, P., Chemical sensing and imaging with metallic nanorods. *Chemical Communications* **2008,** (5), 544-557.

137. Rycenga, M.; Langille, M. R.; Personick, M. L.; Ozel, T.; Mirkin, C. A., Chemically Isolating Hot Spots on Concave Nanocubes. *Nano Letters* **2012,** *12* (12), 6218-6222.

138. Huang, X.; Neretina, S.; El-Sayed, M. A., Gold Nanorods: From Synthesis and Properties to Biological and Biomedical Applications. *Advanced Materials* **2009,** *21* (48), 4880-4910.

139. Banholzer, M. J.; Millstone, J. E.; Qin, L.; Mirkin, C. A., Rationally designed nanostructures for surface-enhanced Raman spectroscopy. *Chemical Society Reviews* **2008,** *37* (5), 885-897.

140. Gersten, J. I., The Effect of Surface-Roughness on Surface Enhanced Raman-Scattering. *J Chem Phys* **1980,** *72* (10), 5779-5780.

141. Tian, F.; Bonnier, F.; Casey, A.; Shanahan, A. E.; Byrne, H. J., Surface enhanced Raman scattering with gold nanoparticles: effect of particle shape. *Analytical Methods* **2014,** *6* (22), 9116-9123.

142. Sivapalan, S. T.; DeVetter, B. M.; Yang, T. K.; van Dijk, T.; Schulmerich, M. V.; Carney, P. S.; Bhargava, R.; Murphy, C. J., Off-Resonance Surface-Enhanced Raman Spectroscopy from Gold Nanorod Suspensions as a Function of Aspect Ratio: Not What We Thought. *ACS Nano* **2013,** *7* (3), 2099-2105.

143. Guerrini, L.; Graham, D., Molecularly-mediated assemblies of plasmonic nanoparticles for Surface-Enhanced Raman Spectroscopy applications. *Chemical Society Reviews* **2012,** *41* (21), 7085-7107.

144. Yaffe, N. R.; Ingram, A.; Graham, D.; Blanch, E. W., A multi-component optimisation of experimental parameters for maximising SERS enhancements. *Journal of Raman Spectroscopy* **2010,** *41* (6), 618-623.

145. Bell, S. E. J.; Sirimuthu, N. M. S., Surface-Enhanced Raman Spectroscopy (SERS) for Sub-Micromolar Detection of DNA/RNA Mononucleotides. *Journal of the American Chemical Society* **2006,** *128* (49), 15580-15581.

146. Papadopoulou, E.; Bell, S. E. J., Label-Free Detection of Single-Base Mismatches in DNA by Surface-Enhanced Raman Spectroscopy. *Angewandte Chemie* **2011,** *123* (39), 9224-9227.

147. Yang, L.; Chen, Y.; Shen, Y.; Yang, M.; Li, X.; Han, X.; Jiang, X.; Zhao, B., SERS strategy based on the modified Au nanoparticles for highly sensitive detection of bisphenol A residues in milk. *Talanta* **2018,** *179*, 37-42.

148. Liszewska, M.; Bartosewicz, B.; Budner, B.; Nasiłowska, B.; Szala, M.; Weyher, J. L.; Dzięcielewski, I.; Mierczyk, Z.; Jankiewicz, B. J., Evaluation of selected SERS substrates for trace detection of explosive materials using portable Raman systems. *Vibrational Spectroscopy* **2019,** *100*, 79-85.

149. Gebavi, H.; Gašparić, V.; Risović, D.; Baran, N.; Albrycht, P. H.; Ivanda, M., Features and advantages of flexible silicon nanowires for SERS applications. *Beilstein Journal of Nanotechnology* **2019,** *10*, 725-734.

150. Horiba Scientific. SERS Substrates. https://www.horiba.com/us/en/scientific/products/raman-spectroscopy/accessories/sers-substrates/ (accessed 21 November 2019).

151. Ocean Optics. SERS Substrates. https://oceanoptics.com/product/sers/ (accessed 21 november 2019).

152. Real Time Analyzers. SERS Products. http://www.rta.biz/products/sers-products/ (accessed 21 November 2019).

153. OndaVia. The OndaVia Story. https://www.ondavia.com/about.

154. OndaVia. Analysis Kits. https://www.ondavia.com/cartridges?page=1 (accessed 4 November 2019).

155. Enhanced Spectrometry. SERS Technology. http://enspectr.com/portfolio/sers-substrates/?done=done&pf=#9da94c02fc (accessed 4 December 2019).

156. Kukushkin, V. I.; Ivanov, N. M.; Novoseltseva, A. A.; Gambaryan, A. S.; Yaminsky, I. V.; Kopylov, A. M.; Zavyalova, E. G., Highly sensitive detection of influenza virus with SERS aptasensor. *PLOS ONE* **2019,** *14* (4), e0216247.

157. StellarNet. SERS Substrate Strips. https://www.stellarnet.us/spectrometers-accessories/sers-substrates/ (accessed 25 November 2019).

158. Hamamatsu. SERS Substrate. https://www.hamamatsu.com/resources/pdf/ssd/j12853_koth1007e.pdf (accessed 25 November 2019).

159. S.T.Japan. Raman SERS Substrate. https://www.stjapan.de/en/shop/accessories-for-spectroscopy-microanalysis/raman-sers-substrate/ (accessed 1 December 2019).

160. Renishaw. EU project delivers new possibilities for SERS sensors. https://www.renishaw.com/en/eu-project-delivers-new-possibilities-for-sers-sensors--24460 (accessed 2 December 2019).

161. Perney, N. M. B.; Baumberg, J. J.; Zoorob, M. E.; Charlton, M. D. B.; Mahnkopf, S.; Netti, C. M., Tuning localized plasmons in nanostructured substrates for surface-enhanced Raman scattering. *Opt. Express* **2006,** *14* (2), 847-857.

162. McNay, G.; Eustace, D.; Smith, W. E.; Faulds, K.; Graham, D., Surface-Enhanced Raman Scattering (SERS) and Surface-Enhanced Resonance Raman Scattering (SERRS): A Review of Applications. *Applied Spectroscopy* **2011,** *65* (8), 825-837.

163. Tahir, M. A.; Zhang, X.; Cheng, H.; Xu, D.; Feng, Y.; Sui, G.; Fu, H.; Valev, V. K.; Zhang, L.; Chen, J., Klarite as a label-free SERS-based assay: a promising approach for atmospheric bioaerosol detection. *Analyst* **2020**.

164. Jin, M.; van Wolferen, H.; Wormeester, H.; van den Berg, A.; Carlen, E. T., Large-area nanogap plasmon resonator arrays for plasmonics applications. *Nanoscale* **2012,** *4* (15), 4712-4718.

165. Setti, G. O.; Mamián-López, M. B.; Pessoa, P. R.; Poppi, R. J.; Joanni, E.; Jesus, D. P., Sputtered gold-coated ITO nanowires by alternating depositions from Indium and ITO targets for application in surface-enhanced Raman scattering. *Applied Surface Science* **2015,** *347*, 17-22.

166. Xie, F.; Drozdowicz-Tomsia, K.; Goldys, E. M., A method to assess modifications of fluorophore radiative rate by plasmonic structures. *Chemical Physics Letters* **2008,** *466* (4), 186-188.

167. Witkowska, E.; Jagielski, T.; Kamińska, A.; Kowalska, A.; Hryncewicz-Gwóźdź, A.; Waluk, J., Detection and identification of human fungal pathogens using surface-enhanced Raman spectroscopy and principal component analysis. *Analytical Methods* **2016,** *8* (48), 8427-8434.

168. Witkowska, E.; Korsak, D.; Kowalska, A.; Księżopolska-Gocalska, M.; Niedziółka-Jönsson, J.; Roźniecka, E.; Michałowicz, W.; Albrycht, P.; Podrażka, M.; Hołyst, R.; Waluk, J.; Kamińska, A., Surface-enhanced Raman spectroscopy introduced into the International Standard Organization (ISO) regulations as an alternative method for detection and identification of pathogens in the food industry. *Analytical and Bioanalytical Chemistry* **2017,** *409* (6), 1555-1567.

169. SERSitive. Products. https://www.sersitive.eu/ (accessed 4 December 2019).

170. Q-SERS. http://www.q-sers.com/q.html (accessed 4 December 2019).

171. Lai, K.; Zhang, Y.; Du, R.; Zhai, F.; Rasco, B. A.; Huang, Y., Determination of chloramphenicol and crystal violet with surface enhanced Raman spectroscopy. *Sensing and Instrumentation for Food Quality and Safety* **2011,** *5* (1), 19-24.

172. Liu, B.; Zhou, P.; Liu, X.; Sun, X.; Li, H.; Lin, M., Detection of Pesticides in Fruits by Surface-Enhanced Raman Spectroscopy Coupled with Gold Nanostructures. *Food and Bioprocess Technology* **2013,** *6* (3), 710-718.

173. Zhang, Y.; Lai, K.; Zhou, J.; Wang, X.; Rasco, B. A.; Huang, Y., A novel approach to determine leucomalachite green and malachite green in fish fillets with surface-enhanced Raman spectroscopy (SERS) and multivariate analyses. *Journal of Raman Spectroscopy* **2012,** *43* (9), 1208-1213.

174. Zhang, Y.; Huang, Y.; Zhai, F.; Du, R.; Liu, Y.; Lai, K., Analyses of enrofloxacin, furazolidone and malachite green in fish products with surface-enhanced Raman spectroscopy. *Food Chemistry* **2012,** *135* (2), 845-850.

175. Metrohm. Metrohm Raman acquires Diagnostic anSERS inc. https://www.metrohm.com/en/company/news/news-raman-sers/ (accessed 4 December 2019).

176. SILMECO. SERS Substrates. https://shop.silmeco.com/?wmc-currency=USD (accessed 4 December 2019).

177. SILMECO. SILMECO SERS Substrates. http://www.silmeco.com/media/12317/silmeco-sers-substrates-serstrate-product-sheet.pdf (accessed 4 December 2019 ).

178. Hakonen, A.; Rindzevicius, T.; Schmidt, M. S.; Andersson, P. O.; Juhlin, L.; Svedendahl, M.; Boisen, A.; Käll, M., Detection of nerve gases using surface-enhanced Raman scattering substrates with high droplet adhesion. *Nanoscale* **2016,** *8* (3), 1305-1308.

179. Lauridsen, R. K.; Sommer, L. M.; Johansen, H. K.; Rindzevicius, T.; Molin, S.; Jelsbak, L.; Engelsen, S. B.; Boisen, A., SERS detection of the biomarker hydrogen cyanide from Pseudomonas aeruginosa cultures isolated from cystic fibrosis patients. *Scientific Reports* **2017,** *7* (1), 45264.

180. Lauridsen, R. K.; Skou, P. B.; Rindzevicius, T.; Wu, K.; Molin, S.; Engelsen, S. B.; Nielsen, K. G.; Johansen, H. K.; Boisen, A., SERS spectroscopy for detection of hydrogen cyanide in breath from children colonised with P. aeruginosa. *Analytical Methods* **2017,** *9* (39), 5757-5762.

181. Lauridsen, R. K.; Rindzevicius, T.; Molin, S.; Johansen, H. K.; Berg, R. W.; Alstrøm, T. S.; Almdal, K.; Larsen, F.; Schmidt, M. S.; Boisen, A., Towards quantitative SERS detection of hydrogen cyanide at ppb level for human breath analysis. *Sensing and Bio-Sensing Research* **2015,** *5*, 84-89.

182. Wong, C. L.; Dinish, U. S.; Schmidt, M. S.; Olivo, M., Non-labeling multiplex surface enhanced Raman scattering (SERS) detection of volatile organic compounds (VOCs). *Analytica Chimica Acta* **2014,** *844*, 54-60.

183. Morelli, L.; Zór, K.; Jendresen, C. B.; Rindzevicius, T.; Schmidt, M. S.; Nielsen, A. T.; Boisen, A., Surface Enhanced Raman Scattering for Quantification of p-Coumaric Acid Produced by Escherichia coli. *Analytical Chemistry* **2017,** *89* (7), 3981-3987.

184. Morelli, L.; Andreasen, S. Z.; Jendresen, C. B.; Nielsen, A. T.; Emnéus, J.; Zór, K.; Boisen, A., Quantification of a bacterial secondary metabolite by SERS combined with SLM extraction for bioprocess monitoring. *Analyst* **2017,** *142* (23), 4553-4559.

185. Ato ID. Substrates shop. http://atoid.com/shop/ (accessed 4 December 2019).

186. ATO ID. New type SERS substrates 'RandaS' and 'MatoS'. https://www.phototechnica.co.jp/wp-content/uploads/2015/02/randa-s-and-mato-s.pdf (accessed 4 December 2019).

187. He, S.; Chua, J.; Tan, E. K. M.; Kah, J. C. Y., Optimizing the SERS enhancement of a facile gold nanostar immobilized paper-based SERS substrate. *RSC Advances* **2017,** *7* (27), 16264-16272.

# Chapter 2

## In-Situ Seed Mediated Approach for Membrane Supported Gold Nanostructures for Surface Enhanced Raman Scattering Applications

## 2.1 Introduction

Surface enhanced Raman scattering (SERS) is a powerful analytical technique that can achieve single molecule detection.[1-4] Development of efficient and reproducible SERS substrates is an active ongoing research field. Most SERS substrates are fabricated using gold or silver nanostructures on rigid substrates, such as silicon or glass, via micro/nanofabrication techniques. The techniques used to fabricate such substrates include nanosphere lithography, electron beam (e-beam) lithography, oblique angle metal film evaporation, and focused ion beam (FIB) milling.[5-9] Although these methods can create uniform SERS substrates with well-defined nanopatterns and high SERS enhancement, they lack fabrication simplicity and affordability, especially in resource limited settings.[10]

Many research groups have been exploring and investigating affordable methods to fabricate SERS substrates. Integration of plasmonic nanoparticles into porous scaffolds, such as paper and paper-like materials, is one of these methods. These scaffolds can be utilized easily to develop flexible SERS substrates where metal nanoparticles are incorporated and stabilized.[11] Plasmonic nanoparticles have been incorporated into the 3D fibrous network of paper and paper-like materials using many methods. For example, White and co-workers have developed a cost-effective ink-jet printing protocol to incorporate metal nanoparticles into paper materials for fabricating SERS substrates.[12-22] Singamaneni's group used an immersion approach where filter papers were soaked for an extended period of time in the colloidal solution of nanoparticles.[23-25] The immersion approach was used also by Mirkin and co-workers to incorporate previously aggregated nanoparticles into paper.[26] In addition, Mirkin's group used the immersion approach to

attach previously synthesized nanoparticles into paper to act as seeds before growing them into anisotropic nanoparticles.[27] Other approaches to incorporate plasmonic nanomaterials into porous substrates include, but are not limited to, brushing,[28] writing with a fountain pen,[29] spraying,[30] screen printing,[31-33] and filtration.[34-35] In all these approaches, plasmonic nanoparticles were synthesized previously, concentrated, and purified before being integrated into the porous scaffolds.

Another simple route that can provide a rapid and cost-effective approach to incorporate nanoparticles into porous substrates is in-situ synthesis of the nanoparticles as presented by Choi's group.[36-40] In their approach, metal nanoparticles have been incorporated into filter paper through a successive ionic layer absorption and reaction (SILAR) technique.[36-40] The group transferred the principles of the SILAR technique from solar cells fabrication to develop SERS substrates based on filter paper. Filter papers were introduced in succession to a metal ion solution, water, reducing agent solution, and water through repeated reaction cycles. This resulted in direct formation of plasmonic nanoparticles at the reaction sites. The researchers showed how SERS enhancement can be optimized through controlling the number of SILAR cycles for different metal nanoparticles. However, their approach depended on the treatment of filter paper by wax printing to produce hydrophobic barrier areas that can help in concentrating nanoparticles in the hydrophilic regions for SERS measurements.[36-38] In addition, wax treatment was necessary to enhance the mechanical stability of the filter paper; otherwise, the material would swell and deform after many cycles of dipping in various reagents in the SILAR procedures.[36-38] Polyvinylidene fluoride (PVDF) filters are an example of porous membranes that already have been used to develop SERS substrates

by filtration without a pre-waxing step.[34-35, 41] SERS substrates based on PVDF membranes can have added benefits, especially when it comes to their mechanical and thermal stability and their chemical resistance against a wide range of chemicals.[42-45]

In this study, we are exploring the integration of gold nanostructures within the 3D porous network of PVDF membranes, combining an in-situ SILAR-like technique and a seed mediated growth protocol. A SILAR-like technique was used to produce nanoseeds, which next were grown into larger nanoparticles. Combining in-situ SILAR and growth protocols with PVDF filters provides a simple method to develop and optimize the SERS performance of these flexible substrates efficiently. We showed that these substrates can be used for detection of some analytes, such as thiabendazole (TBZ), malachite green (MG), and melamine (Mel), as examples of environmentally hazardous substances. We applied also the developed SERS substrate for methimazole (MTZ) measurements in synthetic urine. This shows a wide range of potential applications for the use of these substrates in label free SERS detection related to many fields, including agricultural, pharmaceutical, environmental, and ecological fields.

## 2.2 Experimental

### 2.2.1 Reagents

Gold (III) chloride trihydrate ($HAuCl_4$ $3H_2O$ > 99.9%), hydroxylamine hydrochloride (HH, 99.999%), hydrogen peroxide ($H_2O_2$, 30% (W/W)), 4-nitrobenzenthiol (NBT, 80%), thiabendazole (TBZ ≥ 99%), malachite green oxalate salt (MG, technical grade), melamine (Mel, 99%), Surine™ negative urine control, and methimazole analytical standard (MTZ) were obtained from Sigma-Aldrich. Polyvinylidene fluoride (PVDF)

filters with 0.45-micron pore size and 25 mm in diameter (lot: 7017006) were obtained from Sterlitech. Sodium hydroxide (NaOH) was obtained from Fisherbrand, hydrochloric acid (HCl) from Caledon, and absolute ethanol from Commercial Alcohols. NBT and MG were dissolved in ethanol, while TBZ was dissolved in 0.1 M HCl. Stock solutions of MTZ were prepared using milli-Q water and then diluted ten times using Surine solution to have a final MTZ concentration range from (0–1 mM) using the same volume of artificial urine for each concentration. Milli-Q water with a resistivity of 18.2 MΩ cm was used for all aqueous preparations, unless stated otherwise.

## 2.2.2 Instrumentation

### 2.2.2.1 Fourier transform infrared (FTIR)

FTIR spectra of the bare and modified membranes were collected by a Nicolet 8700 Continuum FTIR Microscope with 128 scans and a resolution of 4 in a transmittance mode.

### 2.2.2.2 Helium ion microscopy (HIM)

Gold nanostructures morphology and 3D network of the PVDF membrane were characterized using a Zeiss Orion Helium ion microscope operated at an acceleration voltage of 30 kV.

### 2.2.2.3 UV-vis diffuse reflectance

UV-vis diffuse reflectance spectra of the substrates were collected by a Carry 5000 UV-vis spectrometer equipped with a home built diffuse reflectance accessory. A white standard, Spectralon, was used before the measurements to adjust the 100% reflectance.

#### 2.2.2.4 Raman spectroscopy

The Raman spectra were collected with a Renishaw in-via confocal Raman microscope using a 785-nm diode laser and a 20x objective (NA = 0.4). The power and integration time are specified for each experiment. A Molectron Power Max 5100 meter was used to measure the laser power at the sample. Point by point mapping was used to map the spectral intensity of NBT for one, two, and four seeding cycles after growth over an area of 20 x 20 μm, with a 2-μm step size (121 spectra were collected), a 10-s integration time for 10 accumulations, and a power of 342 ± 1 μW. Streamline mapping was used to map the spectral intensity of TBZ (10 ppm) for three different substrates of two seeding cycles after growth (2S+G) over an area of 88.8 x 88.8 μm, with a 3.7-μm step size (625 spectra were collected), a 10-s integration time, and a power of 1.4 ± 0.1 mW at the sample. MTZ was spiked in synthetic urine to have a final concentration of MTZ in the range of 0–1 mM. Wire 3.4 software was used for data acquisition and for spectral maps imaging, while Raman spectral data analysis and background subtraction were performed using Spectragryph, an open-source software.[46]

### 2.2.3 In-Situ Seed Mediated Synthesis of Gold Nanostructures on PVDF Membranes

Gold nanostructures were synthesized on PVDF membranes in-situ by combining SILAR-like and growth mediated protocols, as summarized in Figure 2-1. A SILAR process was used to synthesize gold nanoseeds on PVDF membranes before nanostructure growth. PVDF membranes were immersed in a solution of 5 mM $HAuCl_4.3H_2O$ (0.5 mL) and $H_2O_2$ (30% (W/W)) (0.05 mL) for 1 min. We adapted the published procedures to synthesize

gold nanoseeds using $HAuCl_4$ $3H_2O$ as a gold precursor and $H_2O_2$ as a reducing agent in an alkaline medium.[47] $H_2O_2$ works as a reducing agent in an alkaline solution, while in a neutral solution, a very slow gold reduction was observed.[47] Then, the membrane was immersed in a 0.1 M NaOH solution where bubbling was observed. Then, membrane was removed with tweezer and the excess reagents were drained from the edge with a Kimwipe.

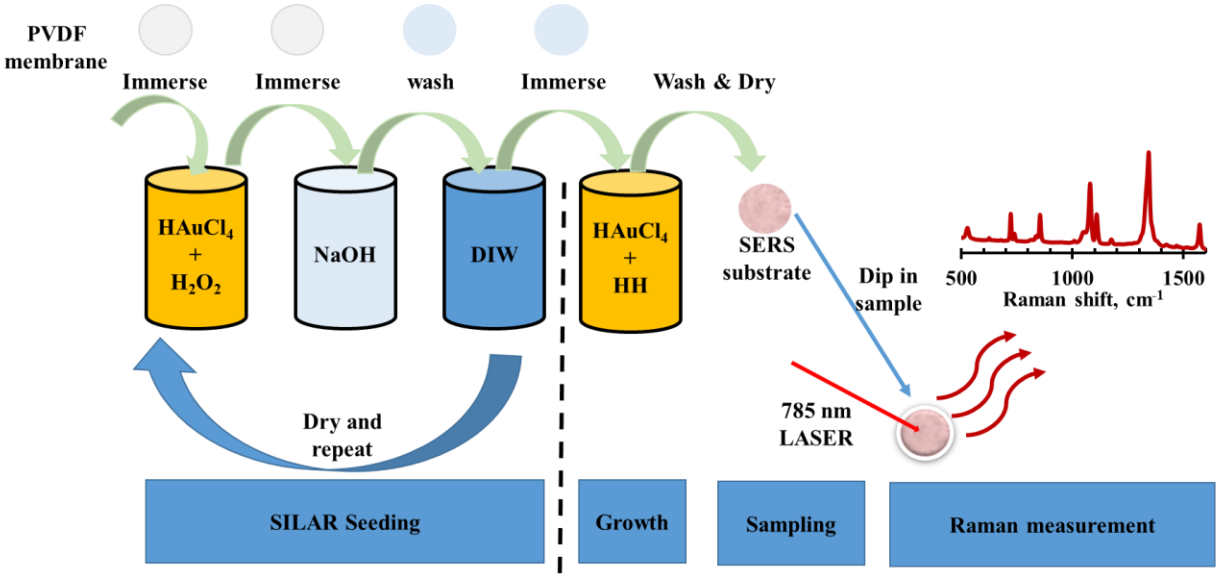


**Figure 2-1. General scheme of combining SILAR and seed mediated growth protocols to develop PVDF SERS substrates.** The first step consists of repeated cycles of SILAR to fabricate the nanoseeds, followed by the growth step then sampling and SERS measurement.

The membrane color changed from white to blue in this step, while the NaOH solution remained colorless. Next, the membrane was washed extensively with Milli-Q water and ethanol to ensure the removal of all excess reagents and was air dried before the growth step. This is considered a one seed cycle (1S), which can be repeated accordingly for multiseed cycles before the growth step (2S, 3S, etc.). Fresh solutions of gold salt and hydrogen peroxide were used for each seeding cycle. The growth step was

adapted from previously published methods where the nanoseeds are grown in $HAuCl_4.3H_2O$ solution using hydroxylamine hydrochloride (HH) as a reducing agent.[48-50] The synthesized membranes with different SILAR seeding cycles (1S, 2S, and 4S) were immersed in a mixture of 5 mM $HAuCl_4.3H_2O$ (0.5mL) and 10 mM HH (0.5mL) for 15 min, and the membrane color changed from blue to red. Then, the membranes were washed extensively with Milli-Q water and ethanol to ensure the removal of all excess reagents. Then, they were air dried and stored in a desiccator at room temperature in the dark. These membranes were denoted as 1S+G, 2S+G, and 4S+G, according to the seeding cycles used before the growth (G) step.

## 2.3 Results and Discussion

### 2.3.1 Proposed Deposition Mechanism

Although $H_2O_2$ is used frequently as an oxidizing agent, it also can function as a reducing agent for $Au^{3+}$ in a basic medium.[47] Figure 2-2 presents our proposed mechanism for the seeding and growth of nanoparticles within the 3D porous network of a PVDF membrane. The manufacturer treats the PVDF membranes in such a way as to render them more hydrophilic than native PVDF. Treatment information is not provided by the vendor, but we assume it involves plasma exposure. Oxygen plasma can impart oxygenated species on PVDF membranes[51], which may work as adsorption nucleation sites for seeding. This treatment may result in a variety of functional groups. However, infrared spectroscopy (see Figure 2-3) provides no evidence of carbonyl and hydroxyl groups. Thus, the oxygen groups are depicted as ethers in Figure 2-2.

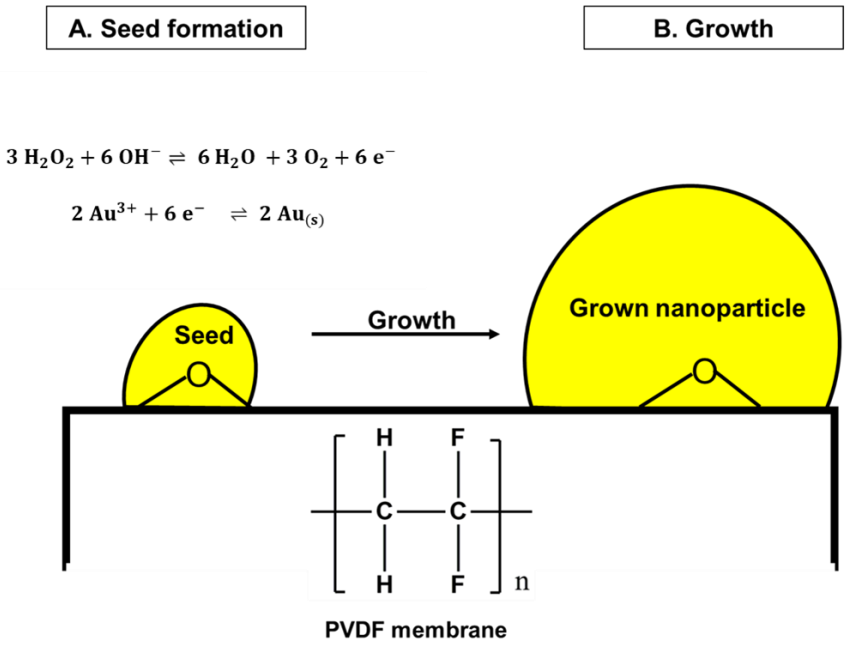


**Figure 2-2. Proposed mechanism for the incorporation of gold nanoparticles onto a PVDF membrane.**

The nanoseeds generation proceeds by the following half-reactions:

$$3\ H_2O_2 + 6\ OH^- \rightleftharpoons 6\ H_2O + 3\ O_2 + 6\ e^- \quad (1)$$

$$2\ Au^{3+} + 6\ e^- \rightleftharpoons 2\ Au_{(s)} \quad (2)$$

The standard potential for reaction 1 is about 0.6 V, which drives the reduction of $Au^{3+}$ in a basic medium, with a standard potential of +1.5 V.[47] This forms the seeds within the membrane, as shown in Figure 2-2A. Then, the seed is grown in a solution of $Au^{3+}$ using HH as a reducing agent[48-50] by electroless growth, as shown in Figure 2-2B.

## 2.3.2 Membrane Stability

Previous studies have shown that PVDF is susceptible to dehydrofluorination upon treatment with sodium hydroxide.[45, 52-53] Removal of HF can lead to changes in the PVDF polymeric structure.[53] This is indicated in the infrared spectrum by the appearance of

bands assigned to a carbon–carbon double bond stretch at 1590–1650 $cm^{-1}$, a carbonyl bond stretch at 1700–1800 $cm^{-1}$, and a carbon–carbon triple bond stretch at 2100 $cm^{-1}$.[45, 52-53] For example, Rabuni et al. reported that a 0.2 M solution of sodium hydroxide can lead to the dehydrofluorination of PVDF membranes after 30 min at 25 °C.[53] In addition, they showed that the effects were more pronounced at longer reaction times and at higher temperatures.[53]

Our procedure involves the use of sodium hydroxide for a short time (1–4 min) to develop our substrates, therefore, we investigated the impact of using a sodium hydroxide solution on the PVDF membrane chemistry by FTIR. We compared the FTIR spectrum of a blank PVDF membrane with that of our substrates after the growth step, which involves the exposure of the membrane to 0.1 M sodium hydroxide. Figure 2-3 contains the infrared spectra of these membranes, showing that the blank PVDF membrane is similar to that of membranes that have been through the seeding and growth process. All membranes showed the characteristic FTIR bands attributed to the PVDF α-phase at 763, 796, 877, and 1070 $cm^{-1}$, along with some other bands that are assigned for the PVDF β-phase at 841, 1273, and 1402 $cm^{-1}$.[45, 52-53] Importantly, we did not observe any significant differences between the FTIR spectra of the blank PVDF and our substrates at the wavenumber range of 1590–2100 $cm^{-1}$. Samples prepared with four seeding cycles and a growth step (4S+G) will have been exposed to 0.1 M NaOH for up to 4 min. This confirms that our procedure does not cause any noticeable degradation of the PVDF membranes.

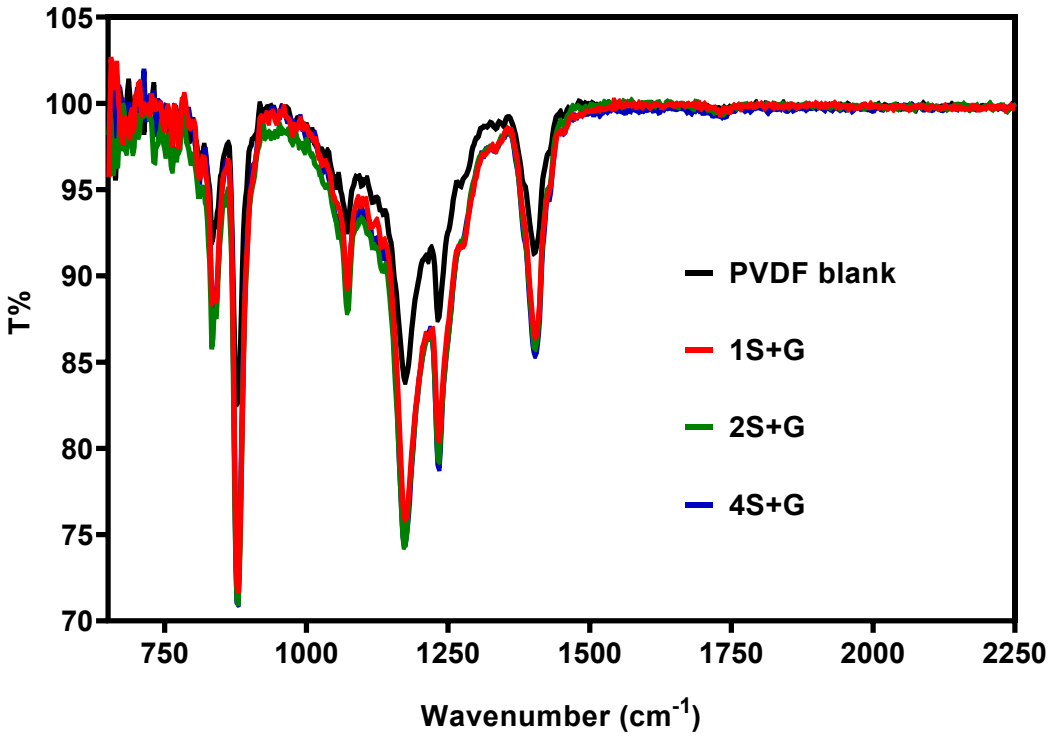


**Figure 2-3. FTIR spectra of a blank PVDF membrane and SERS substrates after the growth step.**

## 2.3.3 SERS Substrates Characterization

### 2.3.3.1 Helium ion microscopy imaging (HIM)

The SERS performance of these substrates depends greatly on the size, shape, and distribution of the gold nanostructure in the membrane. HIM was used to obtain this information. We used HIM, as it has many advantages over traditional scanning electron microscopes (SEM) and field emission scanning electron microscopes (FE-SEM). Some of these advantages include, but are not limited to, high surface contrast without metal sputtering, small probe size, reduced sample damage, long depth of field, and high resolution.[54-55] All of these advantages are preferable for imaging the gold nanostructure without causing any damage to the PVDF membrane itself.

Figure 2-4 contains HIM images of the substrates for the various seeding steps (parts A, B, and C) and the following growth step for each seeding cycle (D, E, and F). Both the seeds and the particles after growth appear quasispherical in shape. The particles were formed randomly into the 3D pores and on the polymeric network of the PVDF membrane. The average particle diameters for the seeding steps and the following growth step are listed in Table 2-1. Figure 2-4 and Table 2-1 show that particles get bigger in size and become closer to each other, as shown in Figure 2-4D, E, and F after the growth step when compared to the particles before the growth step, as shown in Figure 2-4A, B, and C. However, the diameters of the seed particles are similar regardless of the number of seeding cycles. Thus, it is reasonable to expect similarly sized particles after the growth step.

The average particle density of the substrates was estimated after the growth step using high and low magnification HIM images, shown in Figures 2-4 and 2-5. The majority of nanoparticles was attached randomly as individual particles, with the exception of the appearance of a few dimers and trimers. For example, we observed seven dimers and one trimer in Figure 2-4E for the 2S+G substrate. This formation of closely located particles in a 3D architecture is favourable for SERS enhancement.[26]

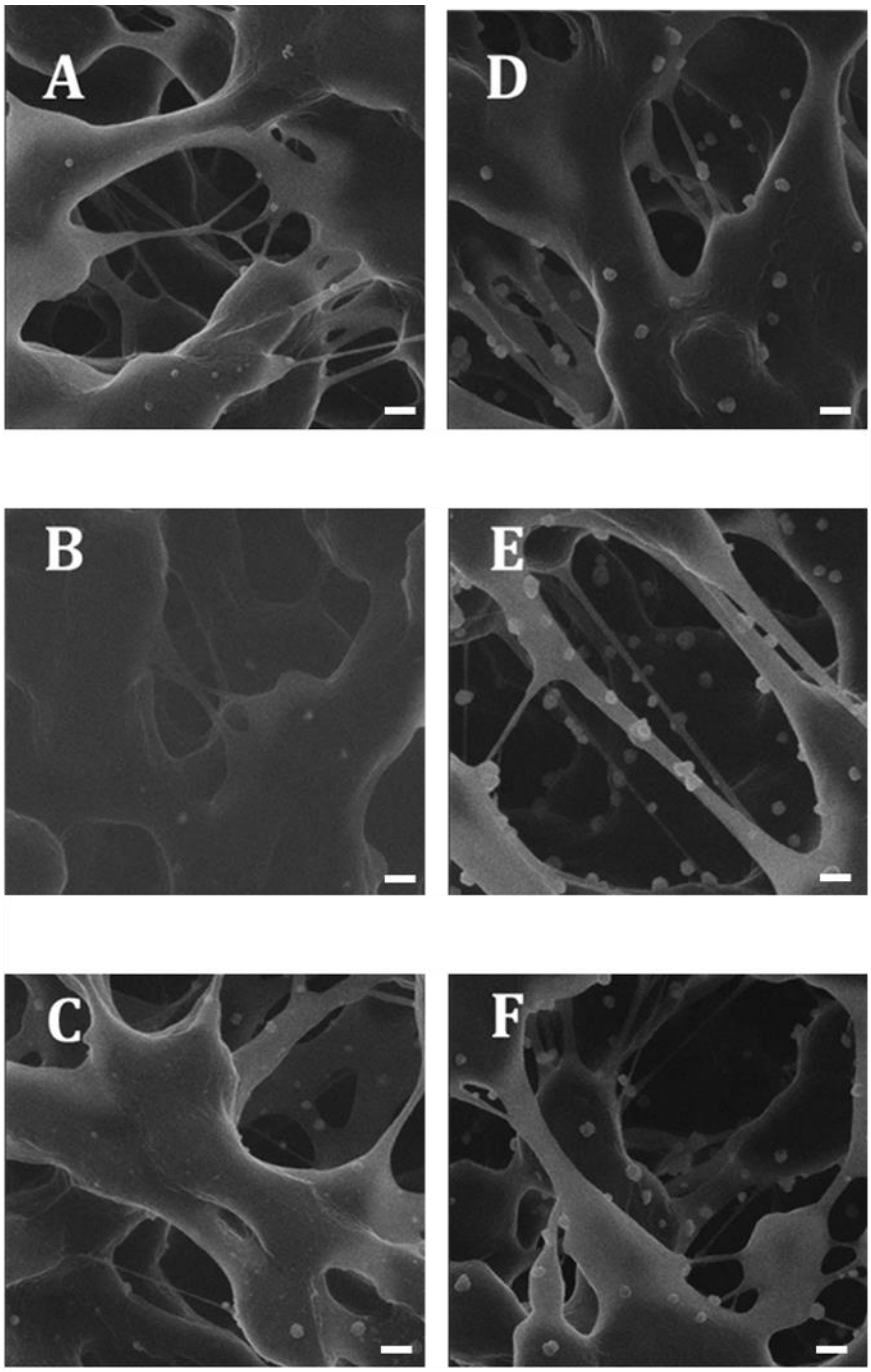


**Figure 2-4. HIM images of the substrates before and after the growth step.** (A), (B), and (C) for 1S, 2S, and 4S and (D), (E), and (F) for 1S+G, 2S+G, and 4S+G, respectively. Scale bar is 200 nm in all images.

**Table 2-1. Average Particle Diameters for Gold Nanoparticles Attached to the PVDF Membrane**

| Membranes | Average particle diameter (nm) ± S. D | Average Particle density (particle/ $\mu m^2$) ± S. D |
|---|---|---|
| 1S | 47 ± 18 | |
| 2S | 52 ± 15 | |
| 4S | 54 ± 20 | |
| 1S+G | 79 ±15 | 5 ± 3 |
| 2S+G | 86 ± 18 | 7 ± 4 |
| 4S+G | 86 ± 16 | 8 ± 3 |

Other features observed during HIM imaging are shown in the lower magnification images in Figure 2-5. Along with a high density of the smaller nanoparticles discussed in Figure 2-4, larger anisotropic gold structures also are formed. While the smaller particles can be observed on the surface and throughout the 3D fibrous network of the PVDF membrane, these larger particles are observed only on the surface. Due to their larger size, we do not believe that these structures play a role in the SERS enhancement discussed later. From Figures 2-4 and 2-5, we can conclude that the growth step has a more pronounced effect to increase particle density to be incorporated into the PVDF membrane.

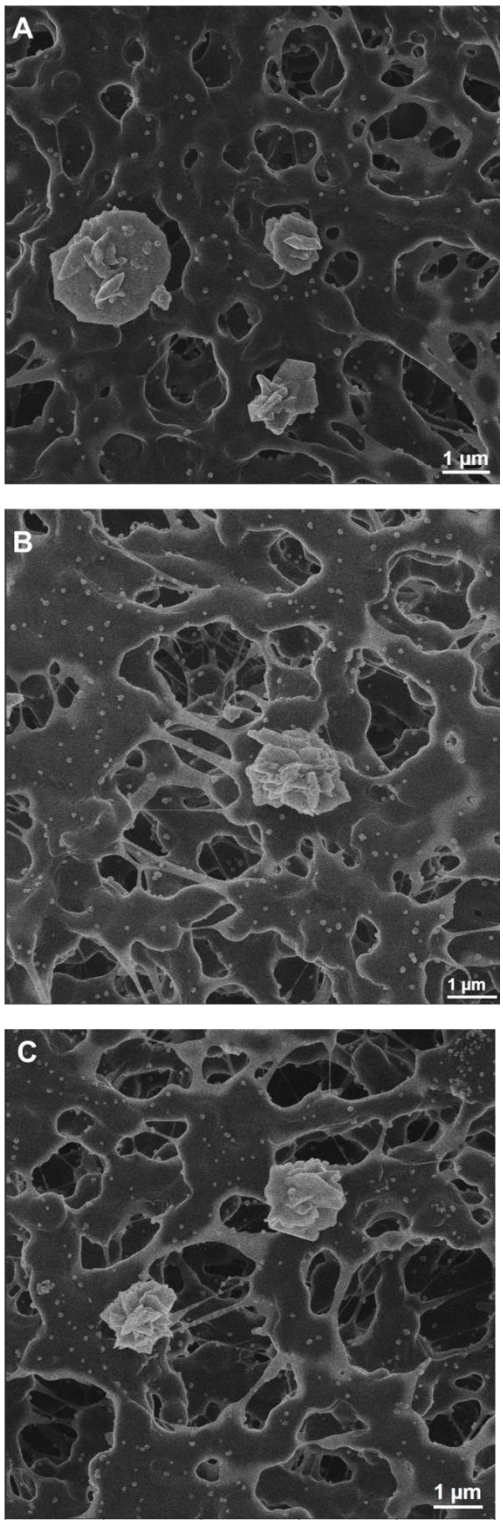


**Figure 2-5. HIM images of the substrates after the growth step.** (A), (B), and (C) of 1S+G, 2S+G, and 4S+G substrates, respectively.

#### 2.3.3.2 UV-vis diffuse reflectance spectroscopy

The enhancement of Raman bands in SERS relies on the plasmonic behavior of the metallic nanostructures. Extinction spectroscopy is one of the most used techniques to study the plasmonic behavior of colloidal metallic nanostructures, based on Mie's theory.[56-57] The wavelength, width, and intensity of the localized surface plasmon resonance (LSPR) band provide information on the size, shape, and concentration of noble metal nanoparticles on transparent substrates and in solutions.[56, 58-60] Although transmission based extinction spectroscopy is a straightforward technique, it is challenging when it comes to nanoparticles attached to opaque surfaces within porous membranes. This is evident in the literature, where most of the published papers concerning paper based plasmonic materials present no extinction spectra[12-22, 37-40] or simply the extinction spectra of the colloidal nanoparticles prior to depositing on a paper substrate.[27, 61]

UV-vis diffuse reflectance spectroscopy has been applied to opaque solids as an alternative technique to UV-vis spectroscopy.[62] This technique has been used to study solid state reactions and provide color measurements and color matching.[62] Reflectance measurements are analogues to transmittance measurements in absorption spectroscopy.[63] However, the diffuse reflectance technique has some limitations that may induce spectral artifacts.[64] These artifacts are due to mainly Fresnel reflectance, changes in scattering coefficients, and samples with high absorptivity.[64] This may lead to a blue shift in band position as an artifact.[64] These limitations were unavoidable for our substrates. One reason was because our substrates have high absorptivity because of the intrinsic LSPR of gold nanoparticles in the visible region. In addition, the size and density

of particles are changing, based on the number of seeding cycles as well as after the growth step, which will lead to changes in the scattering coefficient of the substrates. That is why we used this technique only for a qualitative description of the apparent extinction values of our substrates. For our samples, diffuse reflectance (R) values were converted to log (1/R) values[65] as a qualitative measure of the apparent extinction values. Diffuse reflectance was used to monitor the effects of seeding cycle numbers and the growth step on the plasmonic nature of our samples qualitatively.

Figure 2-6 contains the reflectance spectra (2-6A) and photographs of the substrates after seeding only (Figure 2-6B) and after seeding and growth (Figure 2-6C). As shown in Figure 2-6A, the unmodified PVDF membrane exhibits no spectral features in this region. It is observed that seeding cycles result in an increase in log (1/R) throughout the spectral region as well as an appearance of a band. This band initially is centred at 585 nm for one seeding cycle and blue shifts as a result of multiple seeding cycles. The growth step results in a narrower band at 529 nm for one and two seeding cycles. Growth after four seeding cycles produces a substrate with a significantly higher apparent extinction in the region, with a less developed band at 490 nm. The blue shift in the bands position may be attributed to a spectral artifact due to the high absorptivity of gold nanoparticles in this wavelength range.[64] This blue shift is not due to the particles getting smaller, as is shown in HIM micrographs in Figure 2-4. The increase in the apparent extinction values in this wavelength region may indicate the formation of gold nanoparticles since colloidal gold nanoparticles display an SPR band around 520 nm.[66]

The photographs in parts B and C of Figure 2-6 show the visible color change for different seeding cycles before and after the growth step. Before the growth step, the

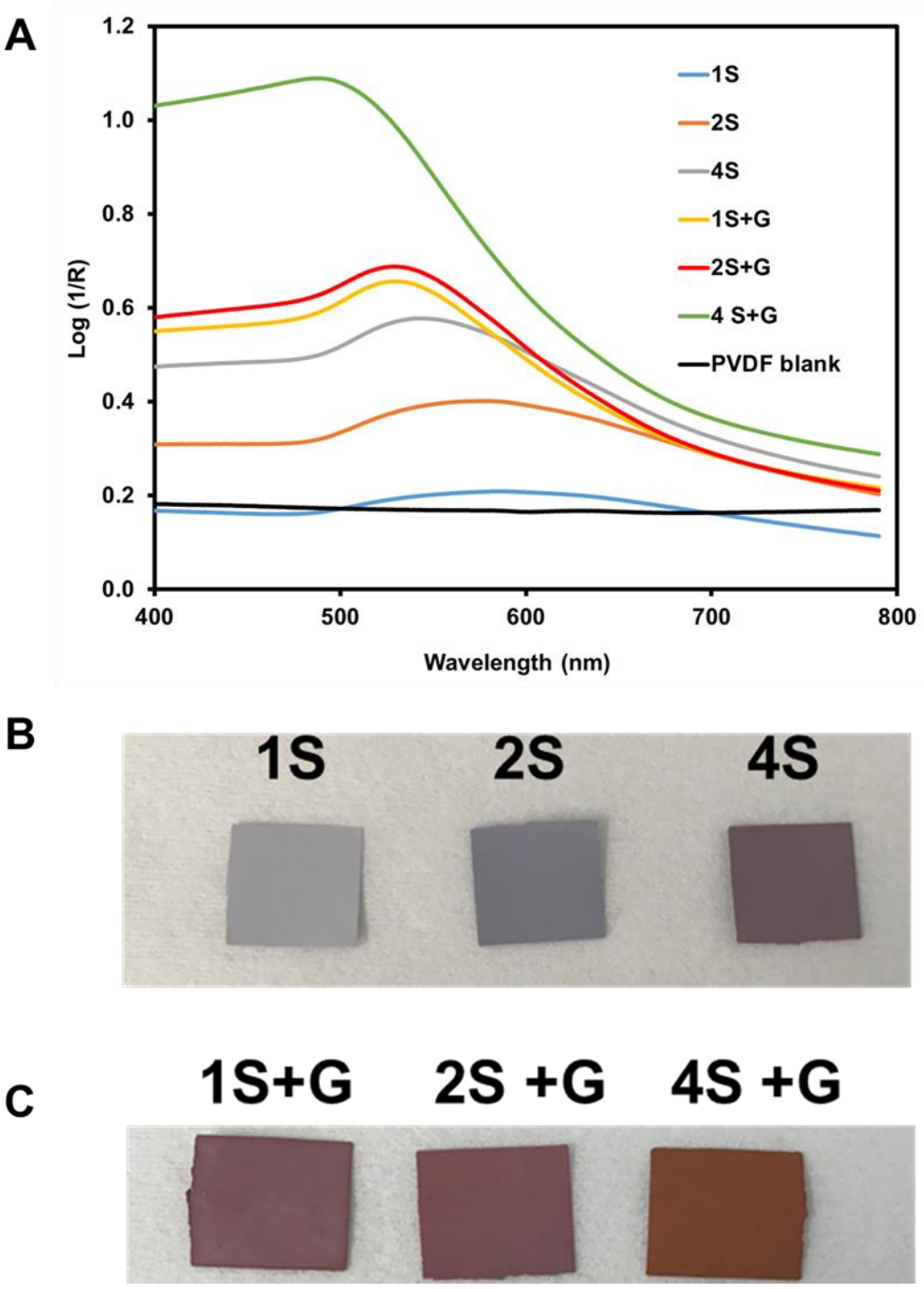


**Figure 2-6. UV-vis diffuse reflectance of the SERS substrates.** (A) UV-vis diffuse reflectance of the SERS substrates before and after growth. (B) and (C) photographs of the substrates before and after growth, respectively.

color of the substrates changed from light blue to purple by increasing the seeding cycles. However, after the growth step, the color of the substrates became red. This may be attributed to the synthesis of gold nanostructures. The red color is visually darker after the growth step by increasing the number of the seeding cycles. We can conclude that the apparent extinction of these substrates can be tuned by changing the number of seeding cycles and by the growth step.

### 2.3.4 Substrate SERS Performance Optimization

#### 2.3.4.1 Impact of the growth step on SERS performance

The benefit of a growth step following a SILAR-like seeding step can be observed easily in the Raman spectra. The seeding cycles used in this work are analogous to the SILAR process. Each seeding cycle consists of four steps of two immersions, followed by washing and drying steps. This means that 1S has four steps, 3S has 12 steps, and 5S has 20 steps. On the other hand, the growth stage has three steps involving immersion into a solution, followed by washing and drying steps. So, 1S+G has seven steps in total. The impact of the growth step after only one seeding cycle (1S+G) on SERS performance was compared to different seeding cycles (1S, 3S, 5S) without growth. Figure 2-7A presents SERS spectra of 4-NBT obtained from the various substrates. Table 2-2 shows major Raman peak assignments for 4-NBT, according to previously published papers.[67-68] The results in Figure 2-7 show that the SERS signal intensities are improved by increasing the number of SILAR-like seeding cycles.

The growth step has a much greater enhancement effect even if only one seeding cycle was used. The nitro stretch peak height at 1335 $cm^{-1}$, normalized to the highest

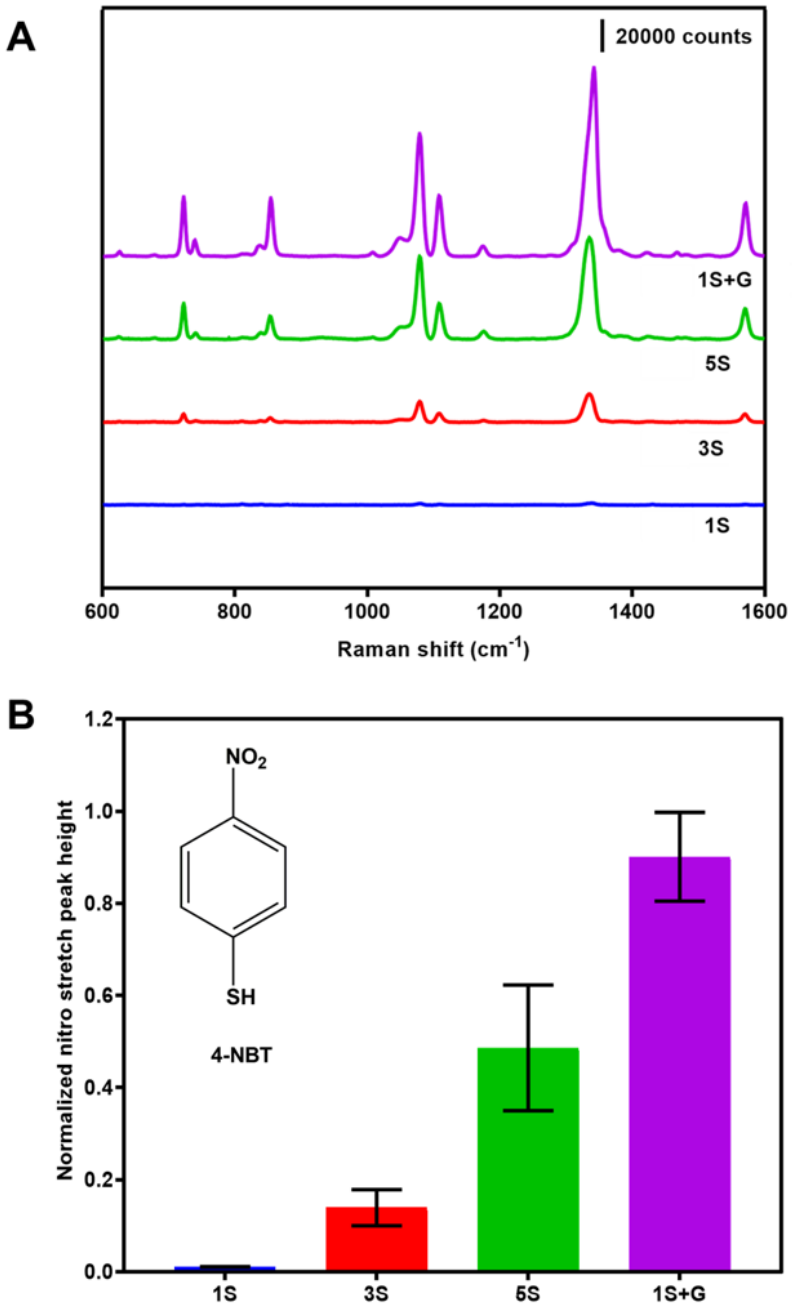


**Figure 2-7. Feasibility of the growth step.** (A) SERS spectra of 4-NBT collected from the SERS substrates prepared by a different number of seeding cycles versus a seed mediated growth approach using only one seeding cycle before growth. Spectra are stacked for more clarification. Spectra are collected and averaged from five different points from each membrane using a 785-nm laser, a 10-s integration time, and for 10 accumulations, with a 342 ± 1 μW power at the sample. (B) Bar chart of the nitro stretch peak height, normalized to the highest value at 1335 $cm^{-1}$ along with the chemical structure of 4-NBT.

**Table 2-2. Major Band Assignments Listed for the SERS Spectrum of 4-NBT on the Surface of the SERS Substrates**

| Band position ($cm^{-1}$) | Assignment [67-68] |
|---|---|
| 1571 | C=C stretch |
| 1335 | Symmetric $NO_2$ stretch |
| 1109 | C–H bending |
| 1079 | C–S stretching |
| 845 | C–H wagging |

value obtained from (1S+G), was used to compare between substrates, as shown in the bar chart of Figure 2-7B. We calculated the ratio of the nitro stretch peak height of 1S+G to the nitro stretch peak height of the other substrates with various seeding cycles. The ratio of 1S+G to 1S was 86 ± 13, while it became 7 ± 2 for 1S+G to 3S and 2 ± 0.3 for 1S+G to 5S. The chemical structure of 4-NBT is shown in Figure 2-7B as well. Figure 2-7 suggests that a seed mediated growth protocol, with only one seeding cycle followed by a growth step, has a superior SERS performance. This performance may be attributed to the plasmonic behaviour change and to the increased size and number of nanoparticles of these substrates after the growth step. The seed mediated protocol also involves fewer steps and reagents than that of the repeated seeding cycles protocol yet with better SERS performance.

#### 2.3.4.2 Number of seeding cycles needed for SERS performance optimization

The SERS performance was optimized for the number of seeding cycles before the growth step. We examined one, two, and four seeding cycles to grow the SERS substrates and used 4-NBT again as the Raman probe to ensure high coverage to the gold nanostructures. These substrates (1S+G, 2S+G, and 4S+G) were probed with point by point Raman mapping to investigate the SERS performance and homogeneity over a relatively large area of the substrates.

Figure 2-8A shows the Raman spectra (average of 121 spectra over an area of 400 $\mu m^2$) collected from each membrane. Figure 2-8B is a bar chart of the average peak area of the symmetric nitro stretch, with the percent relative standard deviation (%RSD) values shown for each substrate. Figures 2-8A and B show that these substrates have a comparable SERS performance, with the 2S+G substrate yielding the highest SERS intensity among the three substrates. In addition, we compared the %RSD values to investigate the point-to-point variability of these substrates. The %RSD values were 11%, 11%, and 8% for the 1S+G, 2S+G, and 4S+G substrates, respectively. It is recommended that SERS substrates should have less than 20% deviation.[69-70] This also supports the fact that the anisotropic microstructures do not contribute to hot spots formation, otherwise, the substrates would have had larger %RSD values. Based on Figure 2-8, we can conclude that our substrates show point-to-point homogeneity over a 400-$\mu m^2$ area in terms of their SERS performance.

Upon further investigation of the collected Raman maps of these substrates, we observed a frequency shift and change in full-width at half maximum (FWHM) of the

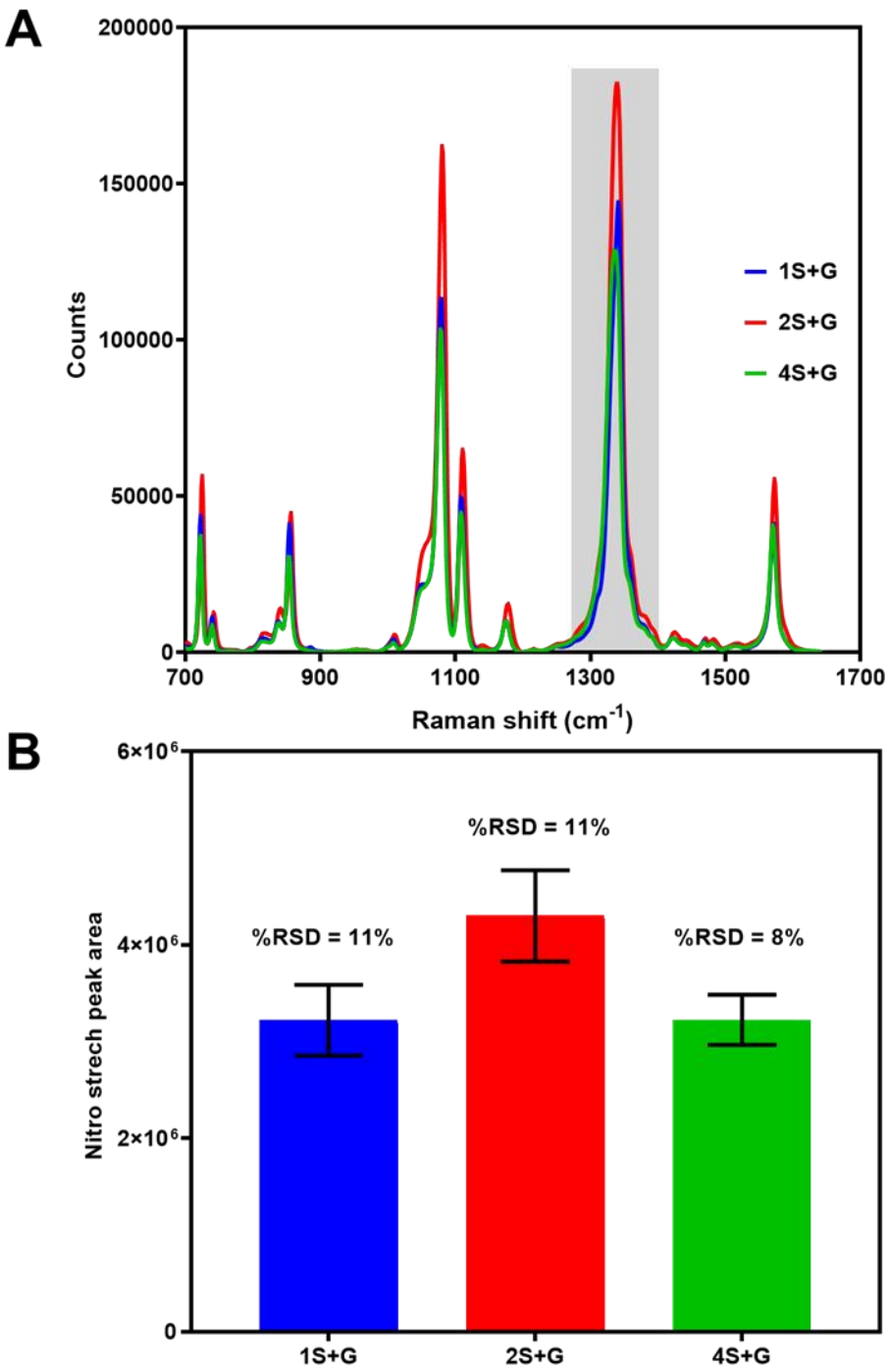


**Figure 2-8. SERS performance optimization.** (A) SERS spectra of 4-NBT (average of 121 spectra over an area of 400 μm$^2$) collected from 1S+G, 2S+G, and 4S+G substrates. (B) Bar chart of the average peak area of the symmetric nitro stretch with %RSD values of theses substrates.

symmetric nitro stretch peak. We used the nitro stretch peak position and FWHM of the substrates as a measure of spatial reproducibility. The data are summarized in Table 2-3.

**Table 2-3. Nitro Stretch Raman Peak Position and FWHM Obtained from Various Substrates**

| Membrane | Mean of nitro stretch peak position ($cm^{-1}$) ± S.D | FWHM ($cm^{-1}$) ± S.D |
|---|---|---|
| 1S+G | 1341 ± 1 | 19.7 ± 0.6 |
| 2S+G | 1337 ± 1 | 21.2 ± 0.6 |
| 4S+G | 1336 ± 1 | 22.7 ± 0.5 |

Table 2-3 shows that the band due to the symmetric nitro stretch is shifted to a lower wavenumber by increasing the number of seeding cycles. The symmetric nitro stretch peak of 2S+G was red shifted by 3.8 $cm^{-1}$ when compared to 1S+G. This red shift in frequency increased to 4.6 $cm^{-1}$ when 4S+G is compared to 1S+G. However, this red shift is not related to the reduction of the nitro group, as we did not observe any Raman bands indicative of aminothiophenol formation.[68, 71] There was also no significant difference in FWHM and peak position observed (about 0.5 $cm^{-1}$) related to ring C-C and C-S stretching modes.[68, 71]

The FWHM of the symmetric nitro stretch Raman band also increased by increasing the number of seeding cycles, by 1.49 and 3.03 $cm^{-1}$ for the 2S+G and 4S+G substrates, respectively, when compared to the 1S+G substrate. These changes also may

be related to the change in the plasmonic behavior, the increase in particle size, and the loading density of these substrates, based on diffuse reflectance data and HIM images. We assume that these may lead to more adsorption and entrapment of 4-NBT molecules onto the gold nanostructures in the 3D porous network of the PVDF membrane by increasing the number of seeding cycles. It has been suggested that the adsorption of a nitro group on gold electrodes can cause a red shift and band broadening of the symmetric nitro stretch in the SERS spectra.[72] An example of one of the collected 2D Raman maps is presented in Figure 2-9 for the 2S+G substrate. We can conclude that the red shift and peak broadening may be attributed to the change in the microenvironment of these substrates by increasing the number of seeding cycles.

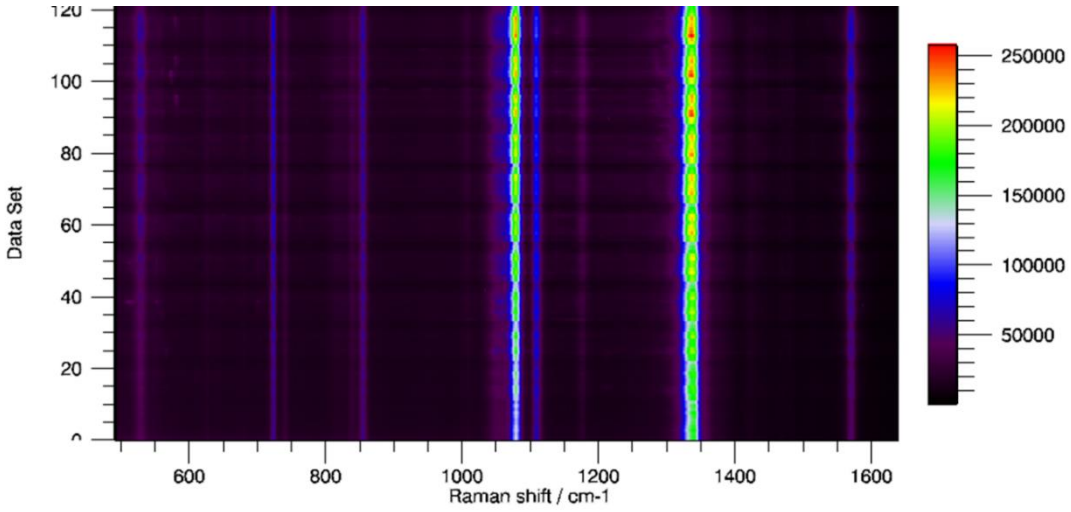


**Figure 2-9. 2D spectral Raman map of 4-NBT from 2S+G substrate.**

## 2.3.5 Applications of The SERS Substrates

### 2.3.5.1 Examples of potential applications

Based on our optimization, we have selected 2S+G substrates to explore their potential range of applications to detect different molecules. We chose four different analyte molecules; thiabendazole (TBZ), melamine (Mel), and malachite green (MG). The chemical structures of these molecules are shown in Figure 2-10. We selected these molecules as examples to show the intersection and applications of these SERS substrates in many fields including agriculture, food, health, and the ecosystem.

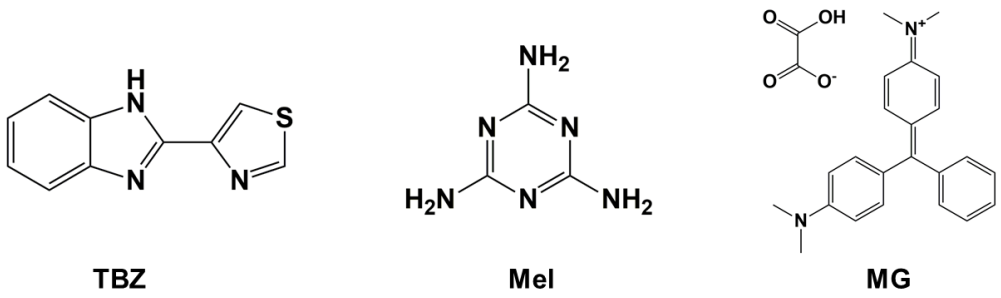


**Figure 2-10. Chemical structures of TBZ, MTZ, Mel, and MG.**

The first example is TBZ, which is used as a broad spectrum anthelmintic drug that is used for animals and humans.[73-75] It is used also as a pesticide and a fungicide to prevent fruits and vegetables from rot, mold, and blight to keep them fresh for storage before any waxing step.[76] While TBZ is less toxic than other pesticides, it may induce side effects, such as hepatotoxicity, nephrotoxicity, teratogenicity, and carcinogenicity.[77]

The second example is Mel, 1,3,5-triazine, which is a nitrogen rich organic compound that is used in plastics and glue industries.[78] In addition, Mel has been used as a milk adulterant to increase its apparent protein content fraudulently since traditional

methods for protein determination, such as the Kjeldahl method, depend only on the nitrogen content.[25, 78] Mel adulterated infants' milk formula has caused an outbreak of kidney diseases in 2008 in China.[79]

The third example is MG, which is an N-methylated diaminotriphenylmethane basic dye that is used in aquaculture industry as an antifungal and an antiprotozoal.[80] Previous studies have shown that MG can cause carcinogenicity, teratogenicity, and reproductive abnormalities in fish and mammals.[81-84] In Canada, MG is permitted to be used for aquarium fish only and is not approved for use on food-producing fish at any step, from the hatchery to the farm.[85]

Figure 2-11 represents the potential qualitative applications of these substrates to identify the previously mentioned molecules. In each case, we collected Raman spectra of each molecule from its solid powder on glass slide, adsorbed on 2S+G substrates, and unmodified PVDF membrane as a control. Figure 2-11A, shows the normal Raman spectrum of TBZ powder in blue. The SERS spectrum obtained from pipetting 1 μL of 100 ppm TBZ solution dissolved in 0.1M HCl on the 2S+G substrate is shown in green. The spectrum obtained under the same conditions from the PVDF membrane as a control is shown in red. The SERS enhancement of the 2S+G substrate is obvious when compared to the control experiment. The TBZ can interact with gold nanoparticles through N and S atoms. We did not observe any bands for the control experiment. Raman bands characteristic of adsorbed TBZ can be observed in the SERS spectrum of Figure 2-11A. These bands are summarized in Table 2-4, using assignments from a previously published paper.[86]

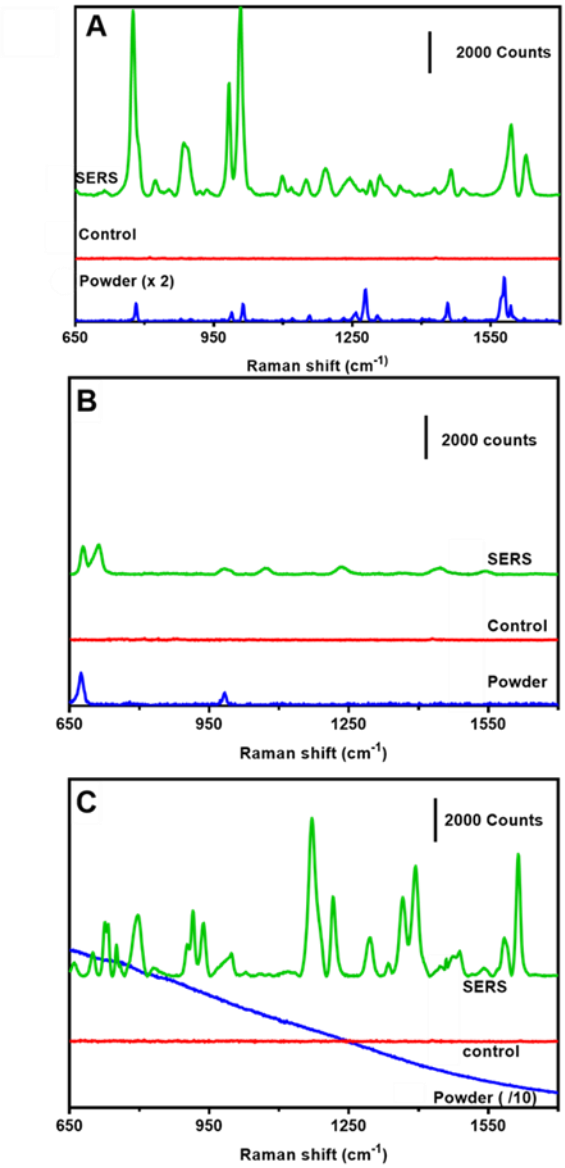


**Figure 2-11. Potential applications of the SERS substrates.** (A) Top (green) is the SERS spectrum of TBZ from a 100-ppm (0.1M HCl) solution on the 2S+G substrate; middle (red) spectrum has the same conditions as the top on an unmodified PVDF membrane; bottom (blue) spectrum is the TBZ powder Raman spectrum. (B) Top (green) is the SERS spectrum of Mel from a 1 mM aqueous solution on the 2S+G substrate; middle (red) spectrum has the same conditions as the top on an unmodified PVDF membrane; bottom (blue) spectrum is the Mel powder Raman spectrum. (C) Top (green) is the SERS spectrum of MG from a 1 mM ethanolic solution on the 2S+G substrate; middle (red) spectrum has the same conditions as the top on an unmodified PVDF membrane; bottom (blue) spectrum is the MG powder Raman spectrum showing high fluorescence background. Spectra were collected and averaged from 20 different points, with a 2-s integration time for five accumulations using a 20x objective and a power of 342 ± 1 μW at the sample. Spectra are stacked for clarification.

**Table 2-4. Major Band Assignments Listed for the SERS Spectrum of TBZ on the Surface of the SERS Substrates**

| Band position ($cm^{-1}$) | Assignment[86] |
|---|---|
| 778 | C–H out-of-plane bending |
| 886 | C–C–S out-of-plane bending and C-H out-of-plane bending |
| 983 | C–S stretching |
| 1008 | C–H out-of-plane bending |
| 1594 | ring stretching and C=N stretching |
| 1626 | C=N stretching |

The same trend was observed by pipetting 1 μL of 1 mM aqueous solutions of Mel (1 nmole) as shown in Figure 2-11B. Raman bands characteristic of adsorbed Mel can be observed in the SERS spectrum of Figure 2-11B. These bands are summarized in Table 2-5, according to a previously published paper.[78] We used Mel as an amine containing molecule that has affinity to bind to gold nanoparticles.

**Table 2-5. Major Band Assignments Listed for the SERS Spectrum of Mel on the Surface of the SERS Substrates**

| Band position ($cm^{-1}$) | Assignment[78] |
|---|---|
| 680 and 714 | ring breathing |
| 985 | C–N–C and N–C–N bending |
| 1070 | ring deformation and $NH_2$ twisting |
| 1477 | C–N stretching and $NH_2$ bending |
| 1543 | C–N stretching and $NH_2$ bending |

No Raman band for the MG powder was observed due to its fluorescence, as shown in Figure 2-11C (blue line). We also did not observe any Raman band for the

control experiment. However, we observed its SERS spectrum on the 2S+G substrate after pipetting 1 μL of its 1 mM ethanolic solution (1 nmole). Raman bands characteristic of adsorbed MG can be observed in the SERS spectrum of Figure 2-11C. These bands are summarized in Table 2-6, according to a previously published paper.[87] We used MG as an example of a fluorescent dye to show the potential capability of our substrates to detect a fluorescent molecule.

**Table 2-6. Major Band Assignments Listed for the SERS Spectrum of MG on the Surface of the SERS Substrates**

| Band position ($cm^{-1}$) | Assignment[87] |
|---|---|
| 1172 | in-plane C–H ring vibration |
| 1220 | C–H rocking |
| 1368 | N-phenyl stretching vibration |
| 1592 | C–C stretching |
| 1616 | C–C stretching |

### 2.3.5.2 Membrane-to-membrane variability

Point-to-point variability within the same substrate and substrate-to-substrate variability are one of the crucial characteristics of any SERS substrate. The recommended variability value should be less than 20% relative standard deviation.[69-70] We decided to investigate membrane-to-membrane and point-to-point reproducibility by Raman mapping of three different membranes where 1μl of 10-ppm TBZ was pipetted. Figure 2-12 shows the membrane-to-membrane and point-to-point variability using Raman

mapping. Figure 2-12A, B, and C are white light images of three different substrates, with a Raman mapped area (88.8 x 88.8 μm) using signal to baseline mapping of the C-H out-of-plane bending peak at 778 $cm^{-1}$. The %RSD within the same membrane is shown on each image and ranged from 11 to 14%. Figure 2-12D is a bar chart plotting of the average peak height of the C-H out-of-plane bend at 778 $cm^{-1}$ (obtained from 625 spectra collected from the Raman mapping of the three substrates).

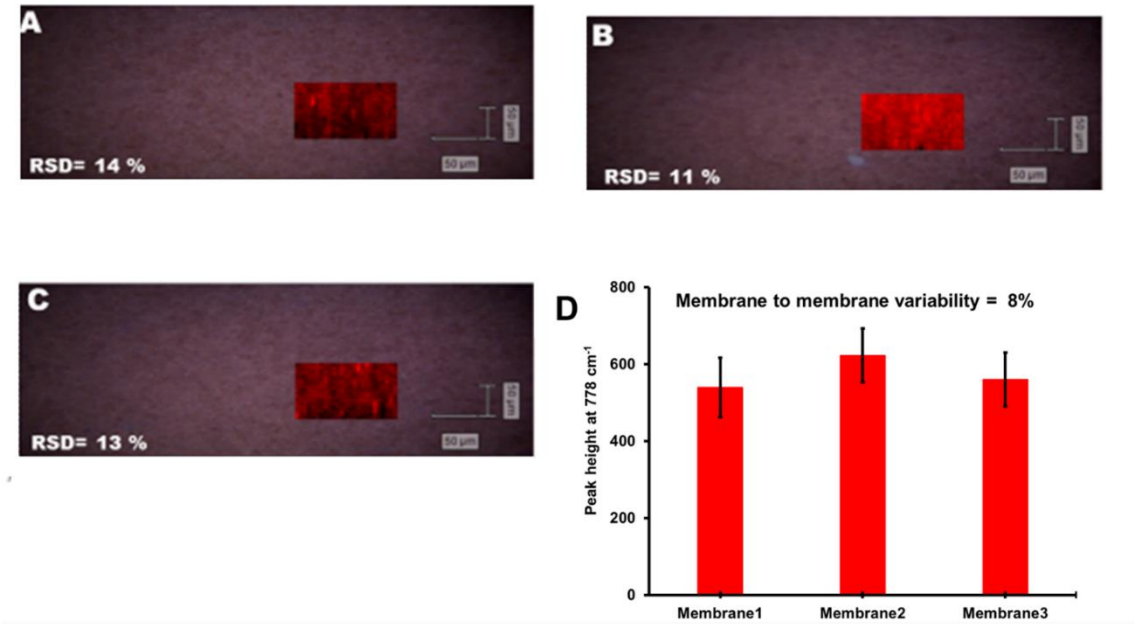


**Figure 2-12. Membrane-to-membrane variability.** (A, B, C) White light images of three different membranes with 10 ppm TBZ showing the Raman mapped area in red (signal to baseline) of the 778 $cm^{-1}$ Raman peak. Each image has the %RSD value at the bottom left showing the point-to-point variability within the same substrate. The scale bar is 50 μm in all images. (D) Bar chart of the membrane-to-membrane variability where the average peak height of the 778 $cm^{-1}$ Raman peak was used to compare between the three membranes.

The %RSD from membrane to membrane was 8%. Based on these %RSD values, our substrates showed comparable results to those of rigid SERS substrates where pre-grown metal nanoparticles were immobilized chemically.[88] We believe that the

formation of nanoparticle clusters and the fact that they are close to each other are the reasons for having point-to-point variability within the same membrane. We can conclude that our substrates demonstrate a lower variation from the 20% recommended %RSD value.[69-70]

#### 2.3.5.3 Methimazole (MTZ) detection and quantitation in urine

Urine is considered a complex matrix because it is composed of inorganic ions, salts, creatinine, creatine, hemoglobin by-products, urea, water soluble toxins, and many other metabolites.[89-90] Beside these metabolites, many drugs can be excreted in urine; methimazole (MTZ) is one example of those drugs.[91-92] MTZ is an antithyroid drug that is used to regulate the production of thyroxine and triiodothyronine.[93-94] MTZ is also the active form of another antithyroid drug called carbimazole.[95] MTZ can cause some side effects, including pharyngitis, liver cirrhosis, nephritis, skin irritation, allergic reactions, and impaired taste and olfaction.[93-94, 96] In addition, MTZ has been reported to be used illegally in animal feed to induce high weight gain by causing more water retention.[93, 97-98] Moreover, MTZ metabolites are reported to have cytotoxic effects.[96]

MTZ has commonly been quantified in urine using chromatographic methods.[94, 99-103] However, these methods require sample extraction, preconcentration, and/or derivatization before analysis by highly trained personnel.[94, 99-103] The limit of detection of MTZ by these chromatographic methods ranges from a concentration of nM to μM.[94, 100-103] SERS methods have been reported for MTZ quantification, but these methods have not been applied to urine.[104-109] In order to expand the applications of our SERS substrates, we decided to explore their analytical performance for MTZ measurements

in artificial urine as a complex matrix. For this purpose, we spiked synthetic urine with methimazole (MTZ) with a final concentration range of 0–1 mM.

Figure 2-13 shows the quantitation of MTZ in synthetic urine (Surine™) after pipetting and drying only 1 µL (0–1 nanomoles) on 2S+G substrates. SERS spectra of MTZ at different concentrations in urine and the associated controls are shown in Figure 2-13A. Each concentration is represented by an average spectrum composed of three samples measured from three different substrates, and each substrate was measured from 20 different spots (n = 60). Urine control shows a Raman band at 1000 $cm^{-1}$ ($I_{urine}$) highlighted in yellow, which is attributed to urea due to symmetric CN vibrations, based on previous publications.[89, 110-112] The most characteristic Raman bands of MTZ can be observed in the SERS spectra of Figure 2-13A. These bands are summarized in Table 2-7, according to previously published papers.[106, 108, 113] The peak used for quantitation is highlighted in light blue and is attributed to the N–C stretching vibration at 1364 $cm^{-1}$ ($I_{MTZ}$). As the concentration of MTZ is increased, the peak intensity also increases. Figure 2-13B is a plot of the peak height of the 1364 $cm^{-1}$ band ($I_{MTZ}$) normalized to the peak height of the urine band ($I_{urine}$) vs. concentration. The plot exhibits a linear portion then curvature at a high concentration. The curvature at high concentration is likely due to saturation of the gold nanostructures. A linear least squares fit of the low concentration portion of the plot can be used as a calibration curve, as shown in the inset of Figure 2-13B. From this linear portion, the limit of detection was determined as 0.2 picomoles.

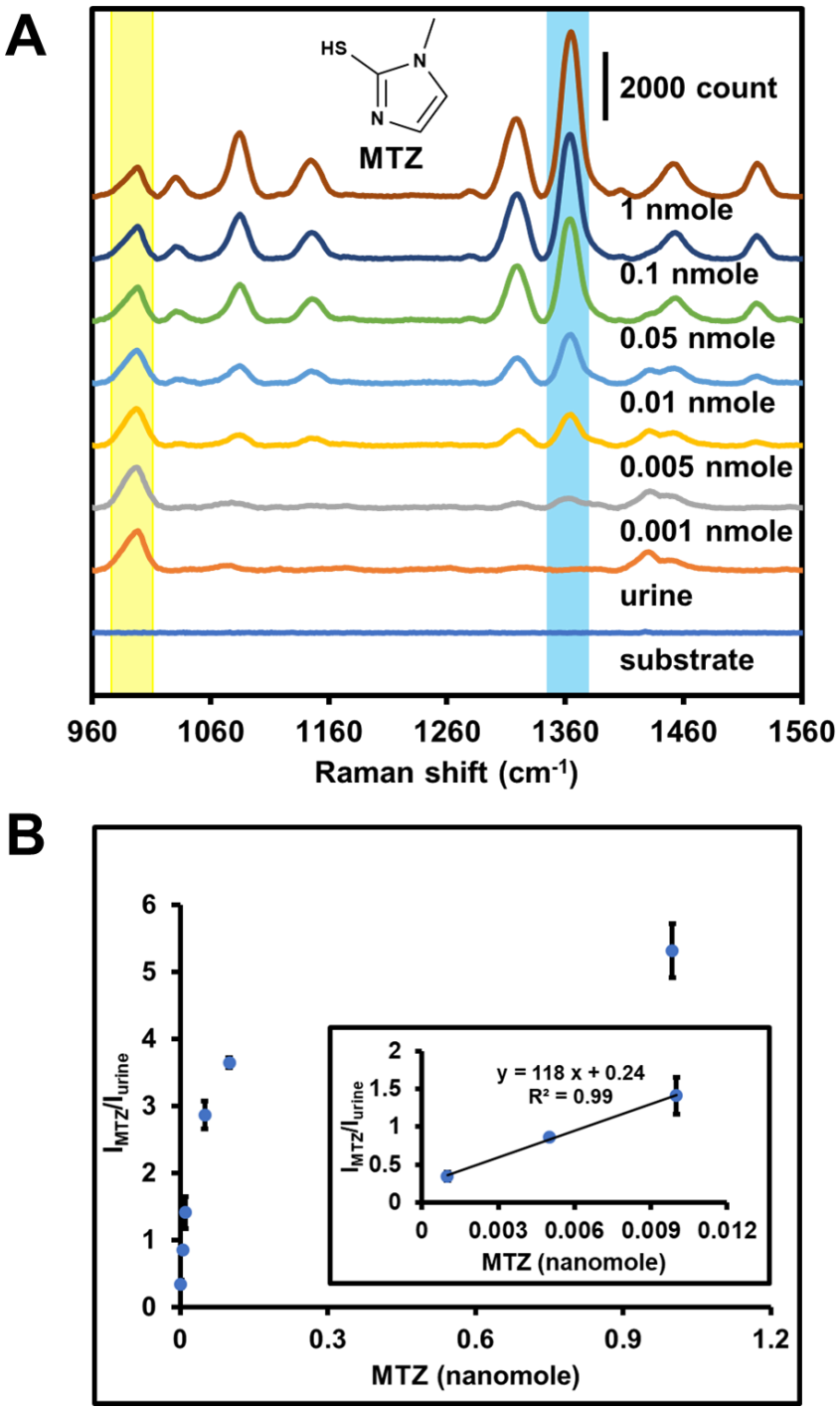


**Figure 2-13. MTZ quantitation in urine.** (A) SERS spectra of different concentrations of MTZ (0–1 nanomoles) obtained from 2S+G substrates. Spectra were collected and averaged from 20 different points with a 2-s integration time for 10 accumulations from three different membranes using a 20x objective and a power of 342 ± 1 μW at the sample. Spectra are stacked for clarification. (B) Calibration curve of MTZ using 2S+G substrates. Inset shows linear least squares fit.

The average point-to-point and membrane-to-membrane variability expressed as %RSD were 15 ± 3% and 9 ± 6%, respectively. From Figure 2-11 to 2-13, we can conclude that the developed method can provide SERS substrates that can be used for rapid detection and quantification of some target analytes. In addition, these substrates can be applied in pharmaceutical analysis as an in-line process control as well as in environmental monitoring.

**Table 2-7. Major Band Assignments Listed for the SERS Spectrum of MTZ on the Surface of the SERS Substrates**

| Band position ($cm^{-1}$) | Assignment[106, 108, 113] |
|---|---|
| 1029 | ring bending, ring C–H bending, and C–S–H bending |
| 1083 | ring C–N stretching and ring C–H bending |
| 1146 | C–S stretching, ring C–H bending, and C–N stretching |
| 1316 | ring C–N stretching, ring bending, and ring C–H bending |
| 1364 | C–N stretching, ring bending, and ring C–H bending |

## 2.4 Conclusions

This work shows that SILAR-like seeding and growth protocols can be combined to develop membrane supported SERS substrates. Gold nanostructures were deposited in-situ within the 3D porous network of the PVDF membranes. The SERS performance of these substrates can be optimized by the number of SILAR cycles used before the growth step. The developed method can reduce SILAR cycles to develop SERS substrates

efficiently and quickly. Our SERS substrates showed less than 20% membrane-to-membrane and point-to-point variability. The substrates can be applied for label-free detection of a wide range of molecules. In-process control and ongoing monitoring for agricultural and pharmaceutical products, as well as environmental and ecosystem testing, can be the target of many fields where these substrates can be utilized in future.

## 2.5 References


1. Kneipp, K.; Wang, Y.; Kneipp, H.; Perelman, L. T.; Itzkan, I.; Dasari, R. R.; Feld, M. S., Single Molecule Detection Using Surface-Enhanced Raman Scattering (SERS). *Physical Review Letters* **1997,** *78* (9), 1667-1670.

2. Nie, S.; Emory, S. R., Probing Single Molecules and Single Nanoparticles by Surface-Enhanced Raman Scattering. *Science* **1997,** *275* (5303), 1102-1106.

3. Sharaabi, Y.; Shegai, T.; Haran, G., Two-state analysis of single-molecule Raman spectra of crystal violet. *Chemical Physics* **2005,** *318* (1), 44-49.

4. Le Ru, E. C.; Meyer, M.; Etchegoin, P. G., Proof of Single-Molecule Sensitivity in Surface Enhanced Raman Scattering (SERS) by Means of a Two-Analyte Technique. *The Journal of Physical Chemistry B* **2006,** *110* (4), 1944-1948.

5. Haynes, C. L.; Van Duyne, R. P., Nanosphere Lithography: A Versatile Nanofabrication Tool for Studies of Size-Dependent Nanoparticle Optics. *The Journal of Physical Chemistry B* **2001,** *105* (24), 5599-5611.

6. Schmidt, M. S.; Hübner, J.; Boisen, A., Large Area Fabrication of Leaning Silicon Nanopillars for Surface Enhanced Raman Spectroscopy. *Advanced Materials* **2012,** *24* (10), OP11-OP18.

7. Kahl, M.; Voges, E.; Kostrewa, S.; Viets, C.; Hill, W., Periodically structured metallic substrates for SERS. *Sensors and Actuators B: Chemical* **1998,** *51* (1), 285-291.

8. Saracut, V.; Giloan, M.; Gabor, M.; Astilean, S.; Farcau, C., Polarization-Sensitive Linear Plasmonic Nanostructures via Colloidal Lithography with Uniaxial Colloidal Arrays. *ACS Applied Materials & Interfaces* **2013,** *5* (4), 1362-1369.

9. Brolo, A. G.; Arctander, E.; Gordon, R.; Leathem, B.; Kavanagh, K. L., Nanohole-Enhanced Raman Scattering. *Nano Letters* **2004,** *4* (10), 2015-2018.

10. Shi, R.; Liu, X.; Ying, Y., Facing Challenges in Real-Life Application of Surface-Enhanced Raman Scattering: Design and Nanofabrication of Surface-Enhanced Raman Scattering Substrates for Rapid Field Test of Food Contaminants. *Journal of Agricultural and Food Chemistry* **2018,** *66* (26), 6525-6543.

11. Schmucker, A. L.; Tadepalli, S.; Liu, K.-K.; Sullivan, C. J.; Singamaneni, S.; Naik, R. R., Plasmonic paper: a porous and flexible substrate enabling nanoparticle-based combinatorial chemistry. *RSC Advances* **2016,** *6* (5), 4136-4144.

12. Yu, W. W.; White, I. M., Inkjet Printed Surface Enhanced Raman Spectroscopy Array on Cellulose Paper. *Analytical Chemistry* **2010,** *82* (23), 9626-9630.

13. Yu, W. W.; White, I. M., Paper-based optofluidic SERS using ink-jet-printed substrates. *Proc. SPIE* **2011,** *7911* (Plasmonics in Biology and Medicine VIII), 791105/1-791105/6.

14. White, I. M., Optofluidic SERS on inkjet-fabricated paper-based substrates. *Proc. SPIE* **2012,** *8264* (Integrated Optics: Devices, Materials, and Technologies XVI), 826414/1-826414/6.

15. Hoppmann, E. P.; White, I. M., A paper-based inkjet-fabricated substrate for SERS detection and differentiation of PCR products. *Proc. SPIE* **2013,** *8718* (Advanced Environmental, Chemical, and Biological Sensing Technologies X), 871804/1-871804/6.

16. Hoppmann, E. P.; Yu, W. W.; White, I. M., Highly sensitive and flexible inkjet printed SERS sensors on paper. *Methods* **2013,** *63* (3), 219-224.

17. Liu, H.; Xu, Y.; Qin, Y.; Sanderson, W.; Crowley, D.; Turner, C. H.; Bao, Y., Ligand-Directed Formation of Gold Tetrapod Nanostructures. *The Journal of Physical Chemistry C* **2013,** *117* (33), 17143-17150.

18. Yu, W. W.; White, I. M., Chromatographic separation and detection of target analytes from complex samples using inkjet printed SERS substrates. *Analyst (Cambridge, U. K.)* **2013,** *138* (13), 3679-3686.

19. Betz, J. F.; Yu, W. W.; Cheng, Y.; White, I. M.; Rubloff, G. W., Simple SERS substrates: powerful, portable, and full of potential. *Phys. Chem. Chem. Phys.* **2014,** *16* (6), 2224-2239.

20. Hoppmann, E. P.; Yu, W. W.; White, I. M., Inkjet-printed fluidic paper devices for chemical and biological analytics using surface enhanced Raman spectroscopy. *IEEE J. Sel. Top. Quantum Electron.* **2014,** *20* (3), 7300510/1-7300510/10.

21. Hoppmann, E. P.; Yu, W. W.; White, I. M., Detection of deoxyribonucleic acid (DNA) targets using polymerase chain reaction (PCR) and paper surface-enhanced Raman spectroscopy (SERS) chromatography. *Appl. Spectrosc.* **2014,** *68* (8), 909-915.

22. Berger, A. G.; Restaino, S. M.; White, I. M., Vertical-flow paper SERS system for therapeutic drug monitoring of flucytosine in serum. *Anal. Chim. Acta* **2017,** *949*, 59-66.

23. Lee, C. H.; Tian, L.; Singamaneni, S., Paper-Based SERS Swab for Rapid Trace Detection on Real-World Surfaces. *ACS Applied Materials & Interfaces* **2010,** *2* (12), 3429-3435.

24. Lee, C. H.; Hankus, M. E.; Tian, L.; Pellegrino, P. M.; Singamaneni, S., Highly Sensitive Surface Enhanced Raman Scattering Substrates Based on Filter Paper Loaded with Plasmonic Nanostructures. *Analytical Chemistry* **2011,** *83* (23), 8953-8958.

25. Abbas, A.; Brimer, A.; Slocik, J. M.; Tian, L.; Naik, R. R.; Singamaneni, S., Multifunctional Analytical Platform on a Paper Strip: Separation, Preconcentration, and Subattomolar Detection. *Analytical Chemistry* **2013,** *85* (8), 3977-3983.

26. Ross, M. B.; Ashley, M. J.; Schmucker, A. L.; Singamaneni, S.; Naik, R. R.; Schatz, G. C.; Mirkin, C. A., Structure–Function Relationships for Surface-Enhanced Raman Spectroscopy-Active Plasmonic Paper. *The Journal of Physical Chemistry C* **2016,** *120* (37), 20789-20797.

27. Ashley, M. J.; Bourgeois, M. R.; Murthy, R. R.; Laramy, C. R.; Ross, M. B.; Naik, R. R.; Schatz, G. C.; Mirkin, C. A., Shape and Size Control of Substrate-Grown Gold Nanoparticles for Surface-Enhanced Raman Spectroscopy Detection of Chemical Analytes. *The Journal of Physical Chemistry C* **2018,** *122* (4), 2307-2314.

28. Zhang, W.; Li, B.; Chen, L.; Wang, Y.; Gao, D.; Ma, X.; Wu, A., Brushing, a simple way to fabricate SERS active paper substrates. *Analytical Methods* **2014,** *6* (7), 2066-2071.

29. Polavarapu, L.; Porta, A. L.; Novikov, S. M.; Coronado-Puchau, M.; Liz-Marzán, L. M., Pen-on-Paper Approach Toward the Design of Universal Surface Enhanced Raman Scattering Substrates. *Small* **2014,** *10* (15), 3065-3071.

30. Herrera-Sandoval, G. M.; Felix-Rivera, H.; Padilla-Jimenez, A. C.; Balaguera-Gelves, M.; Ortega-Zuniga, C. A.; Pacheco-Londono, L. C.; Primera-Pedrozo, O. M.; Fierro, P. M.; Rios-Velazquez, C.; Hernandez-Rivera, S. P. In *Synthesis and characterization of silver nanoparticles and nanostructures for SERS applications*, Nova Science Publishers, Inc.: 2013; pp 59-100.

31. Qu, L.-L.; Li, D.-W.; Xue, J.-Q.; Zhai, W.-L.; Fossey, J. S.; Long, Y.-T., Batch fabrication of disposable screen printed SERS arrays. *Lab on a Chip* **2012,** *12* (5), 876-881.

32. Qu, L.-L.; Song, Q.-X.; Li, Y.-T.; Peng, M.-P.; Li, D.-W.; Chen, L.-X.; Fossey, J. S.; Long, Y.-T., Fabrication of bimetallic microfluidic surface-enhanced Raman scattering sensors on paper by screen printing. *Analytica Chimica Acta* **2013,** *792*, 86-92.

33. Kim, W.-S.; Shin, J.-H.; Park, H.-K.; Choi, S., A low-cost, monometallic, surface-enhanced Raman scattering-functionalized paper platform for spot-on bioassays. *Sensors and Actuators B: Chemical* **2016,** *222*, 1112-1118.

34. Yu, W. W.; White, I. M., A simple filter-based approach to surface enhanced Raman spectroscopy for trace chemical detection. *Analyst* **2012,** *137* (5), 1168-1173.

35. Au - Gao, S.; Au - Glasser, J.; Au - He, L., A Filter-based Surface Enhanced Raman Spectroscopic Assay for Rapid Detection of Chemical Contaminants. *JoVE* **2016,** (108), e53791.

36. Kim, W.; Lee, J.-C.; Shin, J.-H.; Jin, K.-H.; Park, H.-K.; Choi, S., Instrument-Free Synthesizable Fabrication of Label-Free Optical Biosensing Paper Strips for the Early Detection of Infectious Keratoconjunctivitides. *Analytical Chemistry* **2016,** *88* (10), 5531-5537.

37. Kim, W.; Kim, Y.-H.; Park, H.-K.; Choi, S., Facile Fabrication of a Silver Nanoparticle Immersed, Surface-Enhanced Raman Scattering Imposed Paper Platform through Successive Ionic Layer Absorption and Reaction for On-Site Bioassays. *ACS Applied Materials & Interfaces* **2015,** *7* (50), 27910-27917.

38. Kim, W.; Lee, J.-C.; Lee, G.-J.; Park, H.-K.; Lee, A.; Choi, S., Low-Cost Label-Free Biosensing Bimetallic Cellulose Strip with SILAR-Synthesized Silver Core–Gold Shell Nanoparticle Structures. *Analytical Chemistry* **2017,** *89* (12), 6448-6454.

39. Kim, W.; Lee, S. H.; Kim, J. H.; Ahn, Y. J.; Kim, Y.-H.; Yu, J. S.; Choi, S., Paper-Based Surface-Enhanced Raman Spectroscopy for Diagnosing Prenatal Diseases in Women. *ACS Nano* **2018,** *12* (7), 7100-7108.

40. Lee, J.-C.; Kim, W.; Park, H.-K.; Choi, S., Controlling successive ionic layer absorption and reaction cycles to optimize silver nanoparticle-induced localized surface plasmon resonance effects on the paper strip. *Spectrochimica Acta Part A: Molecular and Biomolecular Spectroscopy* **2017,** *174*, 37-43.

41. Tan, C.; Zhang, Z.; Qu, Y.; He, L., Ag2O/TiO2 Nanocomposite Heterostructure as a Dual Functional Semiconducting Substrate for SERS/SEIRAS Application. *Langmuir* **2017,** *33* (22), 5345-5352.

42. Lovinger, A. J., Poly(Vinylidene Fluoride). In *Developments in Crystalline Polymers—1*, Bassett, D. C., Ed. Springer Netherlands: Dordrecht, 1982; pp 195-273.

43. Yeow, M. L.; Liu, Y. T.; Li, K., Isothermal phase diagrams and phase-inversion behavior of poly(vinylidene fluoride)/solvents/additives/water systems. *Journal of Applied Polymer Science* **2003,** *90* (8), 2150-2155.

44. Hashim, N. A.; Liu, F.; Li, K., A simplified method for preparation of hydrophilic PVDF membranes from an amphiphilic graft copolymer. *Journal of Membrane Science* **2009,** *345* (1), 134-141.

45. Awanis Hashim, N.; Liu, Y.; Li, K., Stability of PVDF hollow fibre membranes in sodium hydroxide aqueous solution. *Chemical Engineering Science* **2011,** *66* (8), 1565-1575.

46. Menges, F. Spectragryph - Optical Spectroscopy Software, Version 1.2.10; 2018; http://www.effemm2.de/spectragryph/.

47. Keunen, R.; Macoretta, D.; Cathcart, N.; Kitaev, V., Stable ligand-free stellated polyhedral gold nanoparticles for sensitive plasmonic detection. *Nanoscale* **2016,** *8* (5), 2575-2583.

48. Brown, K. R.; Natan, M. J., Hydroxylamine Seeding of Colloidal Au Nanoparticles in Solution and on Surfaces. *Langmuir* **1998,** *14* (4), 726-728.

49. Brown, K. R.; Lyon, L. A.; Fox, A. P.; Reiss, B. D.; Natan, M. J., Hydroxylamine Seeding of Colloidal Au Nanoparticles. 3. Controlled Formation of Conductive Au Films. *Chemistry of Materials* **2000,** *12* (2), 314-323.

50. Meltzer, S.; Resch, R.; Koel, B. E.; Thompson, M. E.; Madhukar, A.; Requicha, A. A. G.; Will, P., Fabrication of Nanostructures by Hydroxylamine Seeding of Gold Nanoparticle Templates. *Langmuir* **2001,** *17* (5), 1713-1718.

51. Yared, I.; Wang, S.; Wang, M., Effects of Oxygen Plasma and Dopamine Coating on Poly(Vinylidene Fluoride) Microfiltration Membrane for the Resistance to Protein Fouling. *IEEE Transactions on Plasma Science* **2014,** *42* (12), 3847-3857.

52. Kise, H.; Ogata, H., Phase transfer catalysis in dehydrofluorination of poly(vinylidene fluoride) by aqueous sodium hydroxide solutions. *Journal of Polymer Science: Polymer Chemistry Edition* **1983,** *21* (12), 3443-3451.

53. Rabuni, M. F.; Nik Sulaiman, N. M.; Aroua, M. K.; Hashim, N. A., Effects of Alkaline Environments at Mild Conditions on the Stability of PVDF Membrane: An Experimental Study. *Industrial & Engineering Chemistry Research* **2013,** *52* (45), 15874-15882.

54. Notte, J.; Ward, B.; Economou, N.; Hill, R.; Percival, R.; Farkas, L.; McVey, S., An Introduction to the Helium Ion Microscope. *AIP Conference Proceedings* **2007,** *931* (1), 489-496.

55. Joens, M. S.; Huynh, C.; Kasuboski, J. M.; Ferranti, D.; Sigal, Y. J.; Zeitvogel, F.; Obst, M.; Burkhardt, C. J.; Curran, K. P.; Chalasani, S. H.; Stern, L. A.; Goetze, B.; Fitzpatrick, J. A. J., Helium Ion Microscopy (HIM) for the imaging of biological samples at sub-nanometer resolution. *Scientific Reports* **2013,** *3*, 3514.

56. El-Sayed, M. A., Some Interesting Properties of Metals Confined in Time and Nanometer Space of Different Shapes. *Accounts of Chemical Research* **2001,** *34* (4), 257-264.

57. Mulvaney, P., Surface Plasmon Spectroscopy of Nanosized Metal Particles. *Langmuir* **1996,** *12* (3), 788-800.

58. Murphy, C. J.; Sau, T. K.; Gole, A. M.; Orendorff, C. J.; Gao, J.; Gou, L.; Hunyadi, S. E.; Li, T., Anisotropic Metal Nanoparticles: Synthesis, Assembly, and Optical Applications. *The Journal of Physical Chemistry B* **2005,** *109* (29), 13857-13870.

59. Chandra, K.; Culver, K. S. B.; Werner, S. E.; Lee, R. C.; Odom, T. W., Manipulating the Anisotropic Structure of Gold Nanostars using Good's Buffers. *Chemistry of Materials* **2016,** *28* (18), 6763-6769.

60. Haiss, W.; Thanh, N. T. K.; Aveyard, J.; Fernig, D. G., Determination of Size and Concentration of Gold Nanoparticles from UV−Vis Spectra. *Analytical Chemistry* **2007,** *79* (11), 4215-4221.

61. Ross, M. B.; Ashley, M. J.; Schmucker, A. L.; Singamaneni, S.; Naik, R. R.; Schatz, G. C.; Mirkin, C. A., Structure-Function Relationships for Surface-Enhanced Raman Spectroscopy-Active Plasmonic Paper. *J. Phys. Chem. C* **2016,** *120* (37), 20789-20797.

62. Brittain, H. G., 3 - Solid-State Analysis. In *Separation Science and Technology*, Ahuja, S.; Scypinski, S., Eds. Academic Press: 2001; Vol. 3, pp 57-84.

63. Danielson, S. J., 22 - THIN-FILM IMMUNOASSAYS. In *Immunoassay*, Diamandis, E. P.; Christopoulos, T. K., Eds. Academic Press: San Diego, 1996; pp 505-535.

64. Blitz, J. P., Diffuse reflectance spectroscopy. *Modern Techniques in Applied Molecular Spectroscopy* **1998**, 185-219.

65. Viscarra Rossel, R. A.; McGlynn, R. N.; McBratney, A. B., Determining the composition of mineral-organic mixes using UV–vis–NIR diffuse reflectance spectroscopy. *Geoderma* **2006,** *137* (1), 70-82.

66. Link, S.; El-Sayed, M. A., Size and Temperature Dependence of the Plasmon Absorption of Colloidal Gold Nanoparticles. *The Journal of Physical Chemistry B* **1999,** *103* (21), 4212-4217.

67. Skadtchenko, B. O.; Aroca, R., Surface-enhanced Raman scattering of p-nitrothiophenol: Molecular vibrations of its silver salt and the surface complex formed on silver islands and colloids. *Spectrochimica Acta Part A: Molecular and Biomolecular Spectroscopy* **2001,** *57* (5), 1009-1016.

68. Abdelsalam, M. E., Surface enhanced raman scattering of aromatic thiols adsorbed on nanostructured gold surfaces. *Central European Journal of Chemistry* **2009,** *7* (3), 446-453.

69. Natan, M. J., Concluding Remarks Surface enhanced Raman scattering. *Faraday Discussions* **2006,** *132*, 321-328.

70. Lin, X.-M.; Cui, Y.; Xu, Y.-H.; Ren, B.; Tian, Z.-Q., Surface-enhanced Raman spectroscopy: substrate-related issues. *Analytical and Bioanalytical Chemistry* **2009,** *394* (7), 1729-1745.

71. Cui, Q.; Yashchenok, A.; Li, L.; Möhwald, H.; Bargheer, M., Mechanistic study on reduction reaction of nitro compounds catalyzed by gold nanoparticles using in situ SERS monitoring. *Colloids and Surfaces A: Physicochemical and Engineering Aspects* **2015,** *470*, 108-113.

72. Gao, P.; Weaver, M. J., Surface-enhanced raman-spectroscopy as a probe of adsorbate surface bonding - benzene and monosubstituted benzenes adsorbed at gold electrodes. *Journal of Physical Chemistry* **1985,** *89* (23), 5040-5046.

73. Satou, T.; Koga, M.; Koike, K.; Tada, I.; Nikaido, T., Nematocidal activities of thiabendazole and ivermectin against the larvae of Strongyloides ratti and S. venezuelensis. *Veterinary Parasitology* **2001,** *99* (4), 311-322.

74. Cuckler, A. C., Thiabendazole, a new broad spectrum anthelmintic. *Journal of Parasitology* **1961,** *47* (4, Sect. 2), 36-37.

75. Ames, E. R.; Cheney, J. M.; Rubin, R., The efficacy of thiabendazole and bephenium hydroxynaphthoate against Ostertagia ostertagi and Cooperia oncophora in experimentally infected calves. *American journal of veterinary research* **1963,** *24*, 295-299.

76. Alsammarraie, F. K.; Lin, M.; Mustapha, A.; Lin, H.; Chen, X.; Chen, Y.; Wang, H.; Huang, M., Rapid determination of thiabendazole in juice by SERS coupled with novel gold nanosubstrates. *Food Chemistry* **2018,** *259*, 219-225.

77. Jamieson, J. D.; Smith, E. B.; Dalvie, D. K.; Stevens, G. J.; Yanochko, G. M., Myeloperoxidase-mediated bioactivation of 5-hydroxythiabendazole: A possible mechanism of thiabendazole toxicity. *Toxicology in Vitro* **2011,** *25* (5), 1061-1066.

78. Mircescu, N. E.; Oltean, M.; Chiș, V.; Leopold, N., FTIR, FT-Raman, SERS and DFT study on melamine. *Vibrational Spectroscopy* **2012,** *62*, 165-171.

79. Wang, Z.; Luo, H.; Tu, W.; Yang, H.; Wong, W. H.-S.; Wong, W.-T.; Yung, K.-F.; Zhou, N.; Zhang, J.; Li, X.; Wang, Z.; Guo, W.; Mu, D.; Li, F.; Mao, M.; Lau, Y.-L., Melamine-tainted milk product-associated urinary stones in children. *Pediatrics International* **2011,** *53* (4), 489-496.

80. Sudova, E.; Machova, J.; Svobodova, Z.; Vesely, T., Negative effects of malachite green and possibilities of its replacement in the treatment of fish eggs and fish: a review. *Vet. Med.* **2007,** *52* (12), 527-539.

81. Culp, S. J.; Beland, F. A., Malachite green: A toxicological review. *Journal of the American College of Toxicology* **1996,** *15* (3), 219-238.

82. Culp, S. J.; Blankenship, L. R.; Kusewitt, D. F.; Doerge, D. R.; Mulligan, L. T.; Beland, F. A., Toxicity and metabolism of malachite green and leucomalachite green during short-term feeding to Fischer 344 rats and B6C3F1 mice. *Chemico-Biological Interactions* **1999,** *122* (3), 153-170.

83. Fernandes, C.; Lalitha, V. S.; Rao, K. V., Enhancing effect of malachite green on the development of hepatic pre-neoplastic lesions induced by N-nitrosodiethylamine in rats. *Carcinogenesis* **1991,** *12* (5), 839-45.

84. Srivastava, S.; Sinha, R.; Roy, D., Toxicological effects of malachite green. *Aquatic Toxicology* **2004,** *66* (3), 319-329.

85. CFIA Malachite Green - Questions and Answers. http://www.inspection.gc.ca/food/information-for-consumers/fact-sheets-and-infographics/products-and-risks/chemical-hazards/malachite-green/eng/1332268890141/1332268947157 (accessed April 2, 2019).

86. Kim, M. S.; Kim, M. K.; Lee, C. J.; Jung, Y. M.; Lee, M. S., Surface-enhanced Raman Spectroscopy of Benzimidazolic Fungicides: Benzimidazole and Thiabendazole. *B Korean Chem Soc* **2009,** *30* (12), 2930-2934.

87. Chamuah, N.; Bhuyan, N.; Das, P. P.; Ojah, N.; Choudhary, A. J.; Medhi, T.; Nath, P., Gold-coated electrospun PVA nanofibers as SERS substrate for detection of pesticides. *Sensors and Actuators B: Chemical* **2018,** *273*, 710-717.

88. de Albuquerque, C. D. L.; Sobral-Filho, R. G.; Poppi, R. J.; Brolo, A. G., Digital Protocol for Chemical Analysis at Ultralow Concentrations by Surface-Enhanced Raman Scattering. *Analytical Chemistry* **2018,** *90* (2), 1248-1254.

89. Moreira, L. P.; Silveira, L.; Pacheco, M. T. T.; da Silva, A. G.; Rocco, D. D. F. M., Detecting urine metabolites related to training performance in swimming athletes by means of Raman spectroscopy and principal component analysis. *Journal of Photochemistry and Photobiology B: Biology* **2018,** *185*, 223-234.

90. Bouatra, S.; Aziat, F.; Mandal, R.; Guo, A. C.; Wilson, M. R.; Knox, C.; Bjorndahl, T. C.; Krishnamurthy, R.; Saleem, F.; Liu, P.; Dame, Z. T.; Poelzer, J.; Huynh, J.; Yallou, F. S.; Psychogios, N.; Dong, E.; Bogumil, R.; Roehring, C.; Wishart, D. S., The human urine metabolome. *PLoS One* **2013,** *8* (9), e73076.

91. PITTMAN, J. A.; BESCHI, R. J.; SMITHERMAN, T. C., Methimazole: Its Absorption and Excretion in Man and Tissue Distribution in Rats. *The Journal of Clinical Endocrinology & Metabolism* **1971,** *33* (2), 182-185.

92. Okamura, Y.; Shigemasa, C.; Tatsuhara, T., Pharmacokinetics of Methimazole in Normal Subjects and Hyperthyroid Patients. *Endocrinologia Japonica* **1986,** *33* (5), 605-615.

93. Ebrahimzadeh, H.; Asgharinezhad, A. A.; Adlnasab, L.; Shekari, N., Optimization of ion-pair based hollow fiber liquid phase microextraction combined with HPLC–UV for the determination of methimazole in biological samples and animal feed. *Journal of Separation Science* **2012,** *35* (16), 2040-2047.

94. Kuśmierek, K.; Bald, E., Determination of methimazole in urine by liquid chromatography. *Talanta* **2007,** *71* (5), 2121-2125.

95. Skellern, G.; Knight, B.; Low, C.; Alexander, W.; McLarty, D.; Kalk, W., The pharmacokinetics of methimazole after oral administration of carbimazole and methimazole, in hyperthyroid patients. *British Journal of Clinical Pharmacology* **1980,** *9* (2), 137-143.

96. Genter, M. B., Evaluation of olfactory and auditory system effects of the antihyperthyroid drug carbimazole in the Long-Evans rat. *Journal of Biochemical and Molecular Toxicology* **1998,** *12* (5), 305-314.

97. Kong, D.; Chi, Y.; Chen, L.; Dong, Y.; Zhang, L.; Chen, G., Determination of thyreostatics in animal feeds by CE with electrochemical detector. *Electrophoresis* **2009,** *30* (19), 3489-3495.

98. Martínez-Frías, M. L.; Cereijo, A.; Rodríguez-Pinilla, E.; Urioste, M., Methimazole in animal feed and congenital aplasia cutis. *The Lancet* **1992,** *339* (8795), 742-743.

99. Lawrence, J. F.; Iverson, F.; Hanekamp, H. B.; Bos, P.; Frei, R. W., Liquid chromatography with UV absorbance and polarographic detection of ethylenethiourea and related sulfur compounds: Application to rat urine analysis. *Journal of Chromatography A* **1981,** *212* (2), 245-250.

100. Batjoens, P.; De Brabander, H. F.; De Wasch, K., Rapid and high-performance analysis of thyreostatic drug residues in urine using gas chromatography-mass spectrometry. *Journal of Chromatography A* **1996,** *750* (1), 127-132.

101. John Blanchflower, W.; J. Hughes, P.; Cannavan, A.; A. McCoy, M.; Glenn Kennedy, D., Determination of Thyreostats in Thyroid and Urine Using High-performance Liquid Chromatography–Atmospheric Pressure Chemical Ionisation Mass Spectrometry. *Analyst* **1997,** *122* (9), 967-972.

102. Zakrzewski, R., Determination of methimazole in urine with the iodine-azide detection system following its separation by reversed-phase high-performance liquid chromatography. *Journal of Chromatography B* **2008,** *869* (1), 67-74.

103. Tölgyesi, Á.; Giri, A.; Barta, E.; McDonald, T. J.; Sharma, V. K., Determination of Thyreostats in Urine Using Supported Liquid Extraction and Mixed-Mode Cation-Exchange Solid-Phase Extraction: Screening and Confirmatory Methods. *Journal of Chromatographic Science* **2018,** *56* (9), 858-866.

104. Liao, X.; Chen, Y.; Qin, M.; Chen, Y.; Yang, L.; Zhang, H.; Tian, Y., Au–Ag–Au double shell nanoparticles-based localized surface plasmon resonance and surface-enhanced Raman scattering biosensor for sensitive detection of 2-mercapto-1-methylimidazole. *Talanta* **2013,** *117*, 203-208.

105. Saleh, T. A.; Al-Shalalfeh, M. M.; Al-Saadi, A. A., Graphene Dendrimer-stabilized silver nanoparticles for detection of methimazole using Surface-enhanced Raman scattering with computational assignment. *Scientific Reports* **2016,** *6*, 32185.

106. Saleh, T. A.; Al-Shalalfeh, M. M.; Al-Saadi, A. A., Silver nanoparticles for detection of methimazole by surface-enhanced Raman spectroscopy. *Materials Research Bulletin* **2017,** *91*, 173-178.

107. Saleh, T. A.; Al-Shalalfeh, M. M.; Onawole, A. T.; Al-Saadi, A. A., Ultra-trace detection of methimazole by surface-enhanced Raman spectroscopy using gold substrate. *Vibrational Spectroscopy* **2017,** *90*, 96-103.

108. Fei, J.; Wu, L.; Zhang, Y.; Zong, S.; Wang, Z.; Cui, Y., Pharmacokinetics-on-a-Chip Using Label-Free SERS Technique for Programmable Dual-Drug Analysis. *ACS Sensors* **2017,** *2* (6), 773-780.

109. Yang, J.; Cui, Y.; Zong, S.; Zhang, R.; Song, C.; Wang, Z., Tracking Multiplex Drugs and Their Dynamics in Living Cells Using the Label-Free Surface-Enhanced Raman Scattering Technique. *Molecular Pharmaceutics* **2012,** *9* (4), 842-849.

110. Keuleers, R.; Desseyn, H. O.; Rousseau, B.; Van Alsenoy, C., Vibrational Analysis of Urea. *The Journal of Physical Chemistry A* **1999,** *103* (24), 4621-4630.

111. Premasiri, W. R.; Clarke, R. H.; Womble, M. E., Urine analysis by laser Raman spectroscopy. *Lasers in Surgery and Medicine* **2001,** *28* (4), 330-334.

112. Bispo, J. A. M.; Vieira, E. E. d. S.; Jr., L. S.; Fernandes, A. B., Correlating the amount of urea, creatinine, and glucose in urine from patients with diabetes mellitus and hypertension with the risk of developing renal lesions by means of Raman spectroscopy and principal component analysis. *Journal of Biomedical Optics* **2013,** *18* (8), 1-8, 8.

113. Ma, P.; Liang, F.; Yang, Q.; Wang, D.; Sun, Y.; Wang, X.; Gao, D.; Song, D., Highly sensitive SERS probe for mercury(II) using cyclodextrin-protected silver nanoparticles functionalized with methimazole. *Microchimica Acta* **2014,** *181* (9), 975-981.

# Chapter 3

## In-situ Seedless Approach for Membrane Supported Silver Nanocorals as SERS Substrates Using a Handheld Raman Spectrometer

## 3.1 Introduction

As discussed in the previous chapter, surface enhanced Raman scattering (SERS) is becoming a more useful analytical technique. Raman signals can be enhanced by several orders of magnitude due to electromagnetic, chemical, and resonance enhancement mechanisms.[1-7] The capability to reach single molecule detection via these enhancement mechanisms has led to the diversification of research using the technique.[8-11] Impacted research areas include analytical chemistry, polymers, catalysis, materials, biomedical sciences, and forensics.[12-16] In addition, the advent of portable and handheld Raman spectrometers have contributed to extending Raman and SERS applications to the point of need. These include explosive detection, pharmaceutical analysis, environmental monitoring, artwork, and surgery.[17-21]

There are many published reports that involve the use of portable and handheld Raman systems. However, most of this published work relies on the use of rigid SERS substrates.[17, 19, 22-29] These substrates are based on glass, silicon, and gold surfaces that are fabricated using methods such as reactive ion etching, HF etching, oblique angle metal deposition, thermal metal evaporation, and electrodeposition of metal nanostructures.[17, 19, 22-29] These methods require expensive lab equipment and highly trained personnel, which can be a burden in resource limited situations. For example, metal over silicon nanopillar SERS substrates have been reported to accompany the use of handheld Raman spectrometers by different researchers.[22-26] These substrates are fabricated using a maskless procedure that involves reactive ion etching, followed by metal deposition by electron beam evaporation or metal sputtering.[30] The cost of these substrates ranges approximately USD$ 50–80 per substrate.[31] However, SERS substrates based on paper

and polymeric filters prepared by simple chemical methods can provide a cost effective and user friendly alternative over the rigid SERS substrates.[32-45] Little work has been done that couples handheld Raman spectrometers with porous based SERS substrates.[24, 46-48] In these examples, plasmonic nanoparticles were synthesized first using multistep methods to incorporate them into porous substrates.[24, 46-48] An in-situ equipment-free synthesis method for flexible SERS substrates to be coupled with handheld devices has not been demonstrated.

Herein, we present a deviceless and rapid method to develop flexible SERS substrates. Our method is based on an in-situ seedless synthesis of silver nanocorals onto a polyvinylidene fluoride (PVDF) filter. The substrates were characterized using UV-vis diffuse reflectance, Fourier transform infrared (FTIR) spectroscopy, helium ion microscopy (HIM), and Raman spectroscopy. The substrates were optimized based on the loading of silver nanocorals. We applied these substrates for label free detection of methimazole in artificial urine using a handheld Raman spectrometer. The 3D structure of the nanocoral and its incorporation into PVDF membranes generated many hot spots for signal enhancement. These substrates showed reproducible SERS performance from point to point and from substrate to substrate.

## 3.2 Experimental

### 3.2.1 Reagents

Polyvinylidene fluoride (PVDF) filters with a 0.45-micron pore size and 25 mm in diameter (lot: 7017006) were purchased from Sterlitech. Sliver nitrate ($AgNO_3$, ACS-Pur)

and sodium hydroxide were obtained from Fisherbrand. 4-Mercabtobenzonitrile (MBN) was obtained from Combi-Blocks. Hydroxylamine hydrochloride (HH, 99.999% trace metal basis), rhodamine 6G (R6G, dye content ~ 95%), Surine™ negative urine control, and methimazole analytical standard (MTZ) were obtained from Sigma-Aldrich. Absolute ethanol was obtained from Commercial Alcohols. MBN was dissolved in ethanol. Milli-Q water with a resistivity of 18.2 MΩ cm was used for all experiments, unless stated otherwise.

## 3.2.2 Instrumentation

### 3.2.2.1 Fourier transform infrared (FTIR)

Unmodified and modified membranes FTIR spectra were collected by a Nicolet 8700 Continuum FTIR Microscope in transmittance mode using 128 scans with a resolution of 4 $cm^{-1}$.

### 3.2.2.2 Helium ion microscopy (HIM)

Silver nanocorals morphology onto a PVDF membrane was characterized using a Zeiss Orion. The microscope was operated at an acceleration voltage of 30 kV.

### 3.2.2.3 UV-vis diffuse reflectance

UV-vis diffuse reflectance was measured using a Carry 5000 UV-vis spectrometer equipped with a home built diffuse reflectance accessory. The instrument was standardized to 100% reflectance using a white standard (Spectralon).

### 3.2.2.4 Raman spectroscopy

Raman spectra were collected by a TacticID handheld Raman spectrometer (B&W TEK) equipped with a 785-nm diode laser. The power at the sample was 26 ± 1 mW, and all the collected spectra from the handheld spectrometer were normalized to the laser

irradiation time, unless stated otherwise. The SERS performance of the substrates was optimized using a membrane accessory (TacPac adapter). R6G and MBN were the Raman probes used for optimization. One µl of 1 mM ethanolic R6G solution was dropped on three different substrates for each silver nitrate concentration used. Each substrate was measured once to simulate a point and shoot scenario. The substrates were immersed in a 5 µM ethanolic MBN solution and left overnight. Then, they were washed extensively to remove any excess reagents that were not chemisorbed. The substrates were left to air dry, and spectra were collected using a membrane accessory. Three membranes prepared using each concentration of silver nitrate were measured once to simulate a point and shoot situation. For MTZ detection in synthetic urine, a liquid vial accessory was used. Three different substrates were used, and each substrate was measured, after immersion for 30 min, at three different spots by rotating the vial. Raman spectral data analysis and background subtraction were performed using Spectragryph, an open-source software.[49]

### 3.2.3 In-Situ Seedless Synthesis of 3D Silver Nanostructures on PVDF

Silver nanostructures were synthesized in-situ on PVDF membranes, based on a previous publication with some modifications.[50] The steps for the synthesis of the substrate are summarized in Figure 3-1. The PVDF membrane was immersed into a silver nitrate (1–100 mM) solution for 1 min. Then, the membrane was removed with a tweezer, and the excess reagent was drained from the edge using a Kimwipe. Next, the membrane was immersed into a basic solution of HH (100 mM in 0.2 M NaOH) for one minute, the HH acting as the reducing agent here. Bubbling was observed on the membrane upon

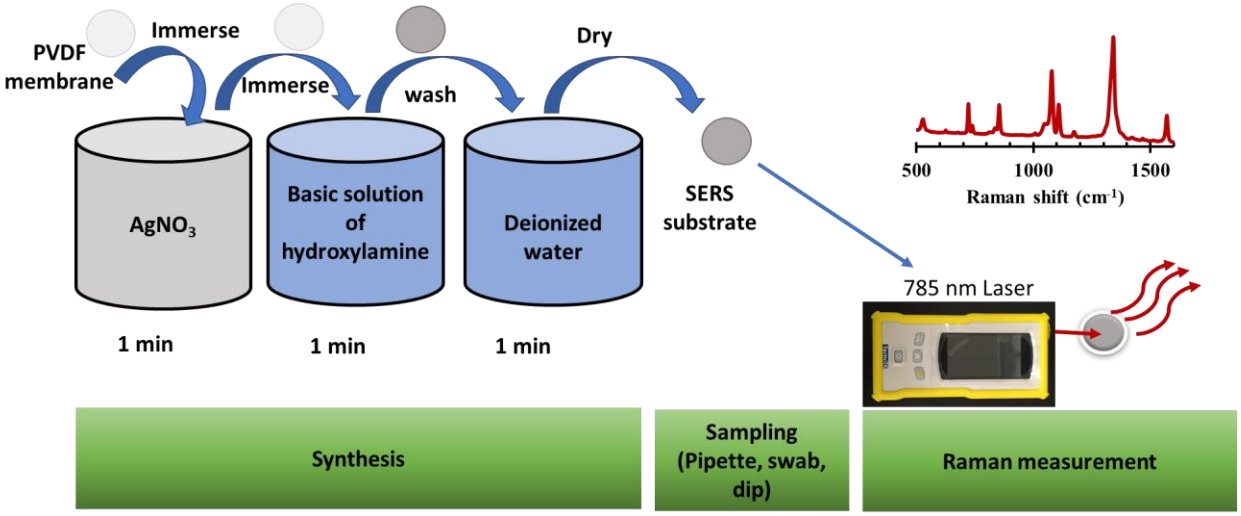


**Figure 3-1. General scheme to develop a silver nanocoral PVDF SERS substrate**.

immersion in HH, and the color of the membrane changed from white to grey at this point, while HH solution remained colorless. Afterward, the membrane was washed extensively with Milli-Q water and ethanol to ensure the removal of all excess reagents. Then, the membranes were air dried and stored in a desiccator away from light. We denoted the membranes as 1mMAg, 20mMAg, 50mMAg, 70mMAg and 100mMAg based on the silver nitrate concentration used.

## 3.3 Results and Discussion

### 3.3.1 SERS Substrate Characterization

In this chapter, FTIR spectroscopy, HIM microscopy and UV-Vis diffuse reflectance are used to characterize our substrates, consistent with the same methods used in Chapter 2.

#### 3.3.1.1 FTIR spectroscopy

As discussed in Chapter 2, FTIR spectroscopy has been used to determine the impact of sodium hydroxide on PVDF membranes.[51-53] Sodium hydroxide treatment may lead to dehydrofluorination of PVDF membranes, which can lead to changes of their polymeric structure.[51-53] Dehydrofluorination is characterized by the appearance of bands attributed to a carbon–carbon double bond stretch at 1590–1650 $cm^{-1}$, a carbonyl bond stretch at 1700–1800 $cm^{-1}$ and a carbon–carbon triple bond stretch at 2100 $cm^{-1}$.[51-53] For example, an experimental study has shown that a solution of 0.2 M sodium hydroxide can cause dehydrofluroination of PVDF membranes after 30 min at 25 °C.[53] The researchers reported also that the degree dehydrofluroination was more pronounced by increasing the reaction time and temperature.[53]

Our procedure uses 0.2 M sodium hydroxide for a short time (1 min) to deposit silver nanostructures on PVDF membranes, then we examine its effect on the chemical structure of PVDF membranes by FTIR. The spectra of our substrates were compared to the blank PVDF membrane spectrum. As depicted in Figure 3-2, the spectra of our substrates are similar to that of the FTIR spectrum of the blank PVDF membrane. In addition, all membranes showed the characteristic FTIR peaks assigned to the PVDF α-phase at 763, 796, 877, and 1070 $cm^{-1}$, and other bands, which are attributed to the PVDF β-phase at 841, 1273, and 1402 $cm^{-1}$.[51-53] Moreover, there was no significant difference between the blank PVDF spectrum and our substrates spectra at the wavenumber range of 1590–2100 $cm^{-1}$. This indicates that our procedure does not result in any noticeable dehydrofluorination of PVDF membranes.

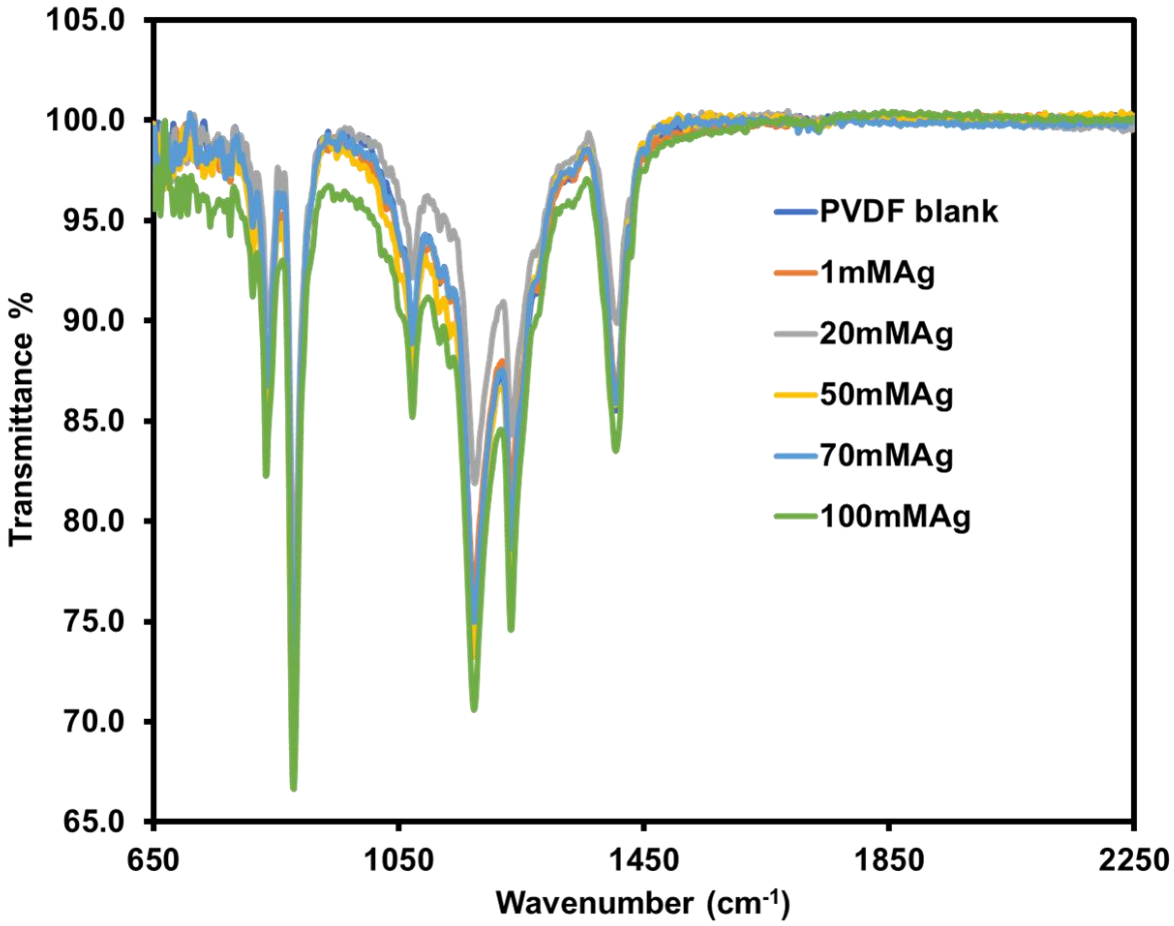


**Figure 3-2. FTIR spectra of blank PVDF membrane and the silver nanocoral substrates with different silver nitrate concentrations.**

### 3.3.1.2 HIM imaging

The size, shape, and distribution of the silver nanostructure in the membrane may affect the SERS performance of these substrates significantly. Helium ion microscopy (HIM) was used to investigate the impact of increasing the silver nitrate concentration on the morphology of the silver nanostructures. It also was used to study how nanoparticles are integrated into the 3D polymeric network of PVDF membranes. HIM has many advantages over traditional scanning electron microscopy. As discussed in Chapter 2, these advantages include small probe size, reduced sample damage, long depth of field and high resolution, and high surface contrast without metal sputtering.[54-55] All of these

advantages are preferable for imaging our silver nanostructures without any metal sputtering required and with no damage to the PVDF membrane.

Figure 3-3 shows HIM images of the substrates using different concentrations of silver nitrate. A similar shape of silver nanobranched structures has been synthesized using electrochemical and chemical methods, with these nanostructures described as nanocoral or coral-like.[56-58] Our silver nanostructures have a 3D shape of nanocorals, with intertwined nanostructured branches. The exact mechanism by which these nanobranched structures are formed is unclear to us, and how the PVDF membranes may impact this mechanism. We observed that the loading density of the silver nanocorals is increased with increasing silver nitrate concentration, as shown in Figure 3-3. The average width of the branches of the nanocorals (n = 20) was calculated to study the impact of increasing the silver nitrate concentration. The average widths were 31 ± 7 nm, 30 ± 7 nm, 35 ± 8 nm, 32 ± 6 nm, and 34 ± 8 nm for 1, 20, 50, and 100 mM $AgNO_3$, respectively. Although the width of the nanocorals branches did not show any significant difference by increasing the silver nitrate concentration, the loading density of the silver nanostructures increased significantly.

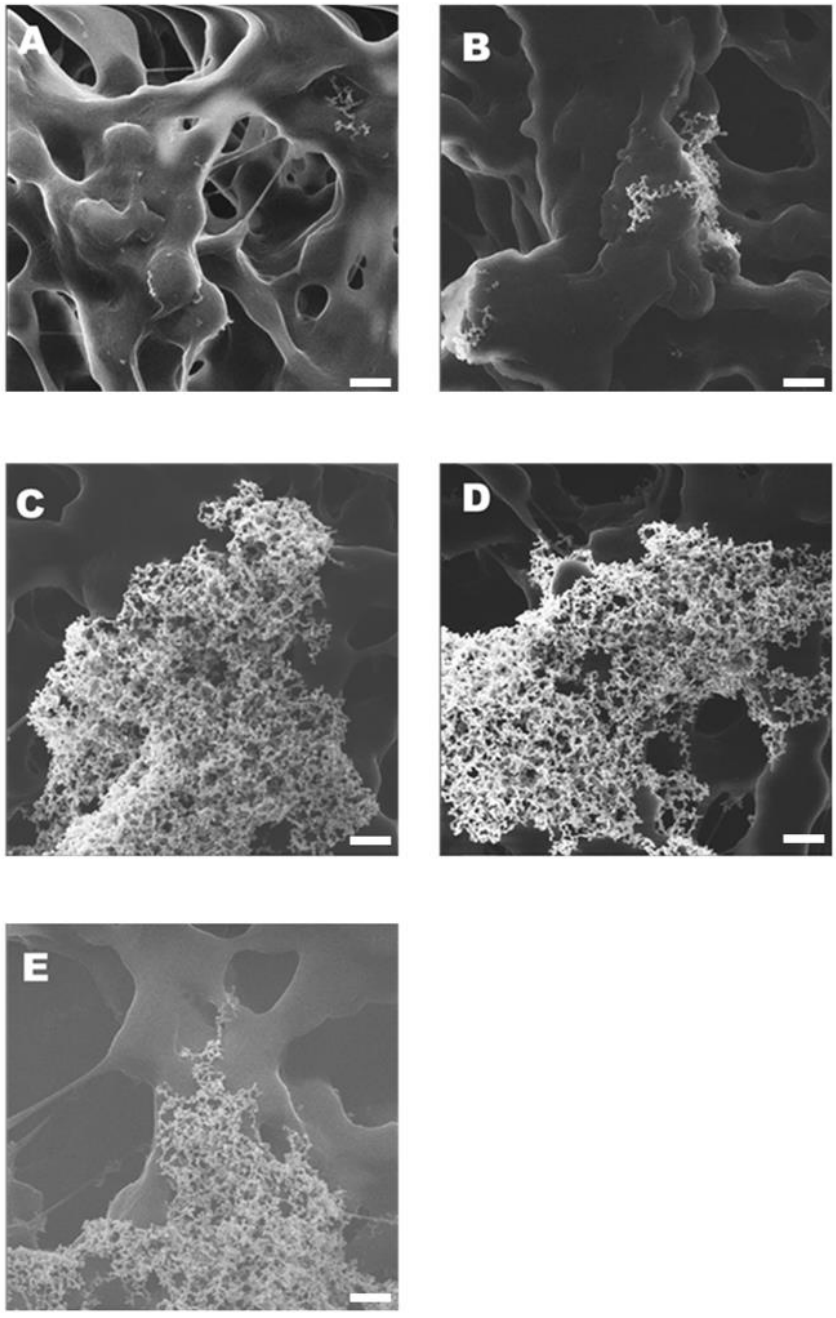


**Figure 3-3. HIM images of the substrates at different $AgNO_3$ concentrations.** (A)1 mM, (B) 10 mM, (C) 50 mM, (D)70 mM, and (E) 100 mM. (Scale bar is 500 nm in all images.)

#### 3.3.1.3 UV-vis diffuse reflectance

As discussed in Chapter 2, the plasmonic behavior of colloidal metallic nanostructures is studied routinely by extinction spectroscopy, based on Mie theory.[59-60] Extinction spectroscopy has been reported to show the effect of shape and size of nanomaterials on the location and number of the localized surface plasmon resonance (LSPR) bands.[59, 61-62] In addition, Haiss et al. estimated the size and concentration of gold nanoparticles using extinction spectroscopy.[63] Although extinction spectroscopy is a well established technique in the case of colloidal nanoparticles, it is challenging when it comes to nanoparticles attached to opaque surfaces within porous membranes. Consequently, most of the published work related to SERS substrates based on porous filters shows no extinction spectra[36-38, 64-75] or only shows extinction spectra of the colloidal nanoparticles before they are attached to the membrane.[35, 76] Thus, we decided to implement UV-vis diffuse reflectance as a qualitative alternative technique to extinction spectroscopy. UV-vis diffuse reflectance has been applied to study solid state reactions, color matching, and color measurements.[77]

Reflectance measurements are analogues to transmittance measurements in absorption spectroscopy.[78] However, spectral artifacts can be induced due to some limitations.[79] These artifacts can be caused by a sample with high absorptivity, changes in scattering coefficients of the samples, and Fresnel reflectance.[79] This may result in a blue shift in the band position as an artifact.[79] These limitations could not be avoided for our substrates due to their high absorptivity because of the intrinsic LSPR of silver nanostructures. In addition, the loading density of silver nanocorals increased with increasing silver nitrate concentration, which would lead to changes in the scattering

coefficient of the substrates. For these reasons, we used this technique for a qualitative description of the apparent extinction values of our substrates. Diffuse reflectance (R) values were transformed to log (1/R) values[80] to study the impact of increasing silver nitrate concentration on the extinction of our substrates qualitatively. As shown in Figure 3-4A, the log (1/R) values of the substrates increased with increasing silver nitrate concentration. The shaded area in the figure shows the appearance of a broad band centered around 380 nm. At low silver nitrate concentrations, the log(1/R) value was similar to the PVDF blank membrane. However, 20 mM silver nitrate produced a significant increase in the log (1/R) values, indicating the formation of silver nanostructures. We also observed a small blue shift (11 nm) in LSPR with increasing silver nitrate concentration, which we attribute as a spectral artifact. Silver nanoparticles prepared with hydroxylamine as a reducing agent in alkaline medium showed a LSPR around 400 nm,[50] which can support that silver nanostructures have been synthesized onto the PVDF membranes.

Figure 3-4B shows a photo of the substrates at different silver nitrate concentrations (0–100 mM). The color of the substrates changed from white (PVDF blank) to grey. As the concentration of silver nitrate increased, the substrates became darker in color. The diffuse reflectance data and grey color of the substrates can be attributed to the in-situ synthesis of silver nanocorals within the porous network of PVDF membranes. Data from diffuse reflectance measurements are summarized in Table 3-1.

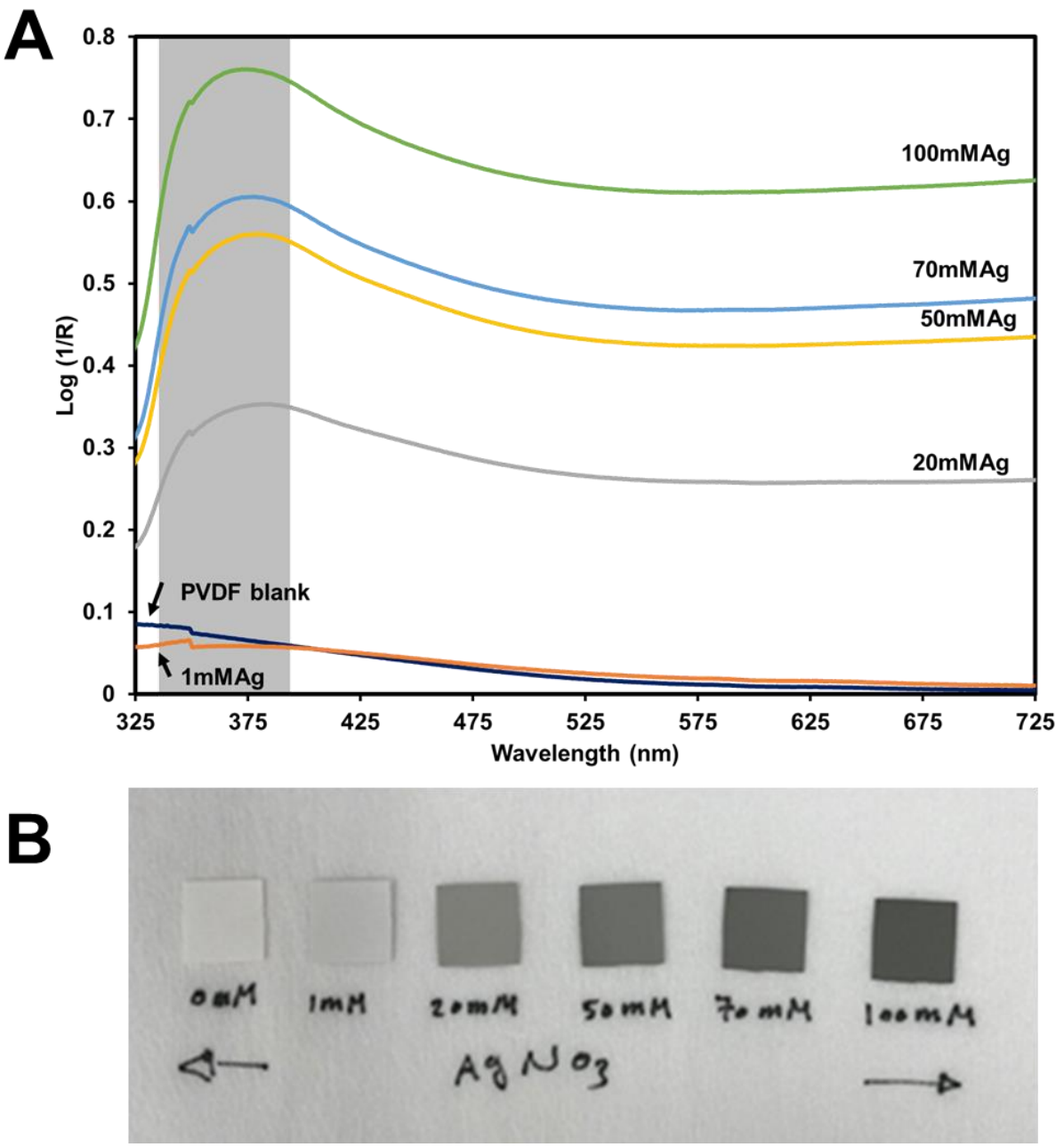


**Figure 3-4. UV-vis diffuse reflectance of the SERS substrates**. (A) UV-vis diffuse reflectance of the substrates at different concentrations of silver nitrate (0–100 mM). (B) Images of the corresponding substrates at different silver nitrate concentrations.

**Table 3-1. Summary of the UV-vis Diffuse Reflectance of the Substrates Using Different Concentrations of Silver Nitrate**

| Membrane | Log (1/R) (a.u) |
|---|---|
| 1mMAg | 0.08 |
| 20mMAg | 0.35 |
| 50mMAg | 0.56 |
| 70mMAg | 0.61 |
| 100mMAg | 0.76 |

### 3.3.2 SERS Performance

The role of silver nitrate concentration on the SERS performance was investigated using a handheld Raman spectrometer. Table 3-2 is a summary of the characteristics and important parameters of the spectrometer used. Figure 3-5 shows photographs of the handheld Raman device used along with different accessories and possible sampling approaches. These accessories include point and shoot adapter, liquid vial adapter, membrane adapter, and polystyrene standard adapter, as shown in Figure 3-5 (A-E). Combining the portability of the handheld Raman device with the flexibility of the developed SERS substrates can offer various sampling approaches, including pipetting, swabbing, and/or immersion, as shown in Figure 3-5 (F-I). Porter and co-workers have shown that TacticID can be used in SERS assays with a SERS performance of approximately one order of magnitude less than that of more sophisticated Raman microscopes when it comes to sensitivity and signal intensity.[29] To examine the SERS

performance of these substrates, two Raman probes were used: the first probe, R6G, is used as an example of a non-specific adsorber; the second probe, MBN, adsorbs specifically and in high coverage through a S–Ag interaction.

**Table 3-2. Summary of The Main Characteristics of The Handheld Raman Spectrometer, TacticID, Provided by the manufacturer, B&W TEK**

| Parameter | Values |
|---|---|
| Dimensions | (19 cm x 10 cm x 5 cm) |
| Weight | 0.9 kg |
| Laser wavelength | 785 nm |
| Spectral resolution | 9 $cm^{-1}$ |
| Power | Max. 300 mW |
| Detector type | Linear CCD array |
| Operating temperature | -20 °C to +50 °C |

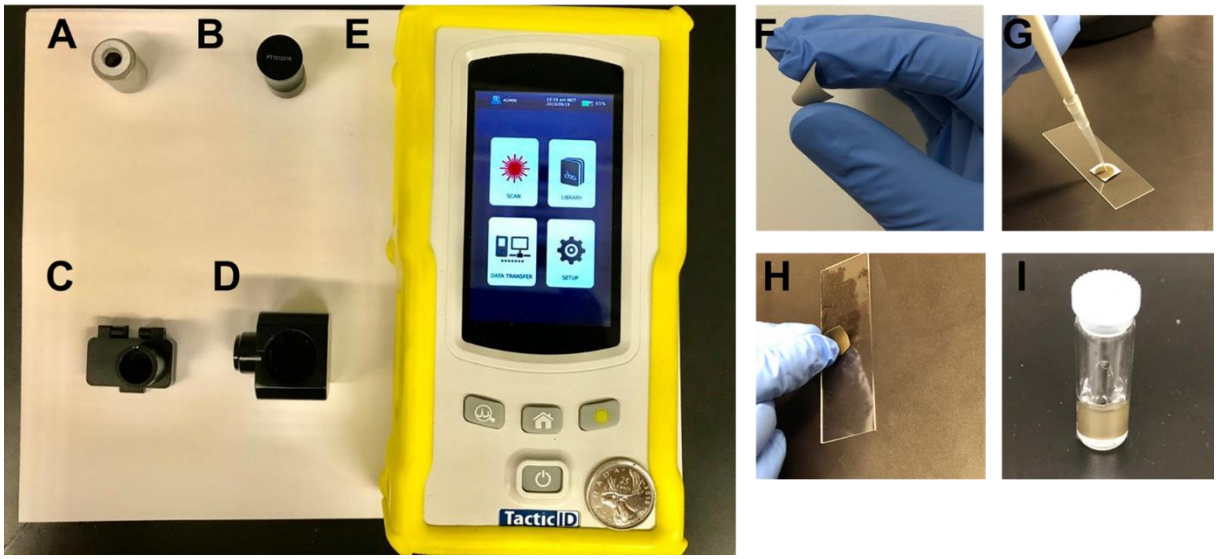


**Figure 3-5. Handheld Raman accessories and substrates applicability.** (A) Point and shoot adapter, (B) polystyrene standard adapter, (C) membrane adapter, (D) vial adapter, (E) handheld device used with a quarter as a scale bar, (F) substrate, bendable and flexible, (G), (H), and (I) images of different sampling approaches, including pipetting, swabbing, and immersion, respectively.

### 3.3.2.1 SERS optimization based on physisorption

R6G was used as a non-thiolated Raman probe to simulate a physisorption scenario using a drop casting sampling approach. R6G adsorbs on silver nanoparticles.[9, 81] One µL of 1 mM ethanolic solution of R6G was dropped on each substrate (1 nmole). We compared the spectral intensity of the substrates at different silver nitrate concentrations, as shown in Figure 3-6. Raman bands characteristic of adsorbed R6G can be observed in Figure 3-6A.

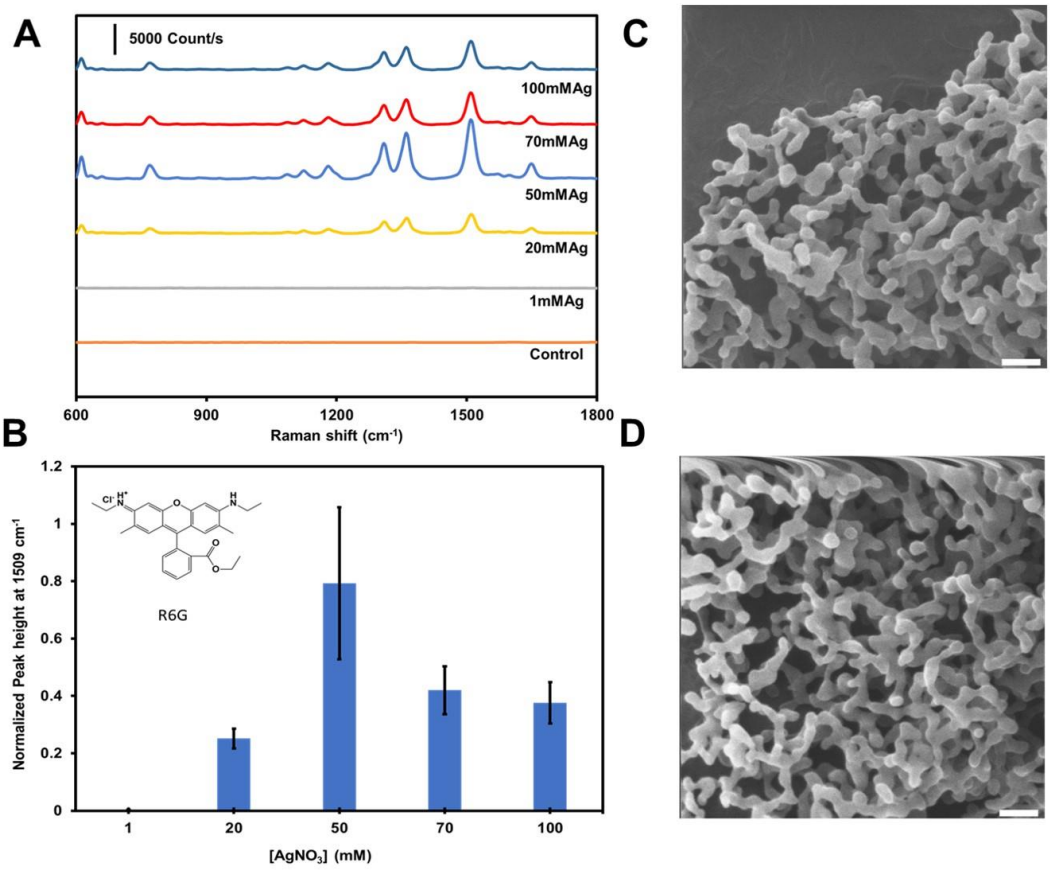


**Figure 3-6. Substrates optimization using R6G.** (A) SERS spectra of R6G on substrates prepared using different $AgNO_3$ concentrations. (B) Bar chart of the normalized peak height to the highest value at 1509 $cm^{-1}$ of R6G from each substrate. The R6G chemical structure is shown on the top left (error bar is standard deviation of three membranes). (C) and (D) HIM images for the substrates synthesized using 50 and 70 mM $AgNO_3$, respectively. (Scale bar is 100 nm.)

We used the normalized peak height to the highest value at 1509 $cm^{-1}$ assigned to the symmetric in-plane C–C stretch of R6G to compare between substrates in Figure 3-6B, where the chemical structure of R6G is shown. We did not observe any Raman band of R6G from the control experiment, where R6G is drop casted on an unmodified PVDF membrane. Table 3-3 shows major Raman peak assignments for R6G, according to previously published papers.[9, 81]

**Table 3-3. Major Band Assignments Listed for the SERS Spectrum of R6G on the Substrates**

| Band position ($cm^{-1}$) | Assignment[9, 81] |
|---|---|
| 1649 | Symmetric in-plane C–C stretch |
| 1575 | |
| 1509 | |
| 1361 | |
| 1311 | |
| 1181 | |
| 1124 | In-plane C–H bend |
| 772 | Out-of-plane C–H bend |

The Raman signal on our substrates was enhanced due to the SERS effect of silver nanocorals. The spectral intensity was improved by increasing the silver nitrate concentration to 50 mM. This may be attributed to the increase of the loading density of silver nanocorals, as presented before in Figure 3-3. However, the spectral intensity was reduced by increasing the silver nitrate concentration beyond 50 mM. Figure 3-6C and D show high magnification HIM micrographs of 50mMAg and 70mMAg substrates, which

appear to be similar. The 50mMAg, 70mMAg, and 100mMAg substrates showed a comparable SERS performance, with the 50mMAg substrate yielding the highest SERS intensity. The silver nanocorals have a 3D architecture, with interconnected branches, which is favourable to generate a lot of hot spots in a 3D volume. We can conclude that the 50mMAg substrates showed the highest enhancement with the physisorption drop casting approach.

#### 3.3.2.2 SERS optimization based on chemisorption

MBN was used as a thiolated Raman probe to ensure binding to the silver nanostructures through a specific thiolate–Ag interaction. This was to investigate the SERS performance of the substrates based on a chemisorption scenario using an immersion sampling approach. Figure 3-7A shows SERS spectra of MBN obtained from the substrates with different silver nitrate concentrations. Raman bands characteristic of chemisorbed MBN are observed in Figure 3-7A. Table 3-4 shows major Raman peak assignments for MBN, according to previously published papers.[82-84]

The nitrile stretch peak height at 2230 $cm^{-1}$ was used to compare the SERS performance of the substrates, based on the silver nitrate concentration in Figure 3-7B, where the chemical structure of MBN is shown. The spectral intensity was enhanced by increasing the silver nitrate concentration to 50 mM. This may be attributed to the increase of the loading density of silver nanocorals. However, the spectral intensity was reduced by increasing silver nitrate concentration beyond 50 mM. Figure 3-7 shows a similar trend in the SERS performance of the substrates when compared to Figure 3-6, with a comparable SERS performance of the substrates that were synthesized with a

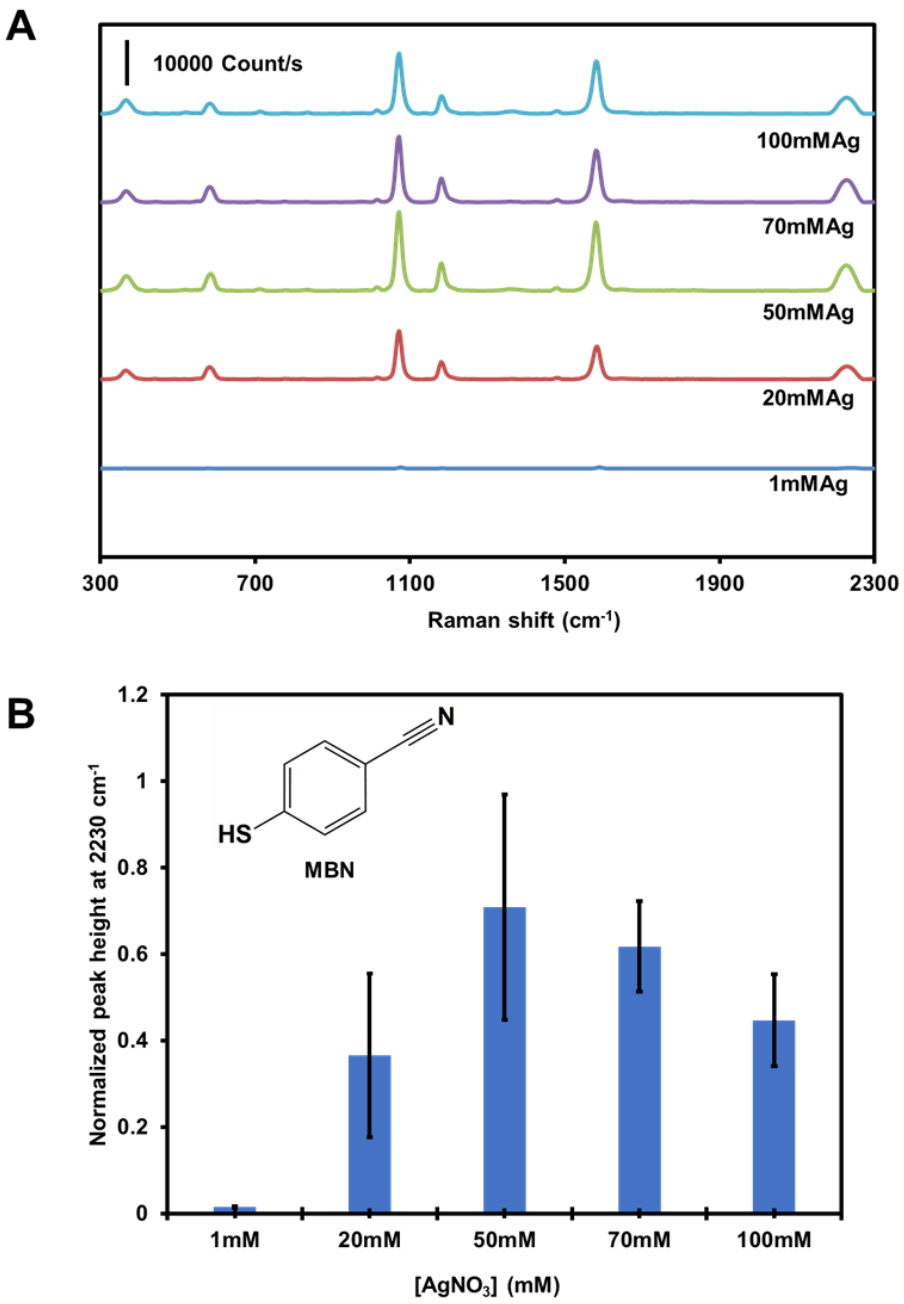


**Figure 3-7. Substrates optimization with MBN.** (A) SERS spectra of MBN from different substrates prepared using 1–100 mM $AgNO_3$. (B) Bar chart of the normalized peak height at 2230 $cm^{-1}$ of MBN on different substrates prepared using 1–100 mM $AgNO_3$ (error bar is standard deviation of three membranes).

silver nitrate concentration between 50 mM and 100 mM. We can conclude that the 50mMAg substrates showed the highest SERS enhancement using both physisorption

and chemisorption approaches. Therefore, we decided to use these substrates in the following section to show their application for methimazole (MTZ) detection.

**Table 3-4. Major Band Assignments Listed for the SERS Spectrum of MBN on the Surface of the Substrates**

| Band position ($cm^{-1}$) | Assignment[82-84] |
|---|---|
| 1071 | C–S and C–C stretching |
| 1182 | C–H bending and C–C stretch |
| 1581 | C–C stretch |
| 2230 | C≡N stretch |

### 3.3.3 Application for Silver Nanocoral PVDF Substrates

As discussed in Chapter 2, methimazole (MTZ) is one of the thyreostatic drugs that is used to treat hyperthyroidism through regulating the production of thyroid hormones.[85-86] Carbimazole is another antithyroid drug that is metabolized to MTZ to be active after administration.[87] Some of MTZ adverse effects include liver cirrhosis, nephritis, pharyngitis, allergic reactions, and skin irritation.[85-86, 88] In addition, MTZ metabolites have been reported to induce cytotoxic effects.[88] Moreover, MTZ has been reported to induce congenital anomalies upon exposure during pregnancy.[89-91] Cases of aplasia cutis, congenital scalp defects, have been reported in Spain and linked to consuming meat contaminated with MTZ during pregnancy.[92] MTZ has been reported to be used illegally in livestock feed to induce fraudulent weight gain by causing water retention.[85, 92-93] As a result, the European union has banned the use of thyreostats in animal feed.

Previous studies have demonstrated that MTZ has to be administered in a large dosage (400–800 mg per animal per day), with an optimum dose of 600 mg per animal per day to induce weight gain.[94-95] Lower doses of MTZ did not show any effect on weight gain.[95] MTZ is excreted mainly in urine, and a range of 5.5–12% of the administered dose of MTZ was reported to be excreted in human urine.[96-98] Stair and Thornhill have reported that 14–21% of the administered dose of MTZ was excreted unchanged in the 24-hour urine volume in albino rats.[98] However, no studies can be found about the pharmacokinetics and excretion of MTZ in cattle. As discussed earlier in Chapter 2, chromatographic techniques are the most common techniques for MTZ quantification in urine.[86, 99-103] The limit of detection of these techniques is reported to have a concentration range from nanomolar to micromolar.[86, 100-103] Although these chromatographic methods are considered the gold standard for MTZ quantification in urine, they include some extra steps, such as sample extraction, preconcentration, and/or derivatization before analysis.[86, 99-103]

Detection of MTZ in urine of farm animals can provide an early preventive warning before consuming meat that may contain MTZ. The average number of daily urination events in beef cattle is reported to be 7.6 events, and the average urine volume for each event is 1.8 L.[104] Given all of that, if we assume that only 1% of the administered dose (600 mg) of MTZ to a cow to induce fraudulent liveweight gain is excreted in urine, the estimated final concentration of MTZ in 24-hour urine would be ~3.8 μM. Our substrates coupled with a handheld Raman device can provide an inexpensive field tool deployable for the application of preliminary qualitative screening of MTZ in beef cattle urine, as shown in Figure 3-8.

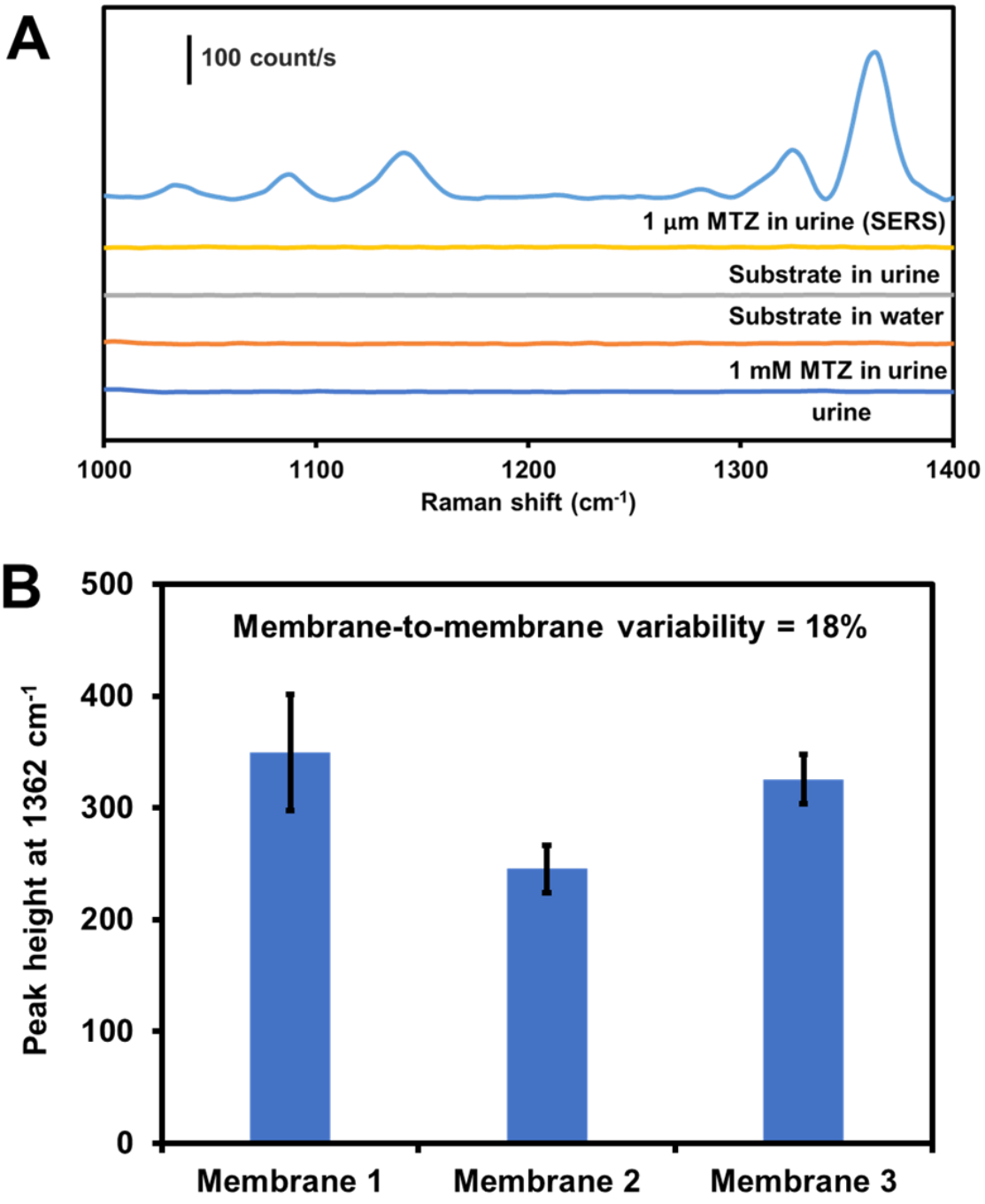


**Figure 3-8. Detection of MTZ in synthetic urine.** (A) Raman spectra of urine blank, 1 mM MTZ in urine, substrate in urine, substrate in water and SERS spectrum of the substrate in µm MTZ in urine using a vial adapter accessory. (B) Bar chart of the peak height at 1364 $cm^{-1}$ of MTZ (error bar is standard deviation of three spots from the same membrane).

Figure 3-8A represents a potential qualitative application of the silver nanocoral SERS substrate to detect MTZ in urine and the associated controls. All spectra in Figure 3-8A were collected from aqueous solutions using a vial adapter accessory. The SERS effect is obvious when the SERS spectrum of 1 μM MTZ in urine solution is compared to the normal Raman spectrum of 1 mM MTZ in urine solution and other associated control experiments. The most characteristic Raman bands of MTZ can be observed in its SERS spectrum, which have been assigned in Chapter 2. The most prominent MTZ Raman band is at 1364 $cm^{-1}$ and is attributed to a combination of a N–C stretching vibration, a ring bend, and a C–N–H in-plane bend.[105-107] We did not observe any Raman bands for the control experiments. MTZ can be adsorbed on silver nanocorals through a Ag–S interaction. It is worth mentioning that a quantitative assay with a linear range of 10 nM-10 μM to determine MTZ in urine and/or in beef would be desired to ensure adherence to the European Union guidelines. We used 1 μM of MTZ, which is less than our estimate of the final concentration of MTZ (~3.8 μM) in the average 24-hour cattle urine volume, as stated previously. In addition, 1 μM of MTZ was similar or less than the limit of detection and quantification of reported chromatographic methods to determine MTZ in urine.[86,103]

The peak height at 1364 $cm^{-1}$ was used to study point-to-point and membrane-to-membrane SERS reproducibility, as shown in Figure 3-8B. Point-to-point variability was determined by the percent relative standard deviation (%RSD) values calculated from three different spots per membrane (n = 3). The point-to-point variability ranged from 7% to 15%, with an average value of 10 ± 4%. The membrane-to-membrane variability was determined using the average of three spots per membrane (n = 3). The membrane-

to-membrane variability was 18%. These values indicate acceptable spot-to-spot and membrane-to-membrane SERS reproducibility and are comparable to other porous SERS substrates.[32, 40, 43-44, 108] In addition, these values also were comparable to those of rigid SERS substrates, where metal nanoparticles were chemically immobilized.[109] We believe that the formation of silver nanocorals with a 3D architecture within the PVDF membrane were distributed well and provided many hot spots for label free detection. Based on the %RSD values, our substrates meet the SERS recommendation parameter to have less than 20% variations.[110-111]

## 3.4 Conclusions

In summary, silver nanocorals have been synthesized via an in-situ deviceless method onto PVDF membranes to be used as SERS substrates. The loading density of the silver nanocorals was the determinant factor for SERS performance optimization of these substrates. SERS performance showed a similar trend using chemisorption and physisorption approaches. The substrates were used for MTZ detection in synthetic urine solution qualitatively showing, homogenous substrate to substrate and point to point reproducibility. Merging porous based SERS substrates and handheld Raman spectrometers can open new avenues for SERS platform development and applications. In future, this method can be applied for on-site synthesis of SERS substrates and detection of various analytes.

## 3.5 References


1. Fleischmann, M.; Hendra, P. J.; McQuillan, A. J., Raman spectra of pyridine adsorbed at a silver electrode. *Chemical Physics Letters* **1974,** *26* (2), 163-166.

2. Jeanmaire, D. L.; Van Duyne, R. P., Surface raman spectroelectrochemistry: Part I. Heterocyclic, aromatic, and aliphatic amines adsorbed on the anodized silver electrode. *Journal of Electroanalytical Chemistry and Interfacial Electrochemistry* **1977,** *84* (1), 1-20.

3. Albrecht, M. G.; Creighton, J. A., Anomalously intense Raman spectra of pyridine at a silver electrode. *Journal of the American Chemical Society* **1977,** *99* (15), 5215-5217.

4. Lombardi, J. R.; Birke, R. L.; Lu, T.; Xu, J., Charge-transfer theory of surface enhanced Raman spectroscopy: Herzberg–Teller contributions. *The Journal of Chemical Physics* **1986,** *84* (8), 4174-4180.

5. Campion, A.; Kambhampati, P., Surface-enhanced Raman scattering. *Chemical Society Reviews* **1998,** *27* (4), 241-250.

6. Kneipp, K.; Kneipp, H.; Itzkan, I.; Dasari, R. R.; Feld, M. S., Surface-enhanced Raman scattering and biophysics. *Journal of Physics: Condensed Matter* **2002,** *14* (18), R597-R624.

7. Lombardi, J. R.; Birke, R. L., A Unified Approach to Surface-Enhanced Raman Spectroscopy. *The Journal of Physical Chemistry C* **2008,** *112* (14), 5605-5617.

8. Kneipp, K.; Wang, Y.; Kneipp, H.; Perelman, L. T.; Itzkan, I.; Dasari, R. R.; Feld, M. S., Single Molecule Detection Using Surface-Enhanced Raman Scattering (SERS). *Physical Review Letters* **1997,** *78* (9), 1667-1670.

9. Nie, S.; Emory, S. R., Probing Single Molecules and Single Nanoparticles by Surface-Enhanced Raman Scattering. *Science* **1997,** *275* (5303), 1102-1106.

10. Sharaabi, Y.; Shegai, T.; Haran, G., Two-state analysis of single-molecule Raman spectra of crystal violet. *Chemical Physics* **2005,** *318* (1), 44-49.

11. Le Ru, E. C.; Meyer, M.; Etchegoin, P. G., Proof of Single-Molecule Sensitivity in Surface Enhanced Raman Scattering (SERS) by Means of a Two-Analyte Technique. *The Journal of Physical Chemistry B* **2006,** *110* (4), 1944-1948.

12. Sharma, B.; Frontiera, R. R.; Henry, A.-I.; Ringe, E.; Van Duyne, R. P., SERS: Materials, applications, and the future. *Materials Today* **2012,** *15* (1), 16-25.

13. Fikiet, M. A.; Khandasammy, S. R.; Mistek, E.; Ahmed, Y.; Halámková, L.; Bueno, J.; Lednev, I. K., Surface enhanced Raman spectroscopy: A review of recent applications in forensic science. *Spectrochimica Acta Part A: Molecular and Biomolecular Spectroscopy* **2018,** *197*, 255-260.

14. Stiles, P. L.; Dieringer, J. A.; Shah, N. C.; Duyne, R. P. V., Surface-Enhanced Raman Spectroscopy. *Annual Review of Analytical Chemistry* **2008,** *1* (1), 601-626.

15. Qian, X. M.; Nie, S. M., Single-molecule and single-nanoparticle SERS: from fundamental mechanisms to biomedical applications. *Chemical Society Reviews* **2008,** *37* (5), 912-920.

16. Pang, S.; Yang, T.; He, L., Review of surface enhanced Raman spectroscopic (SERS) detection of synthetic chemical pesticides. *TrAC Trends in Analytical Chemistry* **2016,** *85*, 73-82.

17. Chen, N.; Ding, P.; Shi, Y.; Jin, T.; Su, Y.; Wang, H.; He, Y., Portable and Reliable Surface-Enhanced Raman Scattering Silicon Chip for Signal-On Detection of Trace Trinitrotoluene Explosive in Real Systems. *Analytical Chemistry* **2017,** *89* (9), 5072-5078.

18. Mojica, E.-R. E.; Zapata, J.; Vedad, J.; Desamero, R. Z. B.; Dai, Z., Analysis of Over-the-Counter Drugs Using Raman Spectroscopy. In *Raman Spectroscopy in the Undergraduate Curriculum*, American Chemical Society: 2018; Vol. 1305, pp 69-91.

19. Sarfo, D. K.; Izake, E. L.; O'Mullane, A. P.; Ayoko, G. A., Molecular recognition and detection of Pb(II) ions in water by aminobenzo-18-crown-6 immobilised onto a nanostructured SERS substrate. *Sensors and Actuators B: Chemical* **2018,** *255*, 1945-1952.

20. Saviello, D.; Di Gioia, A.; Turenne, P.-I.; Trabace, M.; Giorgi, R.; Mirabile, A.; Baglioni, P.; Iacopino, D., Handheld surface-enhanced Raman scattering identification of dye chemical composition in felt-tip pen drawings. *Journal of Raman Spectroscopy* **2019,** *50* (2), 222-231.

21. Karabeber, H.; Huang, R.; Iacono, P.; Samii, J. M.; Pitter, K.; Holland, E. C.; Kircher, M. F., Guiding Brain Tumor Resection Using Surface-Enhanced Raman Scattering Nanoparticles and a Hand-Held Raman Scanner. *ACS Nano* **2014,** *8* (10), 9755-9766.

22. Hakonen, A.; Rindzevicius, T.; Schmidt, M. S.; Andersson, P. O.; Juhlin, L.; Svedendahl, M.; Boisen, A.; Käll, M., Detection of nerve gases using surface-enhanced Raman scattering substrates with high droplet adhesion. *Nanoscale* **2016,** *8* (3), 1305-1308.

23. Hakonen, A.; Wu, K. Y.; Schmidt, M. S.; Andersson, P. O.; Boisen, A.; Rindzevicius, T., Detecting forensic substances using commercially available SERS substrates and handheld Raman spectrometers. *Talanta* **2018,** *189*, 649-652.

24. Hassanain, W. A.; Izake, E. L.; Schmidt, M. S.; Ayoko, G. A., Gold nanomaterials for the selective capturing and SERS diagnosis of toxins in aqueous and biological fluids. *Biosensors and Bioelectronics* **2017,** *91*, 664-672.

25. Agoston, R.; Izake, E. L.; Sivanesan, A.; Lott, W. B.; Sillence, M.; Steel, R., Rapid isolation and detection of erythropoietin in blood plasma by magnetic core gold nanoparticles and portable Raman spectroscopy. *Nanomedicine: Nanotechnology, Biology and Medicine* **2016,** *12* (3), 633-641.

26. Hassanain, W. A.; Izake, E. L.; Ayoko, G. A., Spectroelectrochemical Nanosensor for the Determination of Cystatin C in Human Blood. *Analytical Chemistry* **2018,** *90* (18), 10843-10850.

27. Nuntawong, N.; Eiamchai, P.; Limwichean, S.; Wong-ek, B.; Horprathum, M.; Patthanasettakul, V.; Leelapojanaporn, A.; Nakngoenthong, S.; Chindaudom, P., Trace detection of perchlorate in industrial-grade emulsion explosive with portable surface-enhanced Raman spectroscopy. *Forensic Science International* **2013,** *233* (1), 174-178.

28. Wu, X.; Xu, C.; Tripp, R. A.; Huang, Y.-w.; Zhao, Y., Detection and differentiation of foodborne pathogenic bacteria in mung bean sprouts using field deployable label-free SERS devices. *Analyst* **2013,** *138* (10), 3005-3012.

29. Owens, N. A.; Laurentius, L. B.; Porter, M. D.; Li, Q.; Wang, S.; Chatterjee, D., Handheld Raman Spectrometer Instrumentation for Quantitative Tuberculosis Biomarker Detection: A Performance Assessment for Point-of-Need Infectious Disease Diagnostics. *Applied Spectroscopy* **2018,** *72* (7), 1104-1115.

30. Schmidt, M. S.; Hübner, J.; Boisen, A., Large Area Fabrication of Leaning Silicon Nanopillars for Surface Enhanced Raman Spectroscopy. *Advanced Materials* **2012,** *24* (10), OP11-OP18.

31. SILMECO. SERS Substrates. https://shop.silmeco.com/?wmc-currency=USD (accessed 4 December 2019).

32. Lee, C. H.; Hankus, M. E.; Tian, L.; Pellegrino, P. M.; Singamaneni, S., Highly Sensitive Surface Enhanced Raman Scattering Substrates Based on Filter Paper Loaded with Plasmonic Nanostructures. *Analytical Chemistry* **2011,** *83* (23), 8953-8958.

33. Lee, C. H.; Tian, L.; Singamaneni, S., Paper-Based SERS Swab for Rapid Trace Detection on Real-World Surfaces. *ACS Applied Materials & Interfaces* **2010,** *2* (12), 3429-3435.

34. Abbas, A.; Brimer, A.; Slocik, J. M.; Tian, L.; Naik, R. R.; Singamaneni, S., Multifunctional Analytical Platform on a Paper Strip: Separation, Preconcentration, and Subattomolar Detection. *Analytical Chemistry* **2013,** *85* (8), 3977-3983.

35. Ross, M. B.; Ashley, M. J.; Schmucker, A. L.; Singamaneni, S.; Naik, R. R.; Schatz, G. C.; Mirkin, C. A., Structure–Function Relationships for Surface-Enhanced Raman Spectroscopy-Active Plasmonic Paper. *The Journal of Physical Chemistry C* **2016,** *120* (37), 20789-20797.

36. Yu, W. W.; White, I. M., Inkjet Printed Surface Enhanced Raman Spectroscopy Array on Cellulose Paper. *Analytical Chemistry* **2010,** *82* (23), 9626-9630.

37. Yu, W. W.; White, I. M., Inkjet-printed paper-based SERS dipsticks and swabs for trace chemical detection. *Analyst* **2013,** *138* (4), 1020-1025.

38. Hoppmann, E. P.; Yu, W. W.; White, I. M., Highly sensitive and flexible inkjet printed SERS sensors on paper. *Methods* **2013,** *63* (3), 219-224.

39. Zhang, W.; Li, B.; Chen, L.; Wang, Y.; Gao, D.; Ma, X.; Wu, A., Brushing, a simple way to fabricate SERS active paper substrates. *Analytical Methods* **2014,** *6* (7), 2066-2071.

40. Polavarapu, L.; Porta, A. L.; Novikov, S. M.; Coronado-Puchau, M.; Liz-Marzán, L. M., Pen-on-Paper Approach Toward the Design of Universal Surface Enhanced Raman Scattering Substrates. *Small* **2014,** *10* (15), 3065-3071.

41. Yu, W. W.; White, I. M., A simple filter-based approach to surface enhanced Raman spectroscopy for trace chemical detection. *Analyst* **2012,** *137* (5), 1168-1173.

42. Au - Gao, S.; Au - Glasser, J.; Au - He, L., A Filter-based Surface Enhanced Raman Spectroscopic Assay for Rapid Detection of Chemical Contaminants. *JoVE* **2016,** (108), e53791.

43. Herrera-Sandoval, G. M.; Felix-Rivera, H.; Padilla-Jimenez, A. C.; Balaguera-Gelves, M.; Ortega-Zuniga, C. A.; Pacheco-Londono, L. C.; Primera-Pedrozo, O. M.; Fierro, P. M.; Rios-Velazquez, C.; Hernandez-Rivera, S. P. In *Synthesis and characterization of silver nanoparticles and nanostructures for SERS applications*, Nova Science Publishers, Inc.: 2013; pp 59-100.

44. Qu, L.-L.; Li, D.-W.; Xue, J.-Q.; Zhai, W.-L.; Fossey, J. S.; Long, Y.-T., Batch fabrication of disposable screen printed SERS arrays. *Lab on a Chip* **2012,** *12* (5), 876-881.

45. Kim, W.-S.; Shin, J.-H.; Park, H.-K.; Choi, S., A low-cost, monometallic, surface-enhanced Raman scattering-functionalized paper platform for spot-on bioassays. *Sensors and Actuators B: Chemical* **2016,** *222*, 1112-1118.

46. Zheng, J.; Zhao, C.; Tian, G.; He, L., Rapid screening for ricin toxin on letter papers using surface enhanced Raman spectroscopy. *Talanta* **2017,** *162*, 552-557.

47. Zeng, F.; Duan, W.; Zhu, B.; Mu, T.; Zhu, L.; Guo, J.; Ma, X., Paper-Based Versatile Surface-Enhanced Raman Spectroscopy Chip with Smartphone-Based Raman Analyzer for Point-of-Care Application. *Analytical Chemistry* **2019,** *91* (1), 1064-1070.

48. Zeng, F.; Mou, T.; Zhang, C.; Huang, X.; Wang, B.; Ma, X.; Guo, J., Paper-based SERS analysis with smartphones as Raman spectral analyzers. *Analyst* **2019,** *144* (1), 137-142.

49. Menges, F. Spectragryph - Optical Spectroscopy Software, Version 1.2.10; 2018; http://www.effemm2.de/spectragryph/.

50. Leopold, N.; Lendl, B., A New Method for Fast Preparation of Highly Surface-Enhanced Raman Scattering (SERS) Active Silver Colloids at Room Temperature by Reduction of Silver Nitrate with Hydroxylamine Hydrochloride. *The Journal of Physical Chemistry B* **2003,** *107* (24), 5723-5727.

51. Kise, H.; Ogata, H., Phase transfer catalysis in dehydrofluorination of poly(vinylidene fluoride) by aqueous sodium hydroxide solutions. *Journal of Polymer Science: Polymer Chemistry Edition* **1983,** *21* (12), 3443-3451.

52. Awanis Hashim, N.; Liu, Y.; Li, K., Stability of PVDF hollow fibre membranes in sodium hydroxide aqueous solution. *Chemical Engineering Science* **2011,** *66* (8), 1565-1575.

53. Rabuni, M. F.; Nik Sulaiman, N. M.; Aroua, M. K.; Hashim, N. A., Effects of Alkaline Environments at Mild Conditions on the Stability of PVDF Membrane: An Experimental Study. *Industrial & Engineering Chemistry Research* **2013,** *52* (45), 15874-15882.

54. Notte, J.; Ward, B.; Economou, N.; Hill, R.; Percival, R.; Farkas, L.; McVey, S., An Introduction to the Helium Ion Microscope. *AIP Conference Proceedings* **2007,** *931* (1), 489-496.

55. Joens, M. S.; Huynh, C.; Kasuboski, J. M.; Ferranti, D.; Sigal, Y. J.; Zeitvogel, F.; Obst, M.; Burkhardt, C. J.; Curran, K. P.; Chalasani, S. H.; Stern, L. A.; Goetze, B.; Fitzpatrick, J. A. J., Helium Ion Microscopy (HIM) for the imaging of biological samples at sub-nanometer resolution. *Scientific Reports* **2013,** *3*, 3514.

56. Feng, J.-J.; Hildebrandt, P.; Murgida, D. H., Silver Nanocoral Structures on Electrodes: A Suitable Platform for Protein-Based Bioelectronic Devices. *Langmuir* **2008,** *24* (5), 1583-1586.

57. Wang, Y.; Camargo, P. H. C.; Skrabalak, S. E.; Gu, H.; Xia, Y., A Facile, Water-Based Synthesis of Highly Branched Nanostructures of Silver. *Langmuir* **2008,** *24* (20), 12042-12046.

58. Yuan, L.; Lu, S.; Yang, F.; Wang, Y.; Jia, Y.; Kadhim, M. S.; Yu, Y.; Zhang, Y.; Zhao, Y., A facile room-temperature synthesis of three-dimensional coral-like Ag2S nanostructure with enhanced photocatalytic activity. *Journal of Materials Science* **2019,** *54* (4), 3174-3186.

59. El-Sayed, M. A., Some Interesting Properties of Metals Confined in Time and Nanometer Space of Different Shapes. *Accounts of Chemical Research* **2001,** *34* (4), 257-264.

60. Mulvaney, P., Surface Plasmon Spectroscopy of Nanosized Metal Particles. *Langmuir* **1996,** *12* (3), 788-800.

61. Murphy, C. J.; Sau, T. K.; Gole, A. M.; Orendorff, C. J.; Gao, J.; Gou, L.; Hunyadi, S. E.; Li, T., Anisotropic Metal Nanoparticles: Synthesis, Assembly, and Optical Applications. *The Journal of Physical Chemistry B* **2005,** *109* (29), 13857-13870.

62. Chandra, K.; Culver, K. S. B.; Werner, S. E.; Lee, R. C.; Odom, T. W., Manipulating the Anisotropic Structure of Gold Nanostars using Good's Buffers. *Chemistry of Materials* **2016,** *28* (18), 6763-6769.

63. Haiss, W.; Thanh, N. T. K.; Aveyard, J.; Fernig, D. G., Determination of Size and Concentration of Gold Nanoparticles from UV−Vis Spectra. *Analytical Chemistry* **2007,** *79* (11), 4215-4221.

64. Berger, A. G.; Restaino, S. M.; White, I. M., Vertical-flow paper SERS system for therapeutic drug monitoring of flucytosine in serum. *Anal. Chim. Acta* **2017,** *949*, 59-66.

65. Betz, J. F.; Yu, W. W.; Cheng, Y.; White, I. M.; Rubloff, G. W., Simple SERS substrates: powerful, portable, and full of potential. *Phys. Chem. Chem. Phys.* **2014,** *16* (6), 2224-2239.

66. Hoppmann, E. P.; White, I. M., A paper-based inkjet-fabricated substrate for SERS detection and differentiation of PCR products. *Proc. SPIE* **2013,** *8718* (Advanced Environmental, Chemical, and Biological Sensing Technologies X), 871804/1-871804/6.

67. Hoppmann, E. P.; Yu, W. W.; White, I. M., Inkjet-printed fluidic paper devices for chemical and biological analytics using surface enhanced Raman spectroscopy. *IEEE J. Sel. Top. Quantum Electron.* **2014,** *20* (3), 7300510/1-7300510/10.

68. Hoppmann, E. P.; Yu, W. W.; White, I. M., Detection of deoxyribonucleic acid (DNA) targets using polymerase chain reaction (PCR) and paper surface-enhanced Raman spectroscopy (SERS) chromatography. *Appl. Spectrosc.* **2014,** *68* (8), 909-915.

69. White, I. M., Optofluidic SERS on inkjet-fabricated paper-based substrates. *Proc. SPIE* **2012,** *8264* (Integrated Optics: Devices, Materials, and Technologies XVI), 826414/1-826414/6.

70. Yu, W. W.; White, I. M., Paper-based optofluidic SERS using ink-jet-printed substrates. *Proc. SPIE* **2011,** *7911* (Plasmonics in Biology and Medicine VIII), 791105/1-791105/6.

71. Yu, W. W.; White, I. M., Chromatographic separation and detection of target analytes from complex samples using inkjet printed SERS substrates. *Analyst (Cambridge, U. K.)* **2013,** *138* (13), 3679-3686.

72. Kim, W.; Kim, Y.-H.; Park, H.-K.; Choi, S., Facile Fabrication of a Silver Nanoparticle Immersed, Surface-Enhanced Raman Scattering Imposed Paper Platform through Successive Ionic Layer Absorption and Reaction for On-Site Bioassays. *ACS Applied Materials & Interfaces* **2015,** *7* (50), 27910-27917.

73. Kim, W.; Lee, J.-C.; Lee, G.-J.; Park, H.-K.; Lee, A.; Choi, S., Low-Cost Label-Free Biosensing Bimetallic Cellulose Strip with SILAR-Synthesized Silver Core–Gold Shell Nanoparticle Structures. *Analytical Chemistry* **2017,** *89* (12), 6448-6454.

74. Kim, W.; Lee, S. H.; Kim, J. H.; Ahn, Y. J.; Kim, Y.-H.; Yu, J. S.; Choi, S., Paper-Based Surface-Enhanced Raman Spectroscopy for Diagnosing Prenatal Diseases in Women. *ACS Nano* **2018,** *12* (7), 7100-7108.

75. Lee, J.-C.; Kim, W.; Park, H.-K.; Choi, S., Controlling successive ionic layer absorption and reaction cycles to optimize silver nanoparticle-induced localized surface plasmon resonance effects on the paper strip. *Spectrochimica Acta Part A: Molecular and Biomolecular Spectroscopy* **2017,** *174*, 37-43.

76. Ashley, M. J.; Bourgeois, M. R.; Murthy, R. R.; Laramy, C. R.; Ross, M. B.; Naik, R. R.; Schatz, G. C.; Mirkin, C. A., Shape and Size Control of Substrate-Grown Gold Nanoparticles for Surface-Enhanced Raman Spectroscopy Detection of Chemical Analytes. *The Journal of Physical Chemistry C* **2018,** *122* (4), 2307-2314.

77. Brittain, H. G., 3 - Solid-State Analysis. In *Separation Science and Technology*, Ahuja, S.; Scypinski, S., Eds. Academic Press: 2001; Vol. 3, pp 57-84.

78. Danielson, S. J., 22 - THIN-FILM IMMUNOASSAYS. In *Immunoassay*, Diamandis, E. P.; Christopoulos, T. K., Eds. Academic Press: San Diego, 1996; pp 505-535.

79. Blitz, J. P., Diffuse reflectance spectroscopy. *Modern Techniques in Applied Molecular Spectroscopy* **1998**, 185-219.

80. Viscarra Rossel, R. A.; McGlynn, R. N.; McBratney, A. B., Determining the composition of mineral-organic mixes using UV–vis–NIR diffuse reflectance spectroscopy. *Geoderma* **2006,** *137* (1), 70-82.

81. Pristinski, D.; Tan, S. L.; Erol, M.; Du, H.; Sukhishvili, S., In situ SERS study of Rhodamine 6G adsorbed on individually immobilized Ag nanoparticles. *Journal of Raman Spectroscopy* **2006,** *37* (7), 762-770.

82. Gkogkou, D.; Schreiber, B.; Shaykhutdinov, T.; Ly, H. K.; Kuhlmann, U.; Gernert, U.; Facsko, S.; Hildebrandt, P.; Esser, N.; Hinrichs, K.; Weidinger, I. M.; Oates, T. W. H., Polarization- and Wavelength-Dependent Surface-Enhanced Raman Spectroscopy Using Optically Anisotropic Rippled Substrates for Sensing. *ACS Sensors* **2016,** *1* (3), 318-323.

83. Holze, R., Competition of anchoring groups in adsorption on gold electrodes—a comparative spectroelectrochemical study of 4-mercaptobenzonitrile and aromatic nitriles. *Journal of Solid State Electrochemistry* **2013,** *17* (7), 1869-1879.

84. Villarreal, E.; Li, G. G.; Zhang, Q.; Fu, X.; Wang, H., Nanoscale Surface Curvature Effects on Ligand–Nanoparticle Interactions: A Plasmon-Enhanced Spectroscopic Study of Thiolated Ligand Adsorption, Desorption, and Exchange on Gold Nanoparticles. *Nano Letters* **2017,** *17* (7), 4443-4452.

85. Ebrahimzadeh, H.; Asgharinezhad, A. A.; Adlnasab, L.; Shekari, N., Optimization of ion-pair based hollow fiber liquid phase microextraction combined with HPLC–UV for the determination of methimazole in biological samples and animal feed. *Journal of Separation Science* **2012,** *35* (16), 2040-2047.

86. Kuśmierek, K.; Bald, E., Determination of methimazole in urine by liquid chromatography. *Talanta* **2007,** *71* (5), 2121-2125.

87. Skellern, G.; Knight, B.; Low, C.; Alexander, W.; McLarty, D.; Kalk, W., The pharmacokinetics of methimazole after oral administration of carbimazole and methimazole, in hyperthyroid patients. *British Journal of Clinical Pharmacology* **1980,** *9* (2), 137-143.

88. Genter, M. B., Evaluation of olfactory and auditory system effects of the antihyperthyroid drug carbimazole in the Long-Evans rat. *Journal of Biochemical and Molecular Toxicology* **1998,** *12* (5), 305-314.

89. Clementi, M.; Di Gianantonio, E.; Pelo, E.; Mammi, I.; Basile, R. T.; Tenconi, R., Methimazole embryopathy: Delineation of the phenotype. *American Journal of Medical Genetics* **1999,** *83* (1), 43-46.

90. Diav-Citrin, O.; Ornoy, A., Teratogen update: antithyroid drugs—methimazole, carbimazole, and propylthiouracil. *Teratology* **2002,** *65* (1), 38-44.

91. Cassina, M.; Donà, M.; Di Gianantonio, E.; Clementi, M., Pharmacologic treatment of hyperthyroidism during pregnancy. *Birth Defects Research Part A: Clinical and Molecular Teratology* **2012,** *94* (8), 612-619.

92. Martínez-Frías, M. L.; Cereijo, A.; Rodríguez-Pinilla, E.; Urioste, M., Methimazole in animal feed and congenital aplasia cutis. *The Lancet* **1992,** *339* (8795), 742-743.

93. Kong, D.; Chi, Y.; Chen, L.; Dong, Y.; Zhang, L.; Chen, G., Determination of thyreostatics in animal feeds by CE with electrochemical detector. *ELECTROPHORESIS* **2009,** *30* (19), 3489-3495.

94. BURROUGHS, W.; RAUN, A.; CHENG, E., Effects of Methimazole on Thyroid and Live Weights of Cattle. *Science* **1958,** *128* (3316), 147-147.

95. Burroughs, W.; Raun, A.; Trenkle, A.; Raun, N., Further Observations upon the Effects of Methimazole upon Feedlot Performance and Carcass Characteristics of Fattening Beef Cattle. *Journal of Animal Science* **1960,** *19* (2), 465-469.

96. Pittman, J. A.; Beschi, R. J.; Smitherman, T. C., Methimazole: Its Absorption and Excretion in Man and Tissue Distribution in Rats. *The Journal of Clinical Endocrinology & Metabolism* **1971,** *33* (2), 182-185.

97. Okamura, Y.; Shigemasa, C.; Tatsuhara, T., Pharmacokinetics of Methimazole in Normal Subjects and Hyperthyroid Patients. *Endocrinologia Japonica* **1986,** *33* (5), 605-615.

98. Sitar, D. S.; Thornhill, D. P., Methimazole: Absorption, Metabolism and Excretion in the Albino Rat. *Journal of Pharmacology and Experimental Therapeutics* **1973,** *184* (2), 432-439.

99. Lawrence, J. F.; Iverson, F.; Hanekamp, H. B.; Bos, P.; Frei, R. W., Liquid chromatography with UV absorbance and polarographic detection of ethylenethiourea and related sulfur compounds: Application to rat urine analysis. *Journal of Chromatography A* **1981,** *212* (2), 245-250.

100. Batjoens, P.; De Brabander, H. F.; De Wasch, K., Rapid and high-performance analysis of thyreostatic drug residues in urine using gas chromatography-mass spectrometry. *Journal of Chromatography A* **1996,** *750* (1), 127-132.

101. John Blanchflower, W.; J. Hughes, P.; Cannavan, A.; A. McCoy, M.; Glenn Kennedy, D., Determination of Thyreostats in Thyroid and Urine Using High-performance Liquid Chromatography–Atmospheric Pressure Chemical Ionisation Mass Spectrometry. *Analyst* **1997,** *122* (9), 967-972.

102. Zakrzewski, R., Determination of methimazole in urine with the iodine-azide detection system following its separation by reversed-phase high-performance liquid chromatography. *Journal of Chromatography B* **2008,** *869* (1), 67-74.

103. Tölgyesi, Á.; Giri, A.; Barta, E.; McDonald, T. J.; Sharma, V. K., Determination of Thyreostats in Urine Using Supported Liquid Extraction and Mixed-Mode Cation-Exchange Solid-Phase Extraction: Screening and Confirmatory Methods. *Journal of Chromatographic Science* **2018,** *56* (9), 858-866.

104. Misselbrook, T.; Fleming, H.; Camp, V.; Umstatter, C.; Duthie, C. A.; Nicoll, L.; Waterhouse, T., Automated monitoring of urination events from grazing cattle. *Agriculture, Ecosystems & Environment* **2016,** *230*, 191-198.

105. Fei, J.; Wu, L.; Zhang, Y.; Zong, S.; Wang, Z.; Cui, Y., Pharmacokinetics-on-a-Chip Using Label-Free SERS Technique for Programmable Dual-Drug Analysis. *ACS Sensors* **2017,** *2* (6), 773-780.

106. Ma, P.; Liang, F.; Yang, Q.; Wang, D.; Sun, Y.; Wang, X.; Gao, D.; Song, D., Highly sensitive SERS probe for mercury(II) using cyclodextrin-protected silver nanoparticles functionalized with methimazole. *Microchimica Acta* **2014,** *181* (9), 975-981.

107. Saleh, T. A.; Al-Shalalfeh, M. M.; Al-Saadi, A. A., Silver nanoparticles for detection of methimazole by surface-enhanced Raman spectroscopy. *Materials Research Bulletin* **2017,** *91*, 173-178.

108. Haddad, A.; Comanescu, M. A.; Green, O.; Kubic, T. A.; Lombardi, J. R., Detection and Quantitation of Trace Fentanyl in Heroin by Surface-Enhanced Raman Spectroscopy. *Analytical Chemistry* **2018,** *90* (21), 12678-12685.

109. de Albuquerque, C. D. L.; Sobral-Filho, R. G.; Poppi, R. J.; Brolo, A. G., Digital Protocol for Chemical Analysis at Ultralow Concentrations by Surface-Enhanced Raman Scattering. *Analytical Chemistry* **2018,** *90* (2), 1248-1254.

110. Natan, M. J., Concluding Remarks Surface enhanced Raman scattering. *Faraday Discussions* **2006,** *132*, 321-328.

111. Lin, X.-M.; Cui, Y.; Xu, Y.-H.; Ren, B.; Tian, Z.-Q., Surface-enhanced Raman spectroscopy: substrate-related issues. *Analytical and Bioanalytical Chemistry* **2009,** *394* (7), 1729-1745.

# Chapter 4

# Optimization of Colloidal Gold Nanostars as a SERS Substrate for the Measurements of Methimazole in Urine Using a Handheld Raman Spectrometer*



*Some of the contents of this chapter have been reproduced and/or adapted from the following publication: "Mahmoud, A. Y. F.; Rusin, C. J.; McDermott, M. T., Gold nanostars as a colloidal substrate for in-solution SERS measurements using a handheld Raman spectrometer. *Analyst* **2020,** *145* (4), 1396-1407." with permission from the Royal Society of Chemistry.

## 4.1 Introduction

Anisotropic gold nanostructures have been synthesized in many different shapes, such as rods,[1-2] cubes,[3] bipyramids,[4] cages,[5] prisms,[6] nanostars,[7-9] etc. The localized surface plasmon resonance (LSPR) of these structures is tuneable over a wide wavelength range when compared to spherical nanoparticles.[10-13] Previous reports have shown that plasmonic excitation of anisotropic nanoparticles results in intense electric fields, characteristically localized at their sharp edges.[10-13] This phenomenon is called the "lightening rod" effect [14] and can improve SERS enhancement significantly, providing that the shape and the size of these particles are uniform.[10-13]

Gold nanostars (Au NS) are an example of anisotropic nanoparticles, which have attracted a lot of interest as a possible SERS substrate because of their multiple branches. Byrne and co-workers have shown that the SERS enhancement of R6G adsorbed onto Au NS was more pronounced than that of nanotriangles and nanospheres.[15] Rodríguez-Lorenzo et al. reported a zeptomole detection limit of 1,5-naphtalenedithiol by sandwiching the molecule between a gold substrate and the tips of Au NS.[16] Indrasekara et al. attached Au NS onto a thin gold film using a short amine terminated alkanethiol.[17] The substrate had an enhancement factor up to five orders of magnitude higher than that of gold nanospheres and achieved a femtomolar level of detection of 4-mercaptobenzoic acid.[17] The Haes group has used Au NS functionalized with carboxylic acid terminated alkanethiols for uranyl detection.[18-19] The Hamad–Schifferli group has integrated the use of Au NS in sandwich lateral flow SERS assays for the detection of human immunoglobulin G, Zika, and dengue biomarkers.[20-21]

The Au NS are synthesized via two main approaches, seed-mediated and seedless growth protocols. The first approach is a two-step approach that requires the synthesis of isotropic gold nanoseeds, and anisotropic structures are grown on the seeds.[15-17, 22-24] For example, the nanoseeds are grown into Au NS by the reduction of $HAuCl_4$ using ascorbic acid in the presence of cetyltrimethylammonium bromide and $AgNO_3$.[15, 23] In addition, nanoseeds can be grown into Au NS when $HAuCl_4$ is reduced using N,N-dimethylformamide in the presence of poly(vinylpyrrolidone).[16, 22] Gold nanoseeds also can be grown into Au NS by the reduction of $HAuCl_4$ using ascorbic acid in the presence of HCl and $AgNO_3$.[17, 24]

The second approach is a single step one-pot synthesis approach. In this approach Au NS are synthesized by the reduction of $HAuCl_4$ using Good's buffers. The most commonly used Good's buffer to synthesize Au NS are 4-(2-hydroxyethyl)-1-piperazineethanesulfonic acid (HEPES),[7-8, 25-26] and 4-(2-hydroxyethyl)-1-piperazinepropanesulfonic acid (EPPS).[25-27] A third buffer, 3-(N-morpholino)propanesulfonic acid (MOPS),[25] also has been used to synthesize Au NS. The tertiary amines from the piperazine group form cationic free radicals and act as the reducing agent for Au ions.[7, 25, 28-29] The terminal alkanesulfonate group acts as a shaping-directing agent and promotes bilayer formation on the Au NS.[25-26, 30] The terminal hydroxyl groups promote the bilayer formation and shape stability via hydrogen bonding.[25-26] The hydrophilic nature of the hydroxyl groups also provides water dispersibility and colloidal stability to the Au NS.[26] The simplicity of the one-pot seedless synthesis approach of Au NS using Good's buffers has attracted attention for various applications.[18-21, 27, 31] These nanostars have been applied in many SERS applications

using different synthesis conditions.[18-21] The plasmonic behaviour of Au NS has been optimized systematically by varying some experimental conditions, such as the concentration ratio of Good's buffer to $HAuCl_4$, the choice of Good's buffer, and the pH of the reaction.[25] However, the effect of these various conditions on the SERS performance of these Au NS has not been investigated.[25]

Herein, we are exploring the colloidal SERS performance of Au NS synthesized using HEPES and EPPS buffers at numerous ratios with and without using an aggregating agent. This is to determine the optimal buffer and buffer to gold ratio for colloidal SERS analysis. The Au NS are characterized based on their LSPR, shape and size, and Raman enhancement. This study relied on the use of a handheld Raman spectrometer for in solution SERS performance of these Au NS. After optimization, the Au NS were used as a dispersible substrate to detect a variety of analytes via chemisorption and physisorption mechanisms in solution as a proof-of-concept. A SERS assay was developed to detect and quantify methimazole (MTZ) in synthetic urine. All Raman analyses are performed using a handheld Raman device to show the field deployability aspect of a colloidal Au NS substrate and promote rapid in-process and quality control of the measurements.

## 4.2 Experimental

### 4.2.1 Reagents

Chloroauric acid (99.995%, $HAuCl_4$), 4-(2-hydroxyethyl)-1-piperazineethanesulfonic acid buffer solution (1 M in $H_2O$, HEPES), 4-(2-hydroxyethyl)-1-piperazinepropanesulfonic acid (99.5%, EPPS), sodium chloride (≥99.5%, NaCl), malachite green oxalate salt, technical grade (MG), methimazole (analytical standard,

MTZ), ciprofloxacin (≥98%, Cipro) , and Surine™ negative urine control were purchased from Sigma-Aldrich Canada (Oakville, Ontario). 4-mercaptobenzonitrile (MBN) was purchased from Combi-Blocks, Inc. (San Diego, California, USA) and sodium hydroxide (NaOH) was purchased from Fisher Scientific Canada. Transmission electron microscopy (TEM) grids (400-mesh carbon) were purchased from Electron Microscopy Sciences. Fisherbrand™ Class A clear glass threaded vials (1 dram) were purchased from Fisher Scientific Canada. Deionized (DI) water (18.2 MΩ cm) was used for all syntheses and measurements in this work.

### 4.2.2 Preparation of Gold Nanostars

Au NS were synthesized according to previously developed methods, with slight modifications.[25] The pH of the 1 M HEPES buffer solution was adjusted to 7.20 ± 0.01 using a solution of 1 M NaOH and a Fisher Scientific accumet research AR15 pH meter. Similarly, a solution of 0.5 M EPPS buffer was prepared in DI water, and the pH was adjusted to 7.20 ± 0.01. A stock solution of $HAuCl_4$ (26 mM) was prepared in DI water. The synthesis of Au NS is governed by the ratio of the precursors in solution and is defined as R = [Buffer]/[$HAuCl_4$], where [Buffer] is the concentration of HEPES or EPPS, and [$HAuCl_4$] is held constant at 0.2 mM. The ratios assessed for each buffer in this work are 100, 300, 500, 700, and 1000 (buffer concentration = 20, 60, 100, 140 and 200 mM, respectively). The Good's buffer is mixed initially with DI water at 400 rpm, then $HAuCl_4$ solution is added and mixed for 5 min, after which the solution is removed and stored in the dark for 24 h. Throughout this chapter a "codename" is used to describe the Au NS such as HR100. The first letter (in this case H) is the buffer used, where H stands for

HEPES and E stands for EPPS, the R represents ratio, and the numbers represent the ratio being examined.

### 4.2.3 Characterization

#### 4.2.3.1 UV-vis spectroscopy

UV-vis spectroscopy experiments were carried out using a PerkinElmer Lambda 35 spectrometer. All experiments used a slit width of 1 nm and a scan rate of 960 nm/min. The samples were analyzed in 1.5 mL BRAND® polystyrene disposable cuvettes (unless stated otherwise) and monitored from 400 to 1000 nm.

#### 4.2.3.2 Scanning and transmission electron microscopy

Scanning electron microscopy (SEM) was performed using a Hitachi S-4800 field emission SEM, and transmission electron microscopy (TEM) imaging was performed using a JEOL JEM-ARM200CF S/TEM. Samples underwent a washing step to remove excess buffer by centrifuging three times at 12000 rpm for 10 min, 9000 rpm for 10 min, and 6000 rpm for 10 min (Eppendorf Centrifuge 5417 R). The samples were re-dispersed in water and sonicated for 2 min between centrifugation steps. After the final centrifugation step the sample was concentrated by a factor of 10 for imaging. The sample (10 μL) was drop-casted onto a TEM grid for 10 min, and the excess solution was wicked away. For SEM imaging, the samples were imaged at 30 kV and 20 μA. For TEM imaging, the samples were imaged at 200 kV. Image processing and analysis was completed using Gatan Digital Micrograph software.

#### 4.2.3.3 Dynamic light scattering and zeta potential

Dynamic light scattering (DLS) and zeta potential experiments of Au NS were determined using a Malvern Zetasizer Nano-ZS. The instrument is equipped with a 4-mW HeNe laser

(633 nm) and a 173 ° backscattering angle. The 1-mL aliquot samples were measured in 2.5-mL BRAND® polystyrene disposable cuvettes (pathlength = 1 cm). Each measurement was performed with an equilibrium time of 120 s and at a temperature of 25 °C. For the DLS experiment, the standard deviation is representative of n = 5, with each measurement consisting of 13 sub-runs. For the zeta potential experiment, the standard deviation is representative of n = 3, with each measurement consisting of 20 sub-runs.

### 4.2.4 Raman Analysis

Raman analysis using the Au NS was completed with a B&W Tek TacticID handheld Raman device. The device was automatically calibrated using a polystyrene sample, and all samples were analyzed using a liquid cell adapter at 100% power (300 mW). All measurements were performed in 1-dram vials. The analytes were mixed with the Au NS for 2 min using a vortex before analysis. Studies regarding salt were mixed for an additional 2 min after the addition of NaCl (total of 4 min) before taking the measurement. All samples contained the same concentration of Au NS and a total sample volume of 1 mL.

The SERS performance of the Au NS were compared between the B&W Tek TacticID handheld Raman device and two other Raman systems, Renishaw in-via Raman microscope and DeltaNu benchtop Raman spectrometer. Measurements using the Renishaw Raman microscope were performed using a 90° angle liquid cell holder. The samples underwent the same treatment and were analyzed in the same sample vials. A DeltaNu advantage 785 benchtop Raman spectrometer (SciAps) with 785 nm diode laser was used with a liquid vial holder accessory. The time and power for the laser irradiation

were provided in the text for more clarification. To compare between the different instruments, the spectra were normalized for time and power density (laser power (mW)/laser area in($\mu m^2$)). Care was taken to choose an analyte concentration range that would not aggregate the Au NS before the addition of salt. This ensured partial control over the aggregation throughout the analyses. The spectral analysis was done using Spectragryph, which is an open-source software.[32]

The laser spot size for the DeltaNu and B&W Tek TacticID handheld Raman spectrometer was provided by the manufacturers, however, no further information about their optic systems was provided due to intellectual property rights. The laser spot size for the Renishaw Raman spectrometer at 785 nm was determined using the following equations:

$$d_l = 1.22\lambda \,/\, N.A. \qquad \textbf{(Eq 4–1)}$$

where $d_l$ is the laser spot diameter, $\lambda$ is the laser wavelength in μm, and *N.A.* is the numerical aperture of the objective. Since all samples are solution based, a liquid cell adapter was used to perform the measurements. The objective used had a focal length of 30 mm. The *N.A.* was calculated as follow:

$$f/\# = \text{focal length}/\text{ pupil diameter} \qquad \textbf{(Eq 4–2)}$$

$$N.A. = 1/\,2(f/\#) \qquad \textbf{(Eq 4–3)}$$

The pupil diameter was measured at 10 mm and the *N.A.* was calculated to be 0.17. The spot for the 785 nm laser is assumed to be circular.

## 4.3 Results and Discussion

### 4.3.1 Synthesis and Characterization of Au NS Using HEPES and EPPS Buffers

The synthesis of Au NS in Good's buffers was performed using previously reported methods.[8, 25] The size and shape of the Au NS were manipulated based on the ratio between the [buffer] and [$HAuCl_4$].[25] Figure 4-1 shows the extinction spectra of Au NS synthesized using A) HEPES and B) EPPS at ratios of 100, 300, 500, 700, and 1000. The inset images are a visualization of the LSPR red-shift through a solution colour change from purple/blue to grey as the ratios are increased. In Figure 4-1A, two plasmon resonance modes are observed for all ratios except HR100. The transverse mode is observed between 500 and 560 nm, which is attributed to the core. The longitudinal mode is observed at a longer wavelength, which is attributed to the branches and becomes red-shifted as the ratio increases from 100 to 1000. The transverse mode is from the presence of a spherical core or the presence of spherical nanoparticles within the mixture.[8, 25, 33] The shift in longitudinal plasmon mode previously has been attributed to the change in branch length and the branch tip sharpness.[8] Aside from HR100, the LSPR peak between 500 and 560 nm has a relatively weak extinction, and we suspect that the majority of the sample consists of anisotropic nanostructures. For HR100, the LSPR peak is slightly red-shifted and more intense in comparison to the higher ratios in this range. We hypothesize that the HR100 sample contains more spherical nanoparticles with smaller branch lengths.

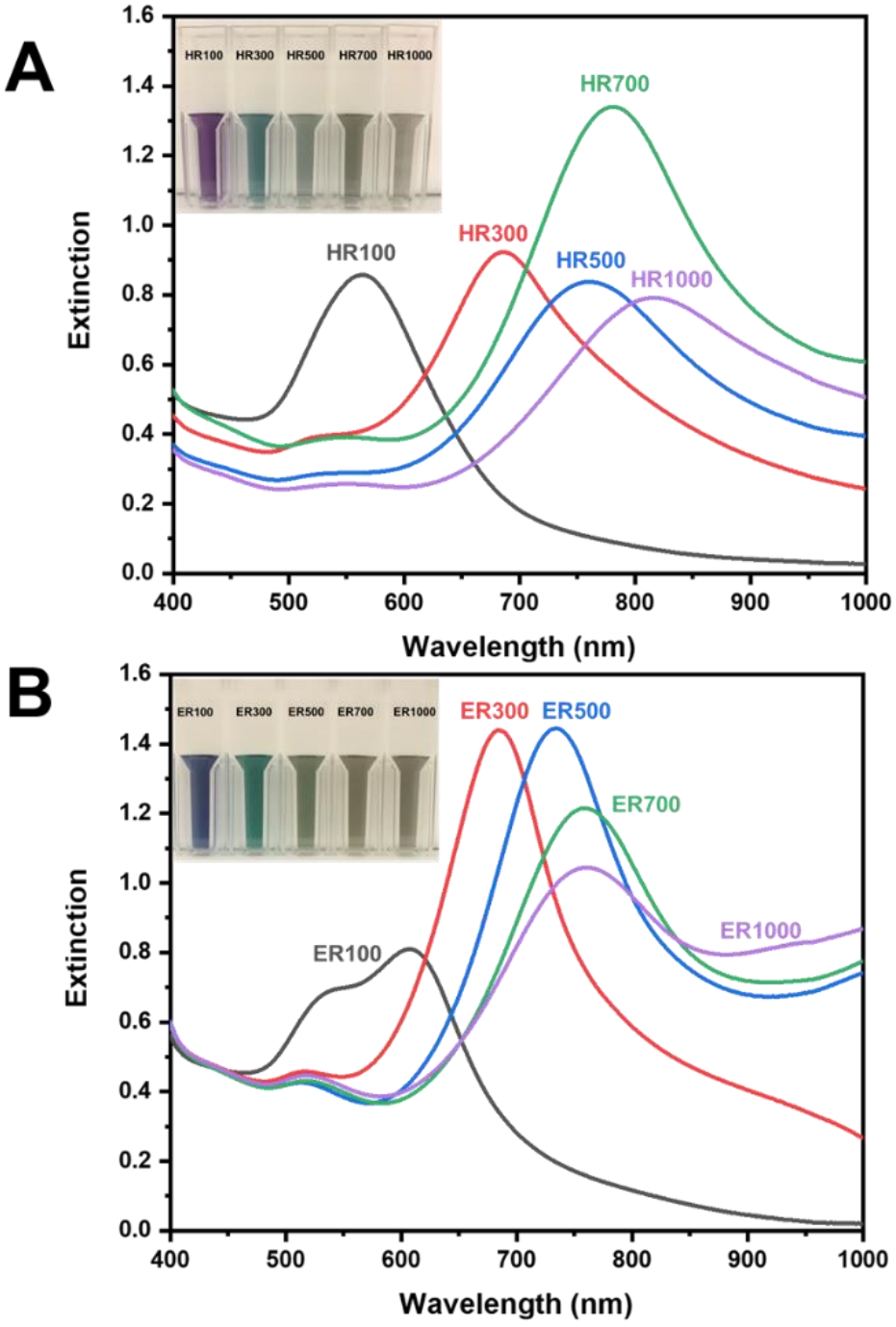


**Figure 4-1. Extinction spectra of Au NS.** (A) HEPES buffer. (B) EPPS buffer. The inset images show the colour of the Au NS solutions at the given ratios.

Nanostars synthesized using EPPS buffer also show two plasmon resonance modes and are red-shifted, as the ratios increased from 100 to 1000, as shown in Figure 4-1B. One notable difference between the HEPES and EPPS Au NS is the presence of both plasmon modes for ER100. Using HEPES buffer, it seems that both modes are overlapped, while for EPPS, $\lambda_{max}$ is at 608 nm with a shoulder at 540 nm. This suggests a spherical core with smaller branch lengths in comparison to nanostars synthesized at higher ratios. Additionally, it is important to note the slight changes in $\lambda_{max}$ at each ratio when comparing HEPES and EPPS. It previously has been reported that different Good's buffers have different interactions with the gold surface and promote different growth directions.[25] Table 4-1 shows the $\lambda_{max}$ at different ratios for each buffer. Figure 4-2 is the UV-vis control spectra of $HAuCl_4$ and the buffers that shows no observed bands.

**Table 4-1. Observation of The Longitudinal LSPR Peak Shift of Au NS at Various [Buffer]/[$HAuCl_4$] Ratios.**

| Au nanostars | $\lambda_{max}$ (nm) |
|---|---|
| HR100 | 566 |
| HR300 | 686 |
| HR500 | 760 |
| HR700 | 781 |
| HR1000 | 817 |
| ER100 | 608 |
| ER300 | 684 |
| ER500 | 734 |
| ER700 | 759 |
| ER1000 | 760 |

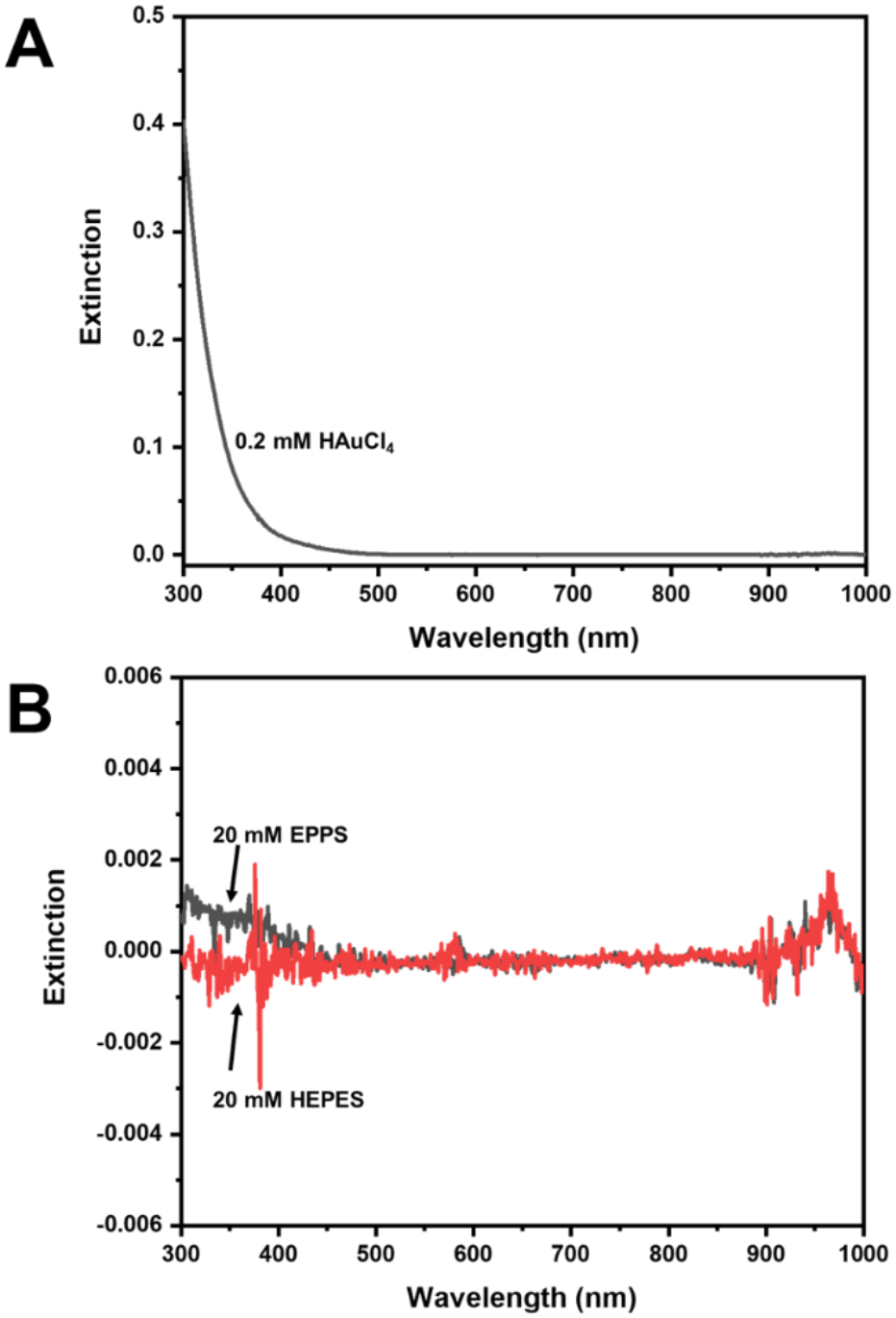


**Figure 4-2. UV-vis control experiments.** (A) Showing the spectrum of $HAuCl_4$ and (B) HEPES and EPPS buffer in a quartz cuvette.

The shape and size of the Au NS at different ratios for each buffer were examined using SEM imaging. Figure 4-3 shows SEM images of Au NS at ratios of 100 and 1000 for

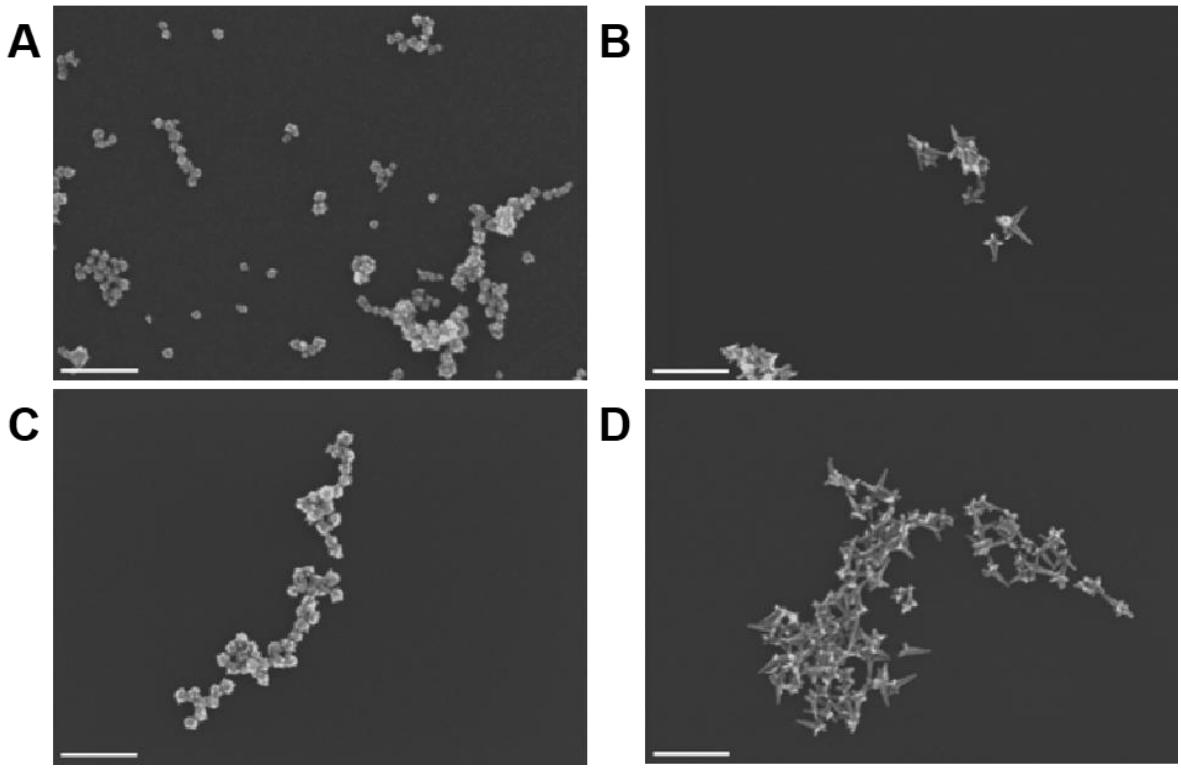


**Figure 4-3. Scanning electron micrograph of Au NS synthesized at different HEPES/$HAuCl_4$ and EPPS/$HAuCl_4$ ratios.** (A) HR100, (B) HR1000, (C) ER100, and (D) ER1000. Scale bars are 200 nm.

both buffers. Figure 4-3A is an image of HR100 nanostars that are approximately 24 ± 4 nm in size (n = 40). The nanostars are uniform in size and branch length, with the majority of the nanostars being spherical, with multiple small branches or roughened surface features.

The size and shape of HR100 Au NS were examined in more detail using TEM imaging, as shown in Figure 4-4. Figures 4-4A and B show that HR100 have a spherical core and multiple small branches extending from the core. There does not seem to be any preferential growth pattern for the branches. The nanostar's core size and branch length were determined as 24 ± 3 nm and 7 ± 3 nm, respectively (n = 40). Figure 4-4C and D are high magnification images of a single gold nanostar and one of its branches, respectively.

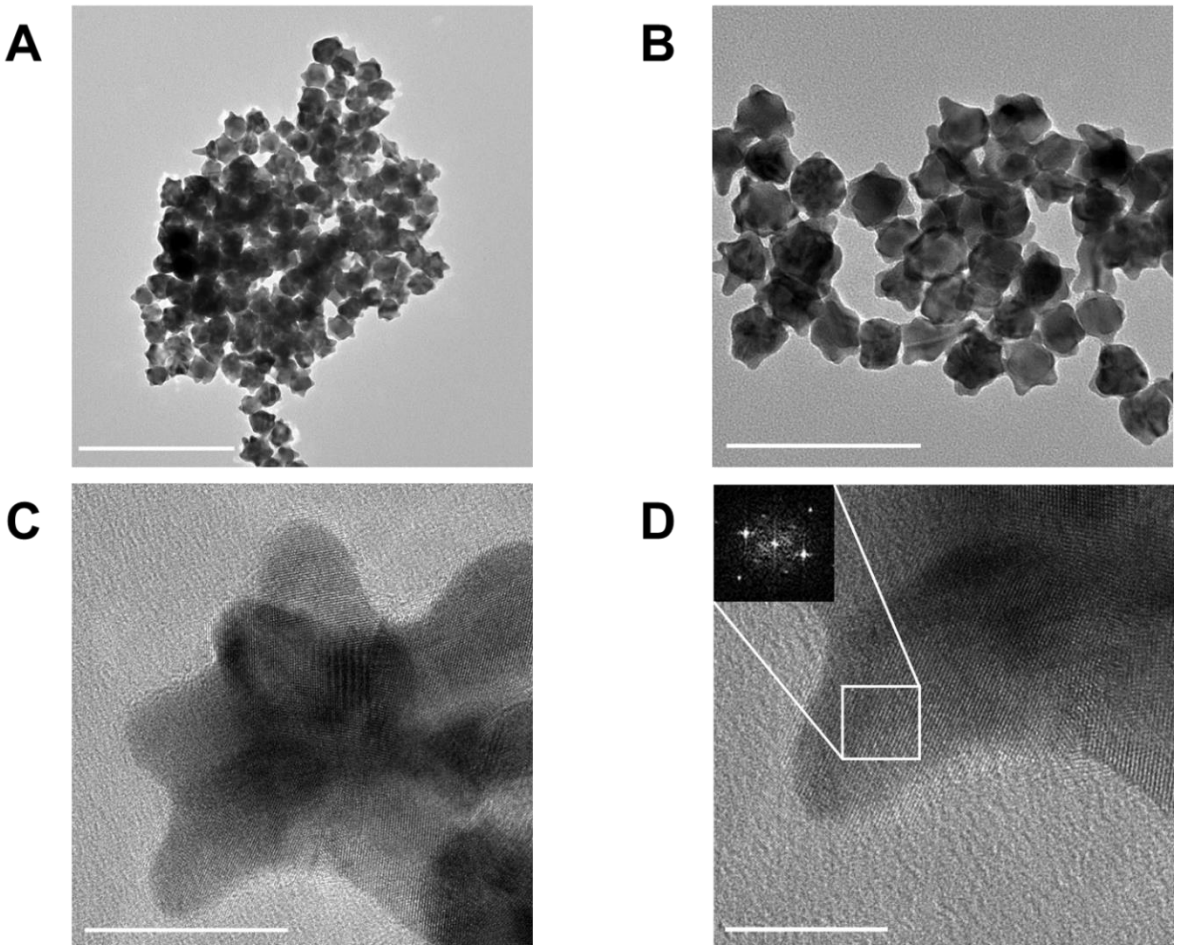


**Figure 4- 4. Transmission electron micrographs of Au NS HR100.** Scale bars: (A) 200 nm, (B) 100 nm, (C) 20 nm, and (D) 10 nm. The inset in D shows the lattice spacing of the Au NS branch based on Fast Fourier Transform (FFT) analysis of the highlighted area.

In Figure 4-4D the lattice spacing along the branch is 0.24 ± 0.02 nm, and this is consistent with the Au face-centred cubic [111] plane. Similar reports are found in the literature for Au NS synthesized using HEPES buffer.[8, 25, 34]

Figure 4-3B shows an image of HR1000 Au NS that appear to no longer have an obvious spherical core. However, the image shows nanoparticles with multiple branches, with lengths much longer than those found in HR100. The SEM images correlate well with the extinction spectra in that at a low ratio the nanostars contain a spherical core with small branches, and we observe a $\lambda_{max}$ that consists of both plasmonic modes. As the ratio

increases, the spherical core disappears, the branch length increases, the plasmon band between 500 and 560 nm nearly disappears, and a $\lambda_{max}$ at 817 nm appears. Similarly, Figure 4-3C and 2D show nanostars for ER100 and ER1000, respectively. The ER100 nanostars are fairly uniform, with a size of 31 ± 4 nm (n = 40). The image shows evidence of multiple branches per nanostar. The ER1000 nanostars also do not show an obvious spherical core nanoparticle and have a longer branch length. While we only examined the d-spacing of HR100, the d-spacing of Au NS synthesized using EPPS buffer has been studied previously, and the additional carbon in the alkanesulfonate for EPPS results in branches in the [110] direction.[25]

### 4.3.2 Au NS as a Colloidal SERS Substrate

The investigation and systematic optimization of colloidal Au NS as a water dispersible SERS substrate with respect to the effect of buffer type and [buffer]/[$HAuCl_4$] ratio has not been explored fully to the best of our knowledge. In this work, the SERS capability of Au NS with the [buffer]/[$HAuCl_4$] ratio ranging from 100 to 1000 was investigated. A ratio within this range commonly is used in the literature. Table 4-2 is a compilation of publications using Au NS within this range for SERS applications.[18-21, 27, 35-36]

Herein, the SERS performance of Au NS synthesized using HEPES and EPPS buffer was examined without any centrifugation or cleaning steps. There are a few reasons for studying the Au NS in the presence of the buffer ligand. First, we aim to develop a feasible SERS platform with a limited amount of synthesis, purification, and analysis steps, and one that requires limited instrument involvement. The presence of the buffer ligands also provides insight into the competition between a thiolated Raman probe, MBN, in this case and the buffer ligands for the nanostar surface sites. This competition offers an

understanding of the colloidal behaviour of the Au NS and their inherent SERS performance. Moreover, we can examine the long-term stability of the Au NS following functionalization with a thiolated Raman probe by monitoring the SERS performance. This reflects the significance of the buffer ligands on the stability of the nanostars post-functionalization.

**Table 4-2. Comparison of Au NS Synthesized Using Good's Buffers for SERS Applications**

| Type of synthesis | Buffer type and ratio | Platform | Application | Reference |
|---|---|---|---|---|
| Seedless/seeded | EPPS R = ~300 | Cellular | SERS imaging of breast cancer cells | [27] |
| Seedless/seeded | EPPS R = 400 | Colloidal | Detection of uranyl | [18] |
| Seedless/seeded | EPPS R = 200 | Surface | Detection of uranyl | [19] |
| Seedless | HEPES R = ~310 | Surface | Lateral flow assay | [20] |
| Seedless | HEPES R = ~625 | Surface | Lateral flow assay | [21] |
| Seedless | HEPES R = 200 | Surface | Development of SERS graphene-nanostar composite nanoprobe | [35] |
| Seedless | HEPES R = 83– 500 | Surface | Synthesis of graphene nanostar nanocomposite | [36] |
| Seedless | HEPES/EPPS R = 100–1000 | Colloidal | SERS optimization and detection | This work |

*Seedless/seeded – Au NS initially are synthesized using a seedless method. The Au NS are used as seeds to produce nanostars with longer branches via addition of $HAuCl_4$.

Figure 4-5A shows the Raman spectra of 5 μM MBN associated with R100 for both HEPES and EPPS buffers. Similarly, Figure 4-5B shows the spectra of MBN at R1000 for both HEPES and EPPS buffers. The Raman band at 1044 $cm^{-1}$ is attributed to the symmetric stretch of sulfonate group of the buffers.[30] In Figure 4-5C, the band at 1044 $cm^{-1}$ can be observed prominently in a control experiment showing the spectra of water, 1 M HEPES, and 0.5 M EPPS buffers.

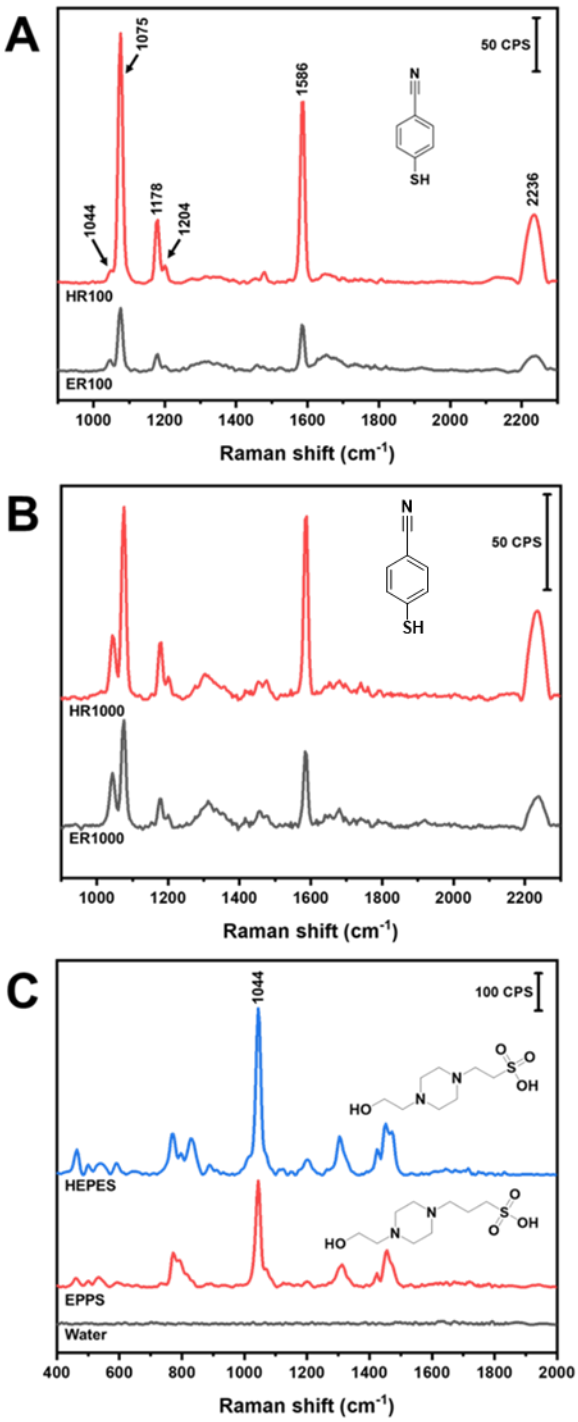


**Figure 4-5. Raman spectra of 5 μM MBN comparing different Au NS.** (A) HR100 and ER100, and (B) HR1000 and ER1000. (C) Raman spectra of water, 0.5 M EPPS, and 1 M HEPES buffer.

The results in Figure 4-5A and 5B indicate that Au NS synthesized using HEPES buffer at the lowest gold to buffer ratio (HR100) have a superior SERS performance. We compared the Au NS synthesized using the two buffers at 100 and 1000 ratios with respect to the three major Raman bands at 1075, 1586, and 2233 $cm^{-1}$. The intensities of these bands for HR100 were approximately four times higher than that of ER100, as shown in Figure 4-5A, while the intensities of these bands for HR1000 were approximately two times higher than those of ER1000, as shown in Figure 4-5B. Table 4-3 shows the major Raman peak assignments for MBN, according to previously published papers.[37-39]

**Table 4-3. Major Band Assignments Listed for the SERS Spectrum of MBN on the Surface of Au NS**

| Band position ($cm^{-1}$) | Assignment[37-39] |
|---|---|
| 1075 | C-S and C-C stretching |
| 1178 | C-H bending and C-C stretch |
| 1204 | C-H bending and C-C≡N stretching modes |
| 1586 | C-C stretch |
| 2233 | C≡N stretch |

An in-depth analysis of three of these major SERS bands of MBN for different [buffer] to [$HAuCl_4$] ratios using HEPES and EPPS is shown in Figure 4-6A and 6B, respectively. Plotted in these figures are the intensities of the three bands at each buffer ratio. In Figure 4-6A, there is variation of the Raman bands intensities with increasing HEPES buffer concentration. However, such a variation was not observed in the case of the EPPS buffer, as shown in Figure 4-6B. The dynamics between the thiolate–gold and the buffer–gold interactions at the nanostar surface may provide an explanation for the Raman enhancement of MBN using different buffers and at different ratios.

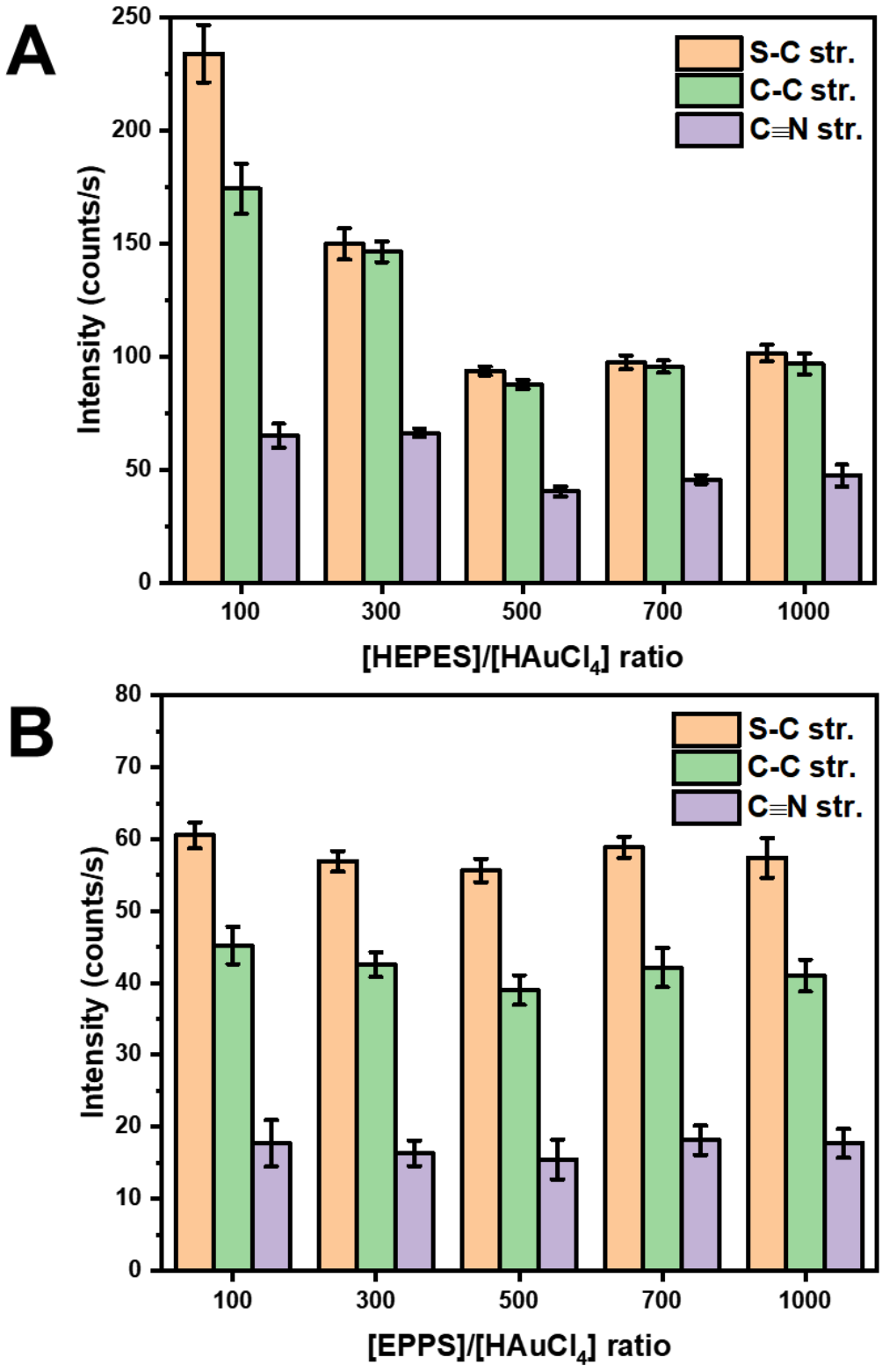


**Figure 4-6. Column graph of the peak height of different vibrational modes of MBN at different buffer/$HAuCl_4$ ratios.** (A) HEPES and (B) EPPS.

HEPES and EPPS molecules act as reducing, shape directing, and stabilizing agents in the synthesis of Au NS.[25, 30] The piperazine contains two cationic free radical tertiary amines that can reduce $Au^{3+}$ to $Au^{0}$.[25, 28] Additionally, the terminal alkanesulfonate group interacts with the Au NS surface and acts as a shape directing agent, while the terminal hydroxyl group acts as a stabilizing agent and facilitates bilayer formation of the buffer ligand.[25-26, 30] Upon addition of MBN to the Au NS, there is a competition between the HEPES or EPPS and the MBN for surface sites. In the case of HEPES buffer, Au NS at a smaller ratio (R100 and R300) provide a higher Raman enhancement compared to those synthesized at a larger ratio (R500, R700, and R1000) (Figure 4-5A). Previous studies suggest that at lower HEPES concentration, the formation of a bilayer is incomplete or collapsed[26, 30] and, in turn, facilitates the adsorption of MBN onto the Au NS surface.

Conversely, at high HEPES concentration (>100 mM) the formation of a bilayer limits the adsorption of MBN. This interaction is observed by monitoring the SERS performance of Au NS at different buffer to gold ratios. In Figure 4-6A, the highest SERS intensity is found at HR100 (20 mM HEPES), twice that of HR1000. As the ratio increases, the SERS intensity gradually decreases (HR300, 60 mM HEPES) and plateaus from HR500 to HR1000 (100–200 mM HEPES). Figure 4-6B is a column graph of MBN peak intensities from ER100 to ER1000. Notably, the peak intensities of MBN are constant regardless of the buffer to gold ratio. One possible explanation involves the binding energy differences between HEPES–HEPES and EPPS–EPPS dimers. A computational study using the polarizable continuum model determined that HEPES–HEPES and EPPS–EPPS dimers have a Gibbs free energy of 25.7 and -1.0 KJ/mol, respectively.[26] Although EPPS has only one extra methylene group more than HEPES, we assume that this may promote a more

densely packed self-assembled monolayer on the Au NS through hydrophobic interactions similar to alkanethiol monolayers.[40] In comparison to HEPES, this could provide a more flexible orientation and configuration of the EPPS and could lead to less available surface sites for Raman active molecules.

Another possible explanation involves the growth direction of the Au NS branches. Chandra et al. have shown that the buffer type impacts the growth direction of Au NS branches. Their results show that Au NS synthesized from HEPES have branches growing in the [111] direction and that Au NS synthesized from EPPS have branches growing in the [110] direction.[25] It is known that the gold crystal face can play a significant role in the surface coverage of thiol-derived monolayers.[41] Thus, surface coverage of MBN on the Au NS can vary for these different crystal faces. The amount of MBN binding to the Au NS possibly could be a result of the different deposition sites produced from HEPES and EPPS.

The above discussion was based on buffer–buffer and buffer–gold interactions, however, another possible explanation for the change in SERS performance at different ratios might be attributed to the changes in size and shape differences at different buffer to gold ratios. A recent study suggests that a different surface curvature can affect the SERS enhancement and the longevity of the colloidal substrate drastically.[39] It is difficult to understand the exact mechanism(s) for the differences in SERS performance at different buffers and ratios. However, the variations of the SERS intensities observed are, at most, a factor of four. We believe that these differences are primarily due to surface coverage of the probe MBN rather than any large electromagnetic differences.

The benefits of using a colloidal SERS substrate are the good reproducibility provided by sample homogeneity and its ease of use. Figure 4-7A shows Raman spectra of MBN from Au NS within the same batch on different days. The peak intensity from the C–S stretching vibration on different days is plotted in Figure 4-7B. The Au NS HR100 were functionalized with 5 μM MBN and measured on day 0. Next, the Au NS were measured after being stored at 4 °C for a given period of time. Over a period of 78 days the Au NS showed a %RSD range of 1–5% within the same day and a %RSD of 8% between days, suggesting good colloidal stability and a long-term storage capability at 4 °C, even after functionalization. This also shows the potential to store Au NS functionalized with a reporter for long-term applications. As a comparison, Figure 4-7C shows SERS spectra of Au NS HR100 modified with 5 μM MBN drop-casted onto a silicon wafer obtained from 100 random points. The %RSD for these 100 points is 51%, which is significantly higher than the %RSD produced from the solution-based substrate, demonstrating the significance of substrate homogeneity in colloidal substrates.

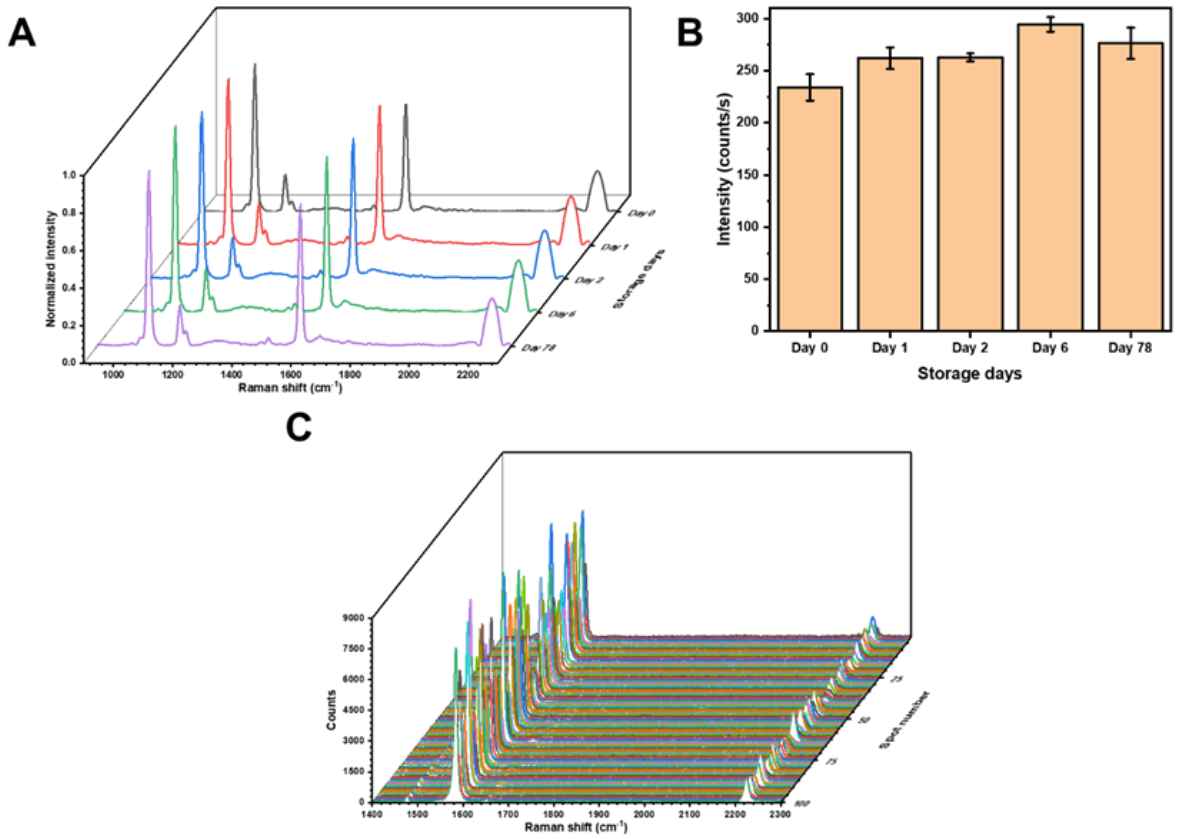


**Figure 4-7. Au NS stability.** (A) Raman spectra of MBN showing signal reproducibility from Au NS substrates. (B) Bar chart of MBN C–S stretch peak intensity showing stability of Au NS in the fridge. (C) Raman spectra of 5 μM MBN drop-casted onto a silicon wafer analyzed using a Renishaw Raman microscope at 785 nm at 100 random points.

### 4.3.3 Rapid Analysis of Analytes Using Colloidal Au NS Nanoaggregates

Aggregating agents commonly are used to enhance the SERS signal by entrapping molecules between interstitial hot spots.[42-45] In this work, NaCl (200 mM) is used to produce dispersible Au NS nanoaggregates to increase the Raman enhancement. Figure 4-8A shows Raman spectra of MBN using Au NS HR100 and ER100 before and after the addition of NaCl. The addition of NaCl results in a significant increase in peak intensity for both HR100 and ER100, with the HR100 formulation exhibiting the highest peak intensity. Figure 4-8B shows the extinction spectra of Au NS HR100, Au NS after the

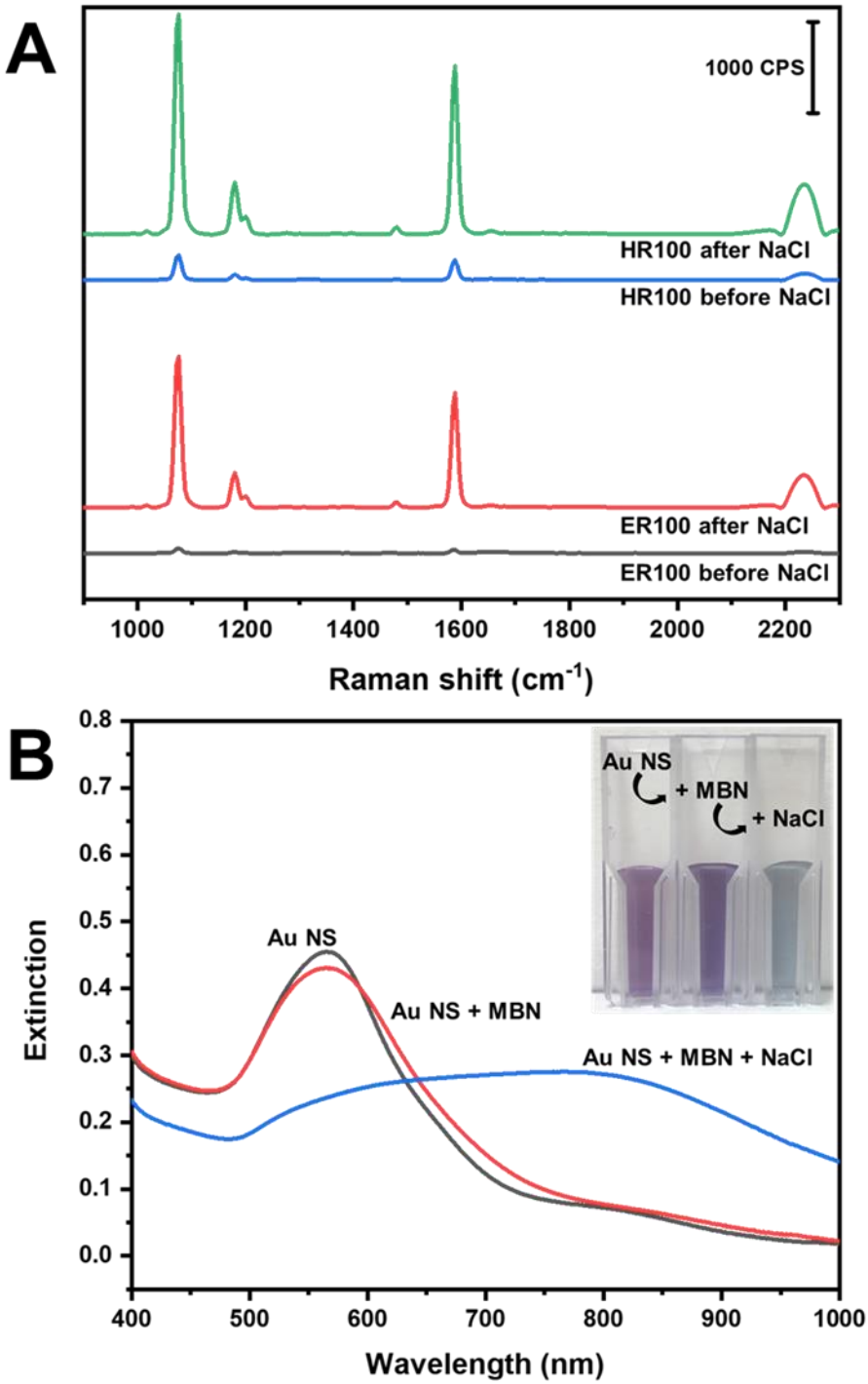


**Figure 4-8. The impact of NaCl addition on Au NS.** (A) Raman spectra of MBN using Au NS R100 before and after salt addition for both HEPES and EPPS buffer. (B) UV-vis spectra showing the extinction of Au NS HR100 after the addition of MBN and after the addition of MBN and NaCl.

addition of MBN (5 μM), and then after the addition of NaCl; the inset is a photograph of the Au NS at each stage. The Au NS HR100 show a LSPR $\lambda_{max}$ at 566 nm, and with the addition of MBN, we observe a slight decrease in the peak intensity and a broadening in the peak width in the 600–775 nm range of the spectrum. We also observe a slight colour change from light purple to dark purple. This is attributed to MBN adsorbing onto the Au NS surface and changing the local dielectric constant. After the addition of NaCl, there is a large red-shift and broadening of the LSPR peak, indicating the formation of Au NS aggregates. The colour of the Au NS changes from a dark purple to a light blue/grey. The UV-vis extinction results are consistent with the formation of Au NS nanoaggregates with the addition of NaCl, and this explains the large enhancement observed in the Raman data.

The size and colloidal stability of the Au NS nanoaggregates were studied using DLS and zeta potential measurements, and the results are shown in Table 4-4. The Au NS HR100 have a z-average diameter of 49.4 ± 0.9 nm. With the addition of MBN, we observe an increase in the z-average diameter due to the adsorption of MBN onto the Au NS surface through a gold–thiol linkage. Addition of NaCl causes the z-average diameter to increase to 379 nm, indicating the formation of Au NS aggregates. The increase in the z-average diameter with the addition of analytes and NaCl is expected. The polydispersity index (PDI) decreases with the addition of MBN and NaCl, indicating the Au NS become more uniformly dispersed. The zeta potential remains relatively constant throughout the additions of MBN and NaCl.

**Table 4-4. Size and Colloidal Stability Study of Au NS Nanoaggregates Using Dynamic Light Scattering and Zeta Potential Measurements**

| Au NS HR100 | z-average diameter (nm)[a] | PDI[a] | Zeta potential (mV)[b] |
|---|---|---|---|
| Unmodified | 49.4 ± 0.9 | 0.38 ± 0.04 | -35 ± 1 |
| + MBN | 54.7 ± 0.4 | 0.29 ± 0.01 | -36.9 ± 0.9 |
| + NaCl | 379 ± 54 | 0.23 ± 0.03 | -34 ± 2 |

[a] n = 5 with each measurement consisting of 13 sub-measurements. Analysis is based on a measurement time of 8 min.
[b] n = 5 with each measurement consisting of 20 sub-measurements. Analysis is based on a measurement time of 5 min.
*pH values of the Au NS solutions were at 6.5–7 and were measured using Accumet pH paper.

Centrifugation of the Au NS was examined as a possible SERS optimization parameter. We wanted to ensure that any excess buffer molecules did not affect the SERS performance of the substrate negatively. The extinction spectra in Figure 4-9A show that centrifugation has no significant effect on the LSPR peak, i.e., peak shifts or broadening (aggregation) after redispersion. The downside to centrifugation is the loss of nanostars, as evidenced by the decrease in LSPR band intensity, thus potentially impacting the Raman enhancement. Figure 4-9B and 9C show the Raman spectra of Au NS HR100, Au NS + MBN, and Au NS + MBN + NaCl before and after centrifugation, respectively. The spectra show similar results, indicating that centrifugation has little to no effect on the substrate and that the excess HEPES buffer at R100 does not impede with analyte adsorption onto Au NS. Since the buffer has no negative impact on detection when using the Au NS, centrifugation is an unnecessary step in the analysis. Moreover, the HEPES buffer is necessary for the Au NS to remain colloidally stable, as previously discussed.

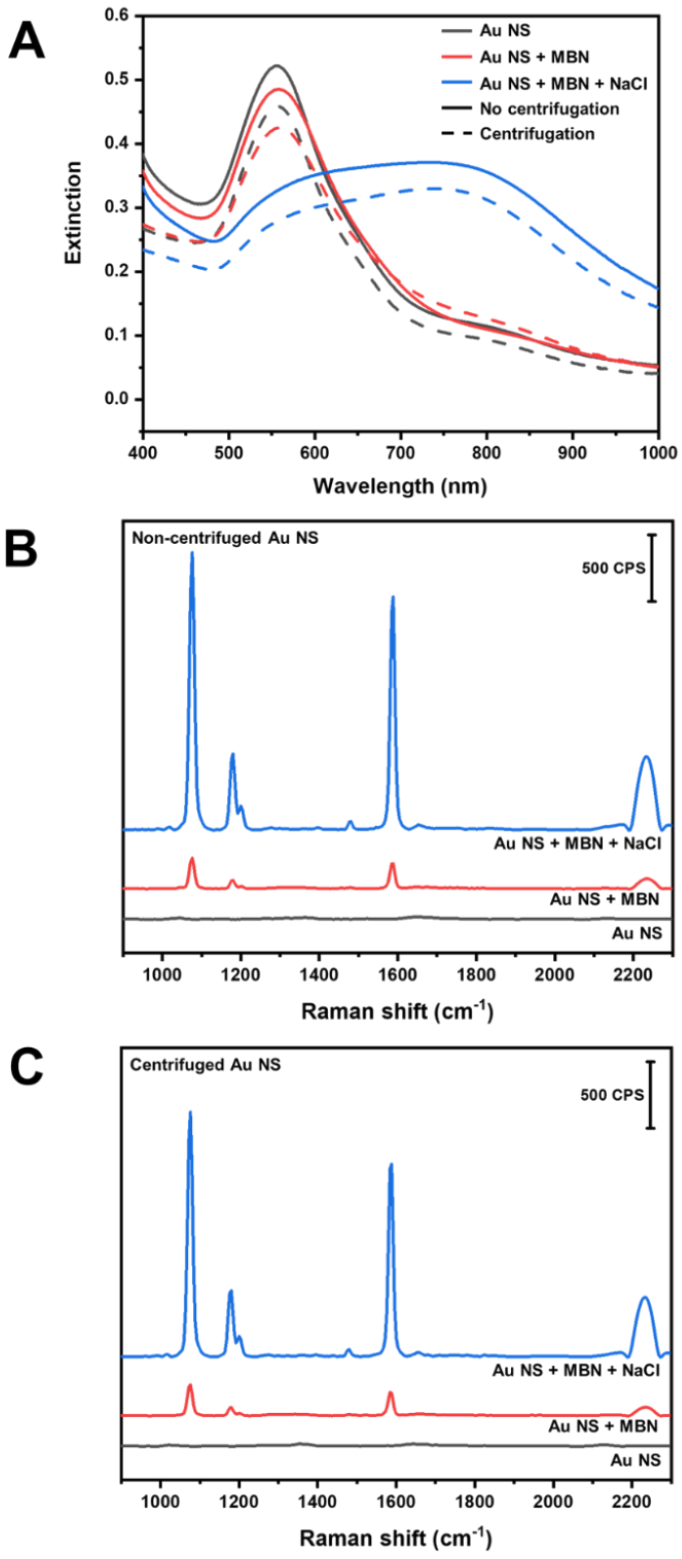


**Figure 4-9.The impact of centrifugation on Au NS.** (A) UV-vis spectra of Au NS HR100 before and after centrifugation (14000 rpm, 10 min) at different stages of the analysis. Raman spectra of MBN using Au NS HR100 showing the effect of centrifugation where (B) before and (C) after centrifugation.

Figure 4-10 shows the Raman spectra of four different analytes, namely TBZ, MTZ, MG, and Cipro, which extend the applications of Au NS for solution-based SERS. All these analytes were detected in solution within 5 min. TBZ and MTZ are examples of sulfur containing molecules that can be adsorbed onto Au NS by chemisorption through thiolate chemistry, while MG and Cipro are examples of non-sulfur containing molecules that can be adsorbed onto Au NS by nitrogen atoms and/or physiosorbed. The rapid detection of two sulfur-containing molecules, TBZ and MTZ, using Au NS HR100 are shown in Figure 4-10A and 10B. TBZ is a common fungicide applied after harvest to prevent mold and rot on fruit and vegetables.[46] The use of TBZ has been classified as likely to be carcinogenic at high concentrations and poses thyroid hormone production imbalance risks.[47-48] Since TBZ is used widely in fruits and vegetables, ranging from applesauce to sweet potatoes, the maximum residue limit (MRL) will differ per commodity. For example, the United States Environmental Protection Agency (US EPA) has set a tolerance limit of 5 ppm and 10 ppm for applesauce and sweet potatoes, respectively (~25–50 μM).[49] Figure 4-10A shows the Raman spectrum of 5 μM TBZ adsorbed onto Au NS before and after the addition of NaCl (200 mM). The major bands are summarized in Table 4-5, according to a previously published paper.[50] The use of colloidal Au NS nanoaggregates shows the capability to detect TBZ well below the set tolerable limit and could be used to detect TBZ in real samples.

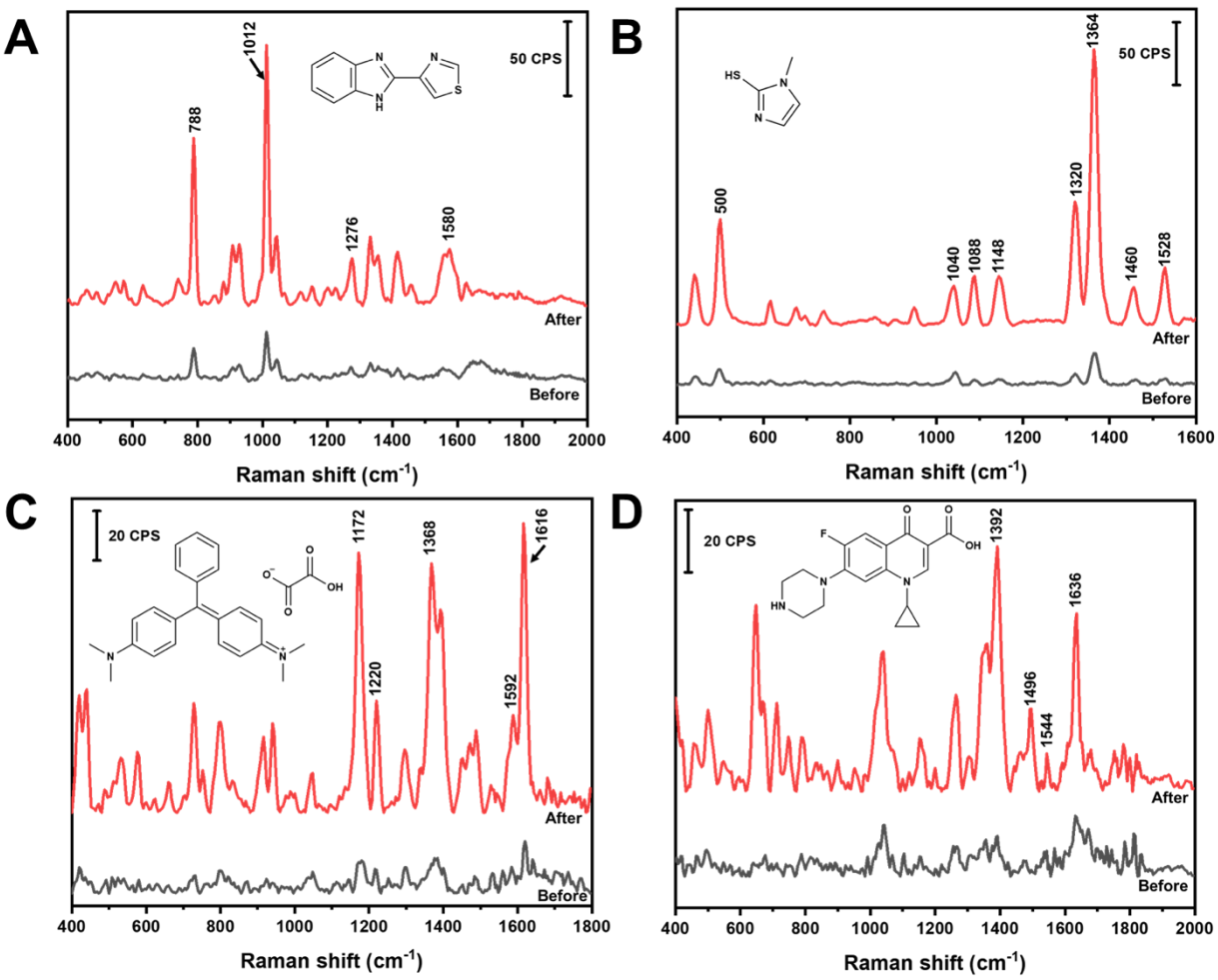


**Figure 4-10. In-solution SERS spectra before and after the addition of NaCl.** (A) 5 μM thiabendazole in 0.1 M HCl, (B) 1 μM methimazole in water, (C) 0.5 μM malachite green in water, and (D) 5 μM ciprofloxacin in 0.1 M HCl using a colloidal Au NS HR100 substrate before and after the addition of NaCl (200 mM).

**Table 4-5. Major Band Assignment Listed for the SERS Spectrum of TBZ on Au NS**

| Band position ($cm^{-1}$) | Assignment[50] |
|---|---|
| 788 | C–H out-of-plane bending |
| 1012 | C–H out-of-plane bending |
| 1276 | ring stretching |
| 1580 | ring stretching and C=N stretching |

MTZ commonly is used as an anti-hormone pharmaceutical to treat hyperthyroidism by regulating the production of thyroxine and triiodothyronine.[51-52] Moreover, MTZ often is applied illegally to animal feed to promote animal weight gain by increasing water retention in tissues.[51, 53] Monitoring and limiting the exposure of MTZ is important, as MTZ is known to have multiple side effects. These side effects include skin irritation, impaired olfaction, allergies, impaired taste, pharyngitis, nephritis, and liver cirrhosis.[51-52, 54] Metabolization of MTZ leads to further MTZ intermediates known to have cytotoxic effects in the body.[54] Figure 4-10B shows the Raman spectrum of 1 μM MTZ before and after the addition of NaCl adsorbed onto Au NS. These bands are summarized in Table 4-6, according to a previously published papers.[55-60] MTZ is looked at in more details below.

**Table 4-6. Major Bands Assignments Listed for the SERS Spectrum of MTZ on Au NS**

| Band position ($cm^{-1}$) | Assignment[55-60] |
|---|---|
| 500 | S–C–N in plane bending |
| 616 | ring out-of-plane bending, ring C–H, and N–H out-of-plane bending |
| 1037 | ring bending, ring C–H bending, and C–S–H bending |
| 1086 | ring C–N stretching and ring C–H bending |
| 1145 | C–S stretching, ring C–H bending, and C–N stretching |
| 1320 | ring C–N stretching, ring bending, and ring C–H bending |
| 1364 | C–N stretching, ring bending, and ring C–H bending |

The detection of two non-sulfur containing molecules (MG and Cipro) using Au NS substrate are shown in Figure 4-10C and 10D. MG is a highly effective fungicide used to mitigate fungi and parasite growth in the aquaculture industry.[61] In Canada, MG is

approved for use only on aquarium fish, and is not permitted for use on food-producing animals/fish.[62] MG and its metabolite, leucomalachite green, are known to reside in fish tissue and are known to have mutagenic and teratogenic effects on humans.[61-62] While its use on aquarium fish is approved, improper disposal or careless treatment of aquarium fish could lead to accidental contamination of surrounding bodies of water and fish. Figure 4-10C shows the in-solution Raman spectrum of 0.5 μM MG adsorbed onto colloidal Au NS before and after the addition of NaCl. These bands are summarized in Table 4-7, according to a previously published paper.[63] MG was used as an example of a fluorescent dye to show the capability of Au NS to detect such a molecule.

**Table 4-7. Major Band Assignments Listed for the SERS Spectrum of MG on Au NS**

| Band position ($cm^{-1}$) | Assignment[63] |
|---|---|
| 1172 | in-plane C–H ring vibration |
| 1220 | C–H rocking |
| 1368 | N-phenyl stretching vibration |
| 1592 | C–C stretching |
| 1616 | C–C stretching |

Cipro is a fluoroquinolone antibiotic used to treat bacterial infections relating to the urinary tract, prostatitis, sinusitis, bones, and joints.[64] Figure 4-10D shows the Raman spectrum of Cipro adsorbed on Au NS before and after the addition of NaCl at a concentration of 5 μM. These bands are summarized in Table 4-8, according to previously published papers.[65-66]

**Table 4-8. Major Band Assignments Listed for the SERS Spectrum of Cipro on Au NS**

| Band position ($cm^{-1}$) | Assignment[65-66] |
|---|---|
| 1392 | symmetric O–C–O stretching |
| 1496 | Asymmetric O–C–O stretching |
| 1544 | quinolone ring ring stretching |
| 1636 | Asymmetric aromatic ring g stretching |

The detection of the analytes described above can be measured rapidly at low μM range (within 5 min) using colloidal Au NS via either chemisorption or physisorption mechanisms using the handheld Raman device. As shown in Figure 4-10, most of the analytes are detectable without the use of NaCl. However, with the addition of NaCl, the analyte signal is enhanced due to the aggregation of the Au NS, subsequently forming more SERS hot spots.

### 4.3.4 Measurements of MTZ in Urine Using Au NS Nanoaggregates

MTZ was chosen as the target molecule for a quantitative method development and measurement in a complex matrix. As noted above, MTZ is an anti-hormonal pharmaceutical used to treat hyperthyroidism, and individuals with MTZ in their system will excrete it in their urine.[51-52] Chromatography commonly is used to detect and quantify MTZ in urine.[52] However, the downside to using chromatography is that it is labour intensive and often requires instrumental expertise, sample extractions, preconcentration, or derivatization treatment before analysis.[51-52] The limit of detection

of MTZ by liquid chromatography methods can range from a concentration of nM to μM.[51-52] A simple and less labour intensive method that can quantify MTZ in urine competitively would be useful. A graphical representation of using Au NS as SERS substrate for MTZ detection is shown in Figure 4-11.

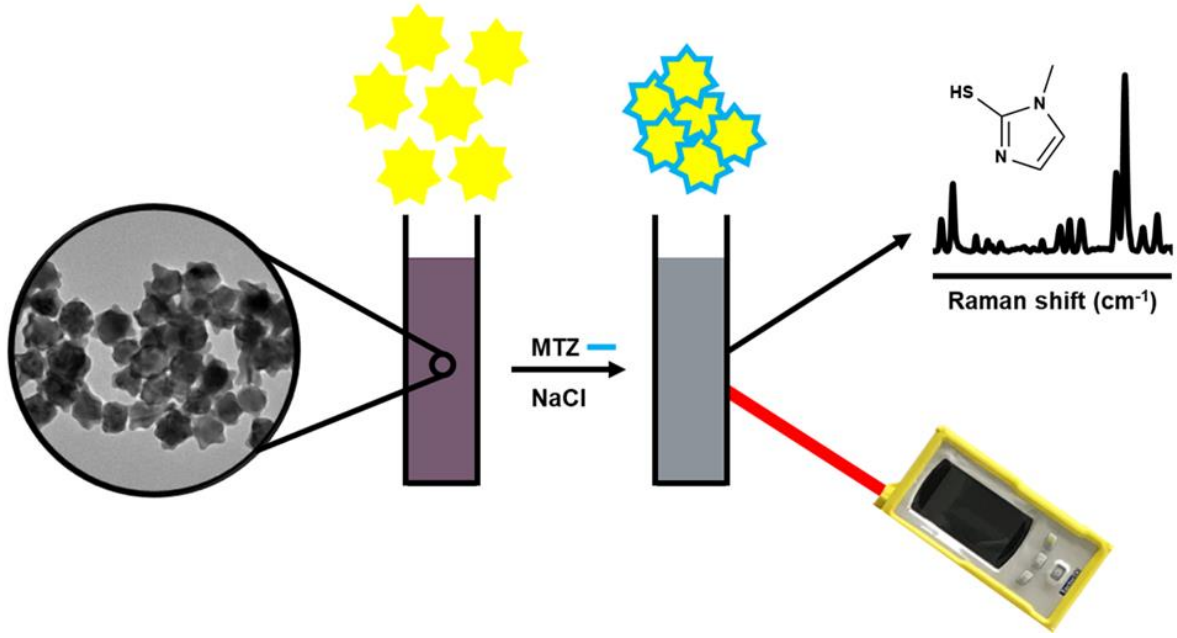


**Figure 4-11. General scheme represents in solution SERS measurement of MTZ using Au NS and a handheld spectrometer.**

#### 4.3.4.1 Method Development

Figure 4-12 shows quantitation of MTZ using colloidal Au NS nanoaggregates as a water dispersible SERS substrate. Raman spectra of MTZ at different concentrations in water are shown in Figure 4-12A. Each concentration is represented by an average spectrum composed of three samples measured three times at different spots in a glass vial (n = 9).

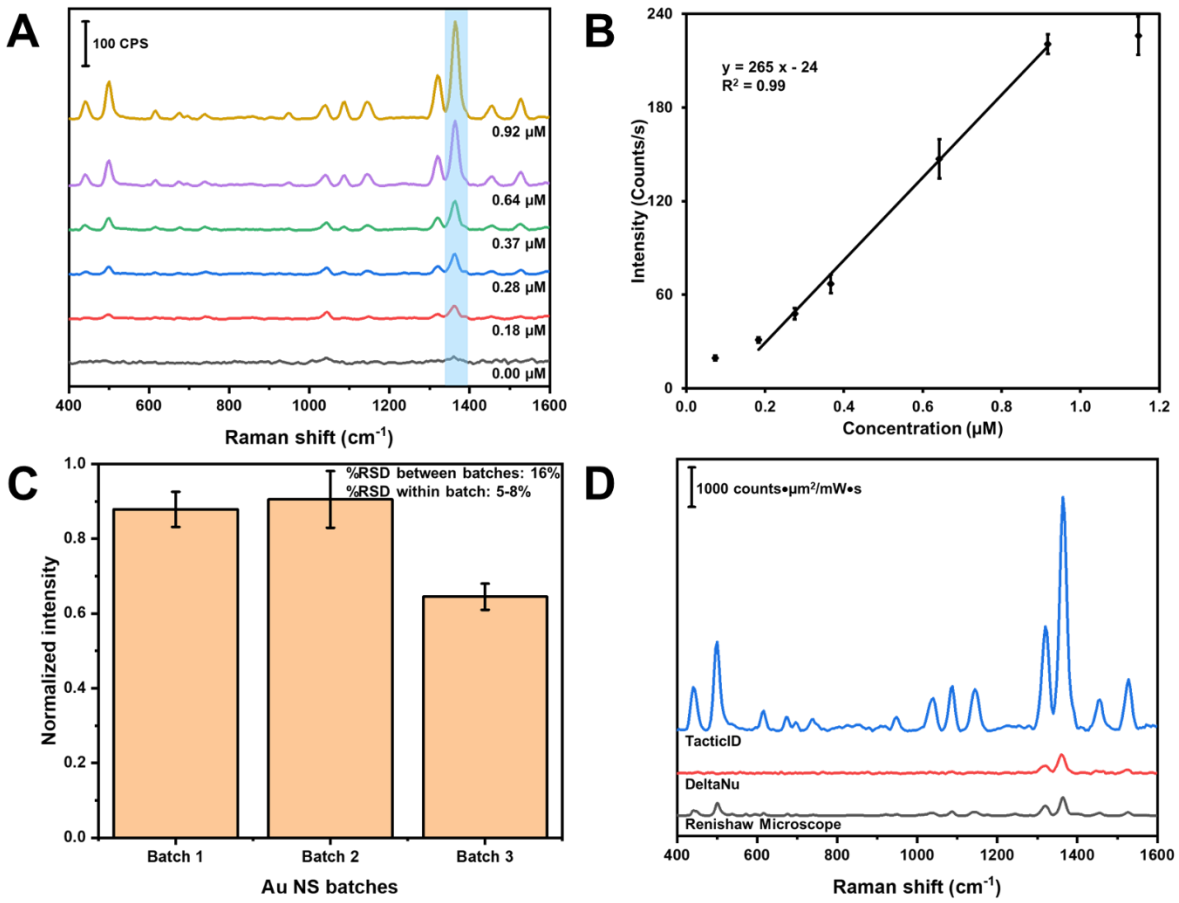


**Figure 4-12. MTZ quantitation.** (A) Raman spectra of MTZ at various concentrations using Au NS HR100 and NaCl. (B) Calibration curve of MTZ using colloidal Au NS HR100. (C) Bar graph of the batch to batch reproducibility of Au NS using MTZ. (D) Instrument comparison in the detection of MTZ (1.15 µM) in urine using Au NS.

The peak used for quantitation is highlighted in light blue and is the N–C stretching vibration at 1364 $cm^{-1}$. As the concentration of MTZ is increased, the peak intensity also increases. Figure 4-12B is a plot of the intensity of the1364 $cm^{-1}$ band vs concentration. The plot exhibits a linear portion and curves at low and high concentrations. The curvature at lower concentration indicates the limit of the measurement. The "levelling-off" at high concentration likely indicates that the adsorption sites on the aggregates are saturated. A linear least square fit of a portion of the plot can be used as a calibration curve. From this linear portion, the limit of detection and limit of quantification were

determined as 0.1 and 0.3 μM, respectively. The dynamic range is determined to be between 0.3 and 0.9 μM.

The batch-to-batch reproducibility of the Au NS was monitored using the peak intensity at 1364 $cm^{-1}$ of MTZ. Figure 4-12C shows a bar chart of the peak intensity using three different Au NS batches. Each batch consists of three samples analyzed three times, each at different spots (n = 9). The percent relative standard deviation (%RSD) between samples within the same batch was between 5 and 8%, while the %RSD between different batches was 16%. %RSD for a range of SERS substrates generally is reported up to about 15–20%.[67]

Figure 4-12D shows the in-solution SERS spectrum of MTZ using different Raman instruments. We compared a Renishaw Raman microscope, a DeltaNu benchtop Raman spectrometer, and a B&W Tek TacticID handheld Raman spectrometer qualitatively. All sample conditions, such as MTZ concentration, sample volume, NaCl concentration, and mixing times, were held constant. The spectra were normalized for the power density and the acquisition time. The peak intensity at 1364 $cm^{-1}$ was determined as 466 ± 28, 493 ± 33 and 5915 ± 320 (counts $\mu m^2$/mW s) for the Renishaw Raman microscope, DeltaNu benchtop Raman spectrometer, and the B&W Tek TacticID handheld Raman spectrometer, respectively. The three Raman systems differ vastly in their optical setup, with some details that could not be given by the vendors due to intellectual property rights. Therefore, the purpose of our comparison here is mainly to show the potential applications of Au NS using different Raman systems, especially a handheld one. The handheld device seems to be the most effective by providing the highest signal intensity in units of Counts $\mu m^2$/mW s. Table 4-9 compares the instrument parameters and the

detection results at 1364 $cm^{-1}$. It also is important to note that the %RSD is relatively consistent amongst all instruments. It is also worth mentioning that the Renishaw Raman microscope provided the highest signal intensity in terms of counts/mW s followed by DeltaNu and TacticID. A typical user may not be concerned about spot size, but power and time are usually known and controlled. While the TacticID handheld device is less expensive than the other spectrometers and provides rapid on location analysis, it does not allow the user to control the acquisition time manually. This can be considered as a shortcoming of TacticID where data has to be normalized and processed after measurements.

**Table 4-9. Comparison of Raman Instruments for the Detection of MTZ**

| | | Instruments | | |
|---|---|---|---|---|
| | | **Renishaw** | **DeltaNu** | **TacticID** |
| **Parameters** | **Power (mW)** | 115 ± 1 | 37 ± 1 | 300.0 ± 0.2 |
| | **Time (s)** | 15 | 10 | N/A* |
| | **Laser spot size (μm²)** | 26 | 491 | 7854 |
| | **Power density (mW/μm²)** | 4.4 | 0.076 | 0.038 |
| **Detection at 1364 $cm^{-1}$** | **Intensity (Counts μm²/mW s)** | 466 ± 28 | 493 ± 33 | 5915 ± 320 |
| | **Intensity (Counts /mW s)** | 18 ± 1 | 1 ± 0.1 | 0.75 ± 0.04 |
| | **%RSD** | 6 | 7 | 5 |

* TacticID does not allow the user to set the acquisition time. The time varies from sample to sample, however, it can be noted and accounted for in the data treatment.

Figure 4-13 shows the Raman spectra of MTZ in the absence and presence of Au NS collected with TacticID. The MTZ in water is at a concentration of 16 mM, and the peak at 1364 $cm^{-1}$ is hardly visible. The MTZ in Au NS nanoaggregates is at a concentration of0.917 µM and shows a large enhancement at 1364 $cm^{-1}$.

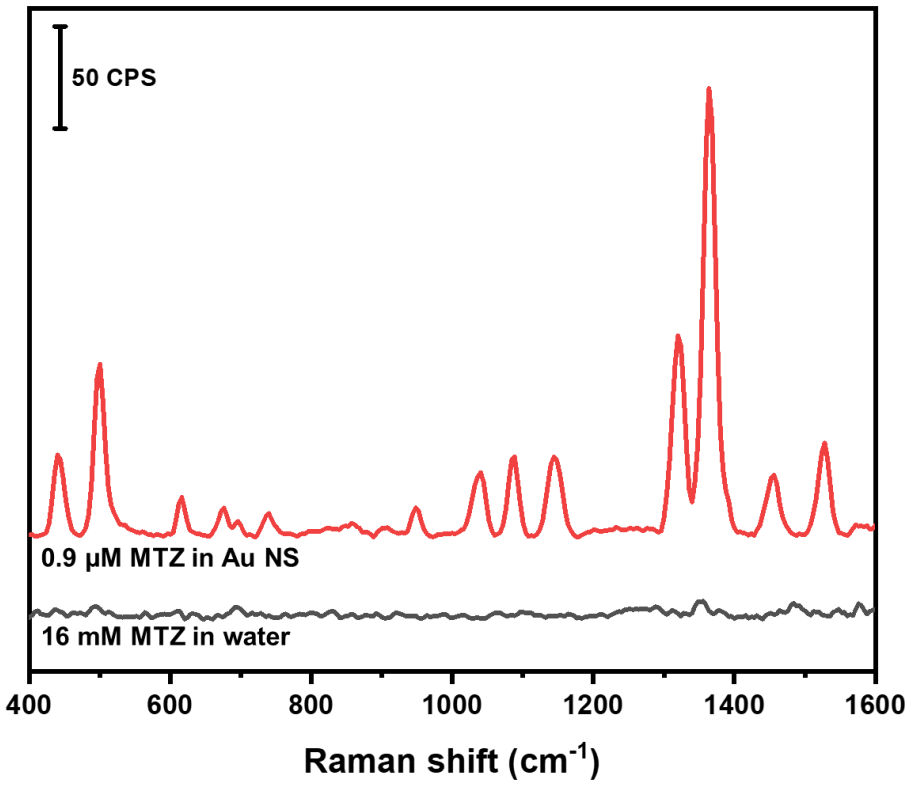


**Figure 4-13. Raman spectra showing the enhancement of methimazole in the presence of Au NS HR100.**

The enhancement factor for Au NS HR100 was determined using the analytical enhancement factor formula[68], as shown as in equation 4-4:

$$A.E.F. = \frac{I_{\mathrm{SERS}}/c_{\mathrm{SERS}}}{I_{\mathrm{Raman}}/c_{\mathrm{Raman}}} \qquad \textbf{(Eq 4–4)}$$

where $I_{\mathrm{SERS}}$ and $I_{\mathrm{Raman}}$ are the peak intensities at 1364 $cm^{-1}$ of MTZ in the presence and in the absence of Au NS HR100, respectively. The $c_{\mathrm{SERS}}$ and $c_{\mathrm{Raman}}$ terms are the solution

concentrations of MTZ in the SERS and normal Raman measurements (0.917 μM and 16 mM), respectively. The enhancement factor from the Au NS was calculated to be $5.2x10^5$. This value falls within the typical enhancement factor value ranges reported in the literature.[68]

#### 4.3.4.2 Measurement in Complex Matrix

Human urine is a complex matrix consisting of non-protein nitrogenous compounds (e.g., urea), inorganic ions and salts, water soluble toxins, and haemoglobin by-products.[69] Individuals that use MTZ to treat hyperthyroidism will excrete excess amounts in their urine.[51-52] The amount of MTZ retained in tissues can be harmful to the individuals' health;[51] it can be quantified by monitoring the amount of MTZ excreted in urine. In our study, we spiked synthetic urine with MTZ and used our colloidal Au NS SERS substrate to quantify the amount of MTZ. Figure 4-14 shows the Raman spectra of MTZ found in urine, along with the corresponding control experiments. In the urine spectrum, we observe a peak at 1008 $cm^{-1}$.

Based on previous work involving urine analysis, the peak at 1008 $cm^{-1}$ likely corresponds to urea due to a symmetrical CN stretching vibration.[69-72] When urine is spiked with MTZ (0.2 mM as a final concentration), no bands corresponding to MTZ are observed. When urine is mixed with the Au NS nanoaggregate substrate, only the HEPES buffer peak is visible. The disappearance of the 1008 $cm^{-1}$ peak may be due to the dilution of the urine into the Au NS. The urine sample spiked with MTZ (0.5 μM as a final concentration) mixed with the Au NS nanoaggregates shows a large enhancement of MTZ. Using the calibration curve obtained in water (Figure 4-12B), MTZ in urine was examined at 0.5 and 0.8 μM and showed recoveries of nearly 100% (Table 4-10).

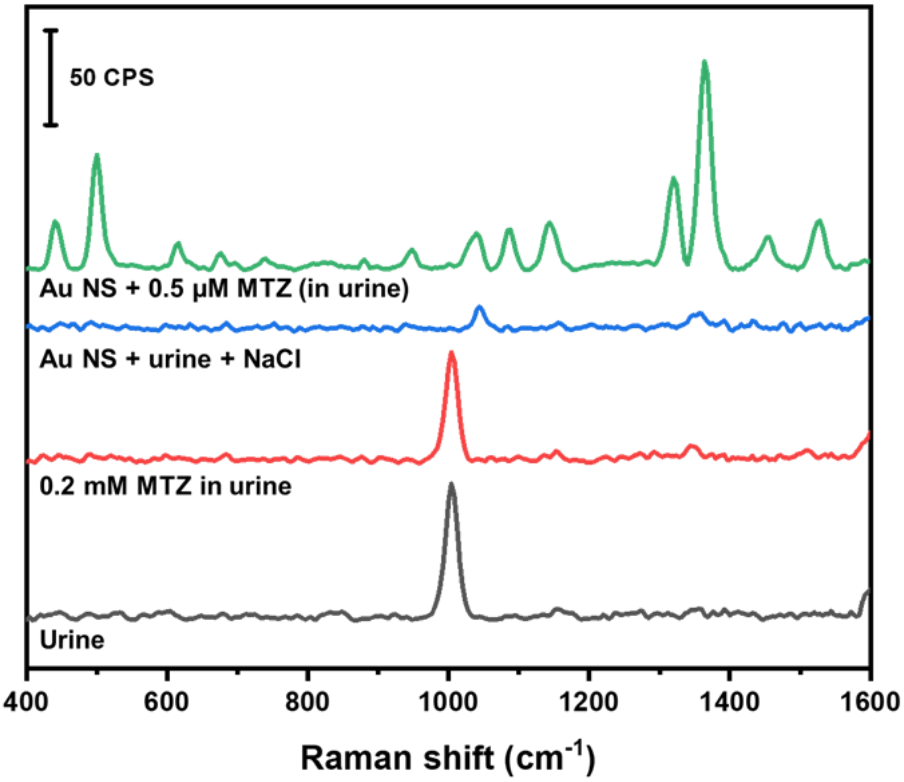


**Figure 4-14. In solution SERS spectrum of MTZ in urine and associated control spectra.**

**Table 4-10. Recoveries of MTZ in Urine Using Au NS Nanoaggregates as a SERS Substrate**

| Spiked amount of MTZ (µM) | Calc. amount of MTZ (µM) | % Recovery | % RSD |
|---|---|---|---|
| 0.5 | 0.495 ± 0.009 | 99 ± 2 | 2% |
| 0.8 | 0.83 ± 0.05 | 104 ± 6 | 5% |

## 4.4 Conclusions

The synthesis of Au NS using HEPES and EPPS buffer were explored systematically to determine the optimal buffer and buffer to gold ratio for colloidal SERS analysis. We determined that Au NS synthesized using HEPES at R=100 produced the highest signal intensities. The SERS signal intensities have been attributed to the thermodynamics and kinetics of adsorption, desorption, and ligand exchange between the buffer molecules and the Raman probe. This relationship is complicated but can be attributed mainly to the surface coverage of the probe molecule. The HR100 Au NS are stable in the long term (>2 months in the fridge) after functionalization with the Raman probe (relative standard deviation of 8%). These nanostars potentially could be functionalized and stored for other SERS assay applications. Our colloidal Au NS substrate detected a variety of analytes, notably cipro, TBZ, MG, and MTZ, in less than 5 min. The addition of NaCl significantly improved the Raman intensities through the formation of nanoaggregates. A SERS assay was developed for the detection and quantitation of MTZ. The assay produced a limit of detection of 0.1 μM and a recovery of nearly 100% when MTZ was spiked in urine. The coupling of a water dispersible Au NS SERS substrate with a handheld Raman device promotes on-site and in-process quality control of field analyses.

## 4.5 References


1. Nikoobakht, B.; El-Sayed, M. A., Preparation and Growth Mechanism of Gold Nanorods (NRs) Using Seed-Mediated Growth Method. *Chemistry of Materials* **2003,** *15* (10), 1957-1962.

2. Gole, A.; Murphy, C. J., Seed-Mediated Synthesis of Gold Nanorods: Role of the Size and Nature of the Seed. *Chemistry of Materials* **2004,** *16* (19), 3633-3640.

3. Sau, T. K.; Murphy, C. J., Room Temperature, High-Yield Synthesis of Multiple Shapes of Gold Nanoparticles in Aqueous Solution. *Journal of the American Chemical Society* **2004,** *126* (28), 8648-8649.

4. Kou, X.; Ni, W.; Tsung, C.-K.; Chan, K.; Lin, H.-Q.; Stucky, G. D.; Wang, J., Growth of Gold Bipyramids with Improved Yield and Their Curvature-Directed Oxidation. *Small* **2007,** *3* (12), 2103-2113.

5. Skrabalak, S. E.; Au, L.; Li, X.; Xia, Y., Facile synthesis of Ag nanocubes and Au nanocages. *Nature Protocols* **2007,** *2*, 2182.

6. Pelaz, B.; Grazu, V.; Ibarra, A.; Magen, C.; del Pino, P.; de la Fuente, J. M., Tailoring the Synthesis and Heating Ability of Gold Nanoprisms for Bioapplications. *Langmuir* **2012,** *28* (24), 8965-8970.

7. Ahsan, H.; Masaaki, T.; Guang, W. Y., Formation of Gold Nanoparticles by Good's Buffers. *Bulletin of the Chemical Society of Japan* **2005,** *78* (2), 262-269.

8. Xie, J.; Lee, J. Y.; Wang, D. I. C., Seedless, Surfactantless, High-Yield Synthesis of Branched Gold Nanocrystals in HEPES Buffer Solution. *Chemistry of Materials* **2007,** *19* (11), 2823-2830.

9. Nehl, C. L.; Liao, H.; Hafner, J. H., Optical Properties of Star-Shaped Gold Nanoparticles. *Nano Letters* **2006,** *6* (4), 683-688.

10. Murphy, C. J.; Gole, A. M.; Hunyadi, S. E.; Stone, J. W.; Sisco, P. N.; Alkilany, A.; Kinard, B. E.; Hankins, P., Chemical sensing and imaging with metallic nanorods. *Chemical Communications* **2008,** (5), 544-557.

11. Rycenga, M.; Langille, M. R.; Personick, M. L.; Ozel, T.; Mirkin, C. A., Chemically Isolating Hot Spots on Concave Nanocubes. *Nano Letters* **2012,** *12* (12), 6218-6222.

12. Huang, X.; Neretina, S.; El-Sayed, M. A., Gold Nanorods: From Synthesis and Properties to Biological and Biomedical Applications. *Advanced Materials* **2009,** *21* (48), 4880-4910.

13. Banholzer, M. J.; Millstone, J. E.; Qin, L.; Mirkin, C. A., Rationally designed nanostructures for surface-enhanced Raman spectroscopy. *Chemical Society Reviews* **2008,** *37* (5), 885-897.

14. Gersten, J. I., The Effect of Surface-Roughness on Surface Enhanced Raman-Scattering. *J Chem Phys* **1980,** *72* (10), 5779-5780.

15. Tian, F.; Bonnier, F.; Casey, A.; Shanahan, A. E.; Byrne, H. J., Surface enhanced Raman scattering with gold nanoparticles: effect of particle shape. *Analytical Methods* **2014,** *6* (22), 9116-9123.

16. Rodríguez-Lorenzo, L.; Álvarez-Puebla, R. A.; Pastoriza-Santos, I.; Mazzucco, S.; Stéphan, O.; Kociak, M.; Liz-Marzán, L. M.; García de Abajo, F. J., Zeptomol Detection Through Controlled Ultrasensitive Surface-Enhanced Raman Scattering. *Journal of the American Chemical Society* **2009,** *131* (13), 4616-4618.

17. Indrasekara, A. S. D. S.; Meyers, S.; Shubeita, S.; Feldman, L. C.; Gustafsson, T.; Fabris, L., Gold nanostar substrates for SERS-based chemical sensing in the femtomolar regime. *Nanoscale* **2014,** *6* (15), 8891-8899.

18. Lu, G.; Forbes, T. Z.; Haes, A. J., SERS detection of uranyl using functionalized gold nanostars promoted by nanoparticle shape and size. *Analyst* **2016,** *141* (17), 5137-5143.

19. Lu, G.; Johns, A. J.; Neupane, B.; Phan, H. T.; Cwiertny, D. M.; Forbes, T. Z.; Haes, A. J., Matrix-Independent Surface-Enhanced Raman Scattering Detection of Uranyl Using Electrospun Amidoximated Polyacrylonitrile Mats and Gold Nanostars. *Analytical Chemistry* **2018,** *90* (11), 6766-6772.

20. Sánchez-Purrà, M.; Carré-Camps, M.; de Puig, H.; Bosch, I.; Gehrke, L.; Hamad-Schifferli, K., Surface-Enhanced Raman Spectroscopy-Based Sandwich Immunoassays for Multiplexed Detection of Zika and Dengue Viral Biomarkers. *ACS Infectious Diseases* **2017,** *3* (10), 767-776.

21. Sánchez-Purrà, M.; Roig-Solvas, B.; Rodriguez-Quijada, C.; Leonardo, B. M.; Hamad-Schifferli, K., Reporter Selection for Nanotags in Multiplexed Surface Enhanced Raman Spectroscopy Assays. *ACS Omega* **2018,** *3* (9), 10733-10742.

22. Senthil Kumar, P.; Pastoriza-Santos, I.; Rodríguez-González, B.; Javier García de Abajo, F.; Liz-Marzán, L. M., High-yield synthesis and optical response of gold nanostars. *Nanotechnology* **2007,** *19* (1), 015606.

23. Nalbant Esenturk, E.; Hight Walker, A. R., Surface-enhanced Raman scattering spectroscopy via gold nanostars. *Journal of Raman Spectroscopy* **2009,** *40* (1), 86-91.

24. Yuan, H.; Khoury, C. G.; Hwang, H.; Wilson, C. M.; Grant, G. A.; Vo-Dinh, T., Gold nanostars: surfactant-free synthesis, 3D modelling, and two-photon photoluminescence imaging. *Nanotechnology* **2012,** *23* (7), 075102.

25. Chandra, K.; Culver, K. S. B.; Werner, S. E.; Lee, R. C.; Odom, T. W., Manipulating the Anisotropic Structure of Gold Nanostars using Good's Buffers. *Chemistry of Materials* **2016,** *28* (18), 6763-6769.

26. Liu, H.; Xu, Y.; Qin, Y.; Sanderson, W.; Crowley, D.; Turner, C. H.; Bao, Y., Ligand-Directed Formation of Gold Tetrapod Nanostructures. *The Journal of Physical Chemistry C* **2013,** *117* (33), 17143-17150.

27. Cai, J.; Raghavan, V.; Bai, Y. J.; Zhou, M. H.; Liu, X. L.; Liao, C. Y.; Ma, P.; Shi, L.; Dockery, P.; Keogh, I.; Fan, H. M.; Olivo, M., Controllable synthesis of tetrapod gold nanocrystals with precisely tunable near-infrared plasmon resonance towards highly efficient surface enhanced Raman spectroscopy bioimaging. *Journal of Materials Chemistry B* **2015,** *3* (37), 7377-7385.

28. Grady, J. K.; Chasteen, N. D.; Harris, D. C., Radicals from "Good's" buffers. *Analytical Biochemistry* **1988,** *173* (1), 111-115.

29. Chen, R.; Wu, J.; Li, H.; Cheng, G.; Lu, Z.; Che, C.-M., Fabrication of gold nanoparticles with different morphologies in HEPES buffer. *Rare Metals* **2010,** *29* (2), 180-186.

30. Xi, W.; Haes, A. J., Elucidation of HEPES Affinity to and Structure on Gold Nanostars. *Journal of the American Chemical Society* **2019,** *141* (9), 4034-4042.

31. Dam, D. H. M.; Lee, J. H.; Sisco, P. N.; Co, D. T.; Zhang, M.; Wasielewski, M. R.; Odom, T. W., Direct Observation of Nanoparticle–Cancer Cell Nucleus Interactions. *ACS Nano* **2012,** *6* (4), 3318-3326.

32. Menges, F. Spectragryph - Optical Spectroscopy Software, Version 1.2.10; 2018; http://www.effemm2.de/spectragryph/.

33. Hao, F.; Nehl, C. L.; Hafner, J. H.; Nordlander, P., Plasmon Resonances of a Gold Nanostar. *Nano Letters* **2007,** *7* (3), 729-732.

34. Webb, J. A.; Erwin, W. R.; Zarick, H. F.; Aufrecht, J.; Manning, H. W.; Lang, M. J.; Pint, C. L.; Bardhan, R., Geometry-Dependent Plasmonic Tunability and Photothermal Characteristics of Multibranched Gold Nanoantennas. *The Journal of Physical Chemistry C* **2014,** *118* (7), 3696-3707.

35. Jalani, G.; Cerruti, M., Nano graphene oxide-wrapped gold nanostars as ultrasensitive and stable SERS nanoprobes. *Nanoscale* **2015,** *7* (22), 9990-9997.

36. Nergiz, S. Z.; Gandra, N.; Singamaneni, S., Self-assembled high aspect ratio gold nanostar/graphene oxide hybrid nanorolls. *Carbon* **2014,** *66*, 585-591.

37. Gkogkou, D.; Schreiber, B.; Shaykhutdinov, T.; Ly, H. K.; Kuhlmann, U.; Gernert, U.; Facsko, S.; Hildebrandt, P.; Esser, N.; Hinrichs, K.; Weidinger, I. M.; Oates, T. W. H., Polarization- and Wavelength-Dependent Surface-Enhanced Raman Spectroscopy Using Optically Anisotropic Rippled Substrates for Sensing. *ACS Sensors* **2016,** *1* (3), 318-323.

38. Holze, R., Competition of anchoring groups in adsorption on gold electrodes—a comparative spectroelectrochemical study of 4-mercaptobenzonitrile and aromatic nitriles. *Journal of Solid State Electrochemistry* **2013,** *17* (7), 1869-1879.

39. Villarreal, E.; Li, G. G.; Zhang, Q.; Fu, X.; Wang, H., Nanoscale Surface Curvature Effects on Ligand–Nanoparticle Interactions: A Plasmon-Enhanced Spectroscopic Study of Thiolated Ligand Adsorption, Desorption, and Exchange on Gold Nanoparticles. *Nano Letters* **2017,** *17* (7), 4443-4452.

40. Porter, M. D.; Bright, T. B.; Allara, D. L.; Chidsey, C. E. D., Spontaneously organized molecular assemblies. 4. Structural characterization of n-alkyl thiol monolayers on gold by optical ellipsometry, infrared spectroscopy, and electrochemistry. *Journal of the American Chemical Society* **1987,** *109* (12), 3559-3568.

41. III, N. C.; Chidsey, C. E. D.; Liu, G. y.; Scoles, G., Substrate dependence of the surface structure and chain packing of docosyl mercaptan self-assembled on the (111), (110), and (100) faces of single crystal gold. *The Journal of Chemical Physics* **1993,** *98* (5), 4234-4245.

42. Yaffe, N. R.; Ingram, A.; Graham, D.; Blanch, E. W., A multi-component optimisation of experimental parameters for maximising SERS enhancements. *Journal of Raman Spectroscopy* **2010,** *41* (6), 618-623.

43. Bell, S. E. J.; Sirimuthu, N. M. S., Surface-Enhanced Raman Spectroscopy (SERS) for Sub-Micromolar Detection of DNA/RNA Mononucleotides. *Journal of the American Chemical Society* **2006,** *128* (49), 15580-15581.

44. Papadopoulou, E.; Bell, S. E. J., Label-Free Detection of Single-Base Mismatches in DNA by Surface-Enhanced Raman Spectroscopy. *Angewandte Chemie* **2011,** *123* (39), 9224-9227.

45. Yang, L.; Chen, Y.; Shen, Y.; Yang, M.; Li, X.; Han, X.; Jiang, X.; Zhao, B., SERS strategy based on the modified Au nanoparticles for highly sensitive detection of bisphenol A residues in milk. *Talanta* **2018,** *179*, 37-42.

46. Alsammarraie, F. K.; Lin, M.; Mustapha, A.; Lin, H.; Chen, X.; Chen, Y.; Wang, H.; Huang, M., Rapid determination of thiabendazole in juice by SERS coupled with novel gold nanosubstrates. *Food Chemistry* **2018,** *259*, 219-225.

47. Liou, P.; Nayigiziki, F. X.; Kong, F.; Mustapha, A.; Lin, M., Cellulose nanofibers coated with silver nanoparticles as a SERS platform for detection of pesticides in apples. *Carbohydrate Polymers* **2017,** *157*, 643-650.

48. USEPA, EPA reregistration eligibility decision thabendazole. United States Environmental Protection Agency: 2002.

49. USDA, Pesticide Data Program Annual Summary, Calendar Year 2017. United States Department of Agriculture: 2017.

50. Kim, M. S.; Kim, M. K.; Lee, C. J.; Jung, Y. M.; Lee, M. S., Surface-enhanced Raman Spectroscopy of Benzimidazolic Fungicides: Benzimidazole and Thiabendazole. *B Korean Chem Soc* **2009,** *30* (12), 2930-2934.

51. Ebrahimzadeh, H.; Asgharinezhad, A. A.; Adlnasab, L.; Shekari, N., Optimization of ion-pair based hollow fiber liquid phase microextraction combined with HPLC–UV for the determination of methimazole in biological samples and animal feed. *Journal of Separation Science* **2012,** *35* (16), 2040-2047.

52. Kuśmierek, K.; Bald, E., Determination of methimazole in urine by liquid chromatography. *Talanta* **2007,** *71* (5), 2121-2125.

53. Kong, D.; Chi, Y.; Chen, L.; Dong, Y.; Zhang, L.; Chen, G., Determination of thyreostatics in animal feeds by CE with electrochemical detector. *ELECTROPHORESIS* **2009,** *30* (19), 3489-3495.

54. Genter, M. B., Evaluation of olfactory and auditory system effects of the antihyperthyroid drug carbimazole in the Long-Evans rat. *Journal of Biochemical and Molecular Toxicology* **1998,** *12* (5), 305-314.

55. Fei, J.; Wu, L.; Zhang, Y.; Zong, S.; Wang, Z.; Cui, Y., Pharmacokinetics-on-a-Chip Using Label-Free SERS Technique for Programmable Dual-Drug Analysis. *ACS Sensors* **2017,** *2* (6), 773-780.

56. Ma, P.; Liang, F.; Yang, Q.; Wang, D.; Sun, Y.; Wang, X.; Gao, D.; Song, D., Highly sensitive SERS probe for mercury(II) using cyclodextrin-protected silver nanoparticles functionalized with methimazole. *Microchimica Acta* **2014,** *181* (9), 975-981.

57. Saleh, T. A.; Al-Shalalfeh, M. M.; Al-Saadi, A. A., Silver nanoparticles for detection of methimazole by surface-enhanced Raman spectroscopy. *Materials Research Bulletin* **2017,** *91*, 173-178.

58. Saleh, T. A.; Al-Shalalfeh, M. M.; Onawole, A. T.; Al-Saadi, A. A., Ultra-trace detection of methimazole by surface-enhanced Raman spectroscopy using gold substrate. *Vibrational Spectroscopy* **2017,** *90*, 96-103.

59. Saleh, T. A.; Al-Shalalfeh, M. M.; Al-Saadi, A. A., Graphene Dendrimer-stabilized silver nanoparticles for detection of methimazole using Surface-enhanced Raman scattering with computational assignment. *Scientific Reports* **2016,** *6*, 32185.

60. Muniz-Miranda, M.; Muniz-Miranda, F.; Pedone, A., Raman and DFT study of methimazole chemisorbed on gold colloidal nanoparticles. *Physical Chemistry Chemical Physics* **2016,** *18* (8), 5974-5980.

61. Zhao, Y.; Tian, Y.; Ma, P.; Yu, A.; Zhang, H.; Chen, Y., Determination of melamine and malachite green by surface-enhanced Raman scattering spectroscopy using starch-coated silver nanoparticles as substrates. *Analytical Methods* **2015,** *7* (19), 8116-8122.

62. CFIA Malachite Green - Questions and Answers. http://www.inspection.gc.ca/food/information-for-consumers/fact-sheets-and-infographics/products-and-risks/chemical-hazards/malachite-green/eng/1332268890141/1332268947157 (accessed April 2, 2019).

63. Chamuah, N.; Bhuyan, N.; Das, P. P.; Ojah, N.; Choudhary, A. J.; Medhi, T.; Nath, P., Gold-coated electrospun PVA nanofibers as SERS substrate for detection of pesticides. *Sensors and Actuators B: Chemical* **2018,** *273*, 710-717.

64. Hidi, I. J.; Heidler, J.; Weber, K.; Cialla-May, D.; Popp, J., Ciprofloxacin: pH-dependent SERS signal and its detection in spiked river water using LoC-SERS. *Analytical and Bioanalytical Chemistry* **2016,** *408* (29), 8393-8401.

65. Yang, L.; Qin, X.; Jiang, X.; Gong, M.; Yin, D.; Zhang, Y.; Zhao, B., SERS investigation of ciprofloxacin drug molecules on TiO2 nanoparticles. *Physical Chemistry Chemical Physics* **2015,** *17* (27), 17809-17815.

66. Neugebauer, U.; Szeghalmi, A.; Schmitt, M.; Kiefer, W.; Popp, J.; Holzgrabe, U., Vibrational spectroscopic characterization of fluoroquinolones. *Spectrochimica Acta Part A: Molecular and Biomolecular Spectroscopy* **2005,** *61* (7), 1505-1517.

67. Panneerselvam, R.; Liu, G.-K.; Wang, Y.-H.; Liu, J.-Y.; Ding, S.-Y.; Li, J.-F.; Wu, D.-Y.; Tian, Z.-Q., Surface-enhanced Raman spectroscopy: bottlenecks and future directions. *Chemical Communications* **2018,** *54* (1), 10-25.

68. Le Ru, E. C.; Blackie, E.; Meyer, M.; Etchegoin, P. G., Surface Enhanced Raman Scattering Enhancement Factors: A Comprehensive Study. *The Journal of Physical Chemistry C* **2007,** *111* (37), 13794-13803.

69. Moreira, L. P.; Silveira, L.; Pacheco, M. T. T.; da Silva, A. G.; Rocco, D. D. F. M., Detecting urine metabolites related to training performance in swimming athletes by means of Raman spectroscopy and principal component analysis. *Journal of Photochemistry and Photobiology B: Biology* **2018,** *185*, 223-234.

70. Keuleers, R.; Desseyn, H. O.; Rousseau, B.; Van Alsenoy, C., Vibrational Analysis of Urea. *The Journal of Physical Chemistry A* **1999,** *103* (24), 4621-4630.

71. Premasiri, W. R.; Clarke, R. H.; Womble, M. E., Urine analysis by laser Raman spectroscopy. *Lasers in Surgery and Medicine* **2001,** *28* (4), 330-334.

72. Bispo, J. A. M.; Vieira, E. E. d. S.; Jr., L. S.; Fernandes, A. B., Correlating the amount of urea, creatinine, and glucose in urine from patients with diabetes mellitus and hypertension with the risk of developing renal lesions by means of Raman spectroscopy and principal component analysis. *Journal of Biomedical Optics* **2013,** *18* (8), 1-8, 8.

# Chapter 5

## Graphene–Silver Nanocomposite as a Colloidal SERS Substrate

## 5.1 Introduction

The development of sensitive biosensing platforms that are able to detect and quantify chemical and biological molecules can impact many fields, including biological, forensic, medical, and environmental domains.[1-2] Graphene is a 2D carbon structure with a large surface area and unique electrical, optical, and thermal properties, which make it suitable for a wide spectrum of applications.[3] Graphene and its derivatives, such as graphene oxide (GO) and reduced graphene oxide (RGO), can interact with planar organic molecules through various noncovalent adsorption mechanisms, including π−π stacking, electrostatic, and/or van der Waals forces.[4-9] The interaction of graphene with organic dyes can lead to fluorescence quenching.[4, 7-9] Graphene can bind also to nucleobases and nucleosides.[10]

The capability of graphene to bind to nucleobases and to quench fluorescence has attracted a lot of interest to employ graphene and its derivatives in sensing platforms, based on fluorescence resonance energy transfer (FRET).[11-22] In this platform, single stranded DNA (ssDNA ), RNA, or aptamers labelled with a fluorophore adsorb on the graphene surface, leading to fluorescence quenching.[11-22] However, upon introducing the complementary strands or the target molecule in the case of aptamers, the probed strand detaches from the graphene surface to bind to its complementary strand or target molecule, which results in restoring the fluorescence signal.[11-22] This platform has been extended for cellular imaging due to its water dispersibility and biocompatibility.[23-28]

The capability of graphene to quench fluorescence and adsorb molecules by π−π stacking has extrapolated its use into surface enhanced Raman scattering (SERS). Liu and co-workers showed that graphene can be used as a substrate to suppress fluorescence

background from rhodamine 6G (R6G) and protoporphyrin IX (PPP).[29] This enabled them to observe the resonance Raman signals of these molecules upon adsorption on graphene without the use of plasmonic nanostructures.[29] The same group also showed that the Raman signals of phthalocyanine (PC), crystal violet (CV), R6G, and PPP, using resonant and non-resonant excitation wavelengths, are enhanced upon adsorption on graphene compared to a $SiO_2$/Si substrate due to chemical enhancement.[30] They showed also that the Raman signal intensities reduced with the increase in the number of graphene layers.[30] This led to the introduction of graphene enhanced Raman scattering (GERS).[31] Zhang and co-workers demonstrated using PPP in a distance dependent study that GERS belongs to the chemical enhancement mechanism.[31] Yu et al. showed that by tuning the reduction of GO nanosheets, they can have higher Raman signal intensities than those of mechanically exfoliated graphene.[32] They observed an enhancement factor of up to $10^3$ of rhodamine B (RhB), and they attributed that to the role of electronegative oxygen species in the chemical enhancement mechanism.[32] Nam's group observed a $10^4$ enhancement factor using a large area graphene grown by chemical vapor deposition (CVD) as a SERS substrate.[33] They reached this enhancement level by increasing oxygenated species on graphene using a UV/ozone treatment.[33] Yaghobian and co-workers showed that 4-mercaptobenzoic acid (4-MBA) gave a reproducible GERS effect.[34] However, the SERS enhancement using silver nanoparticles was higher than that of the GERS in that study.[34]

Graphene can offer a large surface area 2D platform for the attachment of plasmonic nanostructures.[35-37] The attachment of metallic nanoparticles can be achieved without the use of capping agents.[35, 38] The size and loading density of metal

nanoparticles can be controlled on a graphene surface, which leads to SERS enhancement tunability.[35, 39] This has led to the development of SERS assays, based on graphene–plasmonic particle nanocomposites and DNA. For example, Fan et al. developed a label free SERS platform, based on a gold nanopopcorn–graphene nanocomposite for the detection of methicillin-resistant Staphylococcus aureus (MRSA) bacteria and DNA sequence related to HIV.[36] The enhancement factor of the nanocomposite was two orders of magnitude higher than that of gold nanopopcorn and nine orders of magnitude higher than that of GO.[36] He and coworkers used a gold–graphene nanocomposite as a SERS substrate for multiplexed DNA detection upon hybridization, with a limit of detection of 10 pM.[40] Lin et al. developed a SERS platform for DNA detection upon hybridization.[41] Their platform depended on the modification of a silver–graphene nanocomposite surface with thiolated DNA on one end. On the other end, a complementary thiolated DNA strand was attached to silver nanoparticles (AgNPs) that were functionalized with 4-MBA as a Raman probe.[41] The hybridization led to an increase in the SERS signal of 4-MBA, as it brought it closer to the surface of the nanocomposite. This SERS platform showed a pM limit of detection.[41] Although graphene–silver nanocomposites have been used in SERS assays for DNA detection, these assays have not utilized the nanocomposites in their colloidal form.[41-45]

Herein, we are presenting the use of a graphene–silver nanocomposite as a colloidal SERS substrate. The plasmonic behavior and SERS performance of this nanocomposite can be tuned by the particle size of AgNPs integrated on the surface. The nanocomposites showed superior SERS performance compared to silver nanoparticles when they are mixed with a dye labelled DNA in a buffer solution. The platform can be

used to detect DNA hybridization, where the SERS signal of a dye-labelled DNA can be reduced upon hybridization with a complementary strand.

## 5.2 Experimental

### 5.2.1 Reagents

Graphite powder (300 mesh) was purchased from Alfa Easer. Potassium permanganate ($KMNO_4$) and sulphuric acid ($H_2SO_4$, 95.0%–98.0%,) were purchased from Caledon. The following reagents were obtained from Sigma-Aldrich: 10-nm citrate capped AgNPs, sodium borohydride ($NaBH_4$, 99.99%), hydrogen peroxide (30% (W/W)), 4-nitrobenzenthiol (NBT, 80%), acetonitrile (ACN, ≥99.9%), anhydrous magnesium chloride ($MgCl_2$, ≥98%), potassium phosphate monobasic ($KH_2PO_4$, ≥99.9%), and potassium phosphate dibasic ($K_2HPO_4$, ≥99.9%). Phosphoric acid ($H_3PO_4$, 85%) was purchased from Fisher Scientific and dialysis membranes with 1000 molecular weight cutoff was purchased from VWR. Cyanine 5 labelled DNA with a sequence of 5'-Cy5-TTG TTA ATT-3' (CY5-DNA) and its complementary DNA (cDNA) strand were purchased from Integrated DNA Technologies, Inc. (IDT). 10 mM potassium phosphate buffer (PPB) containing 9.4 mM $K_2HPO_4$, 0.6 mM $KH_2PO_4$, and 1 mM $MgCl_2$ (pH = 8) was used in all DNA experiments. Deionized (DI) water (18.2 MΩ cm) was used for all syntheses and measurements, unless stated otherwise.

### 5.2.2 Synthesis of Graphene Oxide (GO)

Graphene oxide sheets were synthesized according to previously published methods, with some modifications.[28, 46] In an ice bath, 0.3 g of graphite powder was mixed with a

mixture of concentrated sulphuric and phosphoric acids in a ratio of 9:1 (36:4 mL). Then, 1.8 g $KMnO_4$ were added portion-wise over an hour. *[Warning: This reaction has to be performed with extreme care in an ice bath. The addition of $KMNO_4$ has to be in a portion-wise manner over an hour to ensure cooling of the reaction after each addition. A thermometer has to be used to make sure that the temperature is less than 5 °C before each addition. This mixture presents an explosion hazard. All work has to be performed in an appropriate chemical fume hood with the proper personal protective equipment]* Then, the mixture was stirred for 12 h at 50 °C. Afterwards, the mixture was cooled to room temperature before it was transferred to a beaker containing 40 mL ice water, then 30% $H_2O_2$ was added drop by drop till no bubbling was observed, and the solution color turned light brown. The solution was filtered by vacuum filtration through a nylon filter with a 0.2-µm pore size. The slurry was washed three times with 1 L of 10 % HCL acid and then washed with Milli-Q water extensively. The powder was collected after being air dried and was dissolved in Milli-Q water to make a 0.5% solution (wt./vol.). This solution was transferred into dialysis tubes with a 1K molecular weight cut-off (MWCO) and placed in a 4-L beaker filled with Milli-Q water. Dialysis was performed for two weeks, and the water was changed twice per day. The solution was vacuum filtered again, as before, and the slurry was air-dried. The obtained powder was dissolved to make a 0.4 mg/mL suspension and then sonicated for 40 min for exfoliation. The suspension was kept at 4 °C till further use.

### 5.2.3 Synthesis of Silver–Graphene Nanocomposites (NCs)

Silver–graphene nanocomposites were synthesized according to a previously published paper by Kamat lab, with some modifications.[35] A 5-mL GO suspension (0.2 mg/mL) was

mixed with different volumes of 0.1 M silver nitrate solution to yield a final concentration of silver nitrate of 1.9, 2.9, and 3.8 mM and was stirred for 5 min. Sodium borohydride was used as the reducing agent. A 90-µL aqueous solution of ice-cooled sodium borohydride (130 mM) was added in10-µL portions every 30 s; this led to the appearance of a yellowish color indicating the formation of silver nanoparticles. The solutions were mixed for 10 min after the last addition of sodium borohydride. Nanocomposites were denoted as NC1.9, NC2.9, and NC3.8, according to the silver nitrate concentration used. Nanocomposites were centrifuged for 10 min at 3000 rpm, and the supernatant was removed carefully. The pellets were resuspended in DI water, and the previous step was repeated twice. The pellets were resuspended in DI water to make a final volume of 5 mL and stored at 4 °C. A reduced graphene oxide (RGO) sample was prepared without using any silver nitrate following the same steps.

## 5.2.4 Instrumentation

### 5.2.4.1 Fourier transform infrared (FTIR)

FTIR spectra of the bare and modified membranes were collected by a Nicolet 8700 Continuum FTIR Microscope with 128 scans and a resolution of 4 in absorbance mode.

### 5.2.4.2 Microscopy

**Transmission electron microscopy (TEM)**

Bright field transmission electron microscopy (TEM) was performed using a JEOL 2010 TEM equipped with a LaB6 thermionic emission filament operating at an accelerating voltage of 200 kV. The sample was prepared by placing a drop of GO suspension on a carbon-coated, 200-mesh Cu grid and drying at room temperature.

**Atomic force microscopy (AFM)**

The GO AFM image was collected by a Digital Instruments Nanoscope III Multimode microscope in tapping mode. A 5-μL of graphene oxide solution (0.2 mg/mL) was drop casted on a precleaned silicon wafer by an ozone cleaner (UV0-Cleaner, Model No.42, Jelight Company Inc.) for 10 min and left to air dry at room temperature.

**Scanning electron microscopy (SEM)**

Field emission scanning electron microscopy (FESEM) was performed using Zeiss Sigma FESEM at Nanofab. Samples were prepared by drop casting 5 μL of as prepared nanocomposites on precleaned silicon wafers by an ozone cleaner (UV0-Cleaner, Model No.42, Jelight Company Inc.) for 10 min and left to air dry at room temperature. Image acquisition was conducted with a 5-kV accelerating voltage. Images were analyzed with Gatan Digital Micrograph (version 2.31.734.0).

#### 5.2.4.3 Extinction spectroscopy

Extinction spectra were collected using a double-beam PerkinElmer Lambda 35 spectrometer. All experiments used a slit width of 1 nm and a scan rate of 960 nm/min. The samples were analyzed in quartz cuvettes. All samples were diluted by a factor of four with DI water before measurement, and DI water was used as a blank.

#### 5.2.4.4 Raman spectroscopy

Raman spectra were collected with a Renishaw in-via confocal Raman microscope using a 514.5 nm Ar ion, air-cooled laser; the laser power and integration time are specified for each experiment. Solid and drop casting samples were mounted or dropped on gold coated glass microscope slides. These slides were fabricated by thermally evaporating 10 nm Cr as an adhesive layer, followed by 300 nm Au in a thermal evaporation system, Torr

International. Spectra were collected using a 50x objective. All experiments involving colloidal samples were performed in a quartz cuvette using a 90° angle liquid cell holder, and spectra were collected using a 30x objective. A 5 mM 4-NBT stock solution was prepared in ACN, and the final concentrations after mixing with the nanocomposites was 5 μM. These solutions were left overnight to ensure functionalization. For the CY5 labelled DNA (CY5-DNA) SERS experiment, 1 mL of each of the NCs and 1 mL of 10-nm AgNPs were transferred to 2-mL Eppendorf tubes and centrifuged at 8000 rpm for 10 min, then the supernatant was discarded carefully from each tube without disturbing the pellets. Next, the pellets were mixed with 1 ml of 1 μM CY5-DNA in 10 mM PPB and left for one hour at room temperature before taking Raman measurements. For the DNA hybridization experiment, 250 μL of 1 μM complementary DNA (cDNA) solution were mixed with the NCs containing CY5-DNA from the previous step and left for 1 h at room temperature before measuring them again. Wire 3.4 software was used for data acquisition, background subtraction, and analysis.

## 5.3 Results and Discussion

### 5.3.1 Graphite Chemical Exfoliation to GO Nanosheets

GO can offer a scaffold with a large surface area that can be utilized to deposit nanoparticles for various applications.[35, 47-48]Hummers' method is the most widely used method to exfoliate graphite powder into GO using a strong oxidizing agent in concentrated acids.[46, 49] TEM and AFM were used to characterize the morphology of the synthesized GO. As depicted in Figure 5-1, the chemical exfoliation of graphite powder resulted in thin nanosheets of GO.

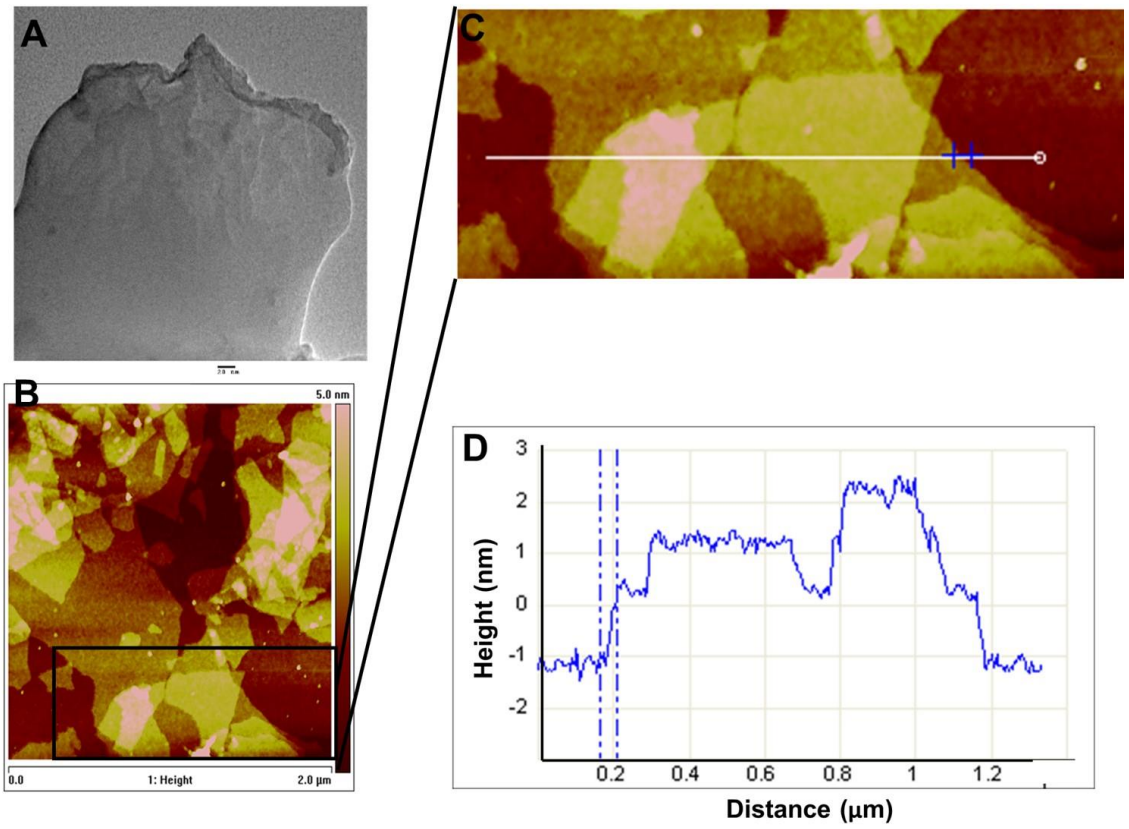


**Figure 5-1. Exfoliation of graphite into GO.** (A) TEM image of GO (scale bar 20 nm). (B) AFM image of GO (scale bar 2 µm). (C) Zoom in AFM image from (B) with a line across three layers of GO. (D) Line profile.

The surface of these nanosheets is flat, but sometimes the edge may wrinkle, as shown in the TEM image in Figure 5-1A. This was observed also by Marcano et al. with a monolayer of GO nanosheet.[46] The AFM image shows that the nanosheets have a microscale size and are arranged randomly in single to few layers. The line profile in Figure 5-1D shows that the layer thickness is about 1.1 ± 0.1 nm for a monolayer, which is consistent with what Mercano et al. had reported.[41] From Figure 5-1, we can conclude that graphite powder has been exfoliated into nanosheets of GO.

### 5.3.2 Vibrational Spectroscopy Characterization of GO Nanosheets

Oxygenated species on GO can function as nucleation sites for the growth of metallic nanoparticles.[35, 47-48] Marcano and co-workers have introduced an improved method to synthesize GO, which depends on using phosphoric acid, sulfuric acid, $KMnO_4$, and the removal of $NaNO_3$ that is used in the traditional Hummers' method.[46] They showed that their method can yield a more hydrophilic GO than that of Hummers' method.[46] As shown in Figure 5-2A and B, the FTIR spectrum of graphite has no observable oxygenated functional groups. However, the spectrum of GO showed bands assigned to C═O and O–H stretches at 1744 and 3450 $cm^{-1}$, respectively.[46] It also showed a band at 1632 $cm^{-1}$ that can be attributed to C═C stretches from unoxidized $sp^2$ carbons.[46] Our results were in agreement with those of Marcano et al.[46]

Raman spectroscopy is one of the most useful techniques that is used to characterize graphitic and carbon-based materials.[50-55] The technique is non-destructive and can provide a lot of information about graphene, such as its purity, number of layers, doping, chemical modification, and method of fabrication.[53-55] For example, Raman spectroscopy has been utilized to differentiate between metallic nanotube, doped graphene, and hard amorphous carbon samples.[55] The main Raman bands that are used to characterize GO are located approximately at 1360 and 1590 $cm^{-1}$. These two bands are called the D band and G band, respectively. The D band is attributed to the symmetry breaking at edges of graphitic planes in $sp^2$ carbon; the position of this band is dependent on the excitation laser wavelength.[50] The G band is attributed to the bond stretching of $sp^2$ carbon atoms; this band is independent of the excitation laser wavelength.[50] The D/G band ratios have been used to determine the graphitic crystalline

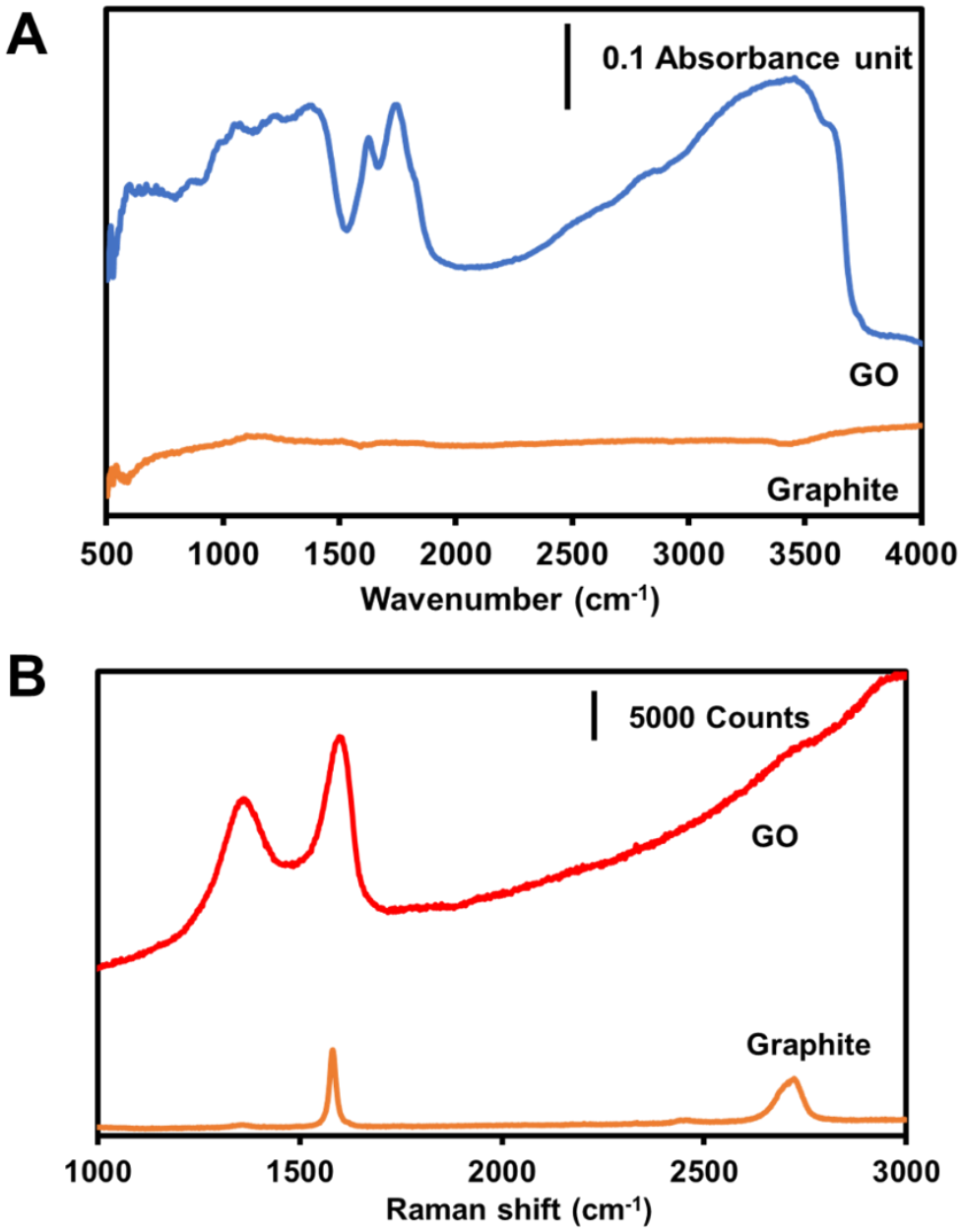


**Figure 5-2. FTIR and Raman spectroscopy characterization of GO.** (A) FTIR and (B) Raman spectra (laser conditions: 30 mW and 200 s integration time).

size.[56-57] Figure 5-2B shows Raman spectra of graphite and GO powders. The Raman spectrum of graphite powder contains the G band at 1585 $cm^{-1}$. It also has another band at 2726 $cm^{-1}$, which is called the 2D band, an overtone of the D band.[50, 58] The Raman spectrum of the powder GO shows D and G bands but not the 2D band, and this was

similar with Marcano et al.[46] Taken all together, the results from TEM, AFM, FTIR, and Raman spectroscopy confirm that the graphite powder has been exfoliated chemically into oxidized nanosheets of GO.

### 5.3.3 Characterization of Nanocomposites

#### 5.3.3.1 Nanocomposite morphology

As discussed in previous chapters of this thesis, the size and shape of metallic nanoparticles play a significant role in SERS enhancement. Graphene oxide can work as a large area scaffold that can be used as a support of many plasmonic nanoparticles and bring them close to each other. [33, 42-43] This can generate many hot spots on the 2D nanosheets. In addition, this scaffold can add more SERS enhancement through the chemical mechanism, whereby molecules are adsorbed on the graphene–metal nanocomposite. SEM was used to study the impact of increasing the silver nitrate concentration on the particle size and morphology of AgNPs. It was used also to investigate how AgNPs are integrated onto the surface of GO.

Figure 5-3 shows SEM images of the nanocomposites prepared using different concentrations of silver nitrate (1.9, 2.9, and 3.8 mM). Spherical AgNPs are formed on GO, and they are randomly distributed within the nanosheets. The average diameters were 6 ± 2, 8 ± 3, and 13 ± 7 nm for NC1.9, NC2.9, and NC3.8 (n = 30), respectively. The particle size increases with increasing silver nitrate concentration, with NC3.8 showing larger particles compared to the other nanocomposites. From Figure 5-3, we can conclude that AgNPs can be deposited randomly on a GO surface as spherical particles, and particle size can be controlled by adjusting the silver nitrate concentration.

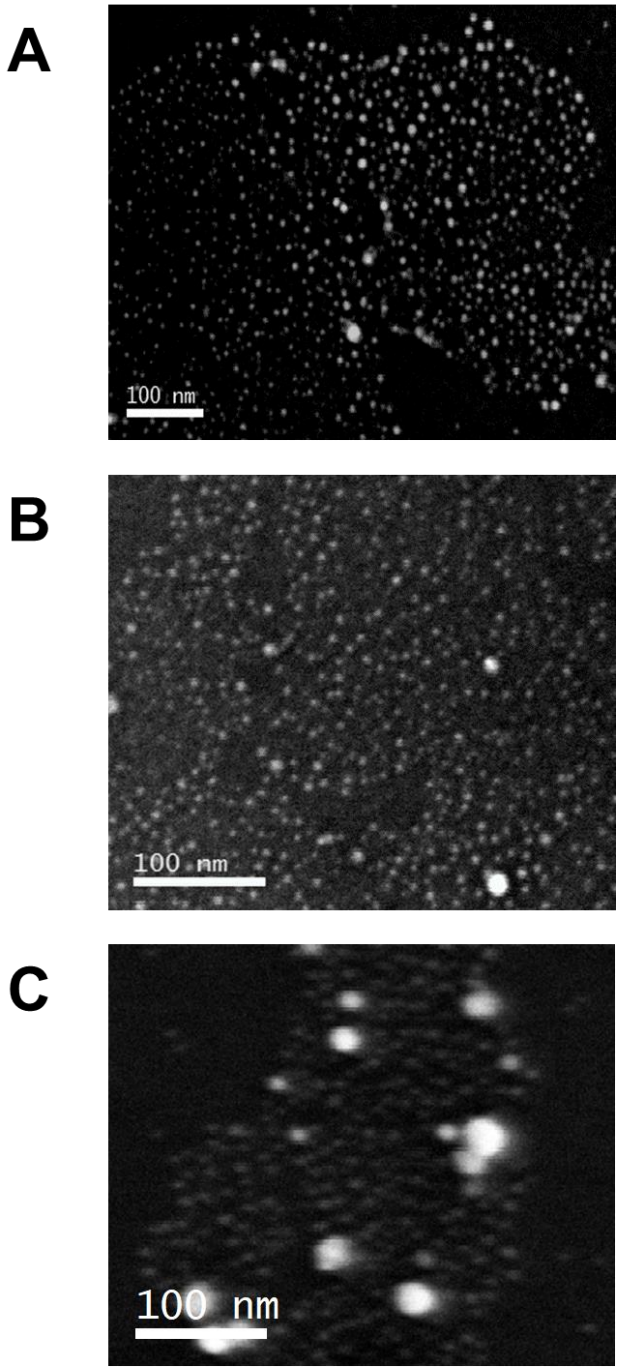


**Figure 5-3. SEM images of nanocomposites.** (A) NC1.9, (B) NC2, and (D) NC3.8.

#### 5.3.3.2 Plasmonic behavior

As discussed in previous chapters of this thesis, the plasmonic behavior of metallic nanostructures plays a crucial role in SERS. Extinction spectroscopy is one of the most used techniques to study the plasmonic behavior of nanocolloidal silver and gold, based on Mie theory.[59-60] Information about the size, shape, and concentration of noble metal nanoparticles can be provided from the wavelength, intensity, and width of the localized surface plasmon resonance (LSPR) band.[59, 61-63]

Figure 5-4 shows the extinction spectra of RGO and the nanocomposites samples. RGO showed a band at 228 nm, attributed to $\pi \rightarrow \pi^*$ transitions due to conjugation, and a shoulder around ~300 nm, attributed to $n \rightarrow \pi^*$ transitions due to carbonyl groups.[46, 64] The nanocomposites exhibit a band centered around 396 nm due to the localized plasmon resonance of the AgNPs. The band intensity increased and became broader with increasing silver nitrate concentration, which can be attributed to the increase in the standard deviation of the particle size, as shown in the SEM images of Figure 5-3. We observed a small red-shift (2–3 nm) in the LSPR of NC3.8 when compared to the other two nanocomposites. Data from extinction spectroscopy measurements are summarized in Table 5-1. The increase in extinction value and the red-shift of NC3.8 can be attributed to the increase in particle size. We did not observe any band in the longer wavelength region, suggesting that the particles are spherical in shape and are not aggregated. This is also consistent with the SEM images in Figure 5-3. We can conclude that the particle size and plasmonic behavior of AgNPs on GO can be tailored by adjusting the silver nitrate concentration.

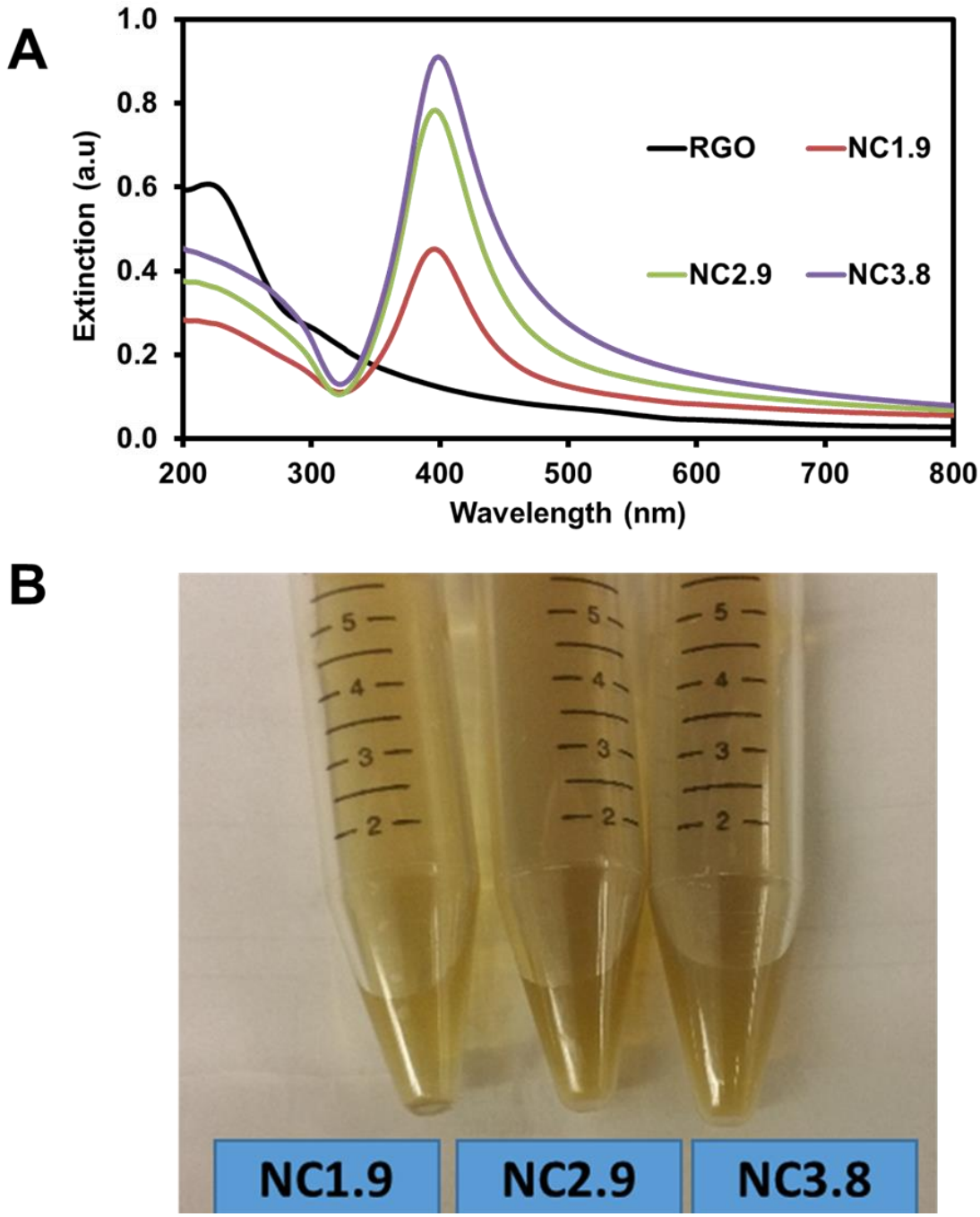


**Figure 5-4. Plasmonic behavior of the nanocomposites.** (A) Extinction spectra of RGO and NCs. (B) Image of colloidal NCs.

**Table 5-1. Summary of the Extinction Spectroscopy Data of the Nanocomposites Using Different Concentrations of Silver Nitrate**

| Nanocomposite | $\lambda_{(max)}$ (nm) | Extinction (a.u) |
|---|---|---|
| NC1.9 | 396 | 0.45 |
| NC2.9 | 397 | 0.78 |
| NC3.8 | 399 | 0.91 |

## 5.3.4 SERS Performance

### 5.3.4.1 Graphene as a Raman probe

GO is a Raman active material with two distinctive Raman bands, the D and G bands at approximately 1360 and 1590 $cm^{-1}$, respectively, as shown in Figure 5-2B. This means that the impact of increasing silver nitrate used for the synthesis of NCs can be probed by the Raman enhancement of these bands using Raman spectroscopy. We investigated two sampling approaches: the first one was to collect the Raman spectra from the colloidal solutions using a liquid cell accessory; the second one was to collect the Raman spectra of NCs from drop casted thin films on a gold slide (300 nm in thickness).

Figure 5-5A shows SERS spectra of NCs collected from their colloidal solutions, while Figure 5-5B shows those collected from drop casted thin films on a gold slide. Both sampling approaches showed that D and G bands are enhanced by increasing silver nitrate concentration. In addition, the D/G band ratios were similar for the two sampling approaches at a different irradiation power and integration time. These ratios were 0.7, 0.6, and 0.6 for NC1.9, NC2.9, and NC3.8, respectively. This suggests that the NCs can be used in solution-based platforms of analysis. We can conclude that NC3.8 showed the highest SERS performance, based on band intensity.

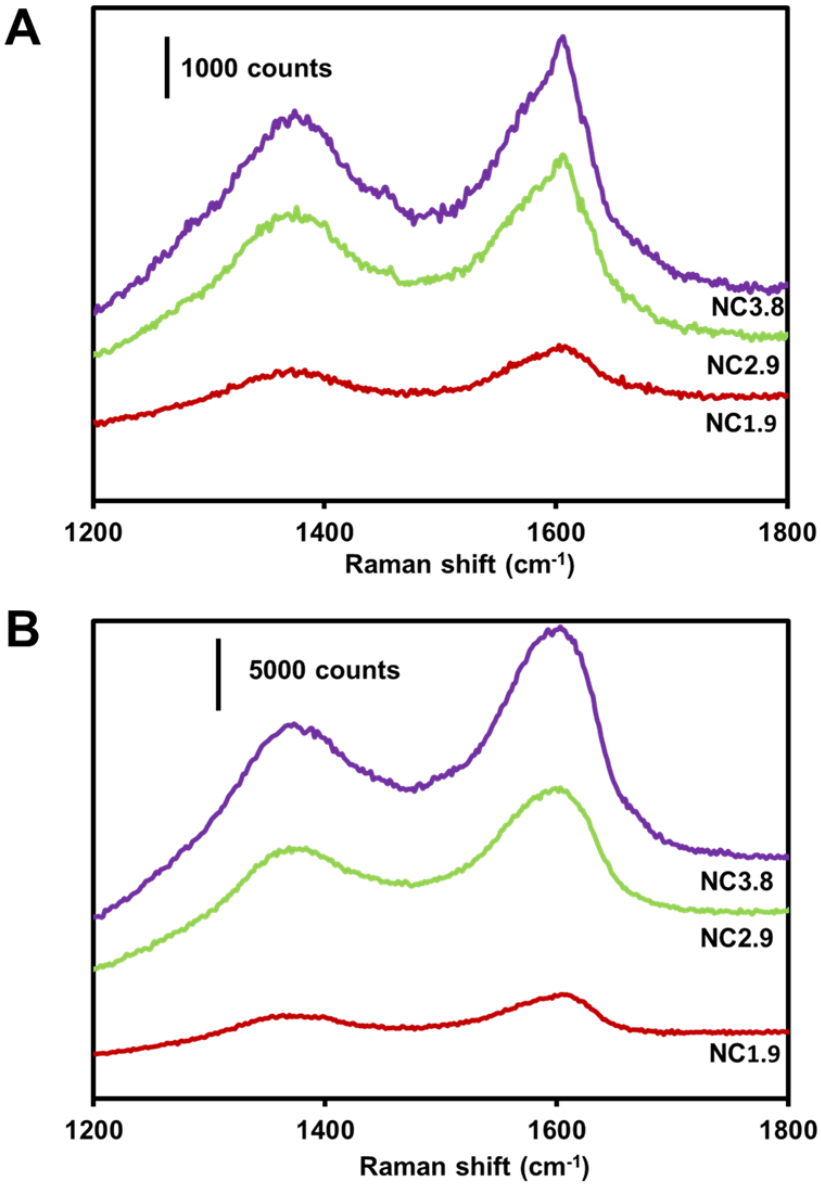


**Figure 5-5. Nanocomposites as Raman probes.** (A) SERS spectra of colloidal NCs in solution (laser conditions: 30 mW for 10 s). (B) SERS spectra of NCs drop casted on a gold slide (laser conditions: 3 mW for 60 s). Spectra averaged from three different samples and stacked for clarity.

#### 5.3.4.2 NBT as a Raman probe

Although D and G bands are enhanced by increasing the silver nitrate concentration, as shown in Figure 5-5, these bands are broad and can interfere with the identification of other molecules. To examine that, we used NBT as a Raman probe. NBT is a thiolated

Raman probe that can adsorb on the NCs through a specific thiolate–Ag interaction. Figure 5-6 shows SERS spectra of colloidal NCs after mixing with NBT. It also shows NBT solution Raman spectra (in ACN) and NBT Raman spectra after mixing with RGO. The final concentration of NBT was 5 μM in all samples. We did not observe any Raman bands indicative of NBT on the control samples. This indicates that no or few NBT molecules were adsorbed on RGO through π–π stacking to exhibit the GERS effect through the chemical enhancement mechanism.

However, Raman bands characteristic of NBT are observed when it is adsorbed on the NCs, as shown in Figure 5-6. These bands are attributed to C–S stretching, symmetric nitro stretching, and C=C stretching, at approximately 1082, 1345, and 1576 $cm^{-1}$, as stated in the previous chapters of this thesis.[65-66] Although NBT Raman bands assigned to the symmetric nitro stretching and C=C stretching are located at similar wavenumbers for the D and G bands of the NCs, these bands appeared narrower and easily distinguishable from the broad D and G bands of the NCs that were demonstrated in Figure 5-5. The NCs showed a comparable SERS performance, with the NC3.8 yielding the highest enhancement, which can be attributed to the effect of the particle size. We also observed Raman bands at 1148 and 1444 $cm^{-1}$, which are attributed to a partial plasmon driven reduction of 4-NBT into aminothiophenol and p,p′-dimercaptoazobenzene.[67-69] We assumed a partial reduction due to the presence of the symmetric nitro stretch Raman band. Previous reports have shown that graphene–metal nanocomposites can induce plasmon driven catalysis for nitro and amino aromatic compounds.[67-69] From Figure 5-6, we can conclude that the NCs can work as colloidal SERS substrates, with NC3.8 having the highest SERS performance.

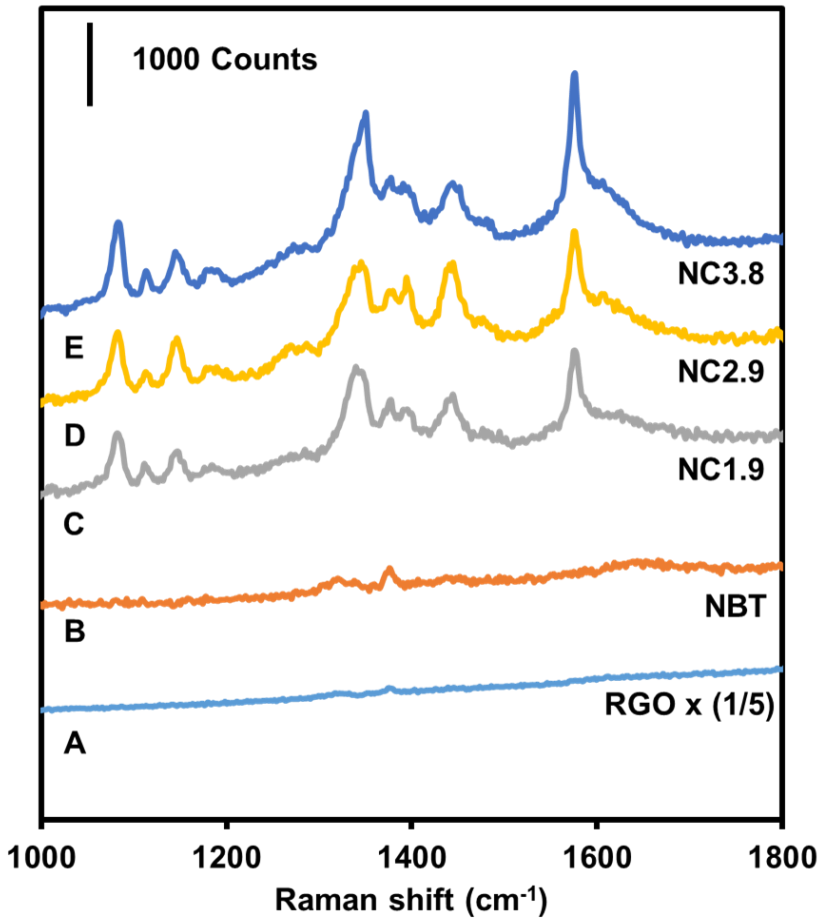


**Figure 5-6. Colloidal SERS behavior of the NCs using NBT as a Raman probe.** (A) Raman spectrum of 5 μM NBT in RGO, (B) Raman spectrum of 5 μM NBT in DI water, (C)SERS spectrum of 5 μM NBT in NC1.9, (D) SERS spectrum of 5 μM NBT in NC2.9, and (E) SERS spectrum of NBT in 5 μM NC3.8. Spectra averaged from three different samples and stacked for clarity (laser conditions: 30 mW and 10 s integration time).

### 5.3.5 Interaction Between NCs and Dye Labelled DNA

Detection of biomolecules such as DNA and proteins has become vitally significant in various fields, including clinical medicine, biosecurity, and food safety.[70-71] Nanocomposites based on graphene–silver have been used for DNA detection.[41-45] However, in these examples of SERS platforms, detection was carried out on the surface of the substrate rather than in a colloidal solution, with a multistep fabrication and functionalization of such platforms. Based on the water dispersibility and colloidal SERS

of the NCs, shown in Figures 5-4, 5-5 and 5-6, we wanted to investigate the capability of NCs to detect a dye labelled DNA without using a thiolated DNA probe and to perform that in a colloidal solution. We also wanted to explore the SERS performance of these NCs to detect such a molecule.

Figure 5-7 shows Raman spectra of a CY5-DNA in PPB solution as a control and when it is mixed with the NCs, along with the chemical structure of CY5 dye. We did not observe any Raman band from the control experiment. However, the Raman spectral intensity of CY5-DNA was enhanced when it is mixed with the NCs. The spectral intensity was more enhanced when NC2.9 and NC3.8 are used rather than NC1.8. The dye can interact also with the NCs through electrostatic and π–π stacking interactions, based on its structure. Raman bands characteristic of CY5 adsorbed on the NCs are summarized in Table 5-2, according to previously published papers.[72-74]

The peak height at 1470 $cm^{-1}$ was used to compare the SERS performance of the three nanocomposites. NC3.8 enhanced the Raman spectral intensity of CY5-DNA more than NC1.9 and NC2.9 by a factor of approximately 14 and 2, respectively. The SERS performance of the NCs was similar to Figures 5-5, 5-6, and 5-7. We attribute this to the particle size effect of silver nanoparticles. We can conclude that NC3.8 showed the highest SERS performance to detect a dye labeled DNA sample in solution.

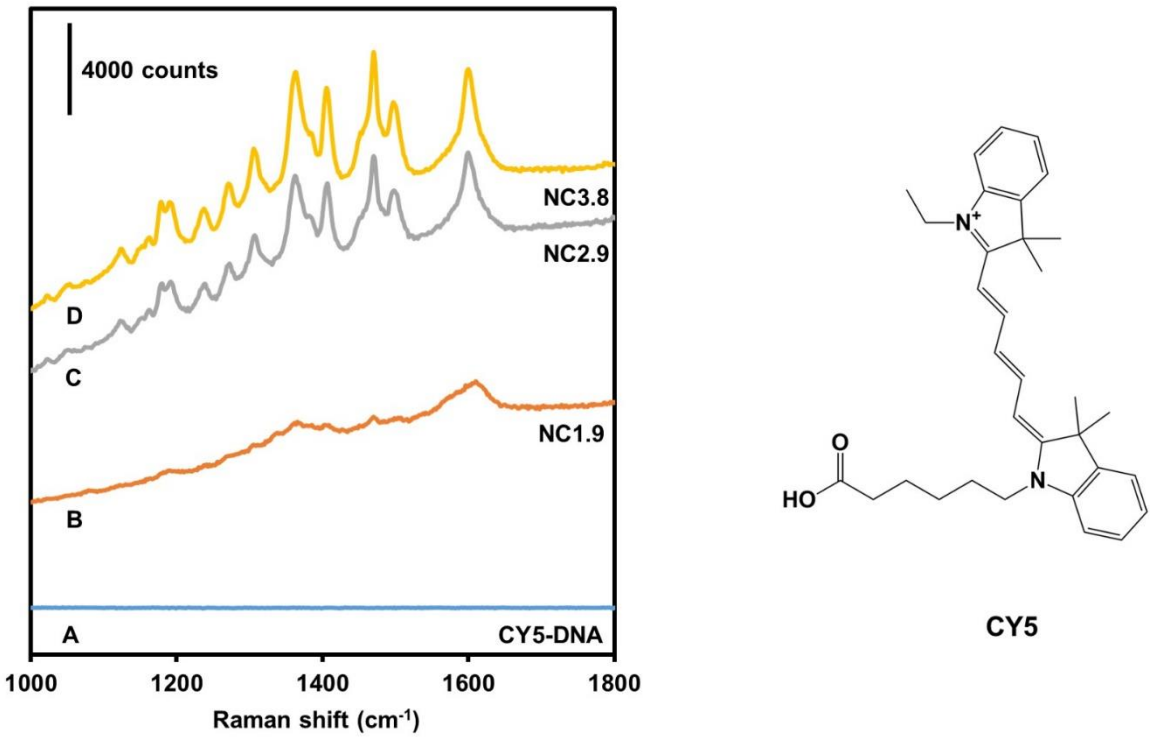


**Figure 5-7. Interaction of NCs with dye labeled ssDNA.** Left (A) Raman spectrum of 1 μM CY5-DNA in PPB, (B) SERS spectrum of 1 μM CY5-DNA in NC1.9 in PPB, (C) SERS spectrum of 1 μM CY5-DNA in NC2.9 in PPB, and (D) SERS spectrum of 1 μM CY5-DNA in NC3.8 in PPB. Spectra averaged from three different samples and stacked for clarity (laser conditions: 30 mW and 10 s integration time). Right, CY5 dye chemical structure is shown.

**Table 5-2. Major Band Assignments Listed for the SERS Spectra of CY5 Adsorbed on the NCs**

| Band position ($cm^{-1}$) | Assignment[72-74] |
|---|---|
| 1123 | C–H in-plane bending |
| 1235 | C–N stretching |
| 1363 | C–O–H bending and C═C stretching |
| 1470 | $CH_3$ bending, C–O–H bending and C═C stretching |
| 1500 | C═C ring stretching |
| 1600 | C═N stretching |

#### 5.3.5.1 Comparison between NC3.8 and 10 nm AgNPs

A number of SERS assays for DNA detection that rely on aggregation of AgNPs to enhance the Raman spectral intensities using an aggregating agent have been reported.[75-80] The particle size of AgNPs ranged from 10 to 150 nm in those examples.[75-80] Here, we selected 10-nm citrate capped AgNPs that have a similar size to the AgNPs on NC 2.9 and NC3.8. Figure 5-8A shows Raman spectra of the CY5-DNA after mixing with the AgNPs and after mixing with NC3.8. We did not observe any Raman band for the CY5-DNA with the AgNPs. In addition, the AgNPs color has changed after mixing with CY5-DNA from yellow to pinkish, indicating aggregation. However, the color of all NCs did not change after mixing with the CY5-DNA, as shown in 5-8B.

This shows that graphene–silver nanocomposites have a superior SERS performance to detect a dye labeled DNA than AgNPs of a similar size. The optimal size range for spherical nanoparticles to be used as SERS substrates is suggested to be approximately 20–100 nm.[81-82] However, a high density of closely spaced AgNPs can be deposited on a GO 2D scaffold with a very large area that can bind to the target molecules; this results in a higher SERS enhancement when compared to colloidal AgNPs of a similar size. From Figure 5-8, we can conclude that the SERS performance and stability of NC3.8 was higher than that of citrate capped AgNPs. The nanocomposite performance depends on a combination of factors, including SERS enhancement through chemical and electromagnetic mechanisms, fluorescence quenching, and AgNPs size.

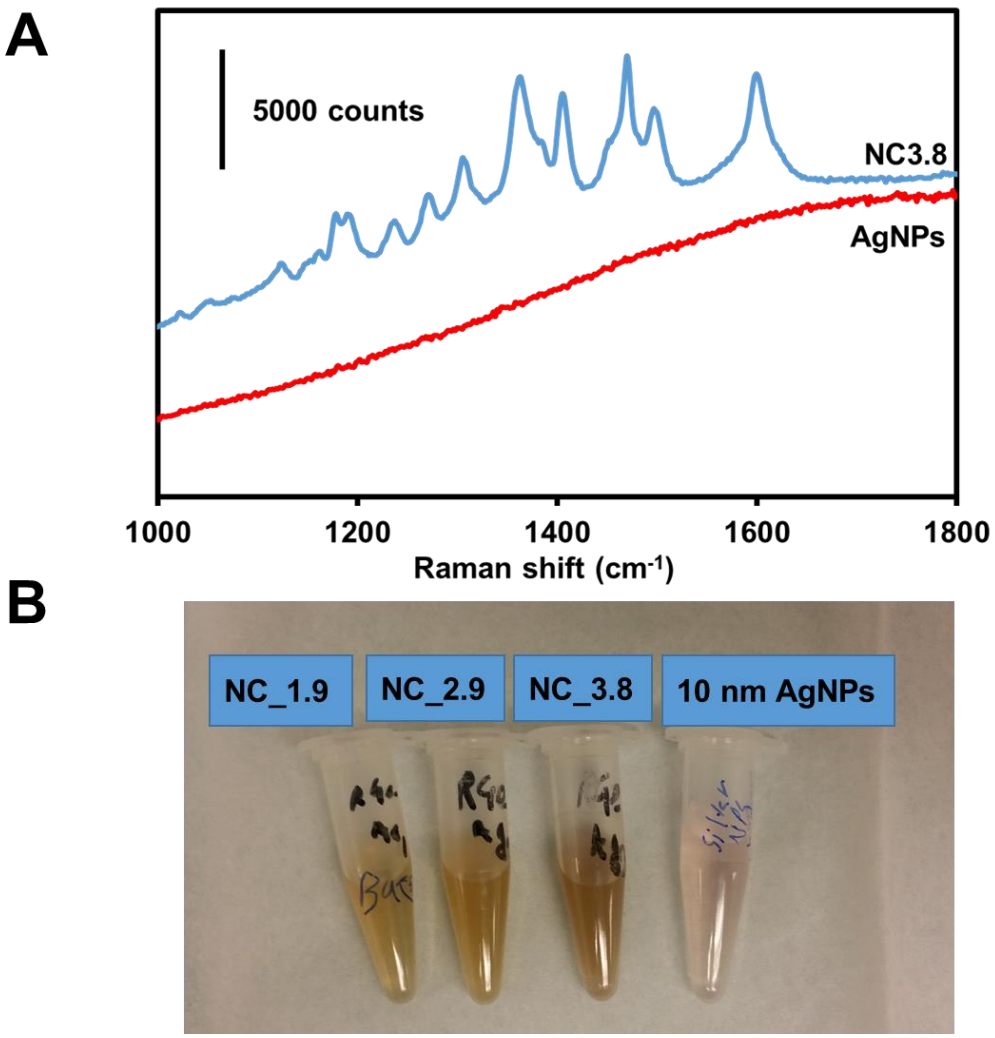


**Figure 5-8. NC3.8 SERS performance compared to AgNPs.** (A) SERS spectra of 1 μM CY5-DNA in PPB after mixing with NC3.8 and with 10 nm AgNPs. (B) An image of the NCs and 10 nm AgNPs after mixing with the CY5-DNA.

### 5.3.5.2 Signal reduction upon DNA Hybridization

Understanding the interaction between the NCs and biomolecules such as DNA is very essential to build a bottom-up bioassay for such a molecule. GO has a higher affinity to bind to ssDNA through hydrogen bonding and π-π stacking to nucleobases, however it has a lower affinity to double strand DNA.[83-86] Based on that, we can detect DNA hybridization upon introducing cDNA to our platform. Figure 5-9A shows a general

representation of the CY5-DNA binding to the nanocomposite in the absence of its cDNA, where the Raman signal is enhanced. However, upon introduction of the cDNA strand, the dye probed ssDNA desorbs away from the nanocomposite surface to hybridize with its complementary. The hybridization event resulted in a reduction in the Raman spectral intensity of the CY5-DNA in our case because of the distance dependence of the SERS effect.[87-89]

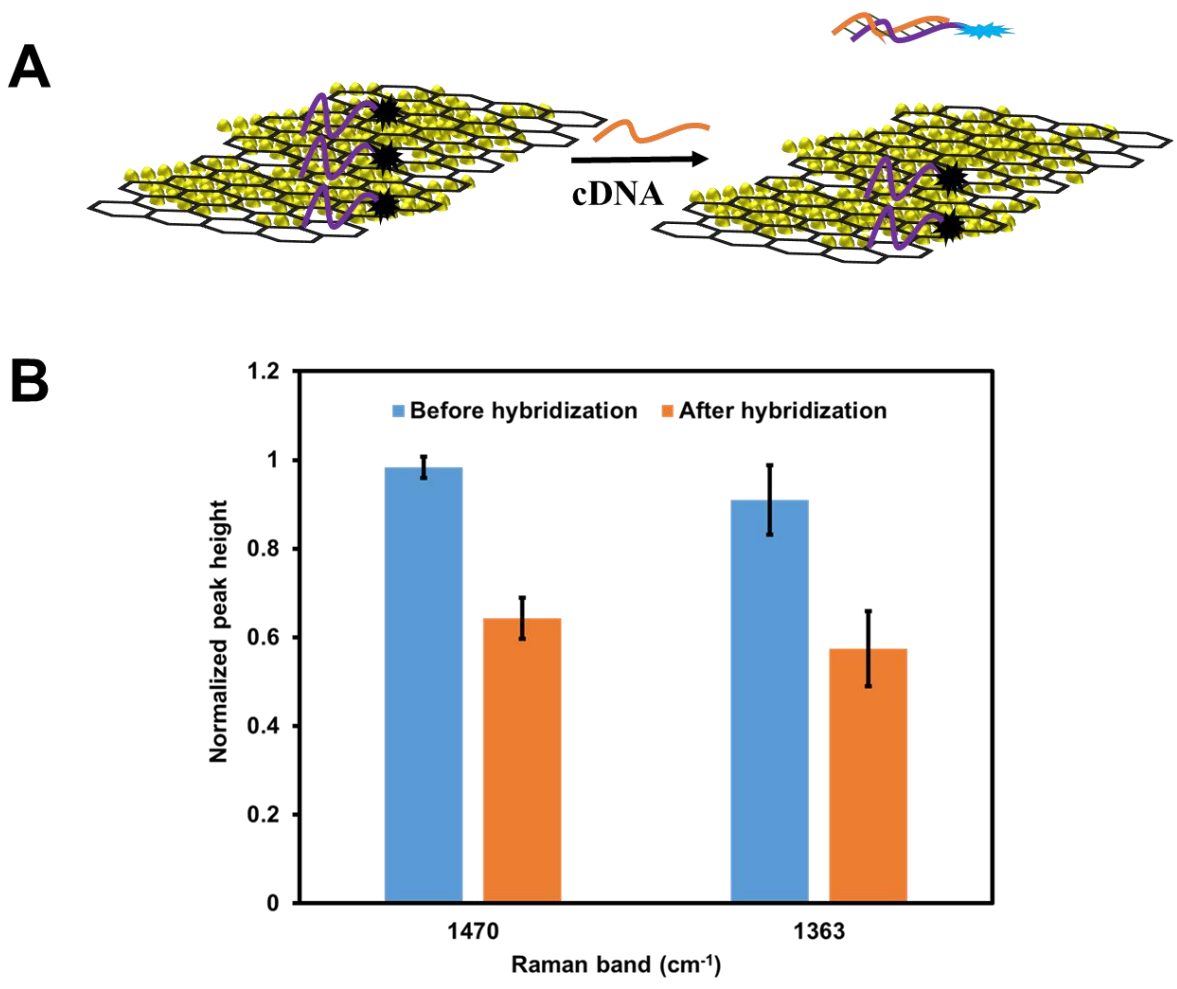


**Figure 5-9. DNA hybridization.** (A) Graphical representation of the adsorption of ssDNA on NC3.8 and its desorption upon hybridization with its cDNA. (B) Bar chart of the Raman bands at 1470 and 1363 $cm^{-1}$ before (blue) and after (orange) hybridization, normalized to their values before hybridization.

Figure 5-9B shows a bar chart of the comparison between peak heights at 1470 and 1363 $cm^{-1}$, before and after hybridization. Each peak was normalized to its highest value before the hybridization step. The percent relative standard deviation (%RSD) was calculated to be 3% and 9% for the 1470 and 1363 $cm^{-1}$ bands, respectively, before hybridization. It became 7% and 15% for the 1470 and 1363 $cm^{-1}$ bands, respectively, after hybridization. These values were less than 20%, which is the recommended threshold for SERS substrates deviation.[90-91] From Figure 5-9, we can conclude that NC3.8 can provide a colloidal SERS substrate that can detect DNA hybridization.

## 5.4 Conclusions

Graphene–silver nanocomposites can provide versatile SERS substrates with a 2D large surface area. Such substrates can interact with a wide spectrum of molecules and can be used on solid as well as in colloidal SERS analyses. The SERS enhancement can be optimized by adjusting the silver nitrate concentration to tailor the particle size and plasmonic behaviour of AgNPs on these substrates. The nanocomposites can be used to detect DNA hybridization using a dye labelled DNA, with superior performance when compared to commercial AgNPs. This dispersible SERS platform can open a new venue in colloidal SERS bioassays using DNA aptamers for various cellular and biomolecular targets.

## 5.5 References


1. Sadik, O. A.; Land Jr., W. H.; Wang, J., Targeting Chemical and Biological Warfare Agents at the Molecular Level. *Electroanalysis* **2003,** *15* (14), 1149-1159.

2. Saha, K.; Agasti, S. S.; Kim, C.; Li, X.; Rotello, V. M., Gold Nanoparticles in Chemical and Biological Sensing. *Chemical Reviews* **2012,** *112* (5), 2739-2779.

3. Geim, A. K.; Novoselov, K. S., The rise of graphene. *Nature Materials* **2007,** *6*, 183.

4. Wojcik, A.; Kamat, P. V., Reduced Graphene Oxide and Porphyrin. An Interactive Affair in 2-D. *ACS Nano* **2010,** *4* (11), 6697-6706.

5. Das, B.; Voggu, R.; Rout, C. S.; Rao, C. N. R., Changes in the electronic structure and properties of graphene induced by molecular charge-transfer. *Chemical Communications* **2008,** (41), 5155-5157.

6. Liu, H.; Gao, J.; Xue, M.; Zhu, N.; Zhang, M.; Cao, T., Processing of Graphene for Electrochemical Application: Noncovalently Functionalize Graphene Sheets with Water-Soluble Electroactive Methylene Green. *Langmuir* **2009,** *25* (20), 12006-12010.

7. Xu, Y.; Bai, H.; Lu, G.; Li, C.; Shi, G., Flexible Graphene Films via the Filtration of Water-Soluble Noncovalent Functionalized Graphene Sheets. *Journal of the American Chemical Society* **2008,** *130* (18), 5856-5857.

8. Geng, J.; Jung, H.-T., Porphyrin Functionalized Graphene Sheets in Aqueous Suspensions: From the Preparation of Graphene Sheets to Highly Conductive Graphene Films. *The Journal of Physical Chemistry C* **2010,** *114* (18), 8227-8234.

9. Treossi, E.; Melucci, M.; Liscio, A.; Gazzano, M.; Samorì, P.; Palermo, V., High-Contrast Visualization of Graphene Oxide on Dye-Sensitized Glass, Quartz, and Silicon by Fluorescence Quenching. *Journal of the American Chemical Society* **2009,** *131* (43), 15576-15577.

10. Varghese, N.; Mogera, U.; Govindaraj, A.; Das, A.; Maiti, P. K.; Sood, A. K.; Rao, C. N. R., Binding of DNA Nucleobases and Nucleosides with Graphene. *ChemPhysChem* **2009,** *10* (1), 206-210.

11. Lu, C.-H.; Yang, H.-H.; Zhu, C.-L.; Chen, X.; Chen, G.-N., A Graphene Platform for Sensing Biomolecules. *Angewandte Chemie International Edition* **2009,** *48* (26), 4785-4787.

12. He, S.; Song, B.; Li, D.; Zhu, C.; Qi, W.; Wen, Y.; Wang, L.; Song, S.; Fang, H.; Fan, C., A Graphene Nanoprobe for Rapid, Sensitive, and Multicolor Fluorescent DNA Analysis. *Advanced Functional Materials* **2010,** *20* (3), 453-459.

13. Li, F.; Huang, Y.; Yang, Q.; Zhong, Z.; Li, D.; Wang, L.; Song, S.; Fan, C., A graphene-enhanced molecular beacon for homogeneous DNA detection. *Nanoscale* **2010,** *2* (6), 1021-1026.

14. Yi, J. W.; Park, J.; Singh, N. J.; Lee, I. J.; Kim, K. S.; Kim, B. H., Quencher-free molecular beacon: Enhancement of the signal-to-background ratio with graphene oxide. *Bioorganic & Medicinal Chemistry Letters* **2011,** *21* (2), 704-706.

15. Dong, H.; Zhang, J.; Ju, H.; Lu, H.; Wang, S.; Jin, S.; Hao, K.; Du, H.; Zhang, X., Highly Sensitive Multiple microRNA Detection Based on Fluorescence Quenching of Graphene Oxide and Isothermal Strand-Displacement Polymerase Reaction. *Analytical Chemistry* **2012,** *84* (10), 4587-4593.

16. Dong, H.; Gao, W.; Yan, F.; Ji, H.; Ju, H., Fluorescence Resonance Energy Transfer between Quantum Dots and Graphene Oxide for Sensing Biomolecules. *Analytical Chemistry* **2010,** *82* (13), 5511-5517.

17. Cao, L.; Cheng, L.; Zhang, Z.; Wang, Y.; Zhang, X.; Chen, H.; Liu, B.; Zhang, S.; Kong, J., Visual and high-throughput detection of cancer cells using a graphene oxide-based FRET aptasensing microfluidic chip. *Lab on a Chip* **2012,** *12* (22), 4864-4869.

18. Chang, H.; Tang, L.; Wang, Y.; Jiang, J.; Li, J., Graphene Fluorescence Resonance Energy Transfer Aptasensor for the Thrombin Detection. *Analytical Chemistry* **2010,** *82* (6), 2341-2346.

19. Wen, Y.; Xing, F.; He, S.; Song, S.; Wang, L.; Long, Y.; Li, D.; Fan, C., A graphene-based fluorescent nanoprobe for silver(i) ions detection by using graphene oxide and a silver-specific oligonucleotide. *Chemical Communications* **2010,** *46* (15), 2596-2598.

20. He, Y.; Wang, Z.-G.; Tang, H.-W.; Pang, D.-W., Low background signal platform for the detection of ATP: When a molecular aptamer beacon meets graphene oxide. *Biosensors and Bioelectronics* **2011,** *29* (1), 76-81.

21. Lu, Z.; Zhang, L.; Deng, Y.; Li, S.; He, N., Graphene oxide for rapid microRNA detection. *Nanoscale* **2012,** *4* (19), 5840-5842.

22. Lee, J.; Kim, J.; Kim, S.; Min, D.-H., Biosensors based on graphene oxide and its biomedical application. *Advanced Drug Delivery Reviews* **2016,** *105*, 275-287.

23. Wang, Y.; Li, Z.; Hu, D.; Lin, C.-T.; Li, J.; Lin, Y., Aptamer/Graphene Oxide Nanocomplex for in Situ Molecular Probing in Living Cells. *Journal of the American Chemical Society* **2010,** *132* (27), 9274-9276.

24. Wang, H.; Zhang, Q.; Chu, X.; Chen, T.; Ge, J.; Yu, R., Graphene Oxide–Peptide Conjugate as an Intracellular Protease Sensor for Caspase-3 Activation Imaging in Live Cells. *Angewandte Chemie International Edition* **2011,** *50* (31), 7065-7069.

25. Ryoo, S.-R.; Lee, J.; Yeo, J.; Na, H.-K.; Kim, Y.-K.; Jang, H.; Lee, J. H.; Han, S. W.; Lee, Y.; Kim, V. N.; Min, D.-H., Quantitative and Multiplexed MicroRNA Sensing in Living Cells Based on Peptide Nucleic Acid and Nano Graphene Oxide (PANGO). *ACS Nano* **2013,** *7* (7), 5882-5891.

26. Kim, S.; Ryoo, S.-R.; Na, H.-K.; Kim, Y.-K.; Choi, B.-S.; Lee, Y.; Kim, D.-E.; Min, D.-H., Deoxyribozyme-loaded nano-graphene oxide for simultaneous sensing and silencing of the hepatitis C virus gene in liver cells. *Chemical Communications* **2013,** *49* (74), 8241-8243.

27. Wang, Y.; Li, Z.; Weber, T. J.; Hu, D.; Lin, C.-T.; Li, J.; Lin, Y., In Situ Live Cell Sensing of Multiple Nucleotides Exploiting DNA/RNA Aptamers and Graphene Oxide Nanosheets. *Analytical Chemistry* **2013,** *85* (14), 6775-6782.

28. Wang, Y.; Tang, L.; Li, Z.; Lin, Y.; Li, J., In situ simultaneous monitoring of ATP and GTP using a graphene oxide nanosheet–based sensing platform in living cells. *Nature Protocols* **2014,** *9*, 1944.

29. Xie, L.; Ling, X.; Fang, Y.; Zhang, J.; Liu, Z., Graphene as a Substrate To Suppress Fluorescence in Resonance Raman Spectroscopy. *Journal of the American Chemical Society* **2009,** *131* (29), 9890-9891.

30. Ling, X.; Xie, L.; Fang, Y.; Xu, H.; Zhang, H.; Kong, J.; Dresselhaus, M. S.; Zhang, J.; Liu, Z., Can Graphene be used as a Substrate for Raman Enhancement? *Nano Letters* **2010,** *10* (2), 553-561.

31. Ling, X.; Zhang, J., First-Layer Effect in Graphene-Enhanced Raman Scattering. *Small* **2010,** *6* (18), 2020-2025.

32. Yu, X.; Cai, H.; Zhang, W.; Li, X.; Pan, N.; Luo, Y.; Wang, X.; Hou, J. G., Tuning Chemical Enhancement of SERS by Controlling the Chemical Reduction of Graphene Oxide Nanosheets. *ACS Nano* **2011,** *5* (2), 952-958.

33. Huh, S.; Park, J.; Kim, Y. S.; Kim, K. S.; Hong, B. H.; Nam, J.-M., UV/Ozone-Oxidized Large-Scale Graphene Platform with Large Chemical Enhancement in Surface-Enhanced Raman Scattering. *ACS Nano* **2011,** *5* (12), 9799-9806.

34. Yaghobian, F.; Korn, T.; Schüller, C., Frequency Shift in Graphene-Enhanced Raman Signal of Molecules. *ChemPhysChem* **2012,** *13* (18), 4271-4275.

35. Murphy, S.; Huang, L.; Kamat, P. V., Reduced Graphene Oxide–Silver Nanoparticle Composite as an Active SERS Material. *The Journal of Physical Chemistry C* **2013,** *117* (9), 4740-4747.

36. Fan, Z.; Kanchanapally, R.; Ray, P. C., Hybrid Graphene Oxide Based Ultrasensitive SERS Probe for Label-Free Biosensing. *The Journal of Physical Chemistry Letters* **2013,** *4* (21), 3813-3818.

37. Muszynski, R.; Seger, B.; Kamat, P. V., Decorating Graphene Sheets with Gold Nanoparticles. *The Journal of Physical Chemistry C* **2008,** *112* (14), 5263-5266.

38. Cassagneau, T.; Fendler, J. H., Preparation and Layer-by-Layer Self-Assembly of Silver Nanoparticles Capped by Graphite Oxide Nanosheets. *The Journal of Physical Chemistry B* **1999,** *103* (11), 1789-1793.

39. Lightcap, I. V.; Murphy, S.; Schumer, T.; Kamat, P. V., Electron Hopping Through Single-to-Few-Layer Graphene Oxide Films. Side-Selective Photocatalytic Deposition of Metal Nanoparticles. *The Journal of Physical Chemistry Letters* **2012,** *3* (11), 1453-1458.

40. He, S.; Liu, K.-K.; Su, S.; Yan, J.; Mao, X.; Wang, D.; He, Y.; Li, L.-J.; Song, S.; Fan, C., Graphene-Based High-Efficiency Surface-Enhanced Raman Scattering-Active Platform for Sensitive and Multiplex DNA Detection. *Analytical Chemistry* **2012,** *84* (10), 4622-4627.

41. Lin, T.-W.; Wu, H.-Y.; Tasi, T.-T.; Lai, Y.-H.; Shen, H.-H., Surface-enhanced Raman spectroscopy for DNA detection by the self-assembly of Ag nanoparticles onto Ag nanoparticle–graphene oxide nanocomposites. *Physical Chemistry Chemical Physics* **2015,** *17* (28), 18443-18448.

42. Ouyang, L.; Hu, Y.; Zhu, L.; Cheng, G. J.; Irudayaraj, J., A reusable laser wrapped graphene-Ag array based SERS sensor for trace detection of genomic DNA methylation. *Biosensors and Bioelectronics* **2017,** *92*, 755-762.

43. Yang, W.; Li, Z.; Lu, Z.; Yu, J.; Huo, Y.; Man, B.; Pan, J.; Si, H.; Jiang, S.; Zhang, C., Graphene-Ag nanoparticles-cicada wings hybrid system for obvious SERS performance and DNA molecular detection. *Opt. Express* **2019,** *27* (3), 3000-3013.

44. Duan, B.; Zhou, J.; Fang, Z.; Wang, C.; Wang, X.; Hemond, H. F.; Chan-Park, M. B.; Duan, H., Surface enhanced Raman scattering by graphene-nanosheet-gapped plasmonic nanoparticle arrays for multiplexed DNA detection. *Nanoscale* **2015,** *7* (29), 12606-12613.

45. Tasi, T.-T.; Lin, T.-W.; Shao, L.-D.; Shen, H.-H., Reversible coupling of 4-nitroaniline molecules to 4-aminothiophenol functionalized on Ag nanoparticle/graphene oxide nanocomposites through the plasmon assisted chemical reaction. *RSC Advances* **2016,** *6* (35), 29453-29459.

46. Marcano, D. C.; Kosynkin, D. V.; Berlin, J. M.; Sinitskii, A.; Sun, Z.; Slesarev, A.; Alemany, L. B.; Lu, W.; Tour, J. M., Improved Synthesis of Graphene Oxide. *ACS Nano* **2010,** *4* (8), 4806-4814.

47. Goncalves, G.; Marques, P. A. A. P.; Granadeiro, C. M.; Nogueira, H. I. S.; Singh, M. K.; Grácio, J., Surface Modification of Graphene Nanosheets with Gold Nanoparticles: The Role of Oxygen Moieties at Graphene Surface on Gold Nucleation and Growth. *Chemistry of Materials* **2009,** *21* (20), 4796-4802.

48. Jasuja, K.; Linn, J.; Melton, S.; Berry, V., Microwave-Reduced Uncapped Metal Nanoparticles on Graphene: Tuning Catalytic, Electrical, and Raman Properties. *The Journal of Physical Chemistry Letters* **2010,** *1* (12), 1853-1860.

49. Hummers, W. S.; Offeman, R. E., Preparation of Graphitic Oxide. *Journal of the American Chemical Society* **1958,** *80* (6), 1339-1339.

50. Wang, Y.; Alsmeyer, D. C.; McCreery, R. L., Raman spectroscopy of carbon materials: structural basis of observed spectra. *Chemistry of Materials* **1990,** *2* (5), 557-563.

51. Allen, M. J.; Tung, V. C.; Kaner, R. B., Honeycomb Carbon: A Review of Graphene. *Chemical Reviews* **2010,** *110* (1), 132-145.

52. Ferrari, A. C.; Basko, D. M., Raman spectroscopy as a versatile tool for studying the properties of graphene. *Nature Nanotechnology* **2013,** *8*, 235.

53. Malard, L. M.; Pimenta, M. A.; Dresselhaus, G.; Dresselhaus, M. S., Raman spectroscopy in graphene. *Physics Reports* **2009,** *473* (5), 51-87.

54. Rao, C. N. R.; Sood, A. K.; Subrahmanyam, K. S.; Govindaraj, A., Graphene: The New Two-Dimensional Nanomaterial. *Angewandte Chemie International Edition* **2009,** *48* (42), 7752-7777.

55. Ferrari, A. C., Raman spectroscopy of graphene and graphite: Disorder, electron–phonon coupling, doping and nonadiabatic effects. *Solid State Communications* **2007,** *143* (1), 47-57.

56. McCreery, R. L., Advanced Carbon Electrode Materials for Molecular Electrochemistry. *Chemical Reviews* **2008,** *108* (7), 2646-2687.

57. Ray, K.; McCreery, R. L., Spatially Resolved Raman Spectroscopy of Carbon Electrode Surfaces: Observations of Structural and Chemical Heterogeneity. *Analytical Chemistry* **1997,** *69* (22), 4680-4687.

58. Vidano, R. P.; Fischbach, D. B.; Willis, L. J.; Loehr, T. M., Observation of Raman band shifting with excitation wavelength for carbons and graphites. *Solid State Communications* **1981,** *39* (2), 341-344.

59. El-Sayed, M. A., Some Interesting Properties of Metals Confined in Time and Nanometer Space of Different Shapes. *Accounts of Chemical Research* **2001,** *34* (4), 257-264.

60. Mulvaney, P., Surface Plasmon Spectroscopy of Nanosized Metal Particles. *Langmuir* **1996,** *12* (3), 788-800.

61. Murphy, C. J.; Sau, T. K.; Gole, A. M.; Orendorff, C. J.; Gao, J.; Gou, L.; Hunyadi, S. E.; Li, T., Anisotropic Metal Nanoparticles: Synthesis, Assembly, and Optical Applications. *The Journal of Physical Chemistry B* **2005,** *109* (29), 13857-13870.

62. Chandra, K.; Culver, K. S. B.; Werner, S. E.; Lee, R. C.; Odom, T. W., Manipulating the Anisotropic Structure of Gold Nanostars using Good's Buffers. *Chemistry of Materials* **2016,** *28* (18), 6763-6769.

63. Haiss, W.; Thanh, N. T. K.; Aveyard, J.; Fernig, D. G., Determination of Size and Concentration of Gold Nanoparticles from UV−Vis Spectra. *Analytical Chemistry* **2007,** *79* (11), 4215-4221.

64. Li, D.; Müller, M. B.; Gilje, S.; Kaner, R. B.; Wallace, G. G., Processable aqueous dispersions of graphene nanosheets. *Nature Nanotechnology* **2008,** *3*, 101.

65. Skadtchenko, B. O.; Aroca, R., Surface-enhanced Raman scattering of p-nitrothiophenol: Molecular vibrations of its silver salt and the surface complex formed on silver islands and colloids. *Spectrochimica Acta Part A: Molecular and Biomolecular Spectroscopy* **2001,** *57* (5), 1009-1016.

66. Abdelsalam, M. E., Surface enhanced raman scattering of aromatic thiols adsorbed on nanostructured gold surfaces. *Central European Journal of Chemistry* **2009,** *7* (3), 446-453.

67. Kang, L.; Chu, J.; Zhao, H.; Xu, P.; Sun, M., Recent progress in the applications of graphene in surface-enhanced Raman scattering and plasmon-induced catalytic reactions. *Journal of Materials Chemistry C* **2015,** *3* (35), 9024-9037.

68. Lin, T.-W.; Tasi, T.-T.; Chang, P.-L.; Cheng, H.-Y., Reversible Association of Nitro Compounds with p-Nitrothiophenol Modified on Ag Nanoparticles/Graphene Oxide Nanocomposites through Plasmon Mediated Photochemical Reaction. *ACS Applied Materials & Interfaces* **2016,** *8* (12), 8315-8322.

69. Liang, X.; You, T.; Liu, D.; Lang, X.; Tan, E.; Shi, J.; Yin, P.; Guo, L., Direct observation of enhanced plasmon-driven catalytic reaction activity of Au nanoparticles supported on reduced graphene oxides by SERS. *Physical Chemistry Chemical Physics* **2015,** *17* (15), 10176-10181.

70. Song, S.; Qin, Y.; He, Y.; Huang, Q.; Fan, C.; Chen, H.-Y., Functional nanoprobes for ultrasensitive detection of biomolecules. *Chemical Society Reviews* **2010,** *39* (11), 4234-4243.

71. Giljohann, D. A.; Mirkin, C. A., Drivers of biodiagnostic development. *Nature* **2009,** *462*, 461.

72. Novara, C.; Petracca, F.; Virga, A.; Rivolo, P.; Ferrero, S.; Chiolerio, A.; Geobaldo, F.; Porro, S.; Giorgis, F., SERS active silver nanoparticles synthesized by inkjet printing on mesoporous silicon. *Nanoscale Research Letters* **2014,** *9* (1), 527.

73. Wu, Y.; Xiao, F.; Wu, Z.; Yu, R., Novel Aptasensor Platform Based on Ratiometric Surface-Enhanced Raman Spectroscopy. *Analytical Chemistry* **2017,** *89* (5), 2852-2858.

74. Jaworska, A.; Pyrak, E.; Kudelski, A., Comparison of the efficiency of generation of Raman radiation by various Raman reporters connected via DNA linkers to different plasmonic nano-structures. *Vibrational Spectroscopy* **2019,** *101*, 34-39.

75. Gracie, K.; Moores, M.; Smith, W. E.; Harding, K.; Girolami, M.; Graham, D.; Faulds, K., Preferential Attachment of Specific Fluorescent Dyes and Dye Labeled DNA Sequences in a Surface Enhanced Raman Scattering Multiplex. *Anal. Chem. (Washington, DC, U. S.)* **2016,** *88* (2), 1147-1153.

76. Guerrini, L.; Krpetic, Z.; van Lierop, D.; Alvarez-Puebla, R. A.; Graham, D., Direct surface-enhanced Raman scattering analysis of DNA duplexes. *Angew. Chem., Int. Ed.* **2015,** *54* (4), 1144-1148.

77. Masetti, M.; Xie, H.-n.; Krpetic, Z.; Recanatini, M.; Alvarez-Puebla, R. A.; Guerrini, L., Revealing DNA Interactions with Exogenous Agents by Surface-Enhanced Raman Scattering. *J. Am. Chem. Soc.* **2015,** *137* (1), 469-476.

78. van Lierop, D.; Krpetic, Z.; Guerrini, L.; Larmour, I. A.; Dougan, J. A.; Faulds, K.; Graham, D., Positively charged silver nanoparticles and their effect on surface-enhanced Raman scattering of dye-labelled oligonucleotides. *Chem. Commun. (Cambridge, U. K.)* **2012,** *48* (66), 8192-8194.

79. van Lierop, D.; Larmour, I. A.; Faulds, K.; Graham, D., SERS primers and their mode of action for pathogen DNA detection. *Anal. Chem. (Washington, DC, U. S.)* **2013,** *85* (3), 1408-1414.

80. Wu, C.-Y.; Lo, W.-Y.; Chiu, C.-R.; Yang, T.-S., Surface enhanced Raman spectra of oligonucleotides induced by spermine. *J. Raman Spectrosc.* **2006,** *37* (8), 799-807.

81. Moskovits, M., Surface-enhanced Raman spectroscopy: a brief retrospective. *Journal of Raman Spectroscopy* **2005,** *36* (6-7), 485-496.

82. Jana, N. R.; Pal, T., Anisotropic Metal Nanoparticles for Use as Surface-Enhanced Raman Substrates. *Advanced Materials* **2007,** *19* (13), 1761-1765.

83. Tian, F.; Lyu, J.; Shi, J.; Yang, M., Graphene and graphene-like two-denominational materials based fluorescence resonance energy transfer (FRET) assays for biological applications. *Biosensors and Bioelectronics* **2017,** *89*, 123-135.

84. Wu, M.; Kempaiah, R.; Huang, P.-J. J.; Maheshwari, V.; Liu, J., Adsorption and Desorption of DNA on Graphene Oxide Studied by Fluorescently Labeled Oligonucleotides. *Langmuir* **2011,** *27* (6), 2731-2738.

85. Park, J. S.; Na, H.-K.; Min, D.-H.; Kim, D.-E., Desorption of single-stranded nucleic acids from graphene oxide by disruption of hydrogen bonding. *Analyst* **2013,** *138* (6), 1745-1749.

86. Jang, H.; Kim, Y.-K.; Kwon, H.-M.; Yeo, W.-S.; Kim, D.-E.; Min, D.-H., A Graphene-Based Platform for the Assay of Duplex-DNA Unwinding by Helicase. *Angewandte Chemie International Edition* **2010,** *49* (33), 5703-5707.

87. Kennedy, B. J.; Spaeth, S.; Dickey, M.; Carron, K. T., Determination of the Distance Dependence and Experimental Effects for Modified SERS Substrates Based on Self-Assembled Monolayers Formed Using Alkanethiols. *The Journal of Physical Chemistry B* **1999,** *103* (18), 3640-3646.

88. Dieringer, J. A.; McFarland, A. D.; Shah, N. C.; Stuart, D. A.; Whitney, A. V.; Yonzon, C. R.; Young, M. A.; Zhang, X.; Van Duyne, R. P., Introductory Lecture Surface enhanced Raman spectroscopy: new materials, concepts, characterization tools, and applications. *Faraday Discussions* **2006,** *132*, 9-26.

89. Ye, Q.; Fang, J.; Sun, L., Surface-Enhanced Raman Scattering from Functionalized Self-Assembled Monolayers. 2. Distance Dependence of Enhanced Raman Scattering from an Azobenzene Terminal Group. *The Journal of Physical Chemistry B* **1997,** *101* (41), 8221-8224.

90. Natan, M. J., Concluding Remarks Surface enhanced Raman scattering. *Faraday Discussions* **2006,** *132*, 321-328.

91. Lin, X.-M.; Cui, Y.; Xu, Y.-H.; Ren, B.; Tian, Z.-Q., Surface-enhanced Raman spectroscopy: substrate-related issues. *Analytical and Bioanalytical Chemistry* **2009,** *394* (7), 1729-1745.

# Chapter 6

# Conclusions and Future Work

## 6.1 Chapter Conclusions

The motivation behind the work in this thesis was to develop cost-effective methods of SERS substrates fabrication. This thesis is divided into two main components, membrane-based and solution-based SERS substrates. Chapters 2 and 3 highlight the fabrication of membrane supported SERS substrates by integrating noble metal nanostructures into the 3D microporous network of polyvinylidene fluoride (PVDF) membranes. Chapters 4 and 5 demonstrate the use and optimization of gold nanostars and graphene–silver nanocomposites as in-solution colloidal SERS substrates.

In Chapter 2 an in-situ deviceless seed-mediated method was developed to fabricate membrane supported gold nanostructures SERS substrates. The incorporation of gold nanostructures into PVDF was achieved by combing SILAR-like seeding and growth protocols. Combining these protocols reduced the number of required steps to optimize the SERS performance of these substrates. Optimization of the SERS performance was based on the number of seeding cycles before the growth step, with two seeding cycles yielding the highest signal intensities. Label-free detection of malachite green, melamine, and thiabendazole using these substrates demonstrates the potential to detect environmentally hazardous analytes. Additionally, a method to quantitate methimazole (MTZ), an anti-hormone pharmaceutical, in urine was developed using these substrates with no sampling preprocessing steps. The substrate-to-substrate and point-to-point variability were less than 20%.

In Chapter 3, another in-situ equipment-free method was developed to fabricate membrane supported silver nanocorals SERS substrates. The nanocorals were integrated into the microporous PVDF membranes using a seedless method. All optimizations and

measurements were completed using a handheld Raman device. The SERS performance was optimized based on the silver nanocorals loading into the membranes. The SERS performance optimization study was performed using two Raman probes to simulate physisorption and chemisorption scenarios. Rhodamine 6G, a Raman probe, was used as an example of a non-specific adsorption. The second probe was mercaptobenzonitrile (MBN), a thiol Raman probe, which can adsorb specifically through a S–Ag interaction. Both approaches demonstrated a similar SERS performance trend. The substrates were used to detect MTZ in synthetic urine, without any preprocessing steps. The substrate-to-substrate and point-to-point variability were also less than 20%.

Chapters 2 and 3 demonstrated cost-effective alternative methods to lithographic ones to fabricate SERS substrates. The main advantages of these substrates are that they are easy to fabricate and use, in addition to being of low cost. Besides, the variation in their SERS performance within the same substrate and from substrate-to-substrate is comparable to other methods used to fabricate SERS substrates like inkjet printing or chemical immobilization of pre-synthesized nanoparticles onto solid substrates.[1-2] These inexpensive equipment-free methods can provide flexible SERS substrates for field-deployable applications, with homogenous SERS reproducibility.

Solution-based SERS platforms can offer another cost-effective, practical, and reproducible approach for SERS analyses. In this approach, the size and shape of plasmonic nanostructures can be controlled and synthesized in large volumes using simple lab equipment. In addition, in-solution SERS can offer an overall higher reproducibility when compared to dried SERS platforms. However, in-solution SERS

platforms are not employed widely as solid-based ones. I investigated two forms of solution-based SERS in Chapters 4 and 5.

Chapter 4 explored gold nanostars (Au NS) as an in-solution SERS substrate. The buffer conditions used in the synthesis of these Au NS can influence their size and shape. The SERS performance of these Au NS synthesized under different buffer conditions was studied systematically. Two different Good's buffers were used here in the synthesis of Au NS at different buffer-to-gold molar ratios, 4-(2-hydroxyethyl)-1-piperazineethanesulfonic acid (HEPES) and 4-(2-hydroxyethyl)-1-piperazinepropanesulfonic acid (EPPS). We demonstrated that the difference in SERS performance between Au NS synthesised using HEPES and EPPS at different ratios was due to mainly the surface coverage of MBN on the Au NS instead of enhanced electromagnetic effects. This finding was counterintuitive based on the sharp features of Au NS and with aligning the laser wavelength with the surface plasmon resonance of Au NS synthesized at higher buffer-to-gold ratios. HR100 (Au NS synthesized using HEPES/gold molar ratio of 100) produced the highest signal intensities. The Au NS showed a %RSD of 8% in signal intensity over 78 days at 4 °C and the ability to detect a variety of analytes in under five minutes through chemisorption and physisorption mechanisms. The addition of NaCl to the Au NS increases the SERS intensity by a factor of about 10 through the formation of nanoaggregates. A SERS assay was developed for the detection and quantitation of MTZ. The assay showed a limit of detection of 0.1 μM and a recovery of nearly 100% when MTZ was spiked in urine. The merging of in-solution substrates and handheld Raman spectrometers open new avenues for rapid and reproducible on-site SERS analysis.

Chapter 5 was based on the exploration of using silver-graphene–nanocomposites as in-solution colloidal SERS substrates. Graphene oxide provides a large 2D surface area, with oxygenated species that can work as nucleation sites to incorporate silver nanoparticles (AgNPs). The SERS performance of graphene–silver nanocomposites was optimized by varying the silver nitrate concentration to control the AgNPs particle size and plasmonic behaviour. We demonstrated that graphene–silver nanocomposites can be used as solid and in-solution SERS substrates. The SERS performance of the nanocomposite was studied using three different Raman probes. The first probe was the graphene itself using its D and G Raman bands. The second probe was 4-nitrobenzenthiol (NBT) as a thiol Raman probe to simulate a chemisorption mechanism. The third probe was a dye labelled ssDNA to simulate a π–π stacking interaction. A proof of concept was demonstrated using a graphene–silver nanocomposite to detect DNA hybridization with a dye-labelled ssDNA; it showed superior performance when compared to commercial AgNPs.

## 6.2 Suggestions for Future Work

The work conducted in this thesis was based on the SERS spectra of the studied molecules upon their direct interaction with the SERS substrates. Generally, this was through chemisorption and physisorption approaches, regardless of the platform used. Although direct interaction between the molecule of interest and the SERS substrate offers a straightforward and easy approach, it still has its own challenges in terms of specificity. This is particularly true with molecules that have a low affinity to interact with plasmonic nanostructures (gold or silver) and/or have a small Raman cross section.

Here, I propose different approaches to circumvent these challenges as future suggestions based on the surface functionalization of the developed SERS substrates in this thesis. For example, polycyclic aromatic hydrocarbons and polychlorinated biphenyls pollutants do not have functional groups that would allow their interaction with gold or silver nanostructures, such as thiols or amines. However, modifying the SERS substrates with alkanethiols will increase their hydrophobicity, and these molecules can be captured through van der Waals forces.[3-5] I also suggest the use of alkane dithiol to functionalize PVDF SERS substrates through thiolate chemistry from one end, while the other thiol end will be used to attach Au NS. This approach can serve two functions at the same time. The first function is to interact and capture the overmentioned pollutants through van der Waals forces.[3-5] The second function is to increase the number of hot spots in the 3D network of the PVDF SERS substrates. The concentration of Au NS and the length of the alkanedithiol used will be significant parameters to investigate in order to optimize the SERS performance of this platform.

Another possible chemical modification for these substrates includes functionalization with macrocycles such as calixarene, pillarenes, and cyclodextrins.[6-8] These macrocycles have hydrophobic cavities that can capture and trap polycyclic aromatic hydrocarbons and polychlorinated biphenyls pollutants.[6-8] This will bring the pollutant molecules in close vicinity to the surface of the SERS substrate and hence enhance the SERS spectral intensity. Interestingly, changing the groups on the lower and upper rims of these macrocycles can control the chemical properties and the shape of the cavity of these macrocycles; this can open a lot of research possibilities to investigate and evaluate.

Biorecognition elements, such as DNA aptamers and antibodies, will improve the specificity of our SERS substrates.[9-10] One approach is to utilize the Raman frequency shift upon interaction with the target biomolecule.[11-12] Another approach to improve the specificity of our SERS substrates is to develop a sandwich assay platform.[9-10] In this case, a biorecognition moiety, such as a primary antibody or DNA aptamer, will be attached to our PVDF SERS substrate to capture its target. Then, Au NS or a graphene–silver nanocomposite functionalized with a secondary antibody and a Raman probe will be introduced. The SERS spectral intensity of the Raman probe will be used to quantify the target concentration. Although this platform is a two-step platform, it can improve the specificity. This approach can offer a multiplexing platform to detect many target molecules using different biorecognition moieties and Raman probes. Moreover, the same principle can be adapted using magnetic beads functionalized with the primary antibodies to design in-solution SERS assays with Au NS or a graphene–silver nanocomposite functionalized with a secondary antibody and a Raman probe.[9-10]

Two chapters in this thesis showed the potential of a handheld Raman spectrometer used with two different types of SERS substrates, flexible PVDF SERS substrates and colloidal Au NS. The portability of the Raman spectrometer and the ease of the synthesis of these substrates can open a lot of pathways for future work to serve field-deployability applications. With this in mind, building an open source Raman/SERS spectral database, where researchers all over the world can contribute to it, is proposed. This database will allow spectroscopists and other experts in many fields to communicate effectively and efficiently. The impact of experimental parameters (laser wavelength, power, irradiation time, SERS substrates, etc.) on the Raman/SERS spectra

can be compared, and evaluated through this database for a tremendous number of molecules (pesticides, pollutants, explosives, DNA, cells, proteins, etc.) in various matrices (water, food, soil, plasma, urine, etc.). This database can offer continuously updated online spectral archives.

Building such a massive database can save a lot of time and effort, when incorporated with artificial intelligence, to be used in various applications. Artificial intelligence can add new dimensions to this database through advanced statistical modeling and algorithms of machine learning. This, in turn, can advance the Raman/SERS applications to unparalleled levels in many fields. Through this open source database, spectroscopists would have access to this database through their mobile devices and would experience no borders. I believe that creating such a mobile application can be very beneficial for global issues, such as climate change, opioid crisis, medical diagnosis, etc.

## 6.3 References


1. Yu, W. W.; White, I. M., Inkjet Printed Surface Enhanced Raman Spectroscopy Array on Cellulose Paper. *Analytical Chemistry* **2010,** *82* (23), 9626-9630.

2. de Albuquerque, C. D. L.; Sobral-Filho, R. G.; Poppi, R. J.; Brolo, A. G., Digital Protocol for Chemical Analysis at Ultralow Concentrations by Surface-Enhanced Raman Scattering. *Analytical Chemistry* **2018,** *90* (2), 1248-1254.

3. Bantz, K. C.; Haynes, C. L., Surface-enhanced Raman scattering detection and discrimination of polychlorinated biphenyls. *Vibrational Spectroscopy* **2009,** *50* (1), 29-35.

4. Jones, C. L.; Bantz, K. C.; Haynes, C. L., Partition layer-modified substrates for reversible surface-enhanced Raman scattering detection of polycyclic aromatic hydrocarbons. *Analytical and Bioanalytical Chemistry* **2009,** *394* (1), 303-311.

5. Bantz, K. C.; Nelson, H. D.; Haynes, C. L., Plasmon-Enabled Study of Self-Assembled Alkanethiol Ordering on Roughened Ag Substrates. *The Journal of Physical Chemistry C* **2012,** *116* (5), 3585-3593.

6. Guerrini, L.; Garcia-Ramos, J. V.; Domingo, C.; Sanchez-Cortes, S., Sensing Polycyclic Aromatic Hydrocarbons with Dithiocarbamate-Functionalized Ag Nanoparticles by Surface-Enhanced Raman Scattering. *Analytical Chemistry* **2009,** *81* (3), 953-960.

7. Montes-García, V.; Fernández-López, C.; Gómez, B.; Pérez-Juste, I.; García-Río, L.; Liz-Marzán, L. M.; Pérez-Juste, J.; Pastoriza-Santos, I., Pillar[5]arene-Mediated Synthesis of Gold Nanoparticles: Size Control and Sensing Capabilities. *Chemistry – A European Journal* **2014,** *20* (27), 8404-8409.

8. Xie, Y.; Wang, X.; Han, X.; Xue, X.; Ji, W.; Qi, Z.; Liu, J.; Zhao, B.; Ozaki, Y., Sensing of polycyclic aromatic hydrocarbons with cyclodextrin inclusion complexes on silver nanoparticles by surface-enhanced Raman scattering. *Analyst* **2010,** *135* (6), 1389-1394.

9. Wang, Z.; Zong, S.; Wu, L.; Zhu, D.; Cui, Y., SERS-Activated Platforms for Immunoassay: Probes, Encoding Methods, and Applications. *Chemical Reviews* **2017,** *117* (12), 7910-7963.

10. Langer, J.; Jimenez de Aberasturi, D.; Aizpurua, J.; Alvarez-Puebla, R. A.; Auguié, B.; Baumberg, J. J.; Bazan, G. C.; Bell, S. E. J.; Boisen, A.; Brolo, A. G.; Choo, J.; Cialla-May, D.; Deckert, V.; Fabris, L.; Faulds, K.; García de Abajo, F. J.; Goodacre, R.; Graham, D.; Haes, A. J.; Haynes, C. L.; Huck, C.; Itoh, T.; Käll, M.; Kneipp,

J.; Kotov, N. A.; Kuang, H.; Le Ru, E. C.; Lee, H. K.; Li, J.-F.; Ling, X. Y.; Maier, S. A.; Mayerhöfer, T.; Moskovits, M.; Murakoshi, K.; Nam, J.-M.; Nie, S.; Ozaki, Y.; Pastoriza-Santos, I.; Perez-Juste, J.; Popp, J.; Pucci, A.; Reich, S.; Ren, B.; Schatz, G. C.; Shegai, T.; Schlücker, S.; Tay, L.-L.; Thomas, K. G.; Tian, Z.-Q.; Van Duyne, R. P.; Vo-Dinh, T.; Wang, Y.; Willets, K. A.; Xu, C.; Xu, H.; Xu, Y.; Yamamoto, Y. S.; Zhao, B.; Liz-Marzán, L. M., Present and Future of Surface-Enhanced Raman Scattering. *ACS Nano* **2019**.

11. Kho, K. W.; Dinish, U. S.; Kumar, A.; Olivo, M., Frequency Shifts in SERS for Biosensing. *ACS Nano* **2012,** *6* (6), 4892-4902.

12. Pilot, R.; Signorini, R.; Durante, C.; Orian, L.; Bhamidipati, M.; Fabris, L., A Review on Surface-Enhanced Raman Scattering. *Biosensors (Basel)* **2019,** *9* (2), 57.

# Bibliography


Abalde-Cela, S.; Aldeanueva-Potel, P.; Mateo-Mateo, C.; Rodríguez-Lorenzo, L.; Alvarez-Puebla, R. A.; Liz-Marzán, L. M., Surface-enhanced Raman scattering biomedical applications of plasmonic colloidal particles. *Journal of The Royal Society Interface* **2010,** *7* (suppl_4), S435-S450.

Abbas, A.; Brimer, A.; Slocik, J. M.; Tian, L.; Naik, R. R.; Singamaneni, S., Multifunctional Analytical Platform on a Paper Strip: Separation, Preconcentration, and Subattomolar Detection. *Analytical Chemistry* **2013,** *85* (8), 3977-3983.

Abdelsalam, M. E., Surface enhanced raman scattering of aromatic thiols adsorbed on nanostructured gold surfaces. *Central European Journal of Chemistry* **2009,** *7* (3), 446-453.

Agoston, R.; Izake, E. L.; Sivanesan, A.; Lott, W. B.; Sillence, M.; Steel, R., Rapid isolation and detection of erythropoietin in blood plasma by magnetic core gold nanoparticles and portable Raman spectroscopy. *Nanomedicine: Nanotechnology, Biology and Medicine* **2016,** *12* (3), 633-641.

Ahsan, H.; Masaaki, T.; Guang, W. Y., Formation of Gold Nanoparticles by Good's Buffers. *Bulletin of the Chemical Society of Japan* **2005,** *78* (2), 262-269.

Albrecht, M. G.; Creighton, J. A., Anomalously intense Raman spectra of pyridine at a silver electrode. *Journal of the American Chemical Society* **1977,** *99* (15), 5215-5217.

Allen, M. J.; Tung, V. C.; Kaner, R. B., Honeycomb Carbon: A Review of Graphene. *Chemical Reviews* **2010,** *110* (1), 132-145.

Alsammarraie, F. K.; Lin, M.; Mustapha, A.; Lin, H.; Chen, X.; Chen, Y.; Wang, H.; Huang, M., Rapid determination of thiabendazole in juice by SERS coupled with novel gold nanosubstrates. *Food Chemistry* **2018,** *259*, 219-225.

Ames, E. R.; Cheney, J. M.; Rubin, R., The efficacy of thiabendazole and bephenium hydroxynaphthoate against Ostertagia ostertagi and Cooperia oncophora in experimentally infected calves. *American journal of veterinary research* **1963,** *24*, 295-299.

American Chemical Society International Historic Chemical Landmarks. The Raman Effect.http://www.acs.org/content/acs/en/education/whatischemistry/landmarks/ramaneffect.html (accessed November 2, 2019).

Ashley, M. J.; Bourgeois, M. R.; Murthy, R. R.; Laramy, C. R.; Ross, M. B.; Naik, R. R.; Schatz, G. C.; Mirkin, C. A., Shape and Size Control of Substrate-Grown Gold Nanoparticles for Surface-Enhanced Raman Spectroscopy Detection of Chemical Analytes. *The Journal of Physical Chemistry C* **2018,** *122* (4), 2307-2314.

Ato ID. Substrates shop. http://atoid.com/shop/ (accessed 4 December 2019).

ATO ID. New type SERS substrates 'RandaS' and 'MatoS'. https://www.phototechnica.co.jp/wp-content/uploads/2015/02/randa-s-and-mato-s.pdf (accessed 4 December 2019).

Au - Gao, S.; Au - Glasser, J.; Au - He, L., A Filter-based Surface Enhanced Raman Spectroscopic Assay for Rapid Detection of Chemical Contaminants. *JoVE* **2016,** (108), e53791.

Awanis Hashim, N.; Liu, Y.; Li, K., Stability of PVDF hollow fibre membranes in sodium hydroxide aqueous solution. *Chemical Engineering Science* **2011,** *66* (8), 1565-1575.

Bailey, M. R.; Pentecost, A. M.; Selimovic, A.; Martin, R. S.; Schultz, Z. D., Sheath-Flow Microfluidic Approach for Combined Surface Enhanced Raman Scattering and Electrochemical Detection. *Analytical Chemistry* **2015,** *87* (8), 4347-4355.

Banholzer, M. J.; Millstone, J. E.; Qin, L.; Mirkin, C. A., Rationally designed nanostructures for surface-enhanced Raman spectroscopy. *Chemical Society Reviews* **2008,** *37* (5), 885-897.

Bantz, K. C.; Haynes, C. L., Surface-enhanced Raman scattering detection and discrimination of polychlorinated biphenyls. *Vibrational Spectroscopy* **2009,** *50* (1), 29-35.

Bantz, K. C.; Nelson, H. D.; Haynes, C. L., Plasmon-Enabled Study of Self-Assembled Alkanethiol Ordering on Roughened Ag Substrates. *The Journal of Physical Chemistry C* **2012,** *116* (5), 3585-3593.

Batjoens, P.; De Brabander, H. F.; De Wasch, K., Rapid and high-performance analysis of thyreostatic drug residues in urine using gas chromatography-mass spectrometry. *Journal of Chromatography A* **1996,** *750* (1), 127-132.

Bell, S. E. J.; Sirimuthu, N. M. S., Surface-Enhanced Raman Spectroscopy (SERS) for Sub-Micromolar Detection of DNA/RNA Mononucleotides. *Journal of the American Chemical Society* **2006,** *128* (49), 15580-15581.

Berger, A. G.; Restaino, S. M.; White, I. M., Vertical-flow paper SERS system for therapeutic drug monitoring of flucytosine in serum. *Anal. Chim. Acta* **2017,** *949*, 59-66.

Berthod, A.; Laserna, J. J.; Winefordner, J. D., Analysis by surface enhanced Raman spectroscopy on silver hydrosols and silver coated filter papers. *Journal of Pharmaceutical and Biomedical Analysis* **1988,** *6* (6), 599-608.

Betz, J. F.; Yu, W. W.; Cheng, Y.; White, I. M.; Rubloff, G. W., Simple SERS substrates: powerful, portable, and full of potential. *Phys. Chem. Chem. Phys.* **2014,** *16* (6), 2224-2239.

Bispo, J. A. M.; Vieira, E. E. d. S.; Jr., L. S.; Fernandes, A. B., Correlating the amount of urea, creatinine, and glucose in urine from patients with diabetes mellitus and hypertension with the risk of developing renal lesions by means of Raman spectroscopy and principal component analysis. *Journal of Biomedical Optics* **2013,** *18* (8), 1-8, 8.

Blitz, J. P., Diffuse reflectance spectroscopy. *Modern Techniques in Applied Molecular Spectroscopy* **1998**, 185-219.

Bolz, A.; Panne, U.; Rurack, K.; Buurman, M., Glass fibre paper-based test strips for sensitive SERS sensing. *Analytical Methods* **2016,** *8* (6), 1313-1318.

Bouatra, S.; Aziat, F.; Mandal, R.; Guo, A. C.; Wilson, M. R.; Knox, C.; Bjorndahl, T. C.; Krishnamurthy, R.; Saleem, F.; Liu, P.; Dame, Z. T.; Poelzer, J.; Huynh, J.; Yallou, F. S.; Psychogios, N.; Dong, E.; Bogumil, R.; Roehring, C.; Wishart, D. S., The human urine metabolome. *PLoS One* **2013,** *8* (9), e73076.

Brittain, H. G., 3 - Solid-State Analysis. In *Separation Science and Technology*, Ahuja, S.; Scypinski, S., Eds. Academic Press: 2001; Vol. 3, pp 57-84.

Brolo, A. G.; Arctander, E.; Gordon, R.; Leathem, B.; Kavanagh, K. L., Nanohole-Enhanced Raman Scattering. *Nano Letters* **2004,** *4* (10), 2015-2018.

Brolo, A. G.; Irish, D. E.; Smith, B. D., Applications of surface enhanced Raman scattering to the study of metal-adsorbate interactions. *Journal of Molecular Structure* **1997,** *405* (1), 29-44.

Brown, K. R.; Lyon, L. A.; Fox, A. P.; Reiss, B. D.; Natan, M. J., Hydroxylamine Seeding of Colloidal Au Nanoparticles. 3. Controlled Formation of Conductive Au Films. *Chemistry of Materials* **2000,** *12* (2), 314-323.

Brown, K. R.; Natan, M. J., Hydroxylamine Seeding of Colloidal Au Nanoparticles in Solution and on Surfaces. *Langmuir* **1998,** *14* (4), 726-728.

BURROUGHS, W.; RAUN, A.; CHENG, E., Effects of Methimazole on Thyroid and Live Weights of Cattle. *Science* **1958,** *128* (3316), 147-147.

Burroughs, W.; Raun, A.; Trenkle, A.; Raun, N., Further Observations upon the Effects of Methimazole upon Feedlot Performance and Carcass Characteristics of Fattening Beef Cattle. *Journal of Animal Science* **1960,** *19* (2), 465-469.

Cai, J.; Raghavan, V.; Bai, Y. J.; Zhou, M. H.; Liu, X. L.; Liao, C. Y.; Ma, P.; Shi, L.; Dockery, P.; Keogh, I.; Fan, H. M.; Olivo, M., Controllable synthesis of tetrapod gold nanocrystals with precisely tunable near-infrared plasmon resonance towards highly efficient surface enhanced Raman spectroscopy bioimaging. *Journal of Materials Chemistry B* **2015,** *3* (37), 7377-7385.

Campion, A.; Kambhampati, P., Surface-enhanced Raman scattering. *Chemical Society Reviews* **1998,** *27* (4), 241-250.

Cao, L.; Cheng, L.; Zhang, Z.; Wang, Y.; Zhang, X.; Chen, H.; Liu, B.; Zhang, S.; Kong, J., Visual and high-throughput detection of cancer cells using a graphene oxide-based FRET aptasensing microfluidic chip. *Lab on a Chip* **2012,** *12* (22), 4864-4869.

Carron, K. T.; Kennedy, B. J., Molecular-specific chromatographic detector using modified SERS substrates. *Analytical Chemistry* **1995,** *67* (18), 3353-3356.

Cassagneau, T.; Fendler, J. H., Preparation and Layer-by-Layer Self-Assembly of Silver Nanoparticles Capped by Graphite Oxide Nanosheets. *The Journal of Physical Chemistry B* **1999,** *103* (11), 1789-1793.

Cassina, M.; Donà, M.; Di Gianantonio, E.; Clementi, M., Pharmacologic treatment of hyperthyroidism during pregnancy. *Birth Defects Research Part A: Clinical and Molecular Teratology* **2012,** *94* (8), 612-619.

CFIA Malachite Green - Questions and Answers. http://www.inspection.gc.ca/food/information-for-consumers/fact-sheets-and-infographics/products-and-risks/chemical-hazards/malachite-green/eng/1332268890141/1332268947157 (accessed April 2, 2019).

Chamuah, N.; Bhuyan, N.; Das, P. P.; Ojah, N.; Choudhary, A. J.; Medhi, T.; Nath, P., Gold-coated electrospun PVA nanofibers as SERS substrate for detection of pesticides. *Sensors and Actuators B: Chemical* **2018,** *273*, 710-717.

Chamuah, N.; Hazarika, A.; Hatiboruah, D.; Nath, P., SERS on paper: an extremely low cost technique to measure Raman signal. *Journal of Physics D: Applied Physics* **2017,** *50* (48), 485601.

Chandra, K.; Culver, K. S. B.; Werner, S. E.; Lee, R. C.; Odom, T. W., Manipulating the Anisotropic Structure of Gold Nanostars using Good's Buffers. *Chemistry of Materials* **2016,** *28* (18), 6763-6769.

Chang, H.; Tang, L.; Wang, Y.; Jiang, J.; Li, J., Graphene Fluorescence Resonance Energy Transfer Aptasensor for the Thrombin Detection. *Analytical Chemistry* **2010,** *82* (6), 2341-2346.

Chen, N.; Ding, P.; Shi, Y.; Jin, T.; Su, Y.; Wang, H.; He, Y., Portable and Reliable Surface-Enhanced Raman Scattering Silicon Chip for Signal-On Detection of Trace Trinitrotoluene Explosive in Real Systems. *Analytical Chemistry* **2017,** *89* (9), 5072-5078.

Chen, R.; Wu, J.; Li, H.; Cheng, G.; Lu, Z.; Che, C.-M., Fabrication of gold nanoparticles with different morphologies in HEPES buffer. *Rare Metals* **2010,** *29* (2), 180-186.

Chen, Y.; Cheng, H.; Tram, K.; Zhang, S.; Zhao, Y.; Han, L.; Chen, Z.; Huan, S., A paper-based surface-enhanced resonance Raman spectroscopic (SERRS) immunoassay using magnetic separation and enzyme-catalyzed reaction. *Analyst* **2013,** *138* (9), 2624-2631.

Clementi, M.; Di Gianantonio, E.; Pelo, E.; Mammi, I.; Basile, R. T.; Tenconi, R., Methimazole embryopathy: Delineation of the phenotype. *American Journal of Medical Genetics* **1999,** *83* (1), 43-46.

Cuckler, A. C., Thiabendazole, a new broad spectrum anthelmintic. *Journal of Parasitology* **1961,** *47* (4, Sect. 2), 36-37.

Cui, Q.; Yashchenok, A.; Li, L.; Möhwald, H.; Bargheer, M., Mechanistic study on reduction reaction of nitro compounds catalyzed by gold nanoparticles using in situ SERS monitoring. *Colloids and Surfaces A: Physicochemical and Engineering Aspects* **2015,** *470*, 108-113.

Culp, S. J.; Beland, F. A., Malachite green: A toxicological review. *Journal of the American College of Toxicology* **1996,** *15* (3), 219-238.

Culp, S. J.; Blankenship, L. R.; Kusewitt, D. F.; Doerge, D. R.; Mulligan, L. T.; Beland, F. A., Toxicity and metabolism of malachite green and leucomalachite green during short-term feeding to Fischer 344 rats and B6C3F1 mice. *Chemico-Biological Interactions* **1999,** *122* (3), 153-170.

Dam, D. H. M.; Lee, J. H.; Sisco, P. N.; Co, D. T.; Zhang, M.; Wasielewski, M. R.; Odom, T. W., Direct Observation of Nanoparticle–Cancer Cell Nucleus Interactions. *ACS Nano* **2012,** *6* (4), 3318-3326.

Danielson, S. J., 22 - THIN-FILM IMMUNOASSAYS. In *Immunoassay*, Diamandis, E. P.; Christopoulos, T. K., Eds. Academic Press: San Diego, 1996; pp 505-535.

Das, B.; Voggu, R.; Rout, C. S.; Rao, C. N. R., Changes in the electronic structure and properties of graphene induced by molecular charge-transfer. *Chemical Communications* **2008,** (41), 5155-5157.

de Albuquerque, C. D. L.; Sobral-Filho, R. G.; Poppi, R. J.; Brolo, A. G., Digital Protocol for Chemical Analysis at Ultralow Concentrations by Surface-Enhanced Raman Scattering. *Analytical Chemistry* **2018,** *90* (2), 1248-1254.

Diav-Citrin, O.; Ornoy, A., Teratogen update: antithyroid drugs—methimazole, carbimazole, and propylthiouracil. *Teratology* **2002,** *65* (1), 38-44.

Dieringer, J. A.; McFarland, A. D.; Shah, N. C.; Stuart, D. A.; Whitney, A. V.; Yonzon, C. R.; Young, M. A.; Zhang, X.; Van Duyne, R. P., Introductory Lecture Surface enhanced Raman spectroscopy: new materials, concepts, characterization tools, and applications. *Faraday Discussions* **2006,** *132* (0), 9-26.

Ding, S.-Y.; You, E.-M.; Tian, Z.-Q.; Moskovits, M., Electromagnetic theories of surface-enhanced Raman spectroscopy. *Chemical Society Reviews* **2017,** *46* (13), 4042-4076.

Dong, H.; Gao, W.; Yan, F.; Ji, H.; Ju, H., Fluorescence Resonance Energy Transfer between Quantum Dots and Graphene Oxide for Sensing Biomolecules. *Analytical Chemistry* **2010,** *82* (13), 5511-5517.

Dong, H.; Zhang, J.; Ju, H.; Lu, H.; Wang, S.; Jin, S.; Hao, K.; Du, H.; Zhang, X., Highly Sensitive Multiple microRNA Detection Based on Fluorescence Quenching of Graphene Oxide and Isothermal Strand-Displacement Polymerase Reaction. *Analytical Chemistry* **2012,** *84* (10), 4587-4593.

Duan, B.; Zhou, J.; Fang, Z.; Wang, C.; Wang, X.; Hemond, H. F.; Chan-Park, M. B.; Duan, H., Surface enhanced Raman scattering by graphene-nanosheet-gapped plasmonic nanoparticle arrays for multiplexed DNA detection. *Nanoscale* **2015,** *7* (29), 12606-12613.

Ebrahimzadeh, H.; Asgharinezhad, A. A.; Adlnasab, L.; Shekari, N., Optimization of ion-pair based hollow fiber liquid phase microextraction combined with HPLC–UV for the determination of methimazole in biological samples and animal feed. *Journal of Separation Science* **2012,** *35* (16), 2040-2047.

El-Sayed, M. A., Some Interesting Properties of Metals Confined in Time and Nanometer Space of Different Shapes. *Accounts of Chemical Research* **2001,** *34* (4), 257-264.

Emory, S. R.; Haskins, W. E.; Nie, S., Direct Observation of Size-Dependent Optical Enhancement in Single Metal Nanoparticles. *Journal of the American Chemical Society* **1998,** *120* (31), 8009-8010.

Enhanced Spectrometry. SERS Technology. http://enspectr.com/portfolio/sers-substrates/?done=done&pf=#9da94c02fc (accessed 4 December 2019)

Evanoff, D. D.; Chumanov, G., Size-Controlled Synthesis of Nanoparticles. 2. Measurement of Extinction, Scattering, and Absorption Cross Sections. *The Journal of Physical Chemistry B* **2004,** *108* (37), 13957-13962.

Fan, M.; Andrade, G. F. S.; Brolo, A. G., A review on the fabrication of substrates for surface enhanced Raman spectroscopy and their applications in analytical chemistry. *Analytica Chimica Acta* **2011,** *693* (1), 7-25.

Fan, Z.; Kanchanapally, R.; Ray, P. C., Hybrid Graphene Oxide Based Ultrasensitive SERS Probe for Label-Free Biosensing. *The Journal of Physical Chemistry Letters* **2013,** *4* (21), 3813-3818.

Fei, J.; Wu, L.; Zhang, Y.; Zong, S.; Wang, Z.; Cui, Y., Pharmacokinetics-on-a-Chip Using Label-Free SERS Technique for Programmable Dual-Drug Analysis. *ACS Sensors* **2017,** *2* (6), 773-780.

Feng, J.-J.; Hildebrandt, P.; Murgida, D. H., Silver Nanocoral Structures on Electrodes: A Suitable Platform for Protein-Based Bioelectronic Devices. *Langmuir* **2008,** *24* (5), 1583-1586.

Fernandes, C.; Lalitha, V. S.; Rao, K. V., Enhancing effect of malachite green on the development of hepatic pre-neoplastic lesions induced by N-nitrosodiethylamine in rats. *Carcinogenesis* **1991,** *12* (5), 839-45.

Ferrari, A. C., Raman spectroscopy of graphene and graphite: Disorder, electron–phonon coupling, doping and nonadiabatic effects. *Solid State Communications* **2007,** *143* (1), 47-57.

Ferrari, A. C.; Basko, D. M., Raman spectroscopy as a versatile tool for studying the properties of graphene. *Nature Nanotechnology* **2013,** *8*, 235.

Fikiet, M. A.; Khandasammy, S. R.; Mistek, E.; Ahmed, Y.; Halámková, L.; Bueno, J.; Lednev, I. K., Surface enhanced Raman spectroscopy: A review of recent applications in forensic science. *Spectrochimica Acta Part A: Molecular and Biomolecular Spectroscopy* **2018,** *197*, 255-260.

Fleischmann, M.; Hendra, P. J.; McQuillan, A. J., Raman spectra of pyridine adsorbed at a silver electrode. *Chemical Physics Letters* **1974,** *26* (2), 163-166.

Gao, P.; Weaver, M. J., SURFACE-ENHANCED RAMAN-SPECTROSCOPY AS A PROBE OF ADSORBATE SURFACE BONDING - BENZENE AND MONOSUBSTITUTED BENZENES ADSORBED AT GOLD ELECTRODES. *Journal of Physical Chemistry* **1985,** *89* (23), 5040-5046.

Gebavi, H.; Gašparić, V.; Risović, D.; Baran, N.; Albrycht, P. H.; Ivanda, M., Features and advantages of flexible silicon nanowires for SERS applications. *Beilstein Journal of Nanotechnology* **2019,** *10*, 725-734.

Geim, A. K.; Novoselov, K. S., The rise of graphene. *Nature Materials* **2007,** *6*, 183.

Geng, J.; Jung, H.-T., Porphyrin Functionalized Graphene Sheets in Aqueous Suspensions: From the Preparation of Graphene Sheets to Highly Conductive Graphene Films. *The Journal of Physical Chemistry C* **2010,** *114* (18), 8227-8234.

Genter, M. B., Evaluation of olfactory and auditory system effects of the antihyperthyroid drug carbimazole in the Long-Evans rat. *Journal of Biochemical and Molecular Toxicology* **1998,** *12* (5), 305-314.

Gersten, J. I., The Effect of Surface-Roughness on Surface Enhanced Raman-Scattering. *J Chem Phys* **1980,** *72* (10), 5779-5780.

Giljohann, D. A.; Mirkin, C. A., Drivers of biodiagnostic development. *Nature* **2009,** *462*, 461.

Gkogkou, D.; Schreiber, B.; Shaykhutdinov, T.; Ly, H. K.; Kuhlmann, U.; Gernert, U.; Facsko, S.; Hildebrandt, P.; Esser, N.; Hinrichs, K.; Weidinger, I. M.; Oates, T. W. H., Polarization- and Wavelength-Dependent Surface-Enhanced Raman Spectroscopy Using Optically Anisotropic Rippled Substrates for Sensing. *ACS Sensors* **2016,** *1* (3), 318-323.

Gole, A.; Murphy, C. J., Seed-Mediated Synthesis of Gold Nanorods: Role of the Size and Nature of the Seed. *Chemistry of Materials* **2004,** *16* (19), 3633-3640.

Goncalves, G.; Marques, P. A. A. P.; Granadeiro, C. M.; Nogueira, H. I. S.; Singh, M. K.; Grácio, J., Surface Modification of Graphene Nanosheets with Gold Nanoparticles: The Role of Oxygen Moieties at Graphene Surface on Gold Nucleation and Growth. *Chemistry of Materials* **2009,** *21* (20), 4796-4802.

Goodacre, R.; Graham, D.; Faulds, K., Recent developments in quantitative SERS: Moving towards absolute quantification. *TrAC Trends in Analytical Chemistry* **2018,** *102*, 359-368.

Gracie, K.; Moores, M.; Smith, W. E.; Harding, K.; Girolami, M.; Graham, D.; Faulds, K., Preferential Attachment of Specific Fluorescent Dyes and Dye Labeled DNA Sequences in a Surface Enhanced Raman Scattering Multiplex. *Anal. Chem. (Washington, DC, U. S.)* **2016,** *88* (2), 1147-1153.

Grady, J. K.; Chasteen, N. D.; Harris, D. C., Radicals from "Good's" buffers. *Analytical Biochemistry* **1988,** *173* (1), 111-115.

Guerrini, L.; Garcia-Ramos, J. V.; Domingo, C.; Sanchez-Cortes, S., Sensing Polycyclic Aromatic Hydrocarbons with Dithiocarbamate-Functionalized Ag Nanoparticles by Surface-Enhanced Raman Scattering. *Analytical Chemistry* **2009,** *81* (3), 953-960.

Guerrini, L.; Graham, D., Molecularly-mediated assemblies of plasmonic nanoparticles for Surface-Enhanced Raman Spectroscopy applications. *Chemical Society Reviews* **2012,** *41* (21), 7085-7107.

Guerrini, L.; Krpetic, Z.; van Lierop, D.; Alvarez-Puebla, R. A.; Graham, D., Direct surface-enhanced Raman scattering analysis of DNA duplexes. *Angew. Chem., Int. Ed.* **2015,** *54* (4), 1144-1148.

Haddad, A.; Comanescu, M. A.; Green, O.; Kubic, T. A.; Lombardi, J. R., Detection and Quantitation of Trace Fentanyl in Heroin by Surface-Enhanced Raman Spectroscopy. *Analytical Chemistry* **2018,** *90* (21), 12678-12685.

Haiss, W.; Thanh, N. T. K.; Aveyard, J.; Fernig, D. G., Determination of Size and Concentration of Gold Nanoparticles from UV−Vis Spectra. *Analytical Chemistry* **2007,** *79* (11), 4215-4221.

Hakonen, A.; Rindzevicius, T.; Schmidt, M. S.; Andersson, P. O.; Juhlin, L.; Svedendahl, M.; Boisen, A.; Käll, M., Detection of nerve gases using surface-enhanced Raman scattering substrates with high droplet adhesion. *Nanoscale* **2016,** *8* (3), 1305-1308.

Hakonen, A.; Wu, K. Y.; Schmidt, M. S.; Andersson, P. O.; Boisen, A.; Rindzevicius, T., Detecting forensic substances using commercially available SERS substrates and handheld Raman spectrometers. *Talanta* **2018,** *189*, 649-652.

Hamamatsu. SERS Substrate. https://www.hamamatsu.com/resources/pdf/ssd/j12853_koth1007e.pdf (accessed 25 November 2019).

Hao, F.; Nehl, C. L.; Hafner, J. H.; Nordlander, P., Plasmon Resonances of a Gold Nanostar. *Nano Letters* **2007,** *7* (3), 729-732.

Hashim, N. A.; Liu, F.; Li, K., A simplified method for preparation of hydrophilic PVDF membranes from an amphiphilic graft copolymer. *Journal of Membrane Science* **2009,** *345* (1), 134-141.

Hasi, W.-L.-J.; Lin, X.; Lou, X.-T.; Lin, S.; Yang, F.; Lin, D.-Y.; Lu, Z.-W., Chloride ion-assisted self-assembly of silver nanoparticles on filter paper as SERS substrate. *Applied Physics A* **2015,** *118* (3), 799-807.

Hassanain, W. A.; Izake, E. L.; Ayoko, G. A., Spectroelectrochemical Nanosensor for the Determination of Cystatin C in Human Blood. *Analytical Chemistry* **2018,** *90* (18), 10843-10850.

Hassanain, W. A.; Izake, E. L.; Schmidt, M. S.; Ayoko, G. A., Gold nanomaterials for the selective capturing and SERS diagnosis of toxins in aqueous and biological fluids. *Biosensors and Bioelectronics* **2017,** *91*, 664-672.

Haynes, C. L.; Van Duyne, R. P., Nanosphere Lithography: A Versatile Nanofabrication Tool for Studies of Size-Dependent Nanoparticle Optics. *The Journal of Physical Chemistry B* **2001,** *105* (24), 5599-5611.

He, S.; Chua, J.; Tan, E. K. M.; Kah, J. C. Y., Optimizing the SERS enhancement of a facile gold nanostar immobilized paper-based SERS substrate. *RSC Advances* **2017,** *7* (27), 16264-16272.

He, S.; Liu, K.-K.; Su, S.; Yan, J.; Mao, X.; Wang, D.; He, Y.; Li, L.-J.; Song, S.; Fan, C., Graphene-Based High-Efficiency Surface-Enhanced Raman Scattering-Active Platform for Sensitive and Multiplex DNA Detection. *Analytical Chemistry* **2012,** *84* (10), 4622-4627.

He, S.; Song, B.; Li, D.; Zhu, C.; Qi, W.; Wen, Y.; Wang, L.; Song, S.; Fang, H.; Fan, C., A Graphene Nanoprobe for Rapid, Sensitive, and Multicolor Fluorescent DNA Analysis. *Advanced Functional Materials* **2010,** *20* (3), 453-459.

He, Y.; Wang, Z.-G.; Tang, H.-W.; Pang, D.-W., Low background signal platform for the detection of ATP: When a molecular aptamer beacon meets graphene oxide. *Biosensors and Bioelectronics* **2011,** *29* (1), 76-81.

Herrera-Sandoval, G. M.; Felix-Rivera, H.; Padilla-Jimenez, A. C.; Balaguera-Gelves, M.; Ortega-Zuniga, C. A.; Pacheco-Londono, L. C.; Primera-Pedrozo, O. M.; Fierro, P. M.; Rios-Velazquez, C.; Hernandez-Rivera, S. P. In *Synthesis and characterization of silver nanoparticles and nanostructures for SERS applications*, Nova Science Publishers, Inc.: 2013; pp 59-100.

Hidi, I. J.; Heidler, J.; Weber, K.; Cialla-May, D.; Popp, J., Ciprofloxacin: pH-dependent SERS signal and its detection in spiked river water using LoC-SERS. *Analytical and Bioanalytical Chemistry* **2016,** *408* (29), 8393-8401.

Holze, R., Competition of anchoring groups in adsorption on gold electrodes—a comparative spectroelectrochemical study of 4-mercaptobenzonitrile and aromatic nitriles. *Journal of Solid State Electrochemistry* **2013,** *17* (7), 1869-1879.

Horiba Scientific. SERS Substrates. https://www.horiba.com/us/en/scientific/products/raman-spectroscopy/accessories/sers-substrates/ (accessed 21 November 2019).

Hoppmann, E. P.; White, I. M., A paper-based inkjet-fabricated substrate for SERS detection and differentiation of PCR products. *Proc. SPIE* **2013,** *8718* (Advanced Environmental, Chemical, and Biological Sensing Technologies X), 871804/1-871804/6.

Hoppmann, E. P.; Yu, W. W.; White, I. M., Detection of deoxyribonucleic acid (DNA) targets using polymerase chain reaction (PCR) and paper surface-enhanced Raman spectroscopy (SERS) chromatography. *Appl. Spectrosc.* **2014,** *68* (8), 909-915.

Hoppmann, E. P.; Yu, W. W.; White, I. M., Highly sensitive and flexible inkjet printed SERS sensors on paper. *Methods* **2013,** *63* (3), 219-224.

Hoppmann, E. P.; Yu, W. W.; White, I. M., Inkjet-printed fluidic paper devices for chemical and biological analytics using surface enhanced Raman spectroscopy. *IEEE J. Sel. Top. Quantum Electron.* **2014,** *20* (3), 7300510/1-7300510/10.

Huang, X.; Neretina, S.; El-Sayed, M. A., Gold Nanorods: From Synthesis and Properties to Biological and Biomedical Applications. *Advanced Materials* **2009,** *21* (48), 4880-4910.

Huang, Z.; Cao, G.; Sun, Y.; Du, S.; Li, Y.; Feng, S.; Lin, J.; Lei, J., Evaluation and Optimization of Paper-Based SERS Substrate for Potential Label-Free Raman Analysis of Seminal Plasma. *Journal of Nanomaterials* **2017,** *2017*, 8.

Huh, S.; Park, J.; Kim, Y. S.; Kim, K. S.; Hong, B. H.; Nam, J.-M., UV/Ozone-Oxidized Large-Scale Graphene Platform with Large Chemical Enhancement in Surface-Enhanced Raman Scattering. *ACS Nano* **2011,** *5* (12), 9799-9806.

Hummers, W. S.; Offeman, R. E., Preparation of Graphitic Oxide. *Journal of the American Chemical Society* **1958,** *80* (6), 1339-1339.

III, N. C.; Chidsey, C. E. D.; Liu, G. y.; Scoles, G., Substrate dependence of the surface structure and chain packing of docosyl mercaptan self-assembled on the (111), (110), and (100) faces of single crystal gold. *The Journal of Chemical Physics* **1993,** *98* (5), 4234-4245.

Indrasekara, A. S. D. S.; Meyers, S.; Shubeita, S.; Feldman, L. C.; Gustafsson, T.; Fabris, L., Gold nanostar substrates for SERS-based chemical sensing in the femtomolar regime. *Nanoscale* **2014,** *6* (15), 8891-8899.

Izquierdo-Lorenzo, I.; García-Ramos, J. V.; Sanchez-Cortes, S., Vibrational characterization and surface-enhanced Raman scattering detection of probenecid doping drug. *Journal of Raman Spectroscopy* **2013,** *44* (10), 1422-1427.

Izquierdo-Lorenzo, I.; Sanchez-Cortes, S.; Garcia-Ramos, J. V., Adsorption of Beta-Adrenergic Agonists Used in Sport Doping on Metal Nanoparticles: A Detection Study Based on Surface-Enhanced Raman Scattering. *Langmuir* **2010,** *26* (18), 14663-14670.

Izquierdo-Lorenzo, I.; Sanchez-Cortes, S.; Garcia-Ramos, J. V., Trace detection ofaminoglutethimide drug by surface-enhanced Raman spectroscopy: a vibrational and adsorption study on gold nanoparticles. *Analytical Methods* **2011,** *3* (7), 1540-1545.

Jalani, G.; Cerruti, M., Nano graphene oxide-wrapped gold nanostars as ultrasensitive and stable SERS nanoprobes. *Nanoscale* **2015,** *7* (22), 9990-9997.

Jamieson, J. D.; Smith, E. B.; Dalvie, D. K.; Stevens, G. J.; Yanochko, G. M., Myeloperoxidase-mediated bioactivation of 5-hydroxythiabendazole: A possible mechanism of thiabendazole toxicity. *Toxicology in Vitro* **2011,** *25* (5), 1061-1066.

Jana, N. R.; Pal, T., Anisotropic Metal Nanoparticles for Use as Surface-Enhanced Raman Substrates. *Advanced Materials* **2007,** *19* (13), 1761-1765.

Jang, H.; Kim, Y.-K.; Kwon, H.-M.; Yeo, W.-S.; Kim, D.-E.; Min, D.-H., A Graphene-Based Platform for the Assay of Duplex-DNA Unwinding by Helicase. *Angewandte Chemie International Edition* **2010,** *49* (33), 5703-5707.

Jasuja, K.; Linn, J.; Melton, S.; Berry, V., Microwave-Reduced Uncapped Metal Nanoparticles on Graphene: Tuning Catalytic, Electrical, and Raman Properties. *The Journal of Physical Chemistry Letters* **2010,** *1* (12), 1853-1860.

Jaworska, A.; Pyrak, E.; Kudelski, A., Comparison of the efficiency of generation of Raman radiation by various Raman reporters connected via DNA linkers to different plasmonic nano-structures. *Vibrational Spectroscopy* **2019,** *101*, 34-39.

Jeanmaire, D. L.; Van Duyne, R. P., Surface raman spectroelectrochemistry: Part I. Heterocyclic, aromatic, and aliphatic amines adsorbed on the anodized silver electrode. *Journal of Electroanalytical Chemistry and Interfacial Electrochemistry* **1977,** *84* (1), 1-20.

Jensen, L.; Zhao, L. L.; Schatz, G. C., Size-Dependence of the Enhanced Raman Scattering of Pyridine Adsorbed on Agn (n = 2−8, 20) Clusters. *The Journal of Physical Chemistry C* **2007,** *111* (12), 4756-4764.

Jin, M.; van Wolferen, H.; Wormeester, H.; van den Berg, A.; Carlen, E. T., Large-area nanogap plasmon resonator arrays for plasmonics applications. *Nanoscale* **2012,** *4* (15), 4712-4718.

Joens, M. S.; Huynh, C.; Kasuboski, J. M.; Ferranti, D.; Sigal, Y. J.; Zeitvogel, F.; Obst, M.; Burkhardt, C. J.; Curran, K. P.; Chalasani, S. H.; Stern, L. A.; Goetze, B.; Fitzpatrick, J. A. J., Helium Ion Microscopy (HIM) for the imaging of biological samples at sub-nanometer resolution. *Scientific Reports* **2013,** *3*, 3514.

John Blanchflower, W.; J. Hughes, P.; Cannavan, A.; A. McCoy, M.; Glenn Kennedy, D., Determination of Thyreostats in Thyroid and Urine Using High-performance Liquid Chromatography–Atmospheric Pressure Chemical Ionisation Mass Spectrometry. *Analyst* **1997,** *122* (9), 967-972.

Jones, C. L.; Bantz, K. C.; Haynes, C. L., Partition layer-modified substrates for reversible surface-enhanced Raman scattering detection of polycyclic aromatic hydrocarbons. *Analytical and Bioanalytical Chemistry* **2009,** *394* (1), 303-311.

Joshi, P.; Santhanam, V., Paper-based SERS active substrates on demand. *RSC Advances* **2016,** *6* (72), 68545-68552.

Kahl, M.; Voges, E.; Kostrewa, S.; Viets, C.; Hill, W., Periodically structured metallic substrates for SERS. *Sensors and Actuators B: Chemical* **1998,** *51* (1), 285-291.

Kambhampati, P.; Child, C. M.; Foster, M. C.; Campion, A., On the chemical mechanism of surface enhanced Raman scattering: Experiment and theory. *The Journal of Chemical Physics* **1998,** *108* (12), 5013-5026.

Kang, L.; Chu, J.; Zhao, H.; Xu, P.; Sun, M., Recent progress in the applications of graphene in surface-enhanced Raman scattering and plasmon-induced catalytic reactions. *Journal of Materials Chemistry C* **2015,** *3* (35), 9024-9037.

Karabeber, H.; Huang, R.; Iacono, P.; Samii, J. M.; Pitter, K.; Holland, E. C.; Kircher, M. F., Guiding Brain Tumor Resection Using Surface-Enhanced Raman Scattering Nanoparticles and a Hand-Held Raman Scanner. *ACS Nano* **2014,** *8* (10), 9755-9766.

Kennedy, B. J.; Milofsky, R.; Carron, K. T., Development of a Cascade Flow Cell for Dynamic Aqueous Phase Detection Using Modified SERS Substrates. *Analytical Chemistry* **1997,** *69* (22), 4708-4715.

Kennedy, B. J.; Spaeth, S.; Dickey, M.; Carron, K. T., Determination of the Distance Dependence and Experimental Effects for Modified SERS Substrates Based on Self-Assembled Monolayers Formed Using Alkanethiols. *The Journal of Physical Chemistry B* **1999,** *103* (18), 3640-3646.

Keuleers, R.; Desseyn, H. O.; Rousseau, B.; Van Alsenoy, C., Vibrational Analysis of Urea. *The Journal of Physical Chemistry A* **1999,** *103* (24), 4621-4630.

Keunen, R.; Macoretta, D.; Cathcart, N.; Kitaev, V., Stable ligand-free stellated polyhedral gold nanoparticles for sensitive plasmonic detection. *Nanoscale* **2016,** *8* (5), 2575-2583.

Kho, K. W.; Dinish, U. S.; Kumar, A.; Olivo, M., Frequency Shifts in SERS for Biosensing. *ACS Nano* **2012,** *6* (6), 4892-4902.

Kim, M. S.; Kim, M. K.; Lee, C. J.; Jung, Y. M.; Lee, M. S., Surface-enhanced Raman Spectroscopy of Benzimidazolic Fungicides: Benzimidazole and Thiabendazole. *B Korean Chem Soc* **2009,** *30* (12), 2930-2934.

Kim, S.; Ryoo, S.-R.; Na, H.-K.; Kim, Y.-K.; Choi, B.-S.; Lee, Y.; Kim, D.-E.; Min, D.-H., Deoxyribozyme-loaded nano-graphene oxide for simultaneous sensing and silencing of the hepatitis C virus gene in liver cells. *Chemical Communications* **2013,** *49* (74), 8241-8243.

Kim, W.-S.; Shin, J.-H.; Park, H.-K.; Choi, S., A low-cost, monometallic, surface-enhanced Raman scattering-functionalized paper platform for spot-on bioassays. *Sensors and Actuators B: Chemical* **2016,** *222*, 1112-1118.

Kim, W.; Kim, Y.-H.; Park, H.-K.; Choi, S., Facile Fabrication of a Silver Nanoparticle Immersed, Surface-Enhanced Raman Scattering Imposed Paper Platform through Successive Ionic Layer Absorption and Reaction for On-Site Bioassays. *ACS Applied Materials & Interfaces* **2015,** *7* (50), 27910-27917.

Kim, W.; Lee, J.-C.; Lee, G.-J.; Park, H.-K.; Lee, A.; Choi, S., Low-Cost Label-Free Biosensing Bimetallic Cellulose Strip with SILAR-Synthesized Silver Core–Gold Shell Nanoparticle Structures. *Analytical Chemistry* **2017,** *89* (12), 6448-6454.

Kim, W.; Lee, J.-C.; Shin, J.-H.; Jin, K.-H.; Park, H.-K.; Choi, S., Instrument-Free Synthesizable Fabrication of Label-Free Optical Biosensing Paper Strips for the Early Detection of Infectious Keratoconjunctivitides. *Analytical Chemistry* **2016,** *88* (10), 5531-5537.

Kim, W.; Lee, S. H.; Kim, J. H.; Ahn, Y. J.; Kim, Y.-H.; Yu, J. S.; Choi, S., Paper-Based Surface-Enhanced Raman Spectroscopy for Diagnosing Prenatal Diseases in Women. *ACS Nano* **2018,** *12* (7), 7100-7108.

Kise, H.; Ogata, H., Phase transfer catalysis in dehydrofluorination of poly(vinylidene fluoride) by aqueous sodium hydroxide solutions. *Journal of Polymer Science: Polymer Chemistry Edition* **1983,** *21* (12), 3443-3451.

Kneipp, K.; Kneipp, H.; Itzkan, I.; Dasari, R. R.; Feld, M. S., Surface-enhanced Raman scattering and biophysics. *Journal of Physics: Condensed Matter* **2002,** *14* (18), R597-R624.

Kneipp, K.; Wang, Y.; Kneipp, H.; Perelman, L. T.; Itzkan, I.; Dasari, R. R.; Feld, M. S., Single Molecule Detection Using Surface-Enhanced Raman Scattering (SERS). *Physical Review Letters* **1997,** *78* (9), 1667-1670.

Kong, D.; Chi, Y.; Chen, L.; Dong, Y.; Zhang, L.; Chen, G., Determination of thyreostatics in animal feeds by CE with electrochemical detector. *ELECTROPHORESIS* **2009,** *30* (19), 3489-3495.

Kong, X.-M.; Reza, M.; Ma, Y.-B.; Hinestroza, J.-P.; Ahvenniemi, E.; Vuorinen, T., Assembly of metal nanoparticles on regenerated fibers from wood sawdust and de-inked pulp: flexible substrates for surface enhanced Raman scattering (SERS) applications. *Cellulose* **2015,** *22* (6), 3645-3655.

Kou, X.; Ni, W.; Tsung, C.-K.; Chan, K.; Lin, H.-Q.; Stucky, G. D.; Wang, J., Growth of Gold Bipyramids with Improved Yield and Their Curvature-Directed Oxidation. *Small* **2007,** *3* (12), 2103-2113.

Krishnan, R. S.; Shankar, R. K., Raman effect: History of the discovery. *Journal of Raman Spectroscopy* **1981,** *10* (1), 1-8.

Kukushkin, V. I.; Ivanov, N. M.; Novoseltseva, A. A.; Gambaryan, A. S.; Yaminsky, I. V.; Kopylov, A. M.; Zavyalova, E. G., Highly sensitive detection of influenza virus with SERS aptasensor. *PLOS ONE* **2019,** *14* (4), e0216247.

Kuśmierek, K.; Bald, E., Determination of methimazole in urine by liquid chromatography. *Talanta* **2007,** *71* (5), 2121-2125.

Lai, K.; Zhang, Y.; Du, R.; Zhai, F.; Rasco, B. A.; Huang, Y., Determination of chloramphenicol and crystal violet with surface enhanced Raman spectroscopy. *Sensing and Instrumentation for Food Quality and Safety* **2011,** *5* (1), 19-24.

Langer, J.; Jimenez de Aberasturi, D.; Aizpurua, J.; Alvarez-Puebla, R. A.; Auguié, B.; Baumberg, J. J.; Bazan, G. C.; Bell, S. E. J.; Boisen, A.; Brolo, A. G.; Choo, J.; Cialla-May, D.; Deckert, V.; Fabris, L.; Faulds, K.; García de Abajo, F. J.; Goodacre, R.; Graham, D.; Haes, A. J.; Haynes, C. L.; Huck, C.; Itoh, T.; Käll, M.; Kneipp, J.; Kotov, N. A.; Kuang, H.; Le Ru, E. C.; Lee, H. K.; Li, J.-F.; Ling, X. Y.; Maier, S. A.; Mayerhöfer, T.; Moskovits, M.; Murakoshi, K.; Nam, J.-M.; Nie, S.; Ozaki, Y.; Pastoriza-Santos, I.; Perez-Juste, J.; Popp, J.; Pucci, A.; Reich, S.; Ren, B.; Schatz, G. C.; Shegai, T.; Schlücker, S.; Tay, L.-L.; Thomas, K. G.; Tian, Z.-Q.; Van Duyne, R. P.; Vo-Dinh, T.; Wang, Y.; Willets, K. A.; Xu, C.; Xu, H.; Xu, Y.; Yamamoto, Y. S.; Zhao, B.; Liz-Marzán, L. M., Present and Future of Surface-Enhanced Raman Scattering. *ACS Nano* **2020,** *14* (1), 28-117.

Laserna, J. J.; Campiglia, A. D.; Winefordner, J. D., Mixture analysis and quantitative determination of nitrogen-containing organic molecules by surface-enhanced Raman spectrometry. *Analytical Chemistry* **1989,** *61* (15), 1697-1701.

Laserna, J. J.; Campiglia, A. D.; Winefordner, J. D., Surface-enhanced Raman spectrometry on a silver-coated filter paper substrate. *Analytica Chimica Acta* **1988,** *208*, 21-30.

Lauridsen, R. K.; Rindzevicius, T.; Molin, S.; Johansen, H. K.; Berg, R. W.; Alstrøm, T. S.; Almdal, K.; Larsen, F.; Schmidt, M. S.; Boisen, A., Towards quantitative SERS detection of hydrogen cyanide at ppb level for human breath analysis. *Sensing and Bio-Sensing Research* **2015,** *5*, 84-89.

Lauridsen, R. K.; Skou, P. B.; Rindzevicius, T.; Wu, K.; Molin, S.; Engelsen, S. B.; Nielsen, K. G.; Johansen, H. K.; Boisen, A., SERS spectroscopy for detection of hydrogen cyanide in breath from children colonised with P. aeruginosa. *Analytical Methods* **2017,** *9* (39), 5757-5762.

Lauridsen, R. K.; Sommer, L. M.; Johansen, H. K.; Rindzevicius, T.; Molin, S.; Jelsbak, L.; Engelsen, S. B.; Boisen, A., SERS detection of the biomarker hydrogen cyanide from Pseudomonas aeruginosa cultures isolated from cystic fibrosis patients. *Scientific Reports* **2017,** *7* (1), 45264.

Lawrence, J. F.; Iverson, F.; Hanekamp, H. B.; Bos, P.; Frei, R. W., Liquid chromatography with UV absorbance and polarographic detection of ethylenethiourea and related sulfur compounds: Application to rat urine analysis. *Journal of Chromatography A* **1981,** *212* (2), 245-250.

Le Ru, E. C.; Blackie, E.; Meyer, M.; Etchegoin, P. G., Surface Enhanced Raman Scattering Enhancement Factors: A Comprehensive Study. *The Journal of Physical Chemistry C* **2007,** *111* (37), 13794-13803.

Le Ru, E. C.; Meyer, M.; Etchegoin, P. G., Proof of Single-Molecule Sensitivity in Surface Enhanced Raman Scattering (SERS) by Means of a Two-Analyte Technique. *The Journal of Physical Chemistry B* **2006,** *110* (4), 1944-1948.

Lee, C. H.; Hankus, M. E.; Tian, L.; Pellegrino, P. M.; Singamaneni, S., Highly Sensitive Surface Enhanced Raman Scattering Substrates Based on Filter Paper Loaded with Plasmonic Nanostructures. *Analytical Chemistry* **2011,** *83* (23), 8953-8958.

Lee, C. H.; Tian, L.; Singamaneni, S., Paper-Based SERS Swab for Rapid Trace Detection on Real-World Surfaces. *ACS Applied Materials & Interfaces* **2010,** *2* (12), 3429-3435.

Lee, J.-C.; Kim, W.; Park, H.-K.; Choi, S., Controlling successive ionic layer absorption and reaction cycles to optimize silver nanoparticle-induced localized surface plasmon resonance effects on the paper strip. *Spectrochimica Acta Part A: Molecular and Biomolecular Spectroscopy* **2017,** *174*, 37-43.

Lee, J.; Kim, J.; Kim, S.; Min, D.-H., Biosensors based on graphene oxide and its biomedical application. *Advanced Drug Delivery Reviews* **2016,** *105*, 275-287.

Lee, P. C.; Meisel, D., Adsorption and surface-enhanced Raman of dyes on silver and gold sols. *The Journal of Physical Chemistry* **1982,** *86* (17), 3391-3395.

Leopold, N.; Lendl, B., A New Method for Fast Preparation of Highly Surface-Enhanced Raman Scattering (SERS) Active Silver Colloids at Room Temperature by Reduction of Silver Nitrate with Hydroxylamine Hydrochloride. *The Journal of Physical Chemistry B* **2003,** *107* (24), 5723-5727.

LeRu, E. C.; Etchegoin, P. G., *Principles of Surface-Enhanced Raman Spectroscopy: And Related Plasmonic Effects*. 2009; p 1-663.

Li, D.; Müller, M. B.; Gilje, S.; Kaner, R. B.; Wallace, G. G., Processable aqueous dispersions of graphene nanosheets. *Nature Nanotechnology* **2008,** *3*, 101.

Li, F.; Huang, Y.; Yang, Q.; Zhong, Z.; Li, D.; Wang, L.; Song, S.; Fan, C., A graphene-enhanced molecular beacon for homogeneous DNA detection. *Nanoscale* **2010,** *2* (6), 1021-1026.

Li, Y.; Zhang, K.; Zhao, J.; Ji, J.; Ji, C.; Liu, B., A three-dimensional silver nanoparticles decorated plasmonic paper strip for SERS detection of low-abundance molecules. *Talanta* **2016,** *147*, 493-500.

Liang, D.; Bowers, J. E., Recent progress in lasers on silicon. *Nature Photonics* **2010,** *4* (8), 511-517.

Liang, X.; You, T.; Liu, D.; Lang, X.; Tan, E.; Shi, J.; Yin, P.; Guo, L., Direct observation of enhanced plasmon-driven catalytic reaction activity of Au nanoparticles supported on reduced graphene oxides by SERS. *Physical Chemistry Chemical Physics* **2015,** *17* (15), 10176-10181.

Liao, W.-J.; Roy, P. K.; Chattopadhyay, S., An ink-jet printed, surface enhanced Raman scattering paper for food screening. *RSC Advances* **2014,** *4* (76), 40487-40493.

Liao, X.; Chen, Y.; Qin, M.; Chen, Y.; Yang, L.; Zhang, H.; Tian, Y., Au–Ag–Au double shell nanoparticles-based localized surface plasmon resonance and surface-enhanced Raman scattering biosensor for sensitive detection of 2-mercapto-1-methylimidazole. *Talanta* **2013,** *117*, 203-208.

Lightcap, I. V.; Murphy, S.; Schumer, T.; Kamat, P. V., Electron Hopping Through Single-to-Few-Layer Graphene Oxide Films. Side-Selective Photocatalytic Deposition of Metal Nanoparticles. *The Journal of Physical Chemistry Letters* **2012,** *3* (11), 1453-1458.

Lin, T.-W.; Tasi, T.-T.; Chang, P.-L.; Cheng, H.-Y., Reversible Association of Nitro Compounds with p-Nitrothiophenol Modified on Ag Nanoparticles/Graphene Oxide Nanocomposites through Plasmon Mediated Photochemical Reaction. *ACS Applied Materials & Interfaces* **2016,** *8* (12), 8315-8322.

Lin, T.-W.; Wu, H.-Y.; Tasi, T.-T.; Lai, Y.-H.; Shen, H.-H., Surface-enhanced Raman spectroscopy for DNA detection by the self-assembly of Ag nanoparticles onto Ag nanoparticle–graphene oxide nanocomposites. *Physical Chemistry Chemical Physics* **2015,** *17* (28), 18443-18448.

Lin, X.-M.; Cui, Y.; Xu, Y.-H.; Ren, B.; Tian, Z.-Q., Surface-enhanced Raman spectroscopy: substrate-related issues. *Analytical and Bioanalytical Chemistry* **2009,** *394* (7), 1729-1745.

Ling, X.; Xie, L.; Fang, Y.; Xu, H.; Zhang, H.; Kong, J.; Dresselhaus, M. S.; Zhang, J.; Liu, Z., Can Graphene be used as a Substrate for Raman Enhancement? *Nano Letters* **2010,** *10* (2), 553-561.

Ling, X.; Zhang, J., First-Layer Effect in Graphene-Enhanced Raman Scattering. *Small* **2010,** *6* (18), 2020-2025.

Link, S.; El-Sayed, M. A., Size and Temperature Dependence of the Plasmon Absorption of Colloidal Gold Nanoparticles. *The Journal of Physical Chemistry B* **1999,** *103* (21), 4212-4217.

Link, S.; Wang, Z. L.; El-Sayed, M. A., Alloy Formation of Gold−Silver Nanoparticles and the Dependence of the Plasmon Absorption on Their Composition. *The Journal of Physical Chemistry B* **1999,** *103* (18), 3529-3533.

Liou, P.; Nayigiziki, F. X.; Kong, F.; Mustapha, A.; Lin, M., Cellulose nanofibers coated with silver nanoparticles as a SERS platform for detection of pesticides in apples. *Carbohydrate Polymers* **2017,** *157*, 643-650.

Liszewska, M.; Bartosewicz, B.; Budner, B.; Nasiłowska, B.; Szala, M.; Weyher, J. L.; Dzięcielewski, I.; Mierczyk, Z.; Jankiewicz, B. J., Evaluation of selected SERS substrates for trace detection of explosive materials using portable Raman systems. *Vibrational Spectroscopy* **2019,** *100*, 79-85.

Liu, B.; Zhou, P.; Liu, X.; Sun, X.; Li, H.; Lin, M., Detection of Pesticides in Fruits by Surface-Enhanced Raman Spectroscopy Coupled with Gold Nanostructures. *Food and Bioprocess Technology* **2013,** *6* (3), 710-718.

Liu, H.; Gao, J.; Xue, M.; Zhu, N.; Zhang, M.; Cao, T., Processing of Graphene for Electrochemical Application: Noncovalently Functionalize Graphene Sheets with Water-Soluble Electroactive Methylene Green. *Langmuir* **2009,** *25* (20), 12006-12010.

Liu, H.; Xu, Y.; Qin, Y.; Sanderson, W.; Crowley, D.; Turner, C. H.; Bao, Y., Ligand-Directed Formation of Gold Tetrapod Nanostructures. *The Journal of Physical Chemistry C* **2013,** *117* (33), 17143-17150.

Lombardi, J. R.; Birke, R. L., A Unified Approach to Surface-Enhanced Raman Spectroscopy. *The Journal of Physical Chemistry C* **2008,** *112* (14), 5605-5617.

Lombardi, J. R.; Birke, R. L.; Lu, T.; Xu, J., Charge-transfer theory of surface enhanced Raman spectroscopy: Herzberg–Teller contributions. *The Journal of Chemical Physics* **1986,** *84* (8), 4174-4180.

Lovinger, A. J., Poly(Vinylidene Fluoride). In *Developments in Crystalline Polymers—1*, Bassett, D. C., Ed. Springer Netherlands: Dordrecht, 1982; pp 195-273.

Lu, C.-H.; Yang, H.-H.; Zhu, C.-L.; Chen, X.; Chen, G.-N., A Graphene Platform for Sensing Biomolecules. *Angewandte Chemie International Edition* **2009,** *48* (26), 4785-4787.

Lu, G.; Forbes, T. Z.; Haes, A. J., SERS detection of uranyl using functionalized gold nanostars promoted by nanoparticle shape and size. *Analyst* **2016,** *141* (17), 5137-5143.

Lu, G.; Johns, A. J.; Neupane, B.; Phan, H. T.; Cwiertny, D. M.; Forbes, T. Z.; Haes, A. J., Matrix-Independent Surface-Enhanced Raman Scattering Detection of Uranyl Using Electrospun Amidoximated Polyacrylonitrile Mats and Gold Nanostars. *Analytical Chemistry* **2018,** *90* (11), 6766-6772.

Lu, Z.; Zhang, L.; Deng, Y.; Li, S.; He, N., Graphene oxide for rapid microRNA detection. *Nanoscale* **2012,** *4* (19), 5840-5842.

Luo, Z.; Fang, Y., SERS of C60/C70 on gold-coated filter paper or filter film influenced by the gold thickness. *Journal of Colloid and Interface Science* **2005,** *283* (2), 459-463.

Ma, P.; Liang, F.; Yang, Q.; Wang, D.; Sun, Y.; Wang, X.; Gao, D.; Song, D., Highly sensitive SERS probe for mercury(II) using cyclodextrin-protected silver nanoparticles functionalized with methimazole. *Microchimica Acta* **2014,** *181* (9), 975-981.

Mahmoud, A. Y. F.; Rusin, C. J.; McDermott, M. T., Gold nanostars as a colloidal substrate for in-solution SERS measurements using a handheld Raman spectrometer. *Analyst* **2020,** *145* (4), 1396-1407.

Malard, L. M.; Pimenta, M. A.; Dresselhaus, G.; Dresselhaus, M. S., Raman spectroscopy in graphene. *Physics Reports* **2009,** *473* (5), 51-87.

Marcano, D. C.; Kosynkin, D. V.; Berlin, J. M.; Sinitskii, A.; Sun, Z.; Slesarev, A.; Alemany, L. B.; Lu, W.; Tour, J. M., Improved Synthesis of Graphene Oxide. *ACS Nano* **2010,** *4* (8), 4806-4814.

Marques, P. A. A. P.; Nogueira, H. I. S.; Pinto, R. J. B.; Neto, C. P.; Trindade, T., Silver-bacterial cellulosic sponges as active SERS substrates. *Journal of Raman Spectroscopy* **2008,** *39* (4), 439-443.

Martínez-Frías, M. L.; Cereijo, A.; Rodríguez-Pinilla, E.; Urioste, M., Methimazole in animal feed and congenital aplasia cutis. *The Lancet* **1992,** *339* (8795), 742-743.

Masetti, M.; Xie, H.-n.; Krpetic, Z.; Recanatini, M.; Alvarez-Puebla, R. A.; Guerrini, L., Revealing DNA Interactions with Exogenous Agents by Surface-Enhanced Raman Scattering. *J. Am. Chem. Soc.* **2015,** *137* (1), 469-476.

McCreery, R. L., Advanced Carbon Electrode Materials for Molecular Electrochemistry. *Chemical Reviews* **2008,** *108* (7), 2646-2687.

McCreery, R. L., Raman spectroscopy for chemical analysis. John Wiley & Sons: New York :, 2000.

McCreery, R. L., Raman Spectroscopy of Surfaces. In *Raman Spectroscopy for Chemical Analysis*, WINEFORDNER, J. D., Ed. Wiely: 2000; pp 373-413.

McFarland, A. D.; Young, M. A.; Dieringer, J. A.; Van Duyne, R. P., Wavelength-Scanned Surface-Enhanced Raman Excitation Spectroscopy. *The Journal of Physical Chemistry B* **2005,** *109* (22), 11279-11285.

McNay, G.; Eustace, D.; Smith, W. E.; Faulds, K.; Graham, D., Surface-Enhanced Raman Scattering (SERS) and Surface-Enhanced Resonance Raman Scattering (SERRS): A Review of Applications. *Applied Spectroscopy* **2011,** *65* (8), 825-837.

Mehn, D.; Morasso, C.; Vanna, R.; Bedoni, M.; Prosperi, D.; Gramatica, F., Immobilised gold nanostars in a paper-based test system for surface-enhanced Raman spectroscopy. *Vibrational Spectroscopy* **2013,** *68*, 45-50.

Meltzer, S.; Resch, R.; Koel, B. E.; Thompson, M. E.; Madhukar, A.; Requicha, A. A. G.; Will, P., Fabrication of Nanostructures by Hydroxylamine Seeding of Gold Nanoparticle Templates. *Langmuir* **2001,** *17* (5), 1713-1718.

Metrohm. Metrohm Raman acquires Diagnostic anSERS inc. https://www.metrohm.com/en/company/news/news-raman-sers/ (accessed 4 December 2019).

Meyer, M.; Le Ru, E. C.; Etchegoin, P. G., Self-Limiting Aggregation Leads to Long-Lived Metastable Clusters in Colloidal Solutions. *The Journal of Physical Chemistry B* **2006,** *110* (12), 6040-6047.

Mircescu, N. E.; Oltean, M.; Chiş, V.; Leopold, N., FTIR, FT-Raman, SERS and DFT study on melamine. *Vibrational Spectroscopy* **2012,** *62*, 165-171.

Misselbrook, T.; Fleming, H.; Camp, V.; Umstatter, C.; Duthie, C. A.; Nicoll, L.; Waterhouse, T., Automated monitoring of urination events from grazing cattle. *Agriculture, Ecosystems & Environment* **2016,** *230*, 191-198.

Mojica, E.-R. E.; Zapata, J.; Vedad, J.; Desamero, R. Z. B.; Dai, Z., Analysis of Over-the-Counter Drugs Using Raman Spectroscopy. In *Raman Spectroscopy in the Undergraduate Curriculum*, American Chemical Society: 2018; Vol. 1305, pp 69-91.

Montes-García, V.; Fernández-López, C.; Gómez, B.; Pérez-Juste, I.; García-Río, L.; Liz-Marzán, L. M.; Pérez-Juste, J.; Pastoriza-Santos, I., Pillar[5]arene-Mediated Synthesis of Gold Nanoparticles: Size Control and Sensing Capabilities. *Chemistry – A European Journal* **2014,** *20* (27), 8404-8409.

Moreira, L. P.; Silveira, L.; Pacheco, M. T. T.; da Silva, A. G.; Rocco, D. D. F. M., Detecting urine metabolites related to training performance in swimming athletes by means of Raman spectroscopy and principal component analysis. *Journal of Photochemistry and Photobiology B: Biology* **2018,** *185*, 223-234.

Morelli, L.; Andreasen, S. Z.; Jendresen, C. B.; Nielsen, A. T.; Emnéus, J.; Zór, K.; Boisen, A., Quantification of a bacterial secondary metabolite by SERS combined with SLM extraction for bioprocess monitoring. *Analyst* **2017,** *142* (23), 4553-4559.

Morelli, L.; Zór, K.; Jendresen, C. B.; Rindzevicius, T.; Schmidt, M. S.; Nielsen, A. T.; Boisen, A., Surface Enhanced Raman Scattering for Quantification of p-Coumaric Acid Produced by Escherichia coli. *Analytical Chemistry* **2017,** *89* (7), 3981-3987.

Morton, S. M.; Ewusi-Annan, E.; Jensen, L., Controlling the non-resonant chemical mechanism of SERS using a molecular photoswitch. *Physical Chemistry Chemical Physics* **2009,** *11* (34), 7424-7429.

Morton, S. M.; Silverstein, D. W.; Jensen, L., Theoretical Studies of Plasmonics using Electronic Structure Methods. *Chemical Reviews* **2011,** *111* (6), 3962-3994.

Mosier-Boss, P. A., Review of SERS Substrates for Chemical Sensing. *Nanomaterials* **2017,** *7* (6), 142.

Moskovits, M., Surface-enhanced Raman spectroscopy: a brief retrospective. *Journal of Raman Spectroscopy* **2005,** *36* (6-7), 485-496.

Moskovits, M., Surface-enhanced spectroscopy. *Reviews of Modern Physics* **1985,** *57* (3), 783-826.

Moskovits, M., Surface roughness and the enhanced intensity of Raman scattering by molecules adsorbed on metals. *The Journal of Chemical Physics* **1978,** *69* (9), 4159-4161.

Mulvaney, P., Surface Plasmon Spectroscopy of Nanosized Metal Particles. *Langmuir* **1996,** *12* (3), 788-800.

Muniz-Miranda, M.; Muniz-Miranda, F.; Pedone, A., Raman and DFT study of methimazole chemisorbed on gold colloidal nanoparticles. *Physical Chemistry Chemical Physics* **2016,** *18* (8), 5974-5980.

Murphy, C. J.; Gole, A. M.; Hunyadi, S. E.; Stone, J. W.; Sisco, P. N.; Alkilany, A.; Kinard, B. E.; Hankins, P., Chemical sensing and imaging with metallic nanorods. *Chemical Communications* **2008,** (5), 544-557.

Murphy, C. J.; Gole, A. M.; Stone, J. W.; Sisco, P. N.; Alkilany, A. M.; Goldsmith, E. C.; Baxter, S. C., Gold Nanoparticles in Biology: Beyond Toxicity to Cellular Imaging. *Accounts of Chemical Research* **2008,** *41* (12), 1721-1730.

Murphy, C. J.; Sau, T. K.; Gole, A. M.; Orendorff, C. J.; Gao, J.; Gou, L.; Hunyadi, S. E.; Li, T., Anisotropic Metal Nanoparticles: Synthesis, Assembly, and Optical Applications. *The Journal of Physical Chemistry B* **2005,** *109* (29), 13857-13870.

Murphy, S.; Huang, L.; Kamat, P. V., Reduced Graphene Oxide–Silver Nanoparticle Composite as an Active SERS Material. *The Journal of Physical Chemistry C* **2013,** *117* (9), 4740-4747.

Muszynski, R.; Seger, B.; Kamat, P. V., Decorating Graphene Sheets with Gold Nanoparticles. *The Journal of Physical Chemistry C* **2008,** *112* (14), 5263-5266.

Nalbant Esenturk, E.; Hight Walker, A. R., Surface-enhanced Raman scattering spectroscopy via gold nanostars. *Journal of Raman Spectroscopy* **2009,** *40* (1), 86-91.

Natan, M. J., Concluding Remarks Surface enhanced Raman scattering. *Faraday Discussions* **2006,** *132* (0), 321-328.

Nehl, C. L.; Liao, H.; Hafner, J. H., Optical Properties of Star-Shaped Gold Nanoparticles. *Nano Letters* **2006,** *6* (4), 683-688.

Nergiz, S. Z.; Gandra, N.; Singamaneni, S., Self-assembled high aspect ratio gold nanostar/graphene oxide hybrid nanorolls. *Carbon* **2014,** *66*, 585-591.

Neugebauer, U.; Szeghalmi, A.; Schmitt, M.; Kiefer, W.; Popp, J.; Holzgrabe, U., Vibrational spectroscopic characterization of fluoroquinolones. *Spectrochimica Acta Part A: Molecular and Biomolecular Spectroscopy* **2005,** *61* (7), 1505-1517.

Ngo, Y. H.; Li, D.; Simon, G. P.; Garnier, G., Gold Nanoparticle–Paper as a Three-Dimensional Surface Enhanced Raman Scattering Substrate. *Langmuir* **2012,** *28* (23), 8782-8790.

Nie, S.; Emory, S. R., Probing Single Molecules and Single Nanoparticles by Surface-Enhanced Raman Scattering. *Science* **1997,** *275* (5303), 1102-1106.

Nikoobakht, B.; El-Sayed, M. A., Preparation and Growth Mechanism of Gold Nanorods (NRs) Using Seed-Mediated Growth Method. *Chemistry of Materials* **2003,** *15* (10), 1957-1962.

Niu, Z.; Fang, Y., Surface-enhanced Raman scattering of single-walled carbon nanotubes on silver-coated and gold-coated filter paper. *Journal of Colloid and Interface Science* **2006,** *303* (1), 224-228.

Njoki, P. N.; Lim, I. I. S.; Mott, D.; Park, H.-Y.; Khan, B.; Mishra, S.; Sujakumar, R.; Luo, J.; Zhong, C.-J., Size Correlation of Optical and Spectroscopic Properties for Gold Nanoparticles. *The Journal of Physical Chemistry C* **2007,** *111* (40), 14664-14669.

Notte, J.; Ward, B.; Economou, N.; Hill, R.; Percival, R.; Farkas, L.; McVey, S., An Introduction to the Helium Ion Microscope. *AIP Conference Proceedings* **2007,** *931* (1), 489-496.

Novara, C.; Petracca, F.; Virga, A.; Rivolo, P.; Ferrero, S.; Chiolerio, A.; Geobaldo, F.; Porro, S.; Giorgis, F., SERS active silver nanoparticles synthesized by inkjet printing on mesoporous silicon. *Nanoscale Research Letters* **2014,** *9* (1), 527.

Nuntawong, N.; Eiamchai, P.; Limwichean, S.; Wong-ek, B.; Horprathum, M.; Patthanasettakul, V.; Leelapojanaporn, A.; Nakngoenthong, S.; Chindaudom, P., Trace detection of perchlorate in industrial-grade emulsion explosive with portable surface-enhanced Raman spectroscopy. *Forensic Science International* **2013,** *233* (1), 174-178.

Ocean Optics. SERS Substrates. https://oceanoptics.com/product/sers/ (accessed 21 november 2019).

Okamura, Y.; Shigemasa, C.; Tatsuhara, T., Pharmacokinetics of Methimazole in Normal Subjects and Hyperthyroid Patients. *Endocrinologia Japonica* **1986,** *33* (5), 605-615.

OndaVia. The OndaVia Story. https://www.ondavia.com/about. (accessed 4 November 2019).

OndaVia. Analysis Kits. https://www.ondavia.com/cartridges?page=1 (accessed 4 November 2019).

Otto, A., The 'chemical' (electronic) contribution to surface-enhanced Raman scattering. *Journal of Raman Spectroscopy* **2005,** *36* (6-7), 497-509.

Otto, A., Surface-enhanced Raman scattering of adsorbates. *Journal of Raman Spectroscopy* **1991,** *22* (12), 743-752.

Otto, A.; Mrozek, I.; Grabhorn, H.; Akemann, W., Surface-enhanced Raman scattering. *Journal of Physics: Condensed Matter* **1992,** *4* (5), 1143-1212.

Ouyang, L.; Hu, Y.; Zhu, L.; Cheng, G. J.; Irudayaraj, J., A reusable laser wrapped graphene-Ag array based SERS sensor for trace detection of genomic DNA methylation. *Biosensors and Bioelectronics* **2017,** *92*, 755-762.

Owens, N. A.; Laurentius, L. B.; Porter, M. D.; Li, Q.; Wang, S.; Chatterjee, D., Handheld Raman Spectrometer Instrumentation for Quantitative Tuberculosis Biomarker Detection: A Performance Assessment for Point-of-Need Infectious Disease Diagnostics. *Applied Spectroscopy* **2018,** *72* (7), 1104-1115.

Pang, S.; Yang, T.; He, L., Review of surface enhanced Raman spectroscopic (SERS) detection of synthetic chemical pesticides. *TrAC Trends in Analytical Chemistry* **2016,** *85*, 73-82.

Panneerselvam, R.; Liu, G.-K.; Wang, Y.-H.; Liu, J.-Y.; Ding, S.-Y.; Li, J.-F.; Wu, D.-Y.; Tian, Z.-Q., Surface-enhanced Raman spectroscopy: bottlenecks and future directions. *Chemical Communications* **2018,** *54* (1), 10-25.

Papadopoulou, E.; Bell, S. E. J., Label-Free Detection of Single-Base Mismatches in DNA by Surface-Enhanced Raman Spectroscopy. *Angewandte Chemie* **2011,** *123* (39), 9224-9227.

Park, J. S.; Na, H.-K.; Min, D.-H.; Kim, D.-E., Desorption of single-stranded nucleic acids from graphene oxide by disruption of hydrogen bonding. *Analyst* **2013,** *138* (6), 1745-1749.

Pelaz, B.; Grazu, V.; Ibarra, A.; Magen, C.; del Pino, P.; de la Fuente, J. M., Tailoring the Synthesis and Heating Ability of Gold Nanoprisms for Bioapplications. *Langmuir* **2012,** *28* (24), 8965-8970.

Perney, N. M. B.; Baumberg, J. J.; Zoorob, M. E.; Charlton, M. D. B.; Mahnkopf, S.; Netti, C. M., Tuning localized plasmons in nanostructured substrates for surface-enhanced Raman scattering. *Opt. Express* **2006,** *14* (2), 847-857.

Pilot, R.; Signorini, R.; Durante, C.; Orian, L.; Bhamidipati, M.; Fabris, L., A Review on Surface-Enhanced Raman Scattering. *Biosensors (Basel)* **2019,** *9* (2), 57.

PITTMAN, J. A.; BESCHI, R. J.; SMITHERMAN, T. C., Methimazole: Its Absorption and Excretion in Man and Tissue Distribution in Rats. *The Journal of Clinical Endocrinology & Metabolism* **1971,** *33* (2), 182-185.

Polavarapu, L.; Porta, A. L.; Novikov, S. M.; Coronado-Puchau, M.; Liz-Marzán, L. M., Pen-on-Paper Approach Toward the Design of Universal Surface Enhanced Raman Scattering Substrates. *Small* **2014,** *10* (15), 3065-3071.

Porter, M. D.; Bright, T. B.; Allara, D. L.; Chidsey, C. E. D., Spontaneously organized molecular assemblies. 4. Structural characterization of n-alkyl thiol monolayers on gold by optical ellipsometry, infrared spectroscopy, and electrochemistry. *Journal of the American Chemical Society* **1987,** *109* (12), 3559-3568.

Premasiri, W. R.; Clarke, R. H.; Womble, M. E., Urine analysis by laser Raman spectroscopy. *Lasers in Surgery and Medicine* **2001,** *28* (4), 330-334.

Prikhozhdenko, E. S.; Bratashov, D. N.; Gorin, D. A.; Yashchenok, A. M., Flexible surface-enhanced Raman scattering-active substrates based on nanofibrous membranes. *Nano Research* **2018,** *11* (9), 4468-4488.

Pristinski, D.; Tan, S. L.; Erol, M.; Du, H.; Sukhishvili, S., In situ SERS study of Rhodamine 6G adsorbed on individually immobilized Ag nanoparticles. *Journal of Raman Spectroscopy* **2006,** *37* (7), 762-770.

Qian, X. M.; Nie, S. M., Single-molecule and single-nanoparticle SERS: from fundamental mechanisms to biomedical applications. *Chemical Society Reviews* **2008,** *37* (5), 912-920.

Q-SERS. http://www.q-sers.com/q.html (accessed 4 December 2019).

Qu, L.-L.; Li, D.-W.; Xue, J.-Q.; Zhai, W.-L.; Fossey, J. S.; Long, Y.-T., Batch fabrication of disposable screen printed SERS arrays. *Lab on a Chip* **2012,** *12* (5), 876-881.

Qu, L.-L.; Song, Q.-X.; Li, Y.-T.; Peng, M.-P.; Li, D.-W.; Chen, L.-X.; Fossey, J. S.; Long, Y.-T., Fabrication of bimetallic microfluidic surface-enhanced Raman scattering sensors on paper by screen printing. *Analytica Chimica Acta* **2013,** *792*, 86-92.

Rabuni, M. F.; Nik Sulaiman, N. M.; Aroua, M. K.; Hashim, N. A., Effects of Alkaline Environments at Mild Conditions on the Stability of PVDF Membrane: An Experimental Study. *Industrial & Engineering Chemistry Research* **2013,** *52* (45), 15874-15882.

Raman, C. V.; Krishnan, K. S., A New Type of Secondary Radiation. *Nature* **1928,** *121* (3048), 501-502.

Rao, C. N. R.; Sood, A. K.; Subrahmanyam, K. S.; Govindaraj, A., Graphene: The New Two-Dimensional Nanomaterial. *Angewandte Chemie International Edition* **2009,** *48* (42), 7752-7777.

Ray, K.; McCreery, R. L., Spatially Resolved Raman Spectroscopy of Carbon Electrode Surfaces: Observations of Structural and Chemical Heterogeneity. *Analytical Chemistry* **1997,** *69* (22), 4680-4687.

Real Time Analyzers. SERS Products. http://www.rta.biz/products/sers-products/ (accessed 21 November 2019).

Renishaw. EU project delivers new possibilities for SERS sensors. https://www.renishaw.com/en/eu-project-delivers-new-possibilities-for-sers-sensors--24460 (accessed 2 December 2019).

Restaino, S. M.; White, I. M., A critical review of flexible and porous SERS sensors for analytical chemistry at the point-of-sample. *Analytica Chimica Acta* **2019,** *1060*, 17-29.

Rodríguez-Lorenzo, L.; Álvarez-Puebla, R. A.; Pastoriza-Santos, I.; Mazzucco, S.; Stéphan, O.; Kociak, M.; Liz-Marzán, L. M.; García de Abajo, F. J., Zeptomol Detection Through Controlled Ultrasensitive Surface-Enhanced Raman Scattering. *Journal of the American Chemical Society* **2009,** *131* (13), 4616-4618.

Ross, M. B.; Ashley, M. J.; Schmucker, A. L.; Singamaneni, S.; Naik, R. R.; Schatz, G. C.; Mirkin, C. A., Structure-Function Relationships for Surface-Enhanced Raman Spectroscopy-Active Plasmonic Paper. *J. Phys. Chem. C* **2016,** *120* (37), 20789-20797.

Ross, M. B.; Ashley, M. J.; Schmucker, A. L.; Singamaneni, S.; Naik, R. R.; Schatz, G. C.; Mirkin, C. A., Structure–Function Relationships for Surface-Enhanced Raman Spectroscopy-Active Plasmonic Paper. *The Journal of Physical Chemistry C* **2016,** *120* (37), 20789-20797.

Rycenga, M.; Langille, M. R.; Personick, M. L.; Ozel, T.; Mirkin, C. A., Chemically Isolating Hot Spots on Concave Nanocubes. *Nano Letters* **2012,** *12* (12), 6218-6222.

Ryoo, S.-R.; Lee, J.; Yeo, J.; Na, H.-K.; Kim, Y.-K.; Jang, H.; Lee, J. H.; Han, S. W.; Lee, Y.; Kim, V. N.; Min, D.-H., Quantitative and Multiplexed MicroRNA Sensing in Living Cells Based on Peptide Nucleic Acid and Nano Graphene Oxide (PANGO). *ACS Nano* **2013,** *7* (7), 5882-5891.

Sadik, O. A.; Land Jr., W. H.; Wang, J., Targeting Chemical and Biological Warfare Agents at the Molecular Level. *Electroanalysis* **2003,** *15* (14), 1149-1159.

Saha, K.; Agasti, S. S.; Kim, C.; Li, X.; Rotello, V. M., Gold Nanoparticles in Chemical and Biological Sensing. *Chemical Reviews* **2012,** *112* (5), 2739-2779.

Saleh, T. A.; Al-Shalalfeh, M. M.; Al-Saadi, A. A., Graphene Dendrimer-stabilized silver nanoparticles for detection of methimazole using Surface-enhanced Raman scattering with computational assignment. *Scientific Reports* **2016,** *6*, 32185.

Saleh, T. A.; Al-Shalalfeh, M. M.; Al-Saadi, A. A., Silver nanoparticles for detection of methimazole by surface-enhanced Raman spectroscopy. *Materials Research Bulletin* **2017,** *91*, 173-178.

Saleh, T. A.; Al-Shalalfeh, M. M.; Onawole, A. T.; Al-Saadi, A. A., Ultra-trace detection of methimazole by surface-enhanced Raman spectroscopy using gold substrate. *Vibrational Spectroscopy* **2017,** *90*, 96-103.

Sánchez-Purrà, M.; Carré-Camps, M.; de Puig, H.; Bosch, I.; Gehrke, L.; Hamad-Schifferli, K., Surface-Enhanced Raman Spectroscopy-Based Sandwich Immunoassays for Multiplexed Detection of Zika and Dengue Viral Biomarkers. *ACS Infectious Diseases* **2017,** *3* (10), 767-776.

Sánchez-Purrà, M.; Roig-Solvas, B.; Rodriguez-Quijada, C.; Leonardo, B. M.; Hamad-Schifferli, K., Reporter Selection for Nanotags in Multiplexed Surface Enhanced Raman Spectroscopy Assays. *ACS Omega* **2018,** *3* (9), 10733-10742.

Saracut, V.; Giloan, M.; Gabor, M.; Astilean, S.; Farcau, C., Polarization-Sensitive Linear Plasmonic Nanostructures via Colloidal Lithography with Uniaxial Colloidal Arrays. *ACS Applied Materials & Interfaces* **2013,** *5* (4), 1362-1369.

Sarfo, D. K.; Izake, E. L.; O'Mullane, A. P.; Ayoko, G. A., Molecular recognition and detection of Pb(II) ions in water by aminobenzo-18-crown-6 immobilised onto a nanostructured SERS substrate. *Sensors and Actuators B: Chemical* **2018,** *255*, 1945-1952.

Satou, T.; Koga, M.; Koike, K.; Tada, I.; Nikaido, T., Nematocidal activities of thiabendazole and ivermectin against the larvae of Strongyloides ratti and S. venezuelensis. *Veterinary Parasitology* **2001,** *99* (4), 311-322.

Sau, T. K.; Murphy, C. J., Room Temperature, High-Yield Synthesis of Multiple Shapes of Gold Nanoparticles in Aqueous Solution. *Journal of the American Chemical Society* **2004,** *126* (28), 8648-8649.

Saviello, D.; Di Gioia, A.; Turenne, P.-I.; Trabace, M.; Giorgi, R.; Mirabile, A.; Baglioni, P.; Iacopino, D., Handheld surface-enhanced Raman scattering identification of dye chemical composition in felt-tip pen drawings. *Journal of Raman Spectroscopy* **2019,** *50* (2), 222-231.

Schlücker, S., Surface-Enhanced Raman Spectroscopy: Concepts and Chemical Applications. *Angewandte Chemie International Edition* **2014,** *53* (19), 4756-4795.

Schmidt, M. S.; Hübner, J.; Boisen, A., Large Area Fabrication of Leaning Silicon Nanopillars for Surface Enhanced Raman Spectroscopy. *Advanced Materials* **2012,** *24* (10), OP11-OP18.

Schmucker, A. L.; Tadepalli, S.; Liu, K.-K.; Sullivan, C. J.; Singamaneni, S.; Naik, R. R., Plasmonic paper: a porous and flexible substrate enabling nanoparticle-based combinatorial chemistry. *RSC Advances* **2016,** *6* (5), 4136-4144.

Seney, C. S.; Gutzman, B. M.; Goddard, R. H., Correlation of Size and Surface-Enhanced Raman Scattering Activity of Optical and Spectroscopic Properties for Silver Nanoparticles. *The Journal of Physical Chemistry C* **2009,** *113* (1), 74-80.

Senthil Kumar, P.; Pastoriza-Santos, I.; Rodríguez-González, B.; Javier García de Abajo, F.; Liz-Marzán, L. M., High-yield synthesis and optical response of gold nanostars. *Nanotechnology* **2007,** *19* (1), 015606.

Sequaris, J. M. L.; Koglin, E., Direct analysis of high-performance thin-layer chromatography spots of nucleic purine derivatives by surface-enhanced Raman scattering spectrometry. *Analytical Chemistry* **1987,** *59* (3), 525-527.

SERSitive. Products. https://www.sersitive.eu/ (accessed 4 December 2019).

Setti, G. O.; Mamián-López, M. B.; Pessoa, P. R.; Poppi, R. J.; Joanni, E.; Jesus, D. P., Sputtered gold-coated ITO nanowires by alternating depositions from Indium and ITO targets for application in surface-enhanced Raman scattering. *Applied Surface Science* **2015,** *347*, 17-22.

Shao, J.; Tong, L.; Tang, S.; Guo, Z.; Zhang, H.; Li, P.; Wang, H.; Du, C.; Yu, X.-F., PLLA Nanofibrous Paper-Based Plasmonic Substrate with Tailored Hydrophilicity for Focusing SERS Detection. *ACS Applied Materials & Interfaces* **2015,** *7* (9), 5391-5399.

Sharaabi, Y.; Shegai, T.; Haran, G., Two-state analysis of single-molecule Raman spectra of crystal violet. *Chemical Physics* **2005,** *318* (1), 44-49.

Sharma, B.; Frontiera, R. R.; Henry, A.-I.; Ringe, E.; Van Duyne, R. P., SERS: Materials, applications, and the future. *Materials Today* **2012,** *15* (1), 16-25.

Shi, R.; Liu, X.; Ying, Y., Facing Challenges in Real-Life Application of Surface-Enhanced Raman Scattering: Design and Nanofabrication of Surface-Enhanced Raman Scattering Substrates for Rapid Field Test of Food Contaminants. *Journal of Agricultural and Food Chemistry* **2018,** *66* (26), 6525-6543.

SILMECO. SERS Substrates. https://shop.silmeco.com/?wmc-currency=USD (accessed 4 December 2019).

SILMECO. SILMECO SERS Substrates. http://www.silmeco.com/media/12317/silmeco-sers-substrates-serstrate-product-sheet.pdf (accessed 4 December 2019 ).

Sitar, D. S.; Thornhill, D. P., Methimazole: Absorption, Metabolism and Excretion in the Albino Rat. *Journal of Pharmacology and Experimental Therapeutics* **1973,** *184* (2), 432-439.

Sivapalan, S. T.; DeVetter, B. M.; Yang, T. K.; van Dijk, T.; Schulmerich, M. V.; Carney, P. S.; Bhargava, R.; Murphy, C. J., Off-Resonance Surface-Enhanced Raman Spectroscopy from Gold Nanorod Suspensions as a Function of Aspect Ratio: Not What We Thought. *ACS Nano* **2013,** *7* (3), 2099-2105.

Skadtchenko, B. O.; Aroca, R., Surface-enhanced Raman scattering of p-nitrothiophenol: Molecular vibrations of its silver salt and the surface complex formed on silver islands and colloids. *Spectrochimica Acta Part A: Molecular and Biomolecular Spectroscopy* **2001,** *57* (5), 1009-1016.

Skellern, G.; Knight, B.; Low, C.; Alexander, W.; McLarty, D.; Kalk, W., The pharmacokinetics of methimazole after oral administration of carbimazole and methimazole, in hyperthyroid patients. *British Journal of Clinical Pharmacology* **1980,** *9* (2), 137-143.

Skrabalak, S. E.; Au, L.; Li, X.; Xia, Y., Facile synthesis of Ag nanocubes and Au nanocages. *Nature Protocols* **2007,** *2*, 2182.

Song, S.; Qin, Y.; He, Y.; Huang, Q.; Fan, C.; Chen, H.-Y., Functional nanoprobes for ultrasensitive detection of biomolecules. *Chemical Society Reviews* **2010,** *39* (11), 4234-4243.

Srivastava, S.; Sinha, R.; Roy, D., Toxicological effects of malachite green. *Aquatic Toxicology* **2004,** *66* (3), 319-329.

Srnová-Šloufová, I.; Vlčková, B.; Snoeck, T. L.; Stufkens, D. J.; Matějka, P., Surface-Enhanced Raman Scattering and Surface-Enhanced Resonance Raman Scattering Excitation Profiles of Ag-2,2'-Bipyridine Surface Complexes and of [Ru(bpy)3]2+ on Ag Colloidal Surfaces: Manifestations of the Charge-Transfer Resonance Contributions to the Overall Surface Enhancement of Raman Scattering. *Inorganic Chemistry* **2000,** *39* (16), 3551-3559.

StellarNet. SERS Substrate Strips. https://www.stellarnet.us/spectrometers-accessories/sers-substrates/ (accessed 25 November 2019).

Stiles, P. L.; Dieringer, J. A.; Shah, N. C.; Duyne, R. P. V., Surface-Enhanced Raman Spectroscopy. *Annual Review of Analytical Chemistry* **2008,** *1* (1), 601-626.

S.T.Japan. Raman SERS Substrate. https://www.stjapan.de/en/shop/accessories-for-spectroscopy-microanalysis/raman-sers-substrate/ (accessed 1 December 2019).

Sudova, E.; Machova, J.; Svobodova, Z.; Vesely, T., Negative effects of malachite green and possibilities of its replacement in the treatment of fish eggs and fish: a review. *Vet. Med.* **2007,** *52* (12), 527-539.

Tahir, M. A.; Zhang, X.; Cheng, H.; Xu, D.; Feng, Y.; Sui, G.; Fu, H.; Valev, V. K.; Zhang, L.; Chen, J., Klarite as a label-free SERS-based assay: a promising approach for atmospheric bioaerosol detection. *Analyst* **2020**.

Tan, C.; Zhang, Z.; Qu, Y.; He, L., Ag2O/TiO2 Nanocomposite Heterostructure as a Dual Functional Semiconducting Substrate for SERS/SEIRAS Application. *Langmuir* **2017,** *33* (22), 5345-5352.

Tantra, R.; Brown, R. J. C.; Milton, M. J. T., Strategy to improve the reproducibility of colloidal SERS. *Journal of Raman Spectroscopy* **2007,** *38* (11), 1469-1479.

Tasi, T.-T.; Lin, T.-W.; Shao, L.-D.; Shen, H.-H., Reversible coupling of 4-nitroaniline molecules to 4-aminothiophenol functionalized on Ag nanoparticle/graphene oxide nanocomposites through the plasmon assisted chemical reaction. *RSC Advances* **2016,** *6* (35), 29453-29459.

Tian, F.; Bonnier, F.; Casey, A.; Shanahan, A. E.; Byrne, H. J., Surface enhanced Raman scattering with gold nanoparticles: effect of particle shape. *Analytical Methods* **2014,** *6* (22), 9116-9123.

Tian, F.; Lyu, J.; Shi, J.; Yang, M., Graphene and graphene-like two-denominational materials based fluorescence resonance energy transfer (FRET) assays for biological applications. *Biosensors and Bioelectronics* **2017,** *89*, 123-135.

Tian, L.; Tadepalli, S.; Farrell, M. E.; Liu, K.-K.; Gandra, N.; Pellegrino, P. M.; Singamaneni, S., Multiplexed charge-selective surface enhanced Raman scattering based on plasmonic calligraphy. *Journal of Materials Chemistry C* **2014,** *2* (27), 5438-5446.

Tölgyesi, Á.; Giri, A.; Barta, E.; McDonald, T. J.; Sharma, V. K., Determination of Thyreostats in Urine Using Supported Liquid Extraction and Mixed-Mode Cation-Exchange Solid-Phase Extraction: Screening and Confirmatory Methods. *Journal of Chromatographic Science* **2018,** *56* (9), 858-866.

Treossi, E.; Melucci, M.; Liscio, A.; Gazzano, M.; Samorì, P.; Palermo, V., High-Contrast Visualization of Graphene Oxide on Dye-Sensitized Glass, Quartz, and Silicon by Fluorescence Quenching. *Journal of the American Chemical Society* **2009,** *131* (43), 15576-15577.

Turkevich, J.; Stevenson, P. C.; Hillier, J., The Formation of Colloidal Gold. *The Journal of Physical Chemistry* **1953,** *57* (7), 670-673.

USDA, Pesticide Data Program Annual Summary, Calendar Year 2017. United States Department of Agriculture: 2017.

USEPA, EPA reregistration eligibility decision thabendazole. United States Environmental Protection Agency: 2002.

Valley, N.; Greeneltch, N.; Van Duyne, R. P.; Schatz, G. C., A Look at the Origin and Magnitude of the Chemical Contribution to the Enhancement Mechanism of Surface-Enhanced Raman Spectroscopy (SERS): Theory and Experiment. *The Journal of Physical Chemistry Letters* **2013,** *4* (16), 2599-2604.

van Lierop, D.; Krpetic, Z.; Guerrini, L.; Larmour, I. A.; Dougan, J. A.; Faulds, K.; Graham, D., Positively charged silver nanoparticles and their effect on surface-enhanced Raman scattering of dye-labelled oligonucleotides. *Chem. Commun. (Cambridge, U. K.)* **2012,** *48* (66), 8192-8194.

van Lierop, D.; Larmour, I. A.; Faulds, K.; Graham, D., SERS primers and their mode of action for pathogen DNA detection. *Anal. Chem. (Washington, DC, U. S.)* **2013,** *85* (3), 1408-1414.

Vander Ende, E.; Bourgeois, M. R.; Henry, A.-I.; Chávez, J. L.; Krabacher, R.; Schatz, G. C.; Van Duyne, R. P., Physicochemical Trapping of Neurotransmitters in Polymer-Mediated Gold Nanoparticle Aggregates for Surface-Enhanced Raman Spectroscopy. *Analytical Chemistry* **2019,** *91* (15), 9554-9562.

Varghese, N.; Mogera, U.; Govindaraj, A.; Das, A.; Maiti, P. K.; Sood, A. K.; Rao, C. N. R., Binding of DNA Nucleobases and Nucleosides with Graphene. *ChemPhysChem* **2009,** *10* (1), 206-210.

Vidano, R. P.; Fischbach, D. B.; Willis, L. J.; Loehr, T. M., Observation of Raman band shifting with excitation wavelength for carbons and graphites. *Solid State Communications* **1981,** *39* (2), 341-344.

Villarreal, E.; Li, G. G.; Zhang, Q.; Fu, X.; Wang, H., Nanoscale Surface Curvature Effects on Ligand–Nanoparticle Interactions: A Plasmon-Enhanced Spectroscopic Study of Thiolated Ligand Adsorption, Desorption, and Exchange on Gold Nanoparticles. *Nano Letters* **2017,** *17* (7), 4443-4452.

Viscarra Rossel, R. A.; McGlynn, R. N.; McBratney, A. B., Determining the composition of mineral-organic mixes using UV–vis–NIR diffuse reflectance spectroscopy. *Geoderma* **2006,** *137* (1), 70-82.

Vo-Dinh, T.; Hiromoto, M. Y. K.; Begun, G. M.; Moody, R. L., Surface-enhanced Raman spectrometry for trace organic analysis. *Analytical Chemistry* **1984,** *56* (9), 1667-1670.

Vo-Dinh, T.; Uziel, M.; Morrison, A. L., Surface-Enhanced Raman Analysis of Benzo[A]Pyrene-DNA Adducts on Silver-Coated Cellulose Substrates. *Applied Spectroscopy* **1987,** *41* (4), 605-610.

Wang, H.; Zhang, Q.; Chu, X.; Chen, T.; Ge, J.; Yu, R., Graphene Oxide–Peptide Conjugate as an Intracellular Protease Sensor for Caspase-3 Activation Imaging in Live Cells. *Angewandte Chemie International Edition* **2011,** *50* (31), 7065-7069.

Wang, Y.; Alsmeyer, D. C.; McCreery, R. L., Raman spectroscopy of carbon materials: structural basis of observed spectra. *Chemistry of Materials* **1990,** *2* (5), 557-563.

Wang, Y.; Camargo, P. H. C.; Skrabalak, S. E.; Gu, H.; Xia, Y., A Facile, Water-Based Synthesis of Highly Branched Nanostructures of Silver. *Langmuir* **2008,** *24* (20), 12042-12046.

Wang, Y.; Li, Z.; Hu, D.; Lin, C.-T.; Li, J.; Lin, Y., Aptamer/Graphene Oxide Nanocomplex for in Situ Molecular Probing in Living Cells. *Journal of the American Chemical Society* **2010,** *132* (27), 9274-9276.

Wang, Y.; Li, Z.; Weber, T. J.; Hu, D.; Lin, C.-T.; Li, J.; Lin, Y., In Situ Live Cell Sensing of Multiple Nucleotides Exploiting DNA/RNA Aptamers and Graphene Oxide Nanosheets. *Analytical Chemistry* **2013,** *85* (14), 6775-6782.

Wang, Y.; Tang, L.; Li, Z.; Lin, Y.; Li, J., In situ simultaneous monitoring of ATP and GTP using a graphene oxide nanosheet–based sensing platform in living cells. *Nature Protocols* **2014,** *9*, 1944.

Wang, Z.; Luo, H.; Tu, W.; Yang, H.; Wong, W. H.-S.; Wong, W.-T.; Yung, K.-F.; Zhou, N.; Zhang, J.; Li, X.; Wang, Z.; Guo, W.; Mu, D.; Li, F.; Mao, M.; Lau, Y.-L., Melamine-tainted milk product-associated urinary stones in children. *Pediatrics International* **2011,** *53* (4), 489-496.

Wang, Z.; Zong, S.; Wu, L.; Zhu, D.; Cui, Y., SERS-Activated Platforms for Immunoassay: Probes, Encoding Methods, and Applications. *Chemical Reviews* **2017,** *117* (12), 7910-7963.

Webb, J. A.; Erwin, W. R.; Zarick, H. F.; Aufrecht, J.; Manning, H. W.; Lang, M. J.; Pint, C. L.; Bardhan, R., Geometry-Dependent Plasmonic Tunability and Photothermal Characteristics of Multibranched Gold Nanoantennas. *The Journal of Physical Chemistry C* **2014,** *118* (7), 3696-3707.

Wen, Y.; Xing, F.; He, S.; Song, S.; Wang, L.; Long, Y.; Li, D.; Fan, C., A graphene-based fluorescent nanoprobe for silver(i) ions detection by using graphene oxide and a silver-specific oligonucleotide. *Chemical Communications* **2010,** *46* (15), 2596-2598.

White, I. M., Optofluidic SERS on inkjet-fabricated paper-based substrates. *Proc. SPIE* **2012,** *8264* (Integrated Optics: Devices, Materials, and Technologies XVI), 826414/1-826414/6.

Witkowska, E.; Jagielski, T.; Kamińska, A.; Kowalska, A.; Hryncewicz-Gwóźdź, A.; Waluk, J., Detection and identification of human fungal pathogens using surface-enhanced Raman spectroscopy and principal component analysis. *Analytical Methods* **2016,** *8* (48), 8427-8434.

Witkowska, E.; Korsak, D.; Kowalska, A.; Księżopolska-Gocalska, M.; Niedziółka-Jönsson, J.; Roźniecka, E.; Michałowicz, W.; Albrycht, P.; Podrażka, M.; Hołyst, R.; Waluk, J.; Kamińska, A., Surface-enhanced Raman spectroscopy introduced into the International Standard Organization (ISO) regulations as an alternative method for detection and identification of pathogens in the food industry. *Analytical and Bioanalytical Chemistry* **2017,** *409* (6), 1555-1567.

Wojcik, A.; Kamat, P. V., Reduced Graphene Oxide and Porphyrin. An Interactive Affair in 2-D. *ACS Nano* **2010,** *4* (11), 6697-6706.

Wong, C. L.; Dinish, U. S.; Schmidt, M. S.; Olivo, M., Non-labeling multiplex surface enhanced Raman scattering (SERS) detection of volatile organic compounds (VOCs). *Analytica Chimica Acta* **2014,** *844*, 54-60.

Wu, C.-Y.; Lo, W.-Y.; Chiu, C.-R.; Yang, T.-S., Surface enhanced Raman spectra of oligonucleotides induced by spermine. *J. Raman Spectrosc.* **2006,** *37* (8), 799-807.

Wu, D.; Fang, Y., The adsorption behavior of p-hydroxybenzoic acid on a silver-coated filter paper by surface enhanced Raman scattering. *Journal of Colloid and Interface Science* **2003,** *265* (2), 234-238.

Wu, M.; Kempaiah, R.; Huang, P.-J. J.; Maheshwari, V.; Liu, J., Adsorption and Desorption of DNA on Graphene Oxide Studied by Fluorescently Labeled Oligonucleotides. *Langmuir* **2011,** *27* (6), 2731-2738.

Wu, X.; Xu, C.; Tripp, R. A.; Huang, Y.-w.; Zhao, Y., Detection and differentiation of foodborne pathogenic bacteria in mung bean sprouts using field deployable label-free SERS devices. *Analyst* **2013,** *138* (10), 3005-3012.

Wu, Y.; Xiao, F.; Wu, Z.; Yu, R., Novel Aptasensor Platform Based on Ratiometric Surface-Enhanced Raman Spectroscopy. *Analytical Chemistry* **2017,** *89* (5), 2852-2858.

Xi, W.; Haes, A. J., Elucidation of HEPES Affinity to and Structure on Gold Nanostars. *Journal of the American Chemical Society* **2019,** *141* (9), 4034-4042.

Xia, L.; Chen, M.; Zhao, X.; Zhang, Z.; Xia, J.; Xu, H.; Sun, M., Visualized method of chemical enhancement mechanism on SERS and TERS. *Journal of Raman Spectroscopy* **2014,** *45* (7), 533-540.

Xie, F.; Drozdowicz-Tomsia, K.; Goldys, E. M., A method to assess modifications of fluorophore radiative rate by plasmonic structures. *Chemical Physics Letters* **2008,** *466* (4), 186-188.

Xie, J.; Lee, J. Y.; Wang, D. I. C., Seedless, Surfactantless, High-Yield Synthesis of Branched Gold Nanocrystals in HEPES Buffer Solution. *Chemistry of Materials* **2007,** *19* (11), 2823-2830.

Xie, L.; Ling, X.; Fang, Y.; Zhang, J.; Liu, Z., Graphene as a Substrate To Suppress Fluorescence in Resonance Raman Spectroscopy. *Journal of the American Chemical Society* **2009,** *131* (29), 9890-9891.

Xie, Y.; Wang, X.; Han, X.; Xue, X.; Ji, W.; Qi, Z.; Liu, J.; Zhao, B.; Ozaki, Y., Sensing of polycyclic aromatic hydrocarbons with cyclodextrin inclusion complexes on silver nanoparticles by surface-enhanced Raman scattering. *Analyst* **2010,** *135* (6), 1389-1394.

Xu, Y.; Bai, H.; Lu, G.; Li, C.; Shi, G., Flexible Graphene Films via the Filtration of Water-Soluble Noncovalent Functionalized Graphene Sheets. *Journal of the American Chemical Society* **2008,** *130* (18), 5856-5857.

Yaffe, N. R.; Ingram, A.; Graham, D.; Blanch, E. W., A multi-component optimisation of experimental parameters for maximising SERS enhancements. *Journal of Raman Spectroscopy* **2010,** *41* (6), 618-623.

Yaghobian, F.; Korn, T.; Schüller, C., Frequency Shift in Graphene-Enhanced Raman Signal of Molecules. *ChemPhysChem* **2012,** *13* (18), 4271-4275.

Yang, J.; Cui, Y.; Zong, S.; Zhang, R.; Song, C.; Wang, Z., Tracking Multiplex Drugs and Their Dynamics in Living Cells Using the Label-Free Surface-Enhanced Raman Scattering Technique. *Molecular Pharmaceutics* **2012,** *9* (4), 842-849.

Yang, L.; Chen, Y.; Shen, Y.; Yang, M.; Li, X.; Han, X.; Jiang, X.; Zhao, B., SERS strategy based on the modified Au nanoparticles for highly sensitive detection of bisphenol A residues in milk. *Talanta* **2018,** *179*, 37-42.

Yang, L.; Qin, X.; Jiang, X.; Gong, M.; Yin, D.; Zhang, Y.; Zhao, B., SERS investigation of ciprofloxacin drug molecules on TiO2 nanoparticles. *Physical Chemistry Chemical Physics* **2015,** *17* (27), 17809-17815.

Yang, W.; Li, Z.; Lu, Z.; Yu, J.; Huo, Y.; Man, B.; Pan, J.; Si, H.; Jiang, S.; Zhang, C., Graphene-Ag nanoparticles-cicada wings hybrid system for obvious SERS performance and DNA molecular detection. *Opt. Express* **2019,** *27* (3), 3000-3013.

Yared, I.; Wang, S.; Wang, M., Effects of Oxygen Plasma and Dopamine Coating on Poly(Vinylidene Fluoride) Microfiltration Membrane for the Resistance to Protein Fouling. *IEEE Transactions on Plasma Science* **2014,** *42* (12), 3847-3857.

Ye, Q.; Fang, J.; Sun, L., Surface-Enhanced Raman Scattering from Functionalized Self-Assembled Monolayers. 2. Distance Dependence of Enhanced Raman Scattering from an Azobenzene Terminal Group. *The Journal of Physical Chemistry B* **1997,** *101* (41), 8221-8224.

Yeow, M. L.; Liu, Y. T.; Li, K., Isothermal phase diagrams and phase-inversion behavior of poly(vinylidene fluoride)/solvents/additives/water systems. *Journal of Applied Polymer Science* **2003,** *90* (8), 2150-2155.

Yi, J. W.; Park, J.; Singh, N. J.; Lee, I. J.; Kim, K. S.; Kim, B. H., Quencher-free molecular beacon: Enhancement of the signal-to-background ratio with graphene oxide. *Bioorganic & Medicinal Chemistry Letters* **2011,** *21* (2), 704-706.

Yu, W. W.; White, I. M., Chromatographic separation and detection of target analytes from complex samples using inkjet printed SERS substrates. *Analyst (Cambridge, U. K.)* **2013,** *138* (13), 3679-3686.

Yu, W. W.; White, I. M., Inkjet-printed paper-based SERS dipsticks and swabs for trace chemical detection. *Analyst* **2013,** *138* (4), 1020-1025.

Yu, W. W.; White, I. M., Inkjet Printed Surface Enhanced Raman Spectroscopy Array on Cellulose Paper. *Analytical Chemistry* **2010,** *82* (23), 9626-9630.

Yu, W. W.; White, I. M., Paper-based optofluidic SERS using ink-jet-printed substrates. *Proc. SPIE* **2011,** *7911* (Plasmonics in Biology and Medicine VIII), 791105/1-791105/6.

Yu, W. W.; White, I. M., A simple filter-based approach to surface enhanced Raman spectroscopy for trace chemical detection. *Analyst* **2012,** *137* (5), 1168-1173.

Yu, X.; Cai, H.; Zhang, W.; Li, X.; Pan, N.; Luo, Y.; Wang, X.; Hou, J. G., Tuning Chemical Enhancement of SERS by Controlling the Chemical Reduction of Graphene Oxide Nanosheets. *ACS Nano* **2011,** *5* (2), 952-958.

Yuan, H.; Khoury, C. G.; Hwang, H.; Wilson, C. M.; Grant, G. A.; Vo-Dinh, T., Gold nanostars: surfactant-free synthesis, 3D modelling, and two-photon photoluminescence imaging. *Nanotechnology* **2012,** *23* (7), 075102.

Yuan, L.; Lu, S.; Yang, F.; Wang, Y.; Jia, Y.; Kadhim, M. S.; Yu, Y.; Zhang, Y.; Zhao, Y., A facile room-temperature synthesis of three-dimensional coral-like Ag2S nanostructure with enhanced photocatalytic activity. *Journal of Materials Science* **2019,** *54* (4), 3174-3186.

Zakrzewski, R., Determination of methimazole in urine with the iodine-azide detection system following its separation by reversed-phase high-performance liquid chromatography. *Journal of Chromatography B* **2008,** *869* (1), 67-74.

Zeng, F.; Duan, W.; Zhu, B.; Mu, T.; Zhu, L.; Guo, J.; Ma, X., Paper-Based Versatile Surface-Enhanced Raman Spectroscopy Chip with Smartphone-Based Raman Analyzer for Point-of-Care Application. *Analytical Chemistry* **2019,** *91* (1), 1064-1070.

Zeng, F.; Mou, T.; Zhang, C.; Huang, X.; Wang, B.; Ma, X.; Guo, J., Paper-based SERS analysis with smartphones as Raman spectral analyzers. *Analyst* **2019,** *144* (1), 137-142.

Zhang, W.; Li, B.; Chen, L.; Wang, Y.; Gao, D.; Ma, X.; Wu, A., Brushing, a simple way to fabricate SERS active paper substrates. *Analytical Methods* **2014,** *6* (7), 2066-2071.

Zhang, Y.; Huang, Y.; Zhai, F.; Du, R.; Liu, Y.; Lai, K., Analyses of enrofloxacin, furazolidone and malachite green in fish products with surface-enhanced Raman spectroscopy. *Food Chemistry* **2012,** *135* (2), 845-850.

Zhang, Y.; Lai, K.; Zhou, J.; Wang, X.; Rasco, B. A.; Huang, Y., A novel approach to determine leucomalachite green and malachite green in fish fillets with surface-enhanced Raman spectroscopy (SERS) and multivariate analyses. *Journal of Raman Spectroscopy* **2012,** *43* (9), 1208-1213.

Zhao; Jensen, L.; Schatz, G. C., Pyridine−Ag20 Cluster: A Model System for Studying Surface-Enhanced Raman Scattering. *Journal of the American Chemical Society* **2006,** *128* (9), 2911-2919.

Zhao, Y.; Tian, Y.; Ma, P.; Yu, A.; Zhang, H.; Chen, Y., Determination of melamine and malachite green by surface-enhanced Raman scattering spectroscopy using starch-coated silver nanoparticles as substrates. *Analytical Methods* **2015,** *7* (19), 8116-8122.

Zheng, J.; Zhao, C.; Tian, G.; He, L., Rapid screening for ricin toxin on letter papers using surface enhanced Raman spectroscopy. *Talanta* **2017,** *162*, 552-557.

Zhu, Y.; Li, M.; Yu, D.; Yang, L., A novel paper rag as 'D-SERS' substrate for detection of pesticide residues at various peels. *Talanta* **2014,** *128*, 117-124.